Universität Bremen

Processes of calcification and sedimentation of the tropical marine green macro-alga genus *Halimeda* and effects of ocean acidification on its calcareous microstructure

Thesis for the completion of a Dr. rer. nat.

Department of Geosciences (FB5)

University of Bremen

André Wizemann

Geoecology and Carbonate Sedimentology

Group leader and supervisor: Prof. Dr. Hildegard Westphal

Second referee: Prof. Dr. Helmut Willems

Bremen, June 2015 / colloquium 20.07.2015

z m t bremen

Leibniz Association

Name : André Wizemann Datum: 01.06.2015

Anschrift : Kulenkampffallee 77, 28213 Bremen

Erklärung

Hiermit versichere ich, dass ich

(1) die Arbeit ohne unerlaubte fremde Hilfe angefertigt habe,

(2) keine anderen als die von mir angegebenen Quellen und Hilfsmittel benutzt habe,

(3) die den benutzten Werken wörtlich oder inhaltlich entnommenen Stellen als solche kenntlich gemacht habe und

(4) weder diese noch eine ähnliche Arbeit an einer anderen Abteilung oder Hochschule im Rahmen eines Prüfungsverfahrens vorgelegt, veröffentlicht oder zur Veröffentlichung vorgelegt habe.

Bremen, den 01.06.2015

(Unterschrift)

Table of Contents

Acknowledgments

I want to thank my supervisor Prof. Dr. Hildegard Westphal for the opportunity to conduct research on this fascinating subject at the Leibniz-Center for Tropical Marine Ecology (ZMT), the kind atmosphere in discussions and her constructive and helpful comments on the thesis and the manuscripts. In the same way, I also thank my PhD colleague Fritz Meyer as I would not have been able to conduct the laboratory research without his help and with whom I had fruitful discussions that led to interesting conceptual ideas. A great part of work would not have been possible without the tremendous effort of ZMT technician Sebastian Flotow in preparing petrographic thin-sections of such tiny and fragile biological samples and his continuous aim to advance the techniques. Further, I want to thank all my colleagues of the working group "Carbonate Sedimentology" at ZMT. André Klicpera with whom I shared the office for a long time and later on also Thomas Mann, Peter Müller and Marleen Stuhr. The pleasant atmosphere in the office led to extensive discussions for which I am sorry if I distracted you from your work way too often with some of my "crazy" ideas. I also have to thank Natalia Herrán Navarro, Gita Roshni Narayan, Claire Reymond, and other (co-)members of our group that however here remain unnamed, nevertheless shall feel addressed. Of course, special credits go to Nereo Preto for establishing the "espresso round" during his research stays at ZMT and I think this little custom fits best the nice atmosphere of our working group ;) In the end, Julien Michel shall not be forgotten and I remember with joy and thank him for the great dinners we all shared together at his former place in Bremen. With our group's team spirit, of everybody supporting each another, it was a pleasant working experience that I do not want to miss.

Abstract

Calcifying green macro-algae of the genus *Halimeda* are common organisms in tropical shallow marine environments. These ramified benthic algae grow by forming successional segments that exhibit an internal skeletal microstructure of the calcium carbonate polymorph aragonite. The calcareous segments become part of the sediment after death. As macro-algae of the genus *Halimeda* often occur in large quantities and are able to build extensive bioherms, dropped segments from these algae are considered as an important source for carbonate sediments in many shallow water and coral reef environments. Thus detailed knowledge on the calcification of the alga is crucial for estimations on the carbonate budget and sediment dynamics of tropical settings, as this process directly determines the sediment contribution of *Halimeda*. Furthermore, it is a prerequisite when effects on the formation of its calcium carbonate microstructure under ocean acidification have to be assessed.

In this study, internal microstructural features of segments from the species *Halimeda opuntia*, a cosmopolitan species of the genus *Halimeda*, are investigated using scanning electron microscopy. The first aim is to study the alga´s calcified microstructure in detail in order to be able to explain the formation of skeletal features in relation to known physiological processes of the alga. Thereby, lifetime primary cementation is identified to be an important process for calcium carbonate deposition in the algal segment. The second aim is to determine potential alterations in the formation of these microstructural features due to elevated seawater pCO_2 and the corresponding shift in seawater carbon chemistry. Laboratory experiments show that especially the process of lifetime primary cementation is affected by elevated seawater pCO_2. Based on the microstructural investigations, a theoretical model is developed on how physiological daytime and nighttime processes influence the formation of skeletal features in the genus *Halimeda.* The model also illustrates the basic relationships between changes in the seawater carbon chemistry and changes observed in the skeletal microstructure of the segment under elevated seawater pCO_2.

As a third objective, segments from living *Halimeda* and segments recovered from surface sediments are studied and compared using scanning electron microscopy to investigate the occurrence of post-sedimentary processes that alter the original skeletal microstructure. By the investigation of thin-sections of numerous sedimentary segments, species-specificity of *Halimeda* sediments is observed. Segments found in

sediments predominantly originate from heavily calcified lithophytic species of the genus *Halimeda*, such as from the lineage Opuntia. Microstructural investigations also reveal that the process of lifetime primary cementation strongly determines the preservation potential of *Halimeda* segments in the sediment. Thus ocean acidification is assumed to impair both the alga´s environmental competitiveness (e.g., grazing protection, pathogen defense, structural integrity) and its carbonate sediment contribution to tropical coastlines and reef islands.

Zusammenfassung

Grünalgen der Gattung *Halimeda* gehören zu einer Gruppe von kalzifizierenden Meeresalgen, die häufig in tropischen flachmarinen Lebensräumen anzutreffen sind. Makroalgen der Gattung *Halimeda* bilden nacheinanderfolgende Segmente in verzweigten Ästen die ein extrazelluläres Kalkskelett aus dem Kalziumkarbonat-Polymorph Aragonit besitzen. Nach ihrem Absterben werden die kalzifizierten Segmente Teil des Sediments. Da Algen der Gattung *Halimeda* in großer Anzahl auftreten können und große Bioherme aufbauen werden abgefallene Kalksegmente der Alge als eine bedeutende "Karbonat-Fabrik" in tropischen flachmarinen Lebensräumen und in Korallenriffen angesehen. Ein detailiertes Verständnis des Kalzifizierungsprozesses ist wichtig, da dieser über die Quantität der Sedimentproduktion der Alge mitbestimmt. Desweiteren ist ein umfassendes Wissen über den Kalzifizierungsmechanismus eine Voraussetzung um Auswirkungen auf die Bildung der Kalziumkarbonatmikrostruktur im Bezug auf anthropogene Prozesse, wie der fortschreitenden Ozeanversauerung, erkennen und erklären zu können.

In dieser Arbeit wurden die internen mikrostrukturellen Eigenschaften der Segmente von *Halimeda opuntia*, einer weltweit vorkommenden *Halimeda*-Art, mittels Rasterelektronenmikroskopie untersucht. Ein erstes Ziel war dabei die Kalziumkarbonatmikrostruktur im Detail genauer zu untersuchen und ihre Ausbildung mit bekannten physiologischen Prozessen der Alge zu korrelieren um diese in Einklang mit der Entwicklung der internen Segmentmikrostruktur erklären zu können. Der dabei beobachtete Prozess der primären Zementierung des internen Kalkskelettes zu Lebzeiten führt zu einer hohen Kalzifizierungsdichte der Segmente. Ein weiteres Ziel war es mögliche Veränderungen in der internen Segmentmikrostruktur unter Einfluss einer erhöhten CO_2 Konzentration des Meerwassers und der zugrundeliegenden Veränderung der Meerwasser-Karbonatchemie zu untersuchen. In Laborexperimenten wurde festgestellt, dass der Prozess der primären Zementierung durch einen erhöhten pCO_2 des Meerwassers beeinträchtigt wird. Nachfolgend ist mit Hilfe dieser Ergebnisse ein einfaches Modell erstellt worden um den Einfluss der physiologischen Tag- und Nachtprozesse der Alge auf die Bildung der Skelettstruktur in der Kalkalgengattung *Halimeda* zu veranschaulichen. Das Modell läßt zudem Rückschlüsse auf die grundlegenden Beziehungen zwischen Veränderungen der Meerwasser-Karbonatchemie und

Veränderungen im Karbonatskelett der Segmente zu, welche durch eine erhöhte CO_2 Konzentration des Meerwassers ausgelöst werden.

Neben Segmenten von lebenden *Halimeda* Algen wurden auch Segmente aus dem Sediment mittels Rasterelektronenmikroskopie untersucht um die postsedimetären Prozesse, die die Segment-Mikrokarbonatstruktur nach deren Absterben verändern, zu untersuchen. Durch die Untersuchung von petrographischen Dünnschliffen einer Vielzahl von Segmenten, sowohl von lebenden Algen als auch aus dem Sediment, wurde eine ausgeprägte Artspezifität der *Halimeda* Sedimente festgestellt. Im Sediment indentifizierte vollständig erhaltene Segmente stammen hauptsächlich von stark-kalzifizierenden Arten der Gattung *Halimeda*, so zum Bespiel von der Art *Halimeda opuntia*. Die Mikrostrukturanalysen zeigen darüberhinaus, dass der Prozess der primären Zementierung unmittelbar mit dem Erhaltungspotential eines Segments im Sediment verbunden ist. Auch deshalb könnte eine fortschreitende Ozeanversauerung beides, sowohl die Konkurrenzfähigkeit der Alge in ihrem Lebensraum, als auch ihre Karbonatsedimentproduktion in tropischen Küstengebieten und Riffinseln beeinträchtigen.

Conference contributions

Wizemann A, Westphal H (GV and Sediment Meeting, Hamburg 2012**)**
The impact of ocean acidification on the calcium carbonate precipitation and deposition in tropical shallow seas: the calcareous green alga *Halimeda*

The calcareous green algae *Halimeda sp*. is one of the most important marine sediment producers in the tropics nowadays. *Halimeda sp*. is an extremely fast growing plant and exhibits a rapid lifecycle as well as turnover of its calcified segments. Therefore it contributes vast amounts of calcium carbonate to shallow, coastal ocean, especially in tropical reef environments. *Halimeda* sediments can form large carbonate platforms, which are considered to be a valuable ocean carbonate buffer in the long term. Current anthropogenic CO_2 input to surface ocean waters lowers seawater carbonate ion saturation state. The underlying process, called "Ocean Acidification" (OA), is an upcoming threat for marine calcifying organisms as precipitation of calcium carbonate mineral forms in general depends on the water to be super-saturated with carbonate ions. Here we show the impact of a declining carbonate saturation state on the precipitation of aragonite and early cementation in the calcified segments of the calcareous green algae *Halimeda sp*. In addition to marine laboratory OA-experiments with living plants, our work is also focusing on the impact of OA on *Halimeda* sediments and so point out the consequences for future ocean´s CO_2 uptake and buffering abilities. Therefore we examine recent and historical surface sediment samples, as well as dried plants from several tropical marine locations all over the world. By doing so we receive a general overview to what extent aragonite precipitation and segment cementation in *Halimeda* are already affected and will be affected in the near future.

Wizemann A, Meyer FW, Westphal H (Biodiversity and Health, Berlin 2013)
Acidification impacts on the microstructure in calcifying green algae

The calcareous green alga *Halimeda* spp. is one of the most important marine sediment producers in the tropics nowadays. *Halimeda* spp. is an extremely fast growing plant and exhibits a rapid lifecycle as well as turnover of its calcified segments. Therefore it contributes vast amounts of calcium carbonate to shallow, coastal ocean, especially in tropical reef environments. *Halimeda* sediments can form large carbonate platforms, which are considered

to be a valuable ocean carbonate buffer in the long term. Current anthropogenic CO_2 input to surface ocean waters lowers seawater carbonate ion saturation state. The underlying process, called "Ocean Acidification" (OA), is an upcoming threat for marine calcifying organisms as precipitation of calcium carbonate mineral forms in general depends on the water to be super-saturated with carbonate ions. Here we show the impact of a declining seawater pH and carbonate saturation state on the precipitation of aragonite and early cementation in the calcified segments of the calcareous green alga *Halimeda opuntia*. In addition to marine laboratory OA-experiments with living plants, our work is also focusing on the impact of OA on *Halimeda* sediments and so point out the consequences for future ocean´s CO_2 uptake and buffering abilities. Therefore we examine recent and historical surface sediment samples, as well as dried plants from several tropical marine locations all over the world. By doing so we receive a general overview to what extent aragonite precipitation and segment cementation in *Halimeda* are already affected and will be affected in the near future.

Wizemann A, Meyer FW, Westphal H (International conference on ceolenterate biology, Eilat 2013)

Acidification impacts on the microstructure in calcifying green macro-algae

The current rise in atmospheric carbon dioxide interacting with surface ocean waters lowers the seawater carbonate ion saturation state. The underlying process, known as "Ocean Acidification" (OA), poses a threat to marine calcifying organisms, as precipitation of calcium carbonate mineral forms depends on the seawater being super-saturated with carbonate ions. The calcifying green macro-alga *Halimeda* spp. is an extremely fast growing alga, exhibiting a rapid turnover of its calcified segments, thus contributing vast amounts of calcium carbonate sediment to shallow marine coral reef environments. The carbonate sediment formed by *Halimeda* not only provides a structure-rich habitat, but also contributes to carbonate platform build-up and the oceans carbonate buffer. Here we show the impact of a declining carbonate ion saturation state on the calcification and early cementation on the calcified skeleton of the calcareous green macro-alga *Halimeda opuntia*. By analyzing the microstructure of the internal morphological features in detail via scanning electron microscopy, and relating to the alga´s physiology, we arrive at a new model of calcification, which explains both the biotic and abiotic driven calcification as well as the alterations caused by OA.

Wizemann A, Mann T, Westphal H (GeoFrankfurt 2014)

Halimeda sediments: implications for the interpretation of carbonate sediment origin and transport

Calcareous segments of the green macro-alga *Halimeda* are a common sediment component often found in the carbonate facies of tropical shallow marine environments (Milliman 1974; Drew 1983). As *Halimeda´*s segmental growth rate is rapid (Wefer 1980) and older segments are continuously shed, its total carbonate sediment production may even exceed that of the corals in coral reef environments (Rees et al. 2007). Thus where it is abundant, *Halimeda* largely supports the buildup of carbonate platforms and tropical islands (Hine et al. 1988; Freile et al. 1995; Wienberg et al. 2009). However the interpretation of typical macroscopic *Halimeda* sediments in sedimentological studies is often relatively general, neglecting their species-specific origin (Johns & Moore, 1988). Thus, without recognizing the alga´s biology and its environmental preferences no valid conclusions can be drawn. Here we present a detailed analysis of *Halimeda* plates from sediments sampled worldwide (e.g. GBR, Fiji, Indonesia, Bahamas, Maldives, Zanzibar, Hawaii, Mexico, Brazil). We picked complete plates, digitally photographed them and prepared thin-sections that we analyzed via scanning electron microscopy. Not only are we able to show how these plates get altered in the sediment, we are also able to trace them back to the species or at least the section type of *Halimeda* (Verbruggen & Kooistra, 2004). Consequently, we present evidence that only some species are responsible for typical macroscopic *Halimeda* sediments that are found today. As we are aware of the environmental niche these species inhabit, we are able to precisely determine the area these sediments originate from and how their external and internal microstructure is altered congruent to their age under hydrodynamic and chemo-physical forces. Our investigations show conclusively that these species-specific *Halimeda* sediments must not be interpreted as localized in-situ sediment production and deposition without conducting a detailed analysis of their internal microstructure, their grain shape and their surface structure.

Overview of publications (chapters in this thesis)

Chapter 3: Wizemann A, Meyer FW, Westphal H (2014) A new model for the calcification of the green macro-alga *Halimeda opuntia* (Lamouroux). Coral Reefs 33:951-964
doi:10.1007/s00338-014-1183-9

Halimeda opuntia is a cosmopolitan marine calcifying green alga in shallow tropical marine environments. Besides *Halimeda*'s contribution to a diverse habitat, the alga is an important sediment producer. Fallen calcareous segments of *Halimeda* spp. are a major component of carbonate sediments in many tropical settings and play an important role in reef framework development and carbonate platform build-up. Consequently the calcification of *H. opuntia* accounts for large portions of the carbonate budget in tropical shallow marine ecosystems. Earlier studies investigating the calcification processes of *Halimeda* spp. have tended to focus on the microstructure or the physiology of the alga, thus overlooking the interaction of physiological and abiotic processes behind the formation of the skeleton. By analyzing microstructural skeletal features of *Halimeda* segments with the aid of scanning electron microscopy and relating their occurrence to known physiological processes, we have been able to identify the initiation of calcification within an organic matrix and demonstrate that biologically-induced cementation is an important process in calcification. For the first time, we propose a model for the calcification of *Halimeda* spp. that considers both the alga's physiology and the carbon chemistry of the seawater with respect to the development of different skeletal features. The presence of an organic matrix and earlier detected external carbonic anhydrase activity suggest that *Halimeda* spp. exhibits biotic precipitation of calcium carbonate, as many other species of marine organisms do. On the other hand it is the formation of micro-anhedral carbonate through the alga's metabolism that leads to a cementation of living segments. Precisely this process allows *H. opuntia* to contribute substantial amounts of carbonate sediments to tropical shallow seas.

Chapter 4: Wizemann A, Meyer FW, Hofmann LC, Wild C, Westphal H (2015) Ocean acidification alters the calcareous microstructure of the macro-alga *Halimeda opuntia.* Coral Reefs 34:941-954
doi:10.1007/s00338-015-1288-9

Decreases in seawater pH and carbonate saturation state (Ω) following the continuous increase in atmospheric CO_2 represent a process termed ocean acidification, which is predicted to become a main threat to marine calcifiers in the near future. Segmented, tropical, marine green macro-algae of the genus *Halimeda* form a calcareous skeleton that involves biotically-initiated and -induced calcification processes influenced by cell physiology. As *Halimeda* is an important habitat provider and major carbonate sediment producer in tropical shallow areas, alterations of these processes due to ocean acidification may cause changes in the skeletal microstructure that have major consequences for the alga and its environment, but related knowledge is scarce. This study used scanning electron microscopy to examine changes of the $CaCO_3$ segment microstructure of *Halimeda opuntia* specimens that had been exposed to artificially elevated seawater pCO_2 of ~650 µatm for 45 days. In spite of elevated seawater pCO_2, the calcification of needles, located at the former utricle walls, was not reduced as frequent initiation of new needle-shaped crystals was observed. Abundance of the needles was ~22 % μm^{-2} higher and needle crystal dimensions ~14 % longer. However, those needles were ~42 % thinner compared to the control treatment. Moreover, lifetime cementation of the segments decreased under elevated seawater pCO_2 due to a loss in micro-anhedral carbonate as indicated by significantly thinner calcified rims of central utricles (35 - 173 % compared to the control treatment). Decreased micro-anhedral carbonate suggests that seawater within the inter-utricular space becomes $CaCO_3$ undersaturated ($\Omega < 1$) during nighttime under conditions of elevated seawater pCO_2 thereby favoring $CaCO_3$ dissolution over micro-anhedral carbonate accretion. Less cemented segments of *H. opuntia* may impair the environmental success of the alga, its carbonate sediment contribution, and the temporal storage of atmospheric CO_2 within *Halimeda*-derived sediments.

Chapter 5: Wizemann A, Mann T, Westphal H (2015) Microstructural analyses of sedimentary *Halimeda* segments from the Spermonde Archipelago (SW Sulawesi, Indonesia): a new indicator for sediment transport in tropical reef islands? Facies 61:4 doi:10.1007/s10347-015-0429-5

Understanding the origin of sediments and the direction of sediment transport is a prerequisite for accurate reconstruction of reef island evolution. In tropical settings, island development depends on the accumulation of sediments on the reef flat, which are produced by calcifying organisms such as corals, foraminifera and green macro-algae of the genus *Halimeda*. In certain areas of tropical regions calcareous segments from these algae might account for more than fifty weight percent of the coarser sediment fraction. *Halimeda*-rich sediments typically contain complete segments that become widely distributed to a range of sedimentary settings. However, the exact sedimentary pathway is either mostly unknown or was neglected. Here we show that the alteration of *Halimeda* segments from the Spermonde Archipelago (SW Sulawesi, Indonesia) is related to processes during transport and deposition. Using field observations and scanning electron microscopy we observed that *Halimeda* segments, sampled from the reef flat to the shore on four uninhabited islands, without exception belong to the grain-size class of pebble gravel (1.6 > 0.4 cm; medium to fine pebbles) and reveal characteristic patterns of external and internal microstructural alteration with respect to sampling area. Furthermore, *Halimeda* species from which most of these segments originate preferably inhabit hard substrates in the reef, on the reef crest and the outer reef flat. Thus, the observed distinct microstructural alteration of the segments allows drawing conclusions on sediment transport and deposition. Particularly, rapid secondary cementation may preserve the segments as a sedimentary component for the development and maintenance of reef islands and coastlines in tropical shallow seas.

1. Introduction

1.1 Calcareous green macro-algae genus *Halimeda*

Calcifying green algae of the genus *Halimeda* are cosmopolitan marine macro-algae that inhabit tropical shallow-water environments such as coral reefs, in which they are primary producers of carbonate sediments (Hillis-Colinvaux 1980; Drew 1983). The genus *Halimeda* belongs to the order Bryopsidales (taxon Ulvophyceae), an order of the green algae (Chlorophyta) that is characterized by coenocytic cells, i.e. cells without a cross-wall that allow cell organelles to move freely within the organics of the alga. Macro-algae of the genus *Halimeda* exhibit a segmental habit whereby the calcified leaf-like segments, joined together at tiny uncalcified nodes, form a dumose thallus with several elongated branches (Hillis-Colinvaux 1980). Fragmentation of these segmented branches from the thallus or clones of rhizoidal threads enable *Halimeda* to disperse asexually, which is the common form of reproduction. However, a sexual reproduction cycle exists enabling genetic exchange over gametes (flagellate stage) and zygotes (Hillis-Colinvaux 1980). *Halimeda* grows by sprouting new segments that firstly develop as whitish organic lobes on the distal pole of apical segments on each branch. After ~24 h these segments become green in color, which is an indication that chloroplasts (and other cell organelles) moved into the newly formed segment (Larkum et al. 2011). The segments develop an internal but extracellular calcareous skeleton that consists of the calcium carbonate ($CaCO_3$) polymorph aragonite (Wilbur et al. 1969; Hillis-Colinvaux 1980; Stanley et al. 2010). Based on species-specific internal segment morphology, type of holdfast and growth habit, the genus *Halimeda* is further separated into taxonomic lineages (synonymously also called sections) (Hillis-Colinvaux 1980; Hillis 2001; Verbruggen and Kooistra 2004). The established *Halimeda* lineages (Rhipsalis, Halimeda, Opuntia, Pseudo-Opuntia and Micronesicae) comprise more than 30 morphologically described species. Species within each lineage generally share similar habitat and substrate preferences, as they inhabit specific biological niches in tropical shallow marine environments.

1.1.1 *Halimeda opuntia* (L.) lineage Opuntia

The species morphotype *Halimeda opuntia* (Lamouroux 1816) defines the lineage Opuntia within the genus *Halimeda* (Hillis-Colinvaux 1980; Verbruggen and Kooistra 2004), which encompasses *Halimeda* species that exhibit relatively small segments (< 1 cm) of typical "butterfly" to "fan-like" shape (cf., reniform) or "trident-like" shape (cf., tripartite), depending on sun-leaf and shade-leaf morphotype, respectively (cf., Kooistra and Verbruggen

2005). The numerous segmented branches, typical for macro-algae of this *Halimeda* lineage, are not solely orientated in upright direction, as it is the case in many other algal species of the genus *Halimeda* (Fig. 1). Additionally, algae of the lineage Opuntia do not posses a bulbous holdfast, but thin root-like filaments with which they attach to the substrate. Thus, these specific *Halimeda* species grow predominantly in habitats with hard substrate (e.g., coral reef, reef crest, reef patches on the reef flat) that naturally are not inhabited by *Halimeda* species with a single thick holdfast and of which most are psammophytic sand-dwellers (e.g., lineage Rhipsalis). Moreover the rather bottom-oriented, flattened growth-form and the small, but strongly calcified, segments allow *Halimeda opuntia* to inhabit environments with high water energy, such as the reef crest or wave-exposed patch reefs, but also carbonate knolls in the open ocean (e.g., seamounts and atolls) (Johns and Moore 1988; Hine et al. 1988; Roberts et al. 1988; Ries et al. 2005; Wienberg et al. 2010).

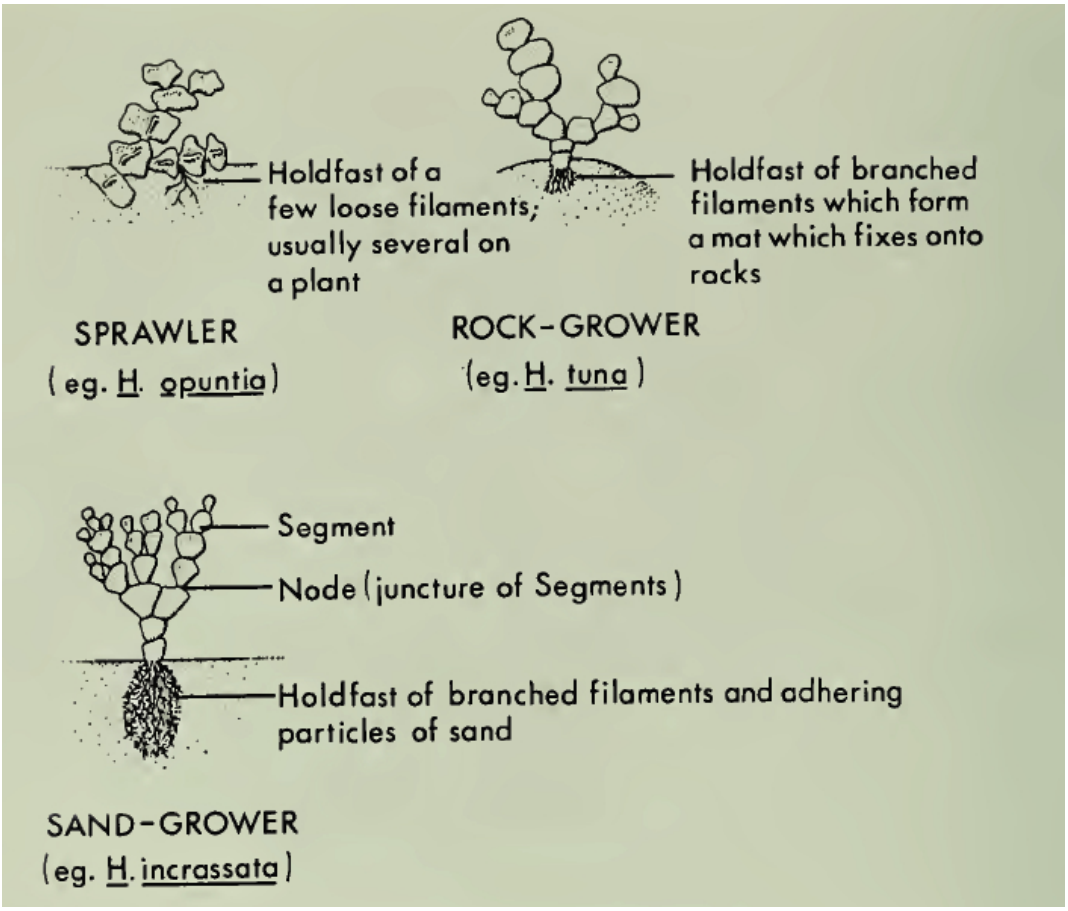

Fig. 1 Different growth forms of green macro-algae genus *Halimeda* and their substrate specificity. Adopted from Hillis-Colinvaux (1980).

1.1.2 The morphological microstructure of the *Halimeda* segment

The internal morphological microstructure of the *Halimeda* segment consists of the calcareous skeleton and the organics (Fig. 2), whereby the cells of the alga are coenocytic (i.e., lacking cross-walls between cells) and form a syncytium (Hillis-Colinvaux 1980). The organic filaments within the segment are termed utricles (U). Utricles are tube-like hierarchical structured filaments that determine the internal morphology of the segment and host the cell organelles. Small primary utricles (pU) are located at the segment rim in the cortex region of the segment. Towards the central part of the segment larger secondary and tertiary utricles (sU and tU) and in the innermost part medullary utricles (mU) are located (i.e. medulla region; Fig. 2b). *Halimeda* calcifies solely extracellular inside open spaces framed by the organic filaments, i.e. the utricles. These open spaces are termed inter-utricular spaces (IUS). As primary utricles located on the rim form small, narrow IUS in contrast to the central secondary, tertiary and medullary utricles, the IUS is separated into a peripheral primary IUS (pIUS) and a secondary IUS (sIUS), sub-peripheral open space that encompasses the inner central and core parts of the segment. The IUS are semi-enclosed and form tiny reaction chambers (< 1 mm^3) where physiological processes of the alga modify the seawater carbon chemistry to support calcification by raising seawater carbonate saturation state (Borowitzka and Larkum 1976a; Borowitzka 1982b). Surrounding seawater enters the IUS and enables ion exchange, e.g. of calcium (Ca^{2+}) ions that are used in calcification (Böhm 1973; Böhm and Goreau 1973; Borowitzka and Larkum 1976a; De Beer and Larkum 2001). The internal morphological organic segment microstructure shaped by the utricles has implications for the segment calcification as it determines dimensions and volume of IUS that is available for calcification. The pIUS of the segment rim that is formed by the small primary utricles is heavier and denser calcified when compared to the wider inner IUS located towards and within the central part of the segment (Multer 1988; Macintyre and Reid 1995).

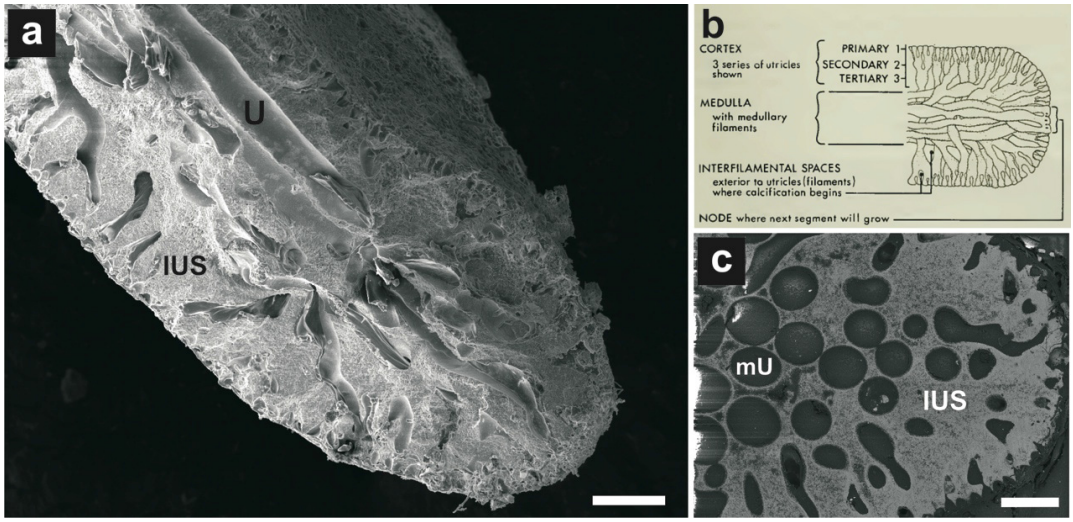

Fig. 2 Internal microstructure of the *Halimeda* segment. (a) Scanning electron microscopic image showing the internal microstructure of a bisected segment from *Halimeda opuntia* that was mounted on a sample-stub (organics lost). (b) Schematic drawing of the organic ultrastructure of the *Halimeda* segment (adopted from Hillis-Colinvaux 1980). (c) Back-scattered electron image of a thin-section from an apical segment of *H. opuntia* showing the $CaCO_3$ skeletal microstructure (in white). U = utricle; IUS = inter-utricular space. Scale bar in (a) and (c) is 100 μm.

1.1.3 The process of calcification in the macro-alga genus *Halimeda*

The process of calcification in *Halimeda* is supposed to be influenced by light and linked to photosynthesis of the alga (Borowitzka and Larkum 1976a, b; Jensen et al. 1985). The most prominent $CaCO_3$ skeletal feature of *Halimeda* are the aragonite needles (Wilbur et al. 1969; Milliman 1974; Macintyre and Reid 1995; Stanley et al. 2010). Based on their prismatic crystal shape that resembles euhedral crystal development it was postulated that precipitation of $CaCO_3$ in *Halimeda* is abiotic, but biologically mediated by photo-physiology (Borowitzka and Larkum 1977; Weiner and Lowenstam 1986). Thereby the alga increases the seawater carbonate ion saturation and the pH in the IUS through uptake of protons (H^+), carbon dioxide (CO_2) and bicarbonate (HCO_3^-) during photosynthesis, which provides conditions necessary for $CaCO_3$ crystallization (Borowitzka 1982a, 1984). However, Macintyre and Reid (1995) recognize different types of needles in the skeleton that are not considered in previous models on calcification of *Halimeda*. Especially the origin of small needles at the utricle wall and the related mechanism of crystal nucleation and crystallization are unknown. Wilbur et al. (1969) proposed that polysaccharide fibers on the utricle walls facing into the IUS accumulate Ca^{2+} ions and act as a scaffold for crystallization. Böhm and Goreau (1973) confirmed the presence of cation-affine acidic sulfated polysaccharides but additionally suggested that a layer of mucilage or an organic matrix is involved in calcification. Nakahara and Bevelander (1978) state the observation of organic envelops surrounding early crystals. In contrast, Borowitzka and Larkum (1977) point out that the initiation of calcification starts between the fibers on the outer utricle wall without an organic matrix present. However, Borowitzka (1982a) recognizes the possibility that an organic matrix may be present and involved in $CaCO_3$ formation but disintegrating soon after crystal nucleation.

1.1.4 The development of the skeletal microstructure of the *Halimeda* segment

In Macintyre and Reid (1995) a new terminology was introduced that is up to now the most detailed description of the $CaCO_3$ skeletal microstructure of *Halimeda*. In the following, the

fundamental steps in the formation of the main skeletal features of the segment microstructure are presented.

At first, $CaCO_3$ precipitation occurs in the *Halimeda* segment in the form of short aragonite needles (< 5 µm) directly on the external cell wall of utricles (Fig. 3). Subsequently, ongoing precipitation of these needles may fill up the smaller primary IUS completely. These short skeletal needles become recrystallized into micron-sized (< 1 µm) aragonite crystals of anhedral shape. Macintyre and Reid (1995) describe these crystals as "mini-micrite". However the term micrite (Folk 1959; Milliman 1974) does not specify the crystal origin and thus does not allow differentiation between abiotic derived $CaCO_3$ precipitation (e.g. intra-granular cementation) from saturated seawater and biotically-induced formation (e.g., recrystallization) from previously formed $CaCO_3$. In the following a new term, "micro-anhedral carbonate (MAC)", is used to describe the type of crystals that are formed solely within living *Halimeda* segments in close dependency to the cell physiology of the alga.

With maturation of the segment, the MAC "front" expands from utricle walls into the IUS (cf., Macintyre and Reid 1995). In the innermost IUS, typically in larger sIUS, long aragonite needles are observed. Long needles may become more than 20 µm in dimension and grow on top of the utricle wall associated MAC layer (Macintyre and Reid 1995). Euhedral and prismatic in shape, these needles fan-out into open and not MAC filled areas of the IUS (Weiner and Lowenstam 1986; Multner 1988; Macintyre and Reid 1995). When the IUS is completely filled with MAC, long needles are absent.

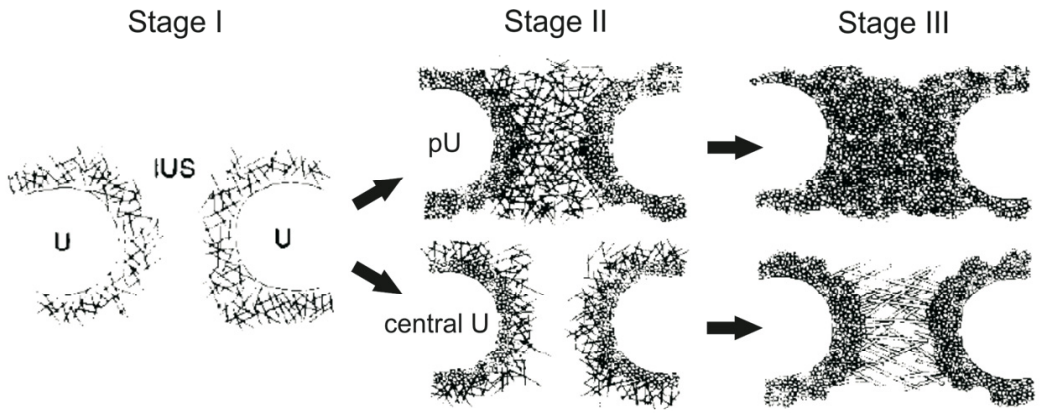

Fig. 3 Schematic drawing of the $CaCO_3$ IUS infilling process in the *Halimeda* segment. Shown are the subsequent stages of segment calcification modified after Macintyre and Reid (1995). In stage (I) short (< 5 µm) skeletal needles are precipitated along extracellular walls of utricles. Stage (II) shows the formation of anhedral crystals (< 1 µm), likely out of recrystallized short needles at the utricle walls. In stage (III), inter-utricular spaces (IUS) between peripheral primary utricles (pU) become filled with anhedral $CaCO_3$ crystals, whereas IUS between central utricles shows abundant growth of long (> 10 µm) euhedral needles. U = utricle; IUS = inter-utricular space.

1.1.5 External carbonic anhydrase activity (eCA) within the IUS

Green macro-algae of the genus *Halimeda* posses extracellular, external carbonic anhydrase activity (eCA) within the IUS (Borowitzka and Larkum 1976b). External CA catalyzes the reversible reaction of $CO_2 + H_2O \leftrightarrow HCO_3^- +$ protons (H^+). Generally, it is understood that eCA in algae and plants provides additional CO_2 for photosynthesis (reviewed by Tsuzuki and Miyachi 1989) to enhance the cell-membrane diffusion gradient outside the cell that promotes the uptake of CO_2. Subsequently, CO_2 uptake may then elevate the seawater carbonate ion saturation within the IUS to allow $CaCO_3$ to precipitate (Borowitzka 1984). Borowitzka and Larkum (1976b) showed that inhibition of eCA with acetazolamide (0.25 mM) terminated the process of calcification in *H. opuntia* during photosynthesis, whereby photosynthesis still occurred at a lower rate of ~25 % of the initial control rate. Noteworthy, *H. opuntia* is well adapted to low light regimes and is able to calcify under such environmental conditions (Goreau 1963; Goreau and Goreau 1973; Böhm 1973; Jensen et al. 1985). Thus, this may contradict the current view that calcification and photosynthesis are tightly coupled. In fact, eCA is well known to play a substantial role in $CaCO_3$ biomineralization of most, if not all, marine organisms (e.g., Mitsunaga et al. 1986; Marin and Luquet 2004; Miyamoto et al. 2005; Tambutté et al. 2007; Rahman et al. 2008; Li et al. 2011; Bonucci et al. 2013; Enrique and Schubert 2014). Interestingly, Hofmann et al. (2014) showed an increase in eCA in *H. opuntia* under elevated seawater pCO_2.

1.2 The process of ocean acidification: present, future and past

The atmosphere and the ocean are in an equilibrium state regarding the concentration of greenhouse gases, such as carbon dioxide (CO_2). Thus, when the atmospheric CO_2 concentration is rising so is the CO_2 concentration of the ocean. When CO_2 enters seawater it rapidly forms carbonic acid (H_2CO_3), which dissociates to bicarbonate ions (HCO_3^-) by the release of protons (hydrogen ions; H^+). As a consequence, this carbonation of the ocean via CO_2 not only lowers seawater pH but also modifies seawater carbon chemistry as it elevates dissolved inorganic carbon (DIC). Higher proton concentration decreases carbonate ion (CO_3^{2-}) saturation as protons react with CO_3^{2-} ions to form HCO_3^-. Subsequently, the carbonate saturation state (Ω) of the seawater decreases as seawater carbon chemistry shifts towards HCO_3^- and CO_2 at the expense of CO_3^{2-} ion concentration. As the whole process creates protons that lower seawater pH and raise the acidity of the ocean it is termed “ocean acidification” (Caldeira and Wickett 2003; Feely et al. 2009). The mean seawater pH already declined during the last century from ~8.2 by 0.1 units to ~8.1, which accounts for an increase in protons (H^+) of roughly 30 % (Orr et al. 2005). It is proposed that seawater pH may decline

up to 0.3 units by the end of this century (i.e., year 2100; Raven et al. 2005; IPCC report 2007, 2013). That may account for an atmospheric CO_2 concentration of more than 1000 parts per million (ppm) CO_2 or a partial pressure of ~1000 micro-atmospheres (µatm) pCO_2 when equilibrated in seawater (Friedlingstein et al. 2006; IPCC report 2007, 2013). In geological times atmospheric CO_2 concentrations were significantly higher as today (Veron 2008). The Cretaceous and the Triassic are two epochs in which the atmospheric CO_2 concentration is estimated to have been even above 3000 ppm over longer periods of time (i.e. hundred-thousands to millions of years). During those times, the ocean pCO_2 resembled the atmospheric CO_2 concentration. However various calcareous reef- and bioherm-building organisms, such as calcareous sponges, bivalves, brachiopods, bryozoans, foraminifers, corals and, rudists flourished during those time periods (Kiessling 2009; Kiessling and Simpson 2011). It is assumed that the shift in carbon chemistry caused by such high concentrations of CO_2 was buffered through a relatively high total alkalinity (> 3000 µmol kg^{-1}) of ocean waters due to enhanced terrestrial weathering processes driven by the high atmospheric CO_2 concentration (e.g, Zeebe 2012). Thus the carbonate saturation state of the water may have remained sufficiently stable, i.e. $CaCO_3$ over-saturated ($\Omega > 1$). Additionally the chemical element composition (e.g., Mg/Ca ratio; Stanley et al. 2010) of the seawater was altered through time, shifting the $CaCO_3$ polymorph that was favored in precipitation (between aragonite - low and high Mg-calcite; Stanley and Hardie 1999; Brennan et al. 2004). Nevertheless, some studies doubt the CO_2 driven elevation of weathering rates to be sufficient for sustainment of a highly alkaline well-buffered ocean (Raymo and Ruddiman 1992; Edmond and Huh 1997; Broecker and Sanyal 1998; Kump et al. 2000). Whatever may prove correct, calcifying organisms (and the process of biological calcification itself) never seemed to be seriously affected over these periods of high pCO_2 as in contrast they were probably well adapted to former seawater carbon chemistry and its elemental composition. Certainly the comparably slow alteration rate of atmospheric CO_2 concentration (likely in the order of millennia) and the long stasis of high CO_2 conditions during these periods may have been supportive for environmental adaptation and niche diversification (Kump et al. 2009). However some major mass extinction events also affecting marine calcifiers (cf., reef gaps; Veron 2008) are linked to rapid increase in atmospheric CO_2 (i.e., in the order of centuries or even faster) and subsequent shift of the ocean carbon chemistry that probably caused conditions of severe $CaCO_3$ undersaturation. Examples with strong evidence therefor are the Paleocene-Eocene Thermal Maximum (PETM; Zachos et al. 2005), the Permian-Triassic event (P/T border; Clarkson et al. 2015) and the End-Triassic event (e.g., Kiessling and Simpson 2011). Undoubtedly, these mass extinctions never are caused by one single factor alone thus very likely it is a combination of many environmental stressors affecting

organisms and time-extents of these (i.e., long stasis, steady state vs. rapid change, short climatic peaks) that lead to such significant natural selection events.

1.2.1 The effect of ocean acidification on marine calcifiers

Nevertheless, present continuous "acidification" of the ocean caused by rising atmospheric CO_2 is thought to influence both calcification and physiology of marine organisms (Kleypas et al. 1999; Feely et al. 2004; Pörtner 2008; Doney et al. 2009; Ries et al. 2009). However, for the process of calcification, it has to be distinguished between active $CaCO_3$ biomineralization and abiotic precipitation of $CaCO_3$ (e.g., Bonucci 2007; Weiss and Marin 2008). Active calcification may not depend on the availability of CO_3^{2-} as HCO_3^- may be widely used by marine calcifiers (Findlay et al. 2009, 2011; Jury et al. 2010; Bertucci et al. 2013; Bach 2015). Thus especially in tropical shallow seas lowered $CaCO_3$ saturation states may not have direct influence on the organism´s ability to calcify as the seawater in the lower latitudes likely remains $CaCO_3$ oversaturated at least until the year 2100 (Feely et al. 2004, 2009; Andersson et al. 2005; Hoegh-Guldberg et al. 2007). Although enzymes drive calcification in many marine organisms, $CaCO_3$ oversaturated seawater is more beneficial, as it reduces the energetic costs for the organisms to maintain and build-up their calcareous skeleton (Wood et al. 2008, 2010; Melzner et al. 2011; Vidal-Dupiol et al. 2013). In contrast, abiotic precipitation of $CaCO_3$ relies on the CO_3^{2-} saturation and is indeed directly impacted by elevated seawater pCO_2. This has consequences not only for the environmental process of marine cementation but also for the calcification of marine organisms, as in some of them, abiotic $CaCO_3$ precipitation may play a substantial role for stability, framework hardening and cementation of their skeletal structure. Thus it is important to understand how the process of calcification and especially the skeletal microstructure is altered under future conditions of ocean acidification. Thereby the skeletal mineralogy is important to consider, as the $CaCO_3$ polymorphs aragonite (precipitated by e.g., corals, calcareous green algae) and high Mg-calcite (precipitated by e.g., echinoderms, crustose coralline algae) are more susceptible to dissolution under low seawater $CaCO_3$ saturation as is low Mg-calcite (Milliman 1974). However that may only apply for structures not stabilized by organic molecules as many calcifying organism of the deep sea (e.g., deep water corals, echinoderms and, mollusks) regularly experience undersaturation ($\Omega_{arag} < 1$) and are able to maintain $CaCO_3$ biomineralization if energy (i.e., food, nutrient supply) is sufficient (e.g., Wood et al. 2008).

1.2.2 Effects of ocean acidification on the calcification of *Halimeda*

Knowledge on how ocean acidification affects the calcification of calcareous macro-algae such as of the genus *Halimeda* is still scarce. Hitherto most studies focused on changes in physiology (photosynthesis, growth rate, metabolism and, nutrient uptake) and changes in calcification rate (alga / segment total $CaCO_3$ content) (e.g., Ries et al. 2009, 2011; Price 2011; Sinutok et al. 2011, 2012; Hofmann et al. 2014). Albeit most of these studies revealed a negative effect on total $CaCO_3$ content caused by elevated seawater pCO_2, only few studies analyzed the $CaCO_3$ skeletal segment microstructure in closer detail (e.g., Robbins et al. 2009; Sinutok et al. 2011). This may be due to the fact that the process of calcification in relation to physiological processes and the resulting formation of microstructural skeletal features observed in segments of *Halimeda* are not yet well understood (e.g., Weiner and Lowenstam 1986; Multer 1988; Macintyre and Reid 1995). Thus microstructural descriptions given for changes of the calcareous skeleton, not only those in context to elevated seawater pCO_2, often are of different accuracy and thus difficult to compare. Nevertheless, the few studies conducted on the segment microstructure of *Halimeda* grown under elevated seawater pCO_2 showed similar alterations in dimensions of aragonite needles, e.g. shifts in crystal dimensions (Robbins et al. 2009; Sinutok et al. 2011) accompanied by increase in crystal abundance (Robbins et al. 2009). However, care must be taken when detailed microstructural analyzes are carried out as a multitude of parameters (e.g., segment age and morphotype, similar and representative areas within the microstructure, environmental parameters and needle type or feature type) have to be considered to allow valid comparative analyses.

1.3 *Halimeda* sediments

Segment production of macro-algae of the genus *Halimeda* is rapid. Wefer (1980) showed that the alga (here of the species of *H. incrassata*) is able to turnover entirely (i.e., all of its segments) in less than 30 days. Thereby its standing stock (lifetime of the alga) may exceed 3 months. During lifetime the alga almost continuously sheds older, mature segments to the sediment. Thus macro-algae of the genus *Halimeda* represent a major carbonate factory in many tropical shallow marine environments. *Halimeda* sediments represent a substrate for a multitude of organisms in coral reef ecosystems and in tropical shallow seas (Wiman and McKendree 1975; Multer 1988; Multer and Clavijo 2004). The alga thus contributes to the development of a diverse habitat that sustains the huge species-richness of these environments (Hillis-Colinvaux 1986; Payri 1988; Jinendradasa and Ekaratne 2000; Nelson 2009). Additionally, sediments of *Halimeda* contribute to the enhancement of the reef framework structure by filling voids between corals or cemented coral-rock but also become transported

over large distances, e.g. onto the shore and into the lagoon where they take part in the buildup and formation of reef islands and carbonate platforms (Jindrich 1969; Drew 1983; Roberts et al. 1987, 1988; Drew and Abel 1988; Hine et al. 1988; Johns and Moore 1988; Orme and Salama 1988; Phipps and Roberts 1988; Freile et al. 1995; Hillis 1997; Pomar and Kendall 2007; Granier 2012). Moreover, calcareous macro-algae, such as of the genus *Halimeda*, fix atmospheric carbon within their calcareous skeleton. Thus they may be a considerable, albeit probably temporary (i.e., centuries), carbon sink and contribute to the short-term carbonate buffer of the ocean (Hillis-Colinvaux 1980; Kinsey and Hopley 1990; Milliman 1993; Rees et al. 2007).

Over long-term (i.e., millennia) biogenic carbonate sediments that consist of the $CaCO_3$ polymorph aragonite and become buried often undergo sedimentary skeletal recrystallization in the process of diagenesis (Reid and Macintyre 1998; Brachert and Dullo 2000; Noé et al. 2006). In *Halimeda* sediments the original aragonite segment skeleton is replaced by more stable $CaCO_3$ polymorphs, such as low Mg-calcite and dolomite or even by other minerals (e.g., observed in petrographic thin-sections of compacted marine sediments, packstones from deep core samples). In some cases, the original microstructure of the former skeleton is preserved as a negative recrystallized imprint. The voids and intra-granular spaces between and inside the segments are filled with a cementing matrix (e.g., of micrite or sparite) thus *Halimeda* sediments often form rudstones (grain-supported) and floatstones (matrix-supported) that are used as indicators for ancient reef-like environments (Manckiewicz 1988; Braga et al. 1996; Martin et al. 1997; Granier 2012). If the original skeletal $CaCO_3$ microstructure is not replaced but dissolved, segments can show remarkable high intra-granular porosity with the segment form stabilized and preserved through secondary (intra-granular) cements, especially when these infill former utricles (cf., formation of microcaverns; Fig. 4). Thus this specific type of preservation may render reef-packstones that contain high quantities of *Halimeda* segments exceptionally good reservoir rocks for natural energy resources (i.e., oil and gas). However that also depends on the overall permeability of the embedding matrix (i.e., open vs. closed porosity; connected vs. unconnected pores), which interlinks the segment "ghost-structures" (microcaverns).

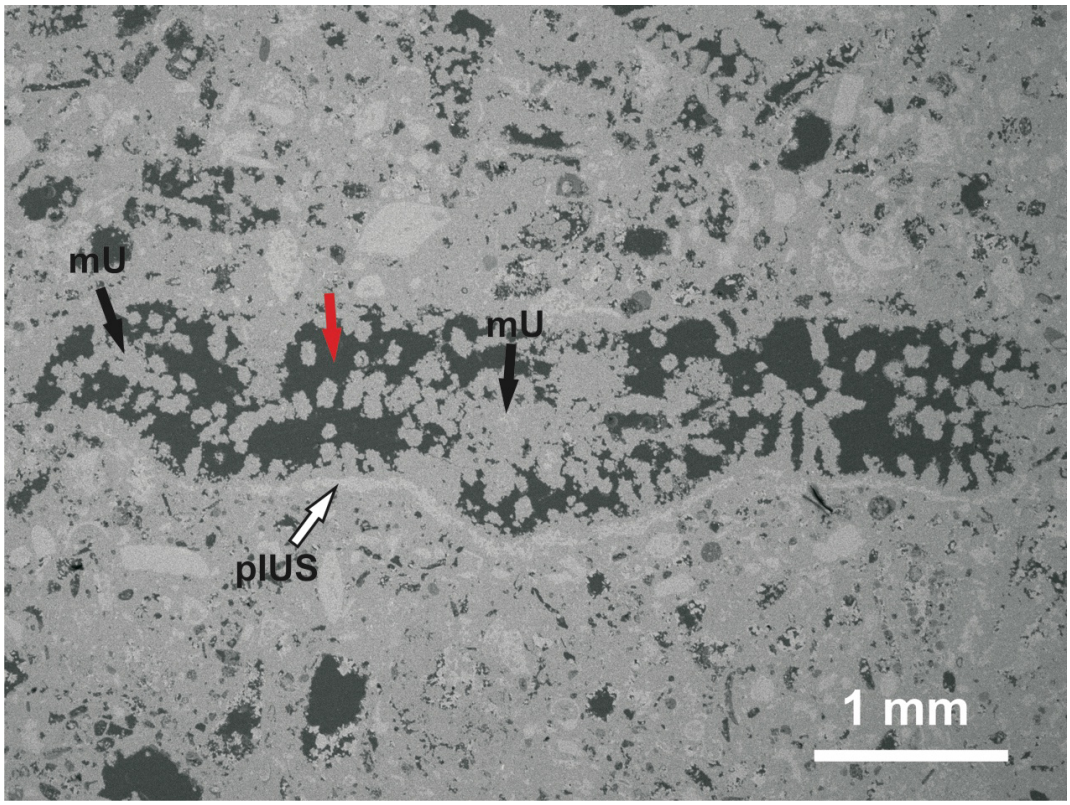

Fig. 4 Back-scattered electron image (BSE-SEM; material contrast imaging) of a thin-section from a *Halimeda* segment (lineage Opuntia) preserved in a CLINO core sample (Upper Pliocene section, ~3.5 - 2 Ma; sample provided by the University of Miami, RSMAS; Eberli et al. 1997) from the western slope of the Great Bahama Bank. Note the infilling of former medullary utricles (mU; black arrows) with $CaCO_3$, likely calcite microspar as indicated by gray value, and the dissolved original aragonite skeletal microstructure in the inner IUS that now forms a microcavern (black embedding medium; red arrow). The original aragonite $CaCO_3$ microstructure of the segment rim (i.e., generally the most calcified part of a segment) is in some parts not replaced (pIUS; white arrow). mU = medullary utricles; pIUS = primary inter-utricular space.

1.3.1 Species-specific sedimentary *Halimeda* segments and their early preservation potential

Segments of different *Halimeda* species differ largely in dimensions but only slightly in external morphology. However, in most studies *Halimeda* segments (also often termed *Halimeda* plates or flakes in sedimentary studies; e.g., Jindrich 1969; Milliman 1974; Alexandersson and Milliman 1981; Hine et al. 1988; Roberts et al. 1988; Freile et al. 1995; Wienberg et al. 2010) sampled from sediments rarely are identified to species level or lineage,

albeit predominantly they are observed in a specific grain size range (pebble gravel, 1.6 > 0.4 cm; e.g., Jindrich 1969, Drew 1983; Drew and Abel 1988; Hine et al. 1988; Roberts et al. 1988; Freile et al. 1995; Wienberg et al. 2010). Thus it is not the segment shape or its size, but rather the extent to which segments of different *Halimeda* species are calcified that determines if they become preserved as complete plates in the sediment (Alexandersson and Milliman 1981; Drew 1983; Multer 1988; Macintyre and Reid 1995; Reid and Macintyre 1998; Perry 2000) and later on may form sedimentary rock (Granier 2012). However, the grade of their calcification strongly depends on the species-specific internal segment morphology and physiology of the alga, as well as the environmental conditions of the habitat they grow in. Subsequently, only heavily calcified segments form typical coarse *Halimeda* sediments and are represented in deeper sedimentary layers (cf., Fig. 4). Most *Halimeda* species, e.g. of the lineages Rhipsalis or Halimeda (Hillis 2001; Verbruggen and Kooistra 2004), but especially those that exhibit rather large and weakly calcified segments (> ~2 cm), do not substantially contribute to typical *Halimeda* sediments as their segments disintegrate rapidly after being shed from the alga and thus do not become preserved in the paleo record (Granier 2012). Segments of these *Halimeda* species may form considerable amounts of carbonate (needle) mud and thus support the fine-grain sediment fraction in tropical settings (< 63 µm) (Neumann and Land 1975; Macintyre and Reid 1992; Milliman and Droxler 1996).

2. Materials and methods

2.1 Laboratory studies

To investigate the segment calcification of the green macro-alga *Halimeda opuntia*, algae were grown under controlled and natural environmental conditions (encompassing light intensity, physical and chemical water parameters, and nutrients) in the marine laboratories of the Leibniz-Center for Tropical Marine Ecology (ZMT) Bremen. To investigate alterations in segment calcification of the alga caused by elevated seawater pCO_2 and subsequent shift in seawater carbon chemistry, algae of the species *Halimeda opuntia* were grown in mesocosms under controlled experimental environmental conditions in the Leibniz ZMT marine facilities.

2.1.1 Setup of seawater aquaria and laboratory conditions

2.1.1.1 Calcification experiment setup

Green macro-algae of the species *Halimeda opuntia* sampled in August 2011 from reefs off Curacao were brought to the marine laboratory facilities of the Leibniz-Center for Tropical Marine Ecology (ZMT) in Bremen (Germany). The algae were acclimatized for more than one month to laboratory conditions (water temperature 27 °C, salinity 35 PSU, pH 8.1) prior the start of the experiment. Afterwards, they were placed in aquaria (35 l; N = 4) filled with pre-filtered natural open ocean seawater (with identical water parameters). T5 full-spectrum light bulbs were installed providing a moderate daylight regime of 150 µmol photons m^{-2} s^{-1}. An electronically controlled air-CO_2 gas-mixing system (HTK® Hamburg, CO_2 provided by Linde® Gas) provided aeration (via bubbling premixed air into the aquaria) whereby the CO_2 concentration of the seawater was adjusted to ambient conditions, i.e. 400 ± 25 µatm pCO_2. Approximately fifty percent of the seawater of each aquarium was exchanged at least twice a week.

2.1.1.2 Elevated pCO_2 experiment in mesocosms

Green macro-algae of the species *Halimeda opuntia*, purchased from Cebu (Philippines; Marina Fauna Inc.®), were brought to the marine laboratory facilities of the Leibniz-Center for Tropical Marine Ecology (ZMT) in Bremen (Germany). The algae were acclimatized for more than one month to laboratory conditions (water temperature 27 °C, salinity 35 PSU, pH 8.1) prior the start of the experiment. Afterwards, algae (N = 9) were placed in mesocosms (256 l; N = 3, algae split evenly) with pre-installed T5 light bulbs providing a moderate daylight regime of 150 µmol photons m^{-2} s^{-1}. For artificial seawater (SW) preparation, sea salt

was diluted in pre-filtered (via reverse-osmosis) UV-treated fresh water from tap in a 35,000 l tank and salinity was adjusted to 35 (PSU). In the 35,000 l tank, seawater total alkalinity (A_T) was pre-adjusted to 2200 +/- 100 µmol kg^{-1}SW with hydrochloric acid (HCl; 1N) prior infilling into the mesocosms. Sufficient time (approx. 2 weeks) was conceded prior to the start of the experiment in order to allow adequate proton equilibration / CO_2 outgassing of the seawater in the tank to reach an initial target seawater pH of 8.1 that was monitored by daily water parameter measurements (pH, temperature and, salinity). During the experiment A_T was measured once a week using an automated titrator (SI Analytics® TitronLine Alpha Plus) and re-adjusted to 2200 +/- 100 µmol kg^{-1}SW by addition of $NaHCO_3$ with a peristaltic pump, when required. Aeration was provided by an electronically controlled CO_2-air gas-mixing system (HTK® Hamburg, CO_2 provided by Linde® Gas) bubbling the premixed air directly into the mesocosms. Thereby, seawater pCO_2 was adjusted to 400 ± 50 µatm for the control treatment (as ambient seawater pCO_2) and 650 ± 50 µatm for the high pCO_2 treatment (as elevated seawater pCO_2), with the latter being the maximum CO_2 concentration (approx. 1500 ppm CO_2 air pressure) supported from the CO_2-air gas-mixing system used in this setup. Approximately ten percent of the seawater in the mesocosms was exchanged once a week to sustain water quality.

2.1.2 Water parameter control and measurements (both experiments)

To control seawater parameters and carbon chemistry during the experiments, pH (NBS-scale), temperature (°C) and salinity (PSU) were measured at least every second day with a multi-probe (WTW® Multi 3410, SenTix® ORP 900 pH probe, TetraCon® 925 conductivity probe). PH probe was calibrated using NBS buffer solution (WTW®) for pH 4.01 and 7. A_T of the seawater was measured once a week with a titrator (SI Analytics® TitronLine Alpha Plus) using 50 mL direct water samples, referenced against seawater Dickson A_T standard batch 111 (Dickson et al. 2003; 2007). Seawater carbon chemistry and $CaCO_3$ saturation state (Ω) were calculated from measured parameters pH_{NBS}, A_T, temperature and salinity with the program CO_2SYS (Pierrot et al. 2006) using K1, K2 constants from Mehrbach et al. (1973) refit by Dickson and Millero (1987).

2.1.3 Laboratory sample collection and preparation for SEM analyses

For the calcification experiment the algae were collected after three months of growth. For the elevated seawater pCO_2 experiment in mesocosms the algae were collected after 45 days. Afterwards the algae were oven-dried at 35 °C for 48 h. Single segments were sampled from the apical, mid-growth and basal section of the algae and afterwards prepared for scanning

electron microscopy (SEM; TESCAN® VEGA3 XMU). Additionally, early young segments, one and two days old, were sampled in both experiments and prepared for SEM analyses.

2.1.3.1 Stub samples

To analyze the microstructural features of *Halimeda* segments, stub samples were prepared. For stub samples segments were cut in the middle plane, mounted with conductive glue on a sample holder (stub, Ø 1 cm) and gold-sputtered for 30s. They were analyzed with the SEM in a range from 2.5 to 10 keV with the detector for secondary electrons (SE).

2.1.3.2 Thin-sections

To analyze the internal $CaCO_3$ microstructural features and $CaCO_3$ density of segments petrographic thin-sections were prepared. Thin-sections were prepared from the middle plane of the segments using a grinding machine. Segments were embedded in epoxy resin and polished to 35 µm thickness. Afterwards, thin-sections were gold-sputtered for 30s and analyzed with the SEM at 10 keV using the detector for back-scattered electrons (BSE-SEM).

2.2 Sedimentary studies

2.2.1 Field sampling and sediment screening

Surface sediment samples (upper 5 cm sediment layer; N = 71) were taken with a hand shovel at four uninhabited islands in the Spermonde Archipelago (SW Sulawesi, Indonesia) during two field trips in October/November 2012 and 2013. On each island transects were sampled from the reef flat in direction to the shore (drift line). The sediments were brought to the ZMT and oven-dried at 40 °C for 48 h. Afterwards the sediment samples were screened for most pristine, i.e. complete and unbroken, *Halimeda* segments. All segments picked were then digitally photographed (Nikon® AW100 using macrofocus) for external morphological analyses (i.e., shape and alteration stages) prior to further processing.

2.2.2 Field sample preparation for SEM analysis

For SEM analyses of the internal $CaCO_3$ microstructure of *Halimeda* segments, thin-sections were prepared. Segments were embedded in epoxy resin, cut in the middle plane and polished to 35 µm thickness. Thin-sections were gold-sputtered for 30s and analyzed with the SEM using the detector for back-scattered electrons (BSE-SEM) at 10 keV. $CaCO_3$ polymorph of

internal cements was inferred from back-scattered electron images (BSE-SEM; gray value) and further analyzed by energy dispersive X-ray (EDX-SEM) with an Oxford® X-Max2 50 mm^2 element detector. Point measurements were conducted at 6 and 10 keV with measurement times adjusted to 120 s (> 300k total counts).

3. Manuscript I :

A new model for the calcification of the green macro-alga *Halimeda opuntia* (Lamouroux)

(2014) Wizemann A, Meyer FW, Westphal H

Coral Reefs 33:951–964

DOI: 10.1007/s00338-014-1183-9

Statement of personal contribution

Manuscript writing:
I wrote the initial manuscript.
(Total contribution: 70%)

Laboratory work:
I helped maintaining the aquaria and performed regular water parameter measurements (pH, salinity, temperature, total alkalinity).
(Total contribution: 40%)

Analyses:
I collected and prepared the samples and conducted scanning electron microscopy.
(Total contribution: 100%)

Idea:
I developed the initial idea of the investigation, analyses and the manuscript.
(Total contribution: 80%)

Coral Reefs (2014) 33:951–964
DOI 10.1007/s00338-014-1183-9

REPORT

A new model for the calcification of the green macro-alga *Halimeda opuntia* (Lamouroux)

André Wizemann · Friedrich W. Meyer · Hildegard Westphal

Received: 29 January 2014 / Accepted: 10 June 2014 / Published online: 20 June 2014

Abstract *Halimeda opuntia* is a cosmopolitan marine calcifying green alga in shallow tropical marine environments. Besides *Halimeda*'s contribution to a diverse habitat, the alga is an important sediment producer. Fallen calcareous segments of *Halimeda* spp. are a major component of carbonate sediments in many tropical settings and play an important role in reef framework development and carbonate platform buildup. Consequently the calcification of *H. opuntia* accounts for large portions of the carbonate budget in tropical shallow marine ecosystems. Earlier studies investigating the calcification processes of *Halimeda* spp. have tended to focus on the microstructure or the physiology of the alga, thus overlooking the interaction of physiological and abiotic processes behind the formation of the skeleton. By analyzing microstructural skeletal features of *Halimeda* segments with the aid of scanning electron microscopy and relating their occurrence to known physiological processes, we have been able to identify the initiation of calcification within an organic matrix and demonstrate that biologically induced cementation is an important process in calcification. For the first time, we propose a model for the calcification of *Halimeda* spp. that considers both the alga's physiology and the carbon chemistry of the seawater with respect to the development of different skeletal features. The presence of an organic matrix and earlier detected external carbonic anhydrase activity suggest that *Halimeda* spp. exhibit biotic precipitation of calcium carbonate, as many other species of marine organisms do. On the other hand, it is the formation of micro-anhedral carbonate through the alga's metabolism that leads to a cementation of living segments. Precisely, this process allows *H. opuntia* to contribute substantial amounts of carbonate sediments to tropical shallow seas.

Keywords Internal microstructure · Organic matrix · Cementation · Carbonate sediments · SEM

Communicated by Biology Editor Dr. Anastazia Banaszak

A. Wizemann (✉) · F. W. Meyer · H. Westphal
Leibniz Center for Tropical Marine Ecology (ZMT), Fahrenheitstraße 6-8, 28359 Bremen, Germany
e-mail: andre.wizemann@zmt-bremen.de

H. Westphal
Faculty of Geosciences, University of Bremen, Klagenfurter Straße 2, 28359 Bremen, Germany

Introduction

The benthic marine green macro-alga *Halimeda opuntia* (Lamouroux 1816) is a common calcareous alga within tropical shallow marine environments. The alga grows in a branched, segmented habit whereby its numerous calcareous segments function in a leaf-like manner (Fig. 1a). The segments are formed in continuous growth of up to one segment per day and per branch (Vroom et al. 2003). The segmental growth of algae of the genus *Halimeda* is rapid, with a complete turnover of ~30 d or even faster (Hillis-Colinvaux 1980; Wefer 1980; Multer 1988; Tussenbroek and van Dijk 2007). Thus, *Halimeda* segments are a major component of tropical shallow marine sediments (Milliman 1974; Drew 1983; Johns and Moore 1988; Freile et al. 1995). In fact, the contribution of *Halimeda* bioherms to the sediment budget of tropical settings might be equal or even exceed the carbonate sediment production of the corals within the reef (Marshall and Davies 1988; Milliman and Droxler 1996; Rees et al. 2007). *Halimeda* spp. and its sediments play a multitude of ecological roles that range

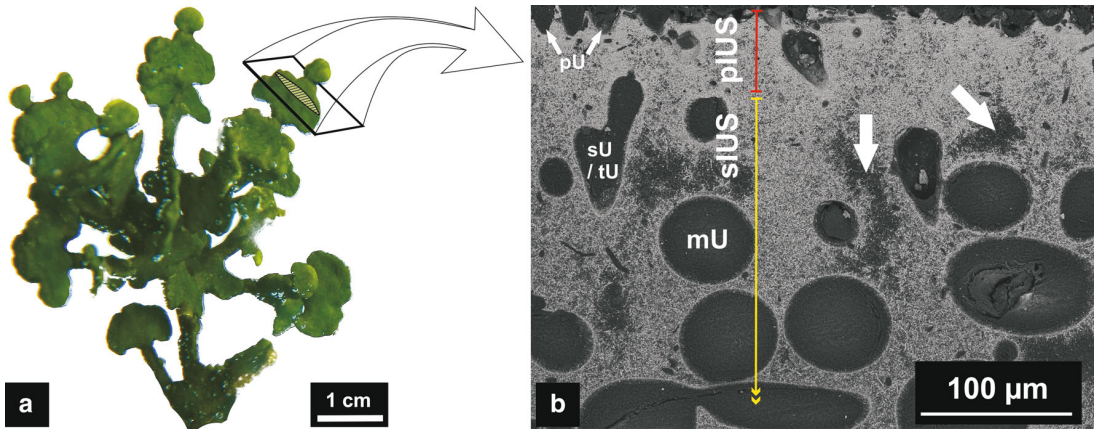

Fig. 1 Illustration of the tropical macro-alga *Halimeda opuntia* and its internal calcareous skeletal structure. **a** Segmented habit of *H. opuntia*. **b** Internal segment microstructure. Scanning Electron Microscope image (via BSE) of a thin-section shows utricles and inter-utricular spaces. *Large arrows* in **b** indicate open areas in the innermost secondary inter-utricular space. *pIUS* primary inter-utricular space, *sIUS* secondary inter-utricular space, *pU/sU/tU/mU* primary/secondary/tertiary/medullary utricle

from habitat and substrate provision (Wiman and McKendree 1975; Multer 1988; Payri 1988; Jinendradasa and Ekaratne 2002; Multer and Clavijo 2004) to the significant contribution to island and carbonate platform buildup (Folk and Robles 1964; Neumann and Land 1975; Roberts et al. 1987; Drew and Abel 1988; Hine et al. 1988; Orme and Salama 1988; Phipps and Roberts 1988; Rao et al. 1994; Hillis 1997; Pomar and Kendall 2007). Moreover, calcareous macro-algae take part in the fixation and long-term storage of atmospheric carbon in tropical coral reef environments (Kinsey and Hopley 1991). Consequently, *Halimeda* sediments can be considered as a carbon sink that contribute to the carbonate buffer of tropical shallow seas (Hillis-Colinvaux 1980; Rees et al. 2007). However, without sufficient knowledge of the processes and mechanisms involved, it is difficult to predict how *Halimeda*'s calcification will respond to environmental changes such as ocean acidification that have the potential to impact the calcification of marine organisms (Hoegh-Guldberg et al. 2007; Doney et al. 2009; Ries et al. 2009). Our goal is to understand the role of physiological processes and chemical seawater parameters on extracellular $CaCO_3$ biomineralization in *H. opuntia.* As the green macro-alga *H. opuntia* is a rather evolutionarily basal algal species, its calcification can be considered primal, thus making it an ideal model organism to study (Hillis 2001; Kleypas et al. 2006). To investigate the calcification of *H. opuntia*, we reared the alga under controlled conditions and analyzed the internal skeletal microstructure of segments using scanning electron microscopy (SEM). We then relate the formation of observed skeletal features to physiological processes of the alga. Subsequently, we propose a new model of skeletal formation that recognizes the close relationship between precipitation of calcium carbonate and the metabolism of the alga as well as the carbon chemistry of the seawater.

Material and methods

Setup of aquaria and seawater parameter measurements

Calcifying green macro-algae of the species *H. opuntia* from reefs of Curaçao (sampled in August 2011 from ~5 m water depth) were acclimatized to laboratory conditions in the marine laboratory facilities of the Leibniz Center for Tropical Marine Ecology (ZMT) in Bremen (Fig. 1a). After acclimatization of several weeks, the algae were individually placed in aquaria (30 L) with preinstalled T5 light bulbs of 150 µE m^{-2} s^{-1} switched in a 12/12 h d/night cycle. During the period of growth UV-sterilized and pre-filtered Atlantic open ocean seawater (SW; unmodified ionic composition) was used. Aeration was provided by an electronically controlled CO_2 gas-mixing system (HTK® Hamburg, Linde® Gas). Fifty percent of the SW was exchanged twice a week. Salinity (S), temperature (T), and pH (NBS scale) were monitored every other day (WTW® Multi 3410, SenTix® ORP 900 pH probe, TetraCon® 925 conductivity probe; Table 1). Total alkalinity (A_T) was measured twice a month by titration of a 50 mL water sample with 0.05 N HCL after Dickson et al. (2007) using an automated titrator (SI Analytics®, TitronLine Alpha Plus) and A_T standard provided by Dickson et al. (2003; batch 111) as certified reference material. Mean values of S, T, pH_{NBS}, and A_T were used to calculate the seawater carbon chemistry and the $CaCO_3$ saturation state (Ω) with the program "CO_2SYS" (Pierrot et al. 2006; Table 1).

Table 1 Measured and calculated physical and chemical seawater (SW) parameters (mean ± SD)

S (PSU)	T (C°)	A_T	pH_{NBS}	TCO_2	pCO_2	HCO_3^-	CO_3^{2-}	CO_2	Ω_{arag}	Ω_{cal}
35.5 ± 0.6	26.8 ± 0.5	2,104 ± 60	8.14 ± 0.05	1,829 ± 57	414 ± 61	1,628 ± 62	190 ± 22	11.2 ± 1.7	3.0 ± 0.3	4.6 ± 0.5

Salinity (S), temperature (T), total alkalinity (A_T), and pH were measured. These parameters were used to calculate the seawater carbon chemistry with the program CO_2SYS (Pierrot et al. 2006) with the use of K1, K2 constants from Merbach et al. (1973), refit by Dickson and Millero (1987). A_T, TCO_2 and carbon species in µmol kg^{-1}SW, pCO_2 in µatm, pH in NBS scale (mol kg^{-1} SW). Ω = $CaCO_3$ saturation state of the seawater; *arag* aragonite, *cal* calcite

Sampling

Proto-segments (day = 0) and young apical segments of the first day (day = 1) were collected after 1 month of experimental duration from selected algae where new segmental growth was observed. Complete algae were collected after 3 months at the end of the experiment. After sampling, the segments were rinsed with distilled water to remove soluble components and oven-dried at 35 °C for 48 h.

Sample preparation and analysis

Thin-sections

To investigate the habit of skeletal features and to get a general overview of the internal microstructure, thin-sections were prepared. For this, segments were embedded in epoxy, cut along the middle plain, and polished to ~35 µm (Fig. 1a, b). Thin-sections were gold sputtered and analyzed with a scanning electron microscope (SEM; TESCAN® VEGA3 XMU) at 10 keV using the detector for back-scattered electrons (BSE).

Stub samples

To investigate the topographical morphology of skeletal features in detail, stub samples were prepared for analysis with an SEM. Segments were cut along the middle plain with a razor blade and fixed on a stub with conductive glue with the cut surface facing upwards. The samples were then gold sputtered and analyzed with the SEM at 10 keV using the secondary electron detector (SE).

A total of $n > 50$ segments of all growing stages (day 1, apical, mid-growth, and basal) were analyzed. Details on the segments presented in the results section are shown in Table 2. The organic matter of the segments was not removed in order to allow identification of organic features on the utricle wall. However, organics were lost in some cases due to preparation techniques.

Table 2 Details on segments presented in the results section

Figure	Segment age	Preparation	SEM-detector	Feature(s) investigated
1b	Mid-growth	Thin-section	BSE	Microstructural overview
3a	Day 1	Stub	SE	Early needles/organic matrix
3b	Apical	Stub	SE	Short needles
3c	Basal	Stub	SE	$CaCO_3$ nuclei
3d	Basal	Stub	SE	Short needles/organic matrix
3f	Basal	Stub	SE	Organic matrix
4a	Apical	Thin-section	BSE	Microstructural overview
4b	Apical	Stub	SE	Long needles
4c	Mid-growth	Stub	SE	Micro-anhedral carbonate of pIUS
4d	Basal	Stub	SE	sIUS with long needles
6	Mid-growth	Thin-section	BSE	Comparison of species

Shown are the preparation technique, the method of analysis via SEM, and the skeletal microstructural features investigated from segments of the first day (day 1), from young, well-developed segments (apical) and from mature segments (mid-growth and basal). *IUS* inter-utricular space (*p* primary, *s* secondary), *SE* secondary electrons, *BSE* back-scattered electrons

Results

The skeleton of a *Halimeda* segment exhibits several microstructural features that appear in a temporal order as depicted in Fig. 2. The subsequent description follows this temporal order. In natural seawater, the calcareous skeleton of *Halimeda* spp. is composed of the $CaCO_3$ polymorph aragonite (Macintyre and Reid 1995; Stanley et al. 2010). In SEM analyses (via back-scattered electrons and energy-dispersive X-ray) of samples investigated no evidence for an alteration of the $CaCO_3$ crystal polymorph was found and so here we follow this assumption. Measured parameters and calculated carbon chemistry of the natural seawater in which the algae were grown in the laboratory facilities are shown in Table 1.

Short aragonite needles

Proto-segments (day = 0), identifiable by their whitish color, do not show any $CaCO_3$ crystals. At the onset of photosynthesis in a new segment (day = 1), the earliest needles are formed directly on the utricle wall in a layer of

a dense organic matrix (Fig. 3a). These short aragonite needles, with a length not exceeding 1 μm, have a random orientation (Fig. 3a). The tissue of the utricle wall exhibits a fibrous, scale-like habit (Fig. 3a).

In a mature segment, fully developed short needles on the utricle wall have a roundish shape and a length of up to ~5 μm (Fig. 3b). Likewise, newly formed short needles are embedded within an organic matrix (Fig. 3d). The matrix is closely attached to the outer utricle wall. In some samples, the matrix is partly disintegrated (Fig. 3e). In other mature segments in which the organic matrix is well-preserved, small roundish nuclei <1 μm are present on the outer utricle wall (Fig. 3c).

Fig. 3 SEM images (via SE) of the internal microstructure of *Halimeda opuntia* from stub samples **a** Short needles within the inter-utricular space of a young segment (day = 1) embedded in an organic matrix (*white frame*). The utricle wall has a fibrous, scale-like habit (*white arrows*). **b** Short needles in a mature segment. *Arrow* indicates the initialization point of needle crystallization (organics lost). **c** Organic utricle wall showing round nuclei of calcium carbonate <1 μm (*arrows*). **d** Newly formed short needles embedded within an organic matrix (*arrows*) on the outer utricle wall of a mature segment. **e** Disintegrated organic matrix (*red arrow*) in a mature segment. The *white arrow* indicates the front of disintegration. *IUS* inter-utricular space, *U* utricle

Micro-anhedral carbonate (MAC)

Micron-sized anhedral crystals of $CaCO_3$ are observed in the vicinity of the outer utricle walls (Fig. 4a, c, d). In a previous study, $CaCO_3$ crystals <1 μm of anhedral shape observed within the internal skeletal microstructure of *Halimeda* spp. were described as "mini-micrite" (Macintyre and Reid 1995) and the process of their formation as "micritization" (Alexandersson 1972, Macintyre and Reid 1995). Generally, the term "micrite" (micro-crystalline calcite; Folk 1959) defines all $CaCO_3$ crystals <4 μm. However, both definitions, "mini-micrite" and "micrite", raise problems of how to distinguish between crystals that have different origins of formation and exhibit different shapes, but are within the same size range. To avoid usage of the term "micrite" and to clearly distinguish between different origins and shapes of the $CaCO_3$ crystals observed in the internal skeletal microstructure of *Halimeda* spp. henceforth, we term all non-needle-like $CaCO_3$ crystals <1 μm that exhibit an anhedral shape and are formed in the living *Halimeda* segment, micro-anhedral carbonate (MAC).

When short needles are present, the MAC always appears on top of these (Fig. 4c, d). Low amounts of short needles are loosely embedded in the MAC (Fig. 4c). Contrary to the formation process of the short needles, an organic matrix is not observed in the context of MAC formation. MAC is more developed within the inter-utricular space (IUS) of mature segments.

Based on our investigation of the internal microstructure of *H. opuntia*, here we distinguish between two parts of the IUS that are defined as follows. The IUS between the peripheral primary utricles (pU) is defined as the primary

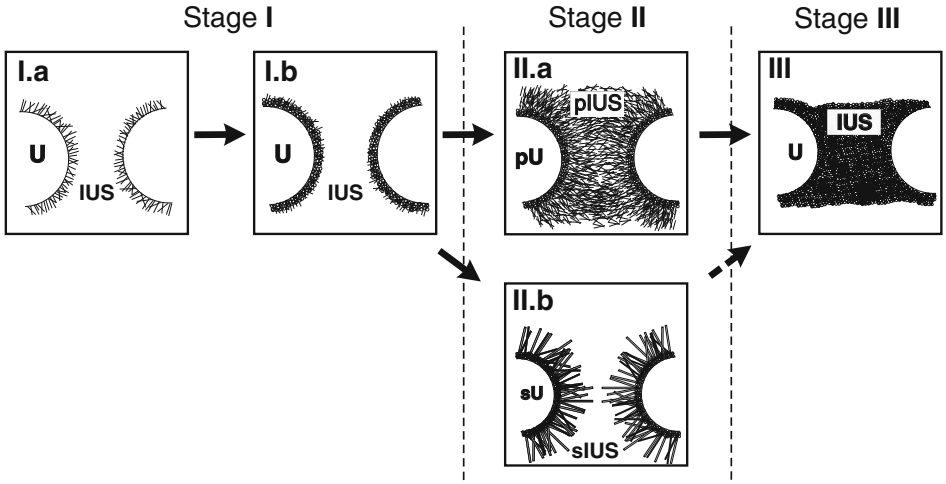

Fig. 2 Calcification stages of *Halimeda* spp. (after Macintyre and Reid 1995). *I.a* Growth of short skeletal needles on the utricle (U) wall followed by *I.b* recrystallization of short needles to micron-sized anhedral crystals. *II.a* Primary utricles (pU)/primary inter-utricular space (pIUS) located on the rim of the segment characterized by dense skeletal needles, or *II.b* secondary utricles (sU)/secondary inter-utricular space (sIUS) located in the inner part of the segment with long euhedral needles. *III* Primary inter-utricular space (pIUS) on the segment rim is filled with micron-sized anhedral crystals, whereas secondary inter-utricular space (sIUS) of the inner part is seldom completely filled (*dashed arrow*) and remains in stage II (cf. II.b). Calcification stage *III* is not developed in all parts of the segment (cf. Fig. 1b)

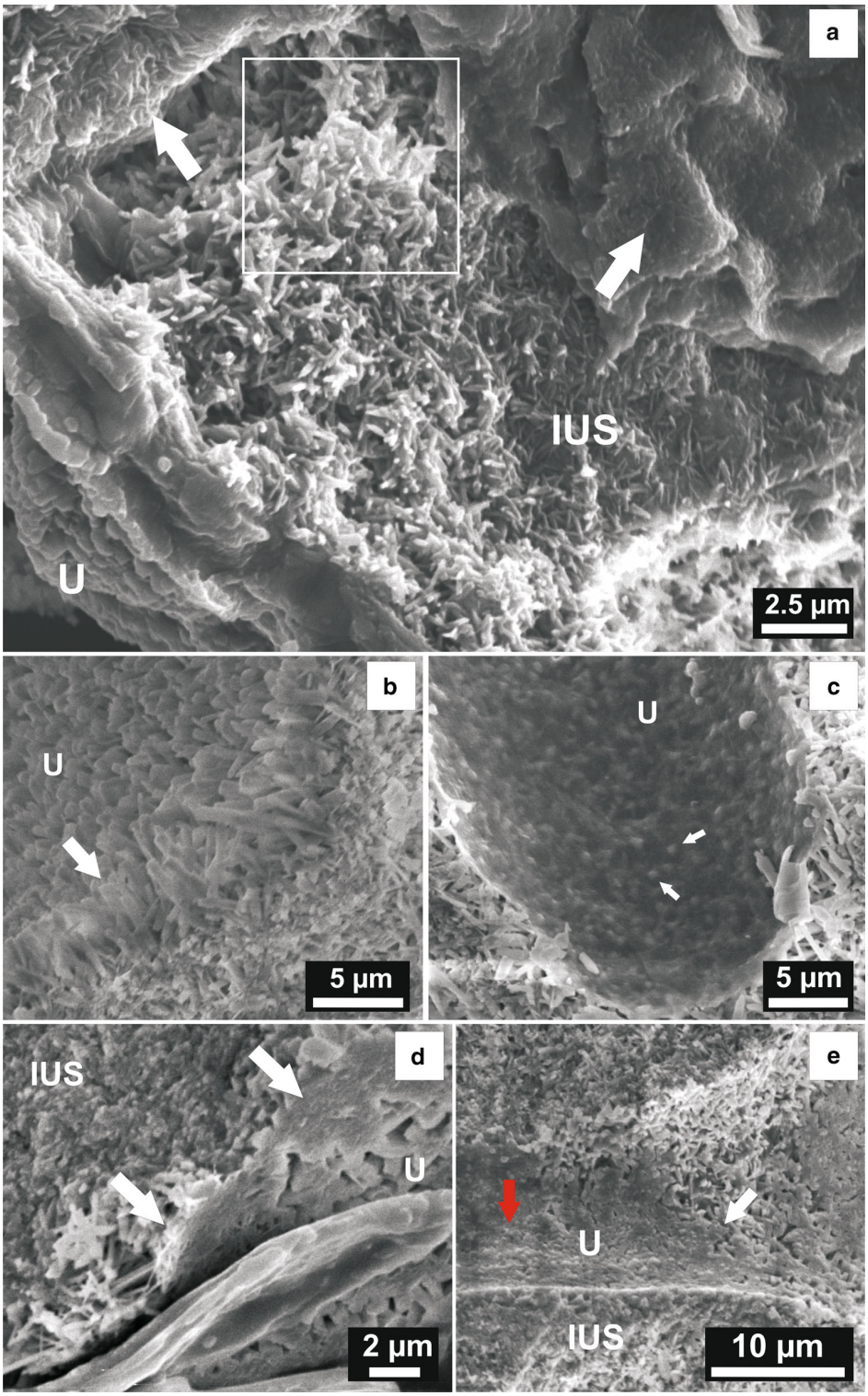
a
IUS
U
2.5 µm
b
U
5 µm
c
U
5 µm
d
IUS
U
2 µm
e
U
IUS
10 µm

inter-utricular space (pIUS). The IUS between the more central secondary, tertiary, and medullary utricles (sU, tU, and mU, respectively) is defined as the secondary inter-utricular space (sIUS) (Figs. 1, 2). The pIUS is entirely filled with MAC (Fig. 4c) and forms a dense rim around the segment (Figs. 1, 4a), whereas the sIUS is not as densely packed with MAC. Within the sIUS, MAC is limited in its extent to the outer walls of larger central utricles (Fig. 4a, b).

Long aragonite needles

Euhedral aragonite needles that are elongated along the c-axis point into open space of the IUS. They are found on top of short needles or MAC and are not attached to the organic utricle wall (Fig. 4a, b, d). In young segments, these long needles reach up to 20 µm in length. In contrast to the roundish habit of the short needles, long needles have a prismatic shape and exhibit a blunt end (Fig. 4b). They predominantly radiate out from a specific location (nucleus) in bundles of several aragonite needles. In older mature segments, long needles appear >20 µm in length as if they continuously extend in length and width congruent to the age of the segment. Where the IUS is filled with MAC, long needles are not observed (Fig. 4c).

Discussion

Our investigations emphasize the relationship between the observed skeletal morphological features and the temporal stage of maturation of a segment. Furthermore, the consecutive and age-related order of appearance of these microstructural features suggest an influence of the physiology of the alga (by its photosynthesis and metabolism) that induces diurnal shifts of seawater carbon chemistry within the inter-utricular space. The calculated $\Omega_{arag} \sim 3.0$ of the natural seawater indicates $CaCO_3$ oversaturated water comparable to present day tropical marine conditions (Table 1; Hoegh-Guldberg et al. 2007).

Primary needles and primary calcification

The onset of calcification in *H. opuntia* is the formation of short aragonite needles (0.5–1 µm) on the outer utricle wall in segments that are 1 d old. Proto-segments (day = 0) do not show any crystal growth even when exposed to light, as chloroplasts for photosynthetic activity are missing (Larkum et al. 2011). Thus, the initiation of calcification seems to be linked to the start of physiological processes. To consider the time-dependent development of the skeletal features here, we define these short needles as "primary needles" and the process of their formation as "primary calcification".

New primary needles are embedded within an organic matrix. This observation implies that the organic matrix is involved in the development of those needles. An extracellular organic matrix is known to be involved in the process of calcification in a variety of marine organisms, such as mollusks, echinoderms, corals, protozoa, and bacteria (Simkiss 1965; Isenberg et al. 1966; Wheeler and Sikes 1984; Simkiss and Wilbur 1989; Mann 2001; Bonucci 2007; Weiss and Marin 2008; Cuif et al. 2012). Nakahara and Bevelander (1978) observed an organic coating on initial needles that precipitated in *Halimeda incrassata*. An organic matrix consists of molecules, such as polysaccharides, proteins, and enzymes, which have major steering functions in the process of calcification (Weiss and Marin 2008; Falini et al. 2013). One of the essential functions of organic matrix molecules is their ability to adsorb and accumulate ions. For example, extracellular acidic polysaccharides or proteoglycans with glycosaminoglycan (GAG) chains exhibit high cation affinity (Bonucci 2007; Arias and Fernández 2008; Salgado et al. 2011). Fibrous elements, presumably organic pectin-hemicellulose fibers (Sikes 1978; Arnott 1982) that are observed in the vicinity of early primary needles on the outer utricle wall suggest that these fibers are involved in the $CaCO_3$ nucleation process. Indeed, Böhm 1973 observed that these fibrous filaments on the utricle wall are acidic (sulfated) polysaccharides with Ca^{2+} affinity. However, observations of primary needles in *Halimeda* growing in a random orientation rules out the possibility that these polysaccharides are directly involved in crystal development or acting as a template (Wilbur et al. 1969). This is supported by findings from Böhm and Goreau (1973) that the polysaccharides exhibit, despite a high Ca^{2+} affinity, only a weak Ca^{2+} binding strength and thus likely function as an intermediate Ca^{2+} pool for calcification. Thus, they might attract Ca^{2+} ions for binding sites (e.g., aspartic ß-pleated sites) of calcifying proteins to promote crystallization (Böhm 1973; Mann 2001).

Roundly shaped nuclei <1 µm, presumably of $CaCO_3$, are located directly on the utricle wall. Their appearance might indicate the start of a calcification event. We propose that these roundish nuclei seen at the utricle wall might (partly) consist of amorphous $CaCO_3$ as indicated by their morphology (Faatz et al. 2004). Acidic polysaccharides on the utricle wall might provide nucleation sites for amorphous $CaCO_3$ that in turn is stabilized by macromolecules (e.g., proteins) within the organic matrix to form aragonite crystals (Zhong and Chu 2010). The initiation of crystallization (nucleation) in biological systems investigated so far was shown to start in vivo and in vitro with a precursor

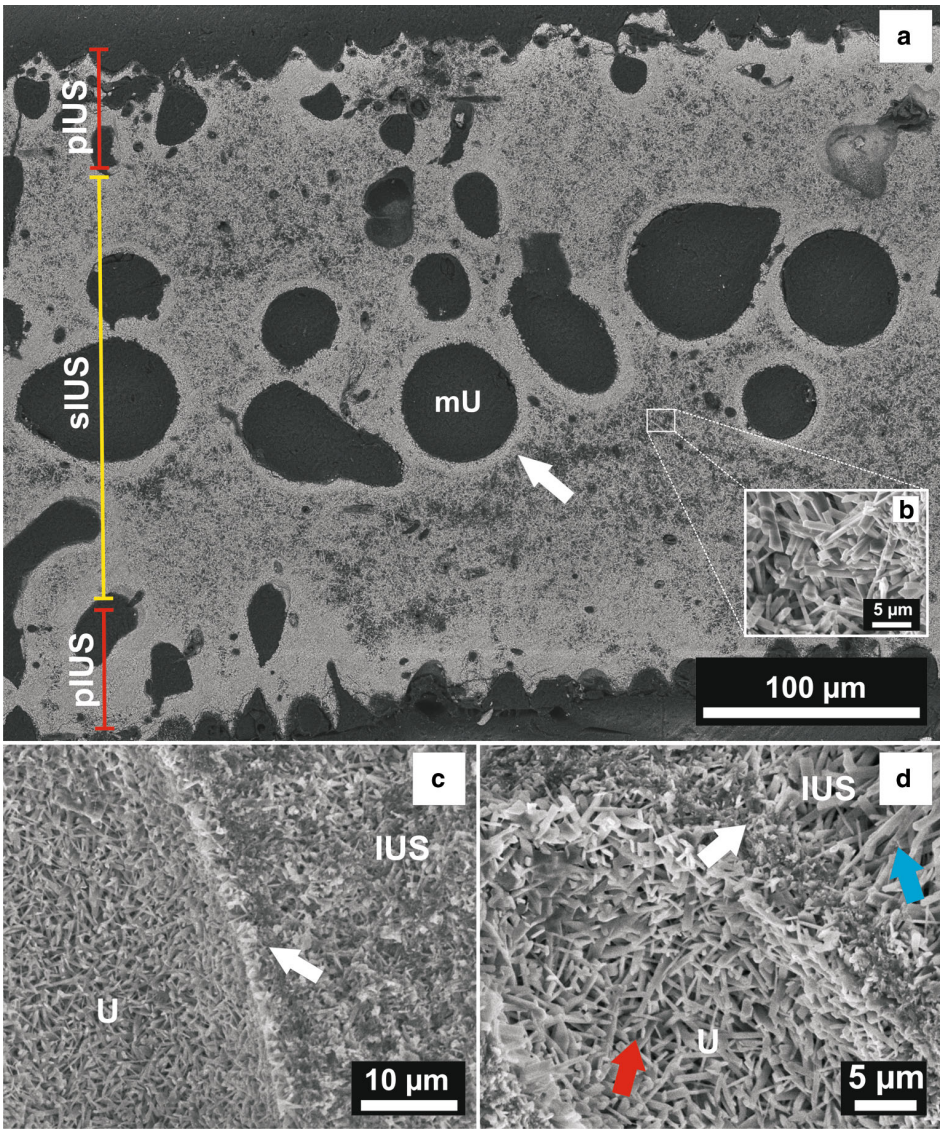

Fig. 4 **a** SEM image (via BSE) of a thin-section from a mature segment shows rims of micro-anhedral carbonate around utricles (*arrow*). **b** Typical orthorhombic long needles within the inner secondary inter-utricular space. **c** Micro-anhedral carbonate filled primary inter-utricular space showing remnants of short needles. A dense meshwork of newly formed needles is present on the utricle wall (*organics lost*) with micro-anhedral carbonate rim of utricle (*arrow*). **d** Microstructure of the secondary inter-utricular space showing short needles (*red arrow*) on the utricle wall, micro-anhedral carbonate rim of utricle (*white arrow*) and long needles (*blue arrow*) of the inter-utricular space (*organics lost*). *pIUS* primary inter-utricular space, *sIUS* secondary inter-utricular space, *U* utricle, *mU* medullary utricle

phase of amorphous $CaCO_3$ (Mann 2001; Addadi et al. 2003, 2006).

In the segments investigated, the organic matrix seems to be in a stage of disintegration when primary needle growth on the utricle wall is observed. Borowitzka (1982b) proposed that early needle formation in *Halimeda* spp. might be associated with a matrix that disintegrates soon after crystal formation. Studies on the calcification of vertebrate bone or dentinogenesis (enamel) show that the organic molecules stabilizing the early crystals have to disintegrate to allow crystallization to proceed (Robinson et al. 1998; Watanabe et al. 2003; Bonucci 2007). Liebezeit and Dawson (1981) postulate a degradation of organic matrix components in mature segments of *Halimeda incrassata* after calcification has reached a certain stage. Primary needle growth and remnants of the organic matrix are also observed in mature, basal segments. This leads to the conclusion that the development of the matrix and its

disintegration is most likely happening at the initiation and for the progression of every calcification event, respectively, as long as the segment is part of the living alga. However, primary calcification in mature segments seems to be limited. Overall thinner and smaller primary needles (<3 μm) are found in a mature segment, which might be due to the insufficient space remaining between the micro-anhedral carbonate and the utricle wall, and thus a consequently restricted exchange of ions with the seawater.

Primary cementation by micro-anhedral carbonate (MAC) formation

Micro-anhedral carbonate (MAC) is precipitated along the outer utricle walls. As suggested by Macintyre and Reid (1995), we propose this MAC to consist mainly of recrystallized $CaCO_3$ from primary calcification. This is supported by the fact that remnants of primary needles are identified within the MAC. The recrystallization and breakdown of the primary needles to anhedral crystals (<1 μm) is most likely induced by the nightly metabolic respiratory activity of the alga exhaling CO_2 into the IUS, which decreases seawater pH and, thereby $CaCO_3$ saturation state within the IUS. This hypothesis is likely for two reasons. First, the initial precipitation of MAC is observed primarily close to the utricle wall, e.g., at the rims of larger central medullary utricles (mU). If this MAC formation was simply intra-granular cementation (Milliman 1974), it is unclear why there was no precipitation of MAC along the abundant long needles in the innermost parts of the IUS. Second, a dense rim that consists of MAC is observed surrounding the segment, which forms within the pIUS. Nightly CO_2 evolution might be highest along the segment rim, where the metabolically derived CO_2 from all algal cells is released into the environment. In addition, the close contact of the segment's surface with the surrounding $CaCO_3$ oversaturated seawater ($\Omega_{arag} \sim 3.0$) may have a buffer effect that allows $CaCO_3$ re-precipitation. Analyses of segments of different age show that first the peripheral primary IUS is filled with MAC until secondly, the more central secondary IUS gains density in MAC. In a young segment, the pIUS is rapidly filled with primary needles, which in turn get recrystallized. Thus, similar to Macintyre and Reid (1995), we observe that the peripheral pIUS between primary utricles (pU) can completely fill with MAC during the lifetime of a segment.

The process of MAC formation during the lifetime of a segment can be considered important for the accumulation of *Halimeda* segments in the sediment as the extent of MAC is a key parameter for the later preservation of a segment in the sediment. A thick stabilizing rim of MAC buildup around the segment during its lifetime is a requirement for later intra-granular cementation. Less MAC filled segments rapidly break apart forming carbonate (needle) mud. Thus, it seems opportune to name this biologically induced early cementation process consistently the "primary cementation" of the segment. It is important to distinguish primary cementation from the subsequent intra-granular cementation of the dead segment. Henceforth, we term this succeeding process the "secondary cementation" of the *Halimeda* segment. Secondary cementation also infills the inner sIUS of the segment that remained open during its lifetime and the utricles, after the organics have disintegrated. Additionally, secondary cements may exhibit a different $CaCO_3$ polymorph than aragonite, namely (low or high) Mg-calcite (Milliman 1974; Alexandersson and Milliman 1981; Reid and Macintyre 1998). As secondary cementation mainly takes place within a dropped segment, no physiological processes of the alga are involved. However, the initiation of secondary cementation is possible in dead segments that are still attached to the living alga (Milliman 1974).

Secondary needles and secondary calcification

Long euhedral needles are observed in the innermost parts of the IUS (especially within the sIUS), extending into available open space. These needles grow more than 20 μm in size on top of the primary needles or the MAC. That indicates formation after that of the primary needles. To describe the time-dependent development and the different location of these long needles, we define them as "secondary needles" and the process of their formation as "secondary calcification".

Secondary needles are elongated in the c-axis and have a typical prismatic aragonite crystal shape with a rather blunt end. Thus, it is assumed that they are precipitated abiotically during daytime photosynthesis. This implies that the seawater pH in the innermost parts of the IUS does not rise above pH $\sim$ 9, as at higher seawater pH aragonite is usually precipitated in a granular crystal shape (De Beer and Larkum 2001; Holcomb et al. 2009). In addition, an organic matrix associated with secondary needles was not detected. In most cases, secondary needles radiated out in bundles from distinct nuclei on top of the MAC layer. Similar observations can be made by the investigation of SEM images of former studies (e.g., Weiner and Lowenstam 1986; Multer 1988; Macintyre and Reid 1995). Therefore, it seems likely that remnants of primary needles on top of the MAC may act as nucleation sites and secondary needles are simply the result of continued crystal growth (Macintyre and Reid 1995). Crystal morphology suggests that $CaCO_3$ oversaturation in the IUS during photosynthesis is not high enough for spontaneous abiotic crystal nucleation, thus it seems rather unlikely that these long needles crystallize on the surface of organic utricle walls without any nuclei of $CaCO_3$ present (Holcomb et al. 2009). That might explain why the

secondary needles are never found attached to the utricle wall between primary needles or remnants of them within the MAC.

The role of external carbonic anhydrase activity in calcification

In a previous study, external carbonic anhydrase activity was detected within the IUS of *Halimeda* spp. (Borowitzka and Larkum 1976b). External carbonic anhydrase activity is one of the essential enzymatic activities recognized within the organic matrix of most marine calcifying organisms (Mitsunaga et al. 1986; Miyamoto et al. 1996, 2005; Tambutté et al. 2007; Moya et al. 2008; Rahman et al. 2008). Studies on the calcification mechanism of marine algae and plants argue that the product of external carbonic anhydrase activity is CO_2 for photosynthesis, by the use of HCO_3^- as a substrate (Simkiss 1965; Borowitzka 1982a). Although for non-calcifying aquatic algae and plants this seems to be most likely the case (reviewed by Tsuzuki and Miyachi 1989), our observation of an organic matrix in *H. opuntia* and other recent analyses on the response of external carbonic anhydrase activity to elevated seawater pCO_2 question this view for calcifying macro-algae (Hofmann et al. 2013, 2014). Generally, it is accepted that external carbonic anhydrase activity catalyzes the hydration of CO_2 to HCO_3^- when present in the calcifying matrix of marine organisms (e.g., in corals, Bertucci et al. 2013). Subsequently, enzymes use HCO_3^- for $CaCO_3$ formation (Weiss and Marin 2008). Although carbonic anhydrase activity may take part in the cell-uptake of HCO_3^- by representing a functional domain in a transport-metabolon of HCO_3^-/H^+ symporters, the occurrence of several coexisting isoforms of carbonic anhydrase domains (e.g., catalytic sites in the tertiary or quarterly structure of calcifying proteins within the organic matrix) is not uncommon (e.g., Marin and Luquet 2004; Bertucci et al. 2013).

Combining our observation of an organic matrix with the previous results of Böhm (1973) on the presence of acidic polysaccharides on the utricle wall and of Borowitzka and Larkum (1976b) and Hofmann et al. (2014) on external carbonic anhydrase activity within the IUS, we conclude that calcification mechanisms similar to those of other marine calcifying organisms are present. Testing this hypothesis exceeds the scope of the current study. However, our study considers external carbonic anhydrase activity as a key feature in the calcification of *Halimeda* spp. Whether this is correct needs to be investigated in future work.

A new model for the calcification in *Halimeda* spp

To place the findings of this study in the context of the present knowledge of $CaCO_3$ biomineralization and of the physiology of the alga, we propose a new model for the calcification in *Halimeda* spp. (Fig. 5). The model is based on Alexandersson (1974) and his work on the skeleton of living coralline red algae. He suggested that it is primarily the metabolism of the alga that contributes to the abiotic formation of "non-biogenic" carbonate crystals within the skeleton. In addition, the model is influenced by the work of Comeau et al. (2012), who proposed a new model for calcification in crustose coralline red algae with the evidence that abiotic re-precipitation of $CaCO_3$ during nighttime should be considered as a common process in skeletal formation.

Daytime processes

Physiological processes that are important for daytime calcification involve photosynthesis, external carbonic anhydrase activity, and cell-uptake of ions. These processes modify seawater parameters like carbon chemistry and ion availability within the inter-utricular space (IUS). HCO_3^- from the seawater is used in the physiology of *Halimeda* spp. for both photosynthesis and calcification. External carbonic anhydrase activity catalyzes H_2O and CO_2 to HCO_3^- and protons (H^+), necessary for nutrient and HCO_3^-/H^+ (proton-driven trans-membrane) symport into the cell. Removal of CO_2 via trans-membrane diffusion and external carbonic anhydrase activity elevates seawater CO_3^{2-} saturation in the IUS. Resulting CO_3^{2-} oversaturation supports biotic primary needle formation, and especially maintains abiotic secondary needle formation. To counteract the decrease in HCO_3^-/CO_2 availability in the IUS, as they are used up in photosynthesis and as a substrate of external carbonic anhydrase activity, calcification might be a "byproduct" to replenish CO_2 for its use in photosynthesis and also for its use in external carbonic anhydrase activity to gain HCO_3^-. In addition, calcification generates H^+ for nutrient trans-membrane symport. In particular, HCO_3^- concentration may drop in the IUS due to biotically driven calcification and active cell import. Thus, we propose here that the primary calcification in *Halimeda* spp. may be HCO_3^- limited. However, Borowitzka and Larkum (1976a) note that in *Halimeda* spp., the use of HCO_3^- in photosynthesis, catalyzed to CO_2 via cell-internal carbonic anhydrase activity, is less efficient compared with the direct use of CO_2.

Other physiological daytime processes not shown in the model

Not included in the model is a light-induced membrane-bound proton pump (presumably a H^+-ATPase; De Beer and Larkum 2001) from the cell to the IUS, as in our view it is not directly involved in the process of

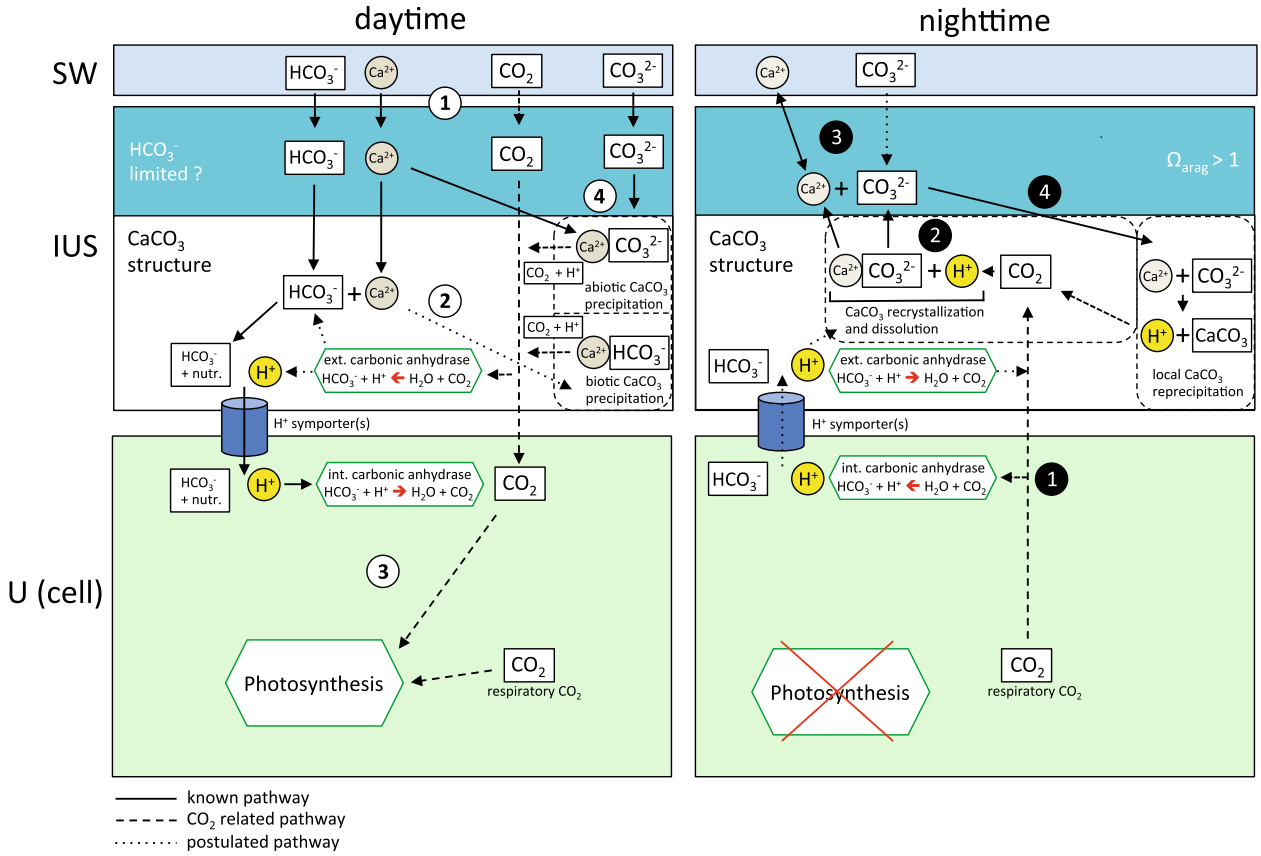

Fig. 5 Model of physiological processes related to calcification in *Halimeda* spp. (modified from Comeau et al. 2012). *Photosynthesis at daytime*: Ca^{2+} ions and inorganic carbon species enter the inter-utricular space (IUS) (*1*). Polysaccharides accumulate Ca^{2+} ions on the utricle wall and increase Ca^{2+} saturation. External carbonic anhydrase activity catalyzes $CO_2 + H_2O$ to $HCO_3^- + H^+$. (Unknown) Organic matrix protein(s)/enzyme(s) initiate and control $CaCO_3$ formation out of HCO_3^- and Ca^{2+} = primary calcification (*2*). Both photosynthesis and external carbonic anhydrase activity extract CO_2 from the IUS. HCO_3^- is cell-imported through H^+/membrane-bound symporter(s) (*3*). Subsequently, seawater $CaCO_3$ saturation state within the IUS gets elevated. $CaCO_3$ precipitates abiotically at nucleation sites due to CO_3^{2-} oversaturation = secondary calcification (*4*). *Respiration at nighttime*: Respiratory CO_2 from cell metabolism enters the IUS (*1*). Rise of seawater pCO_2 lowers seawater $CaCO_3$ saturation state in the IUS. $CaCO_3$, precipitated during daytime, gets partly dissolved and recrystallized (*2*). Inflow of CO_3^{2-} saturated seawater and dissolution of $CaCO_3$ locally elevate $CaCO_3$ saturation state ($\Omega > 1$) (*3*). Abiotic re-precipitation of $CaCO_3$ occurs (*4*). *SW* seawater, *IUS* inter-utricular space, *U* utricle/cell. Also see text for further explanations

calcification and might rather play a role in balancing the internal cell pH. Furthermore, it can be safely assumed that protons discharged to the IUS are (re)used for nutrient symport back into the cell. Nevertheless, a proton efflux during the daytime supports the assumption of a matrix-driven primary calcification, as the pH in the microenvironment at the utricular site of calcification is likely to be comparably low (pH < 9) to allow abiotic precipitation of $CaCO_3$. Likewise not considered is a postulated OH^- efflux from the cell into the IUS during daytime photosynthesis (Borowitzka and Larkum 1976a), as no mechanism and thus no evidence regarding the process was found yet.

Nighttime processes

Physiological cell processes shift during the nighttime from photosynthesis to metabolic respiration. This change affects the seawater carbon chemistry within the inter-utricular space (IUS). Metabolic respiration elevates CO_2 concentration and thus decreases CO_3^{2-} saturation within the IUS. As a consequence, aragonite needles precipitated during the daytime become partially dissolved, recrystallized, and break down to micro-anhedral crystals (<1 µm). $CaCO_3$ saturated seawater that enters the IUS might be sufficient to sustain local abiotic re-precipitation of previously dissolved $CaCO_3$ along possible nucleation sites

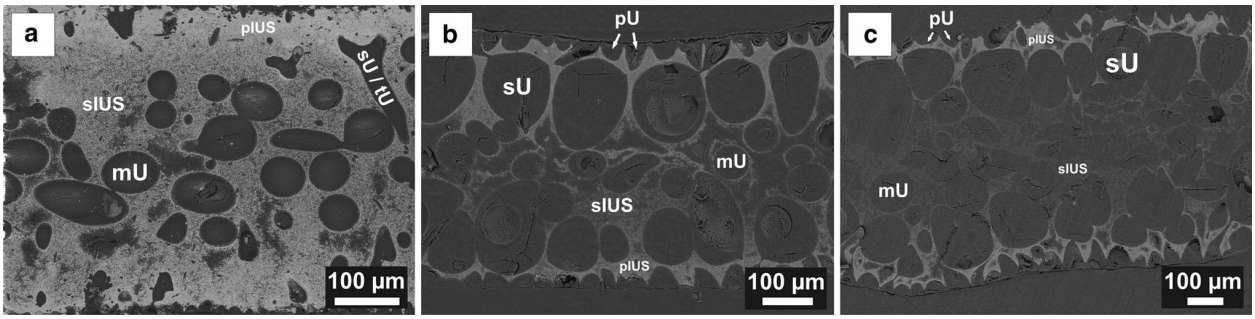

Fig. 6 Comparison of the internal skeletal microstructure of segments from different *Halimeda* species. SEM images (via BSE) of thin-sections from mature segments of **a** *Halimeda opuntia*, **b** *Halimeda copiosa* and **c** *Halimeda cuneata*. Note the difference in dimensions of secondary, medullary utricles, and the respective volume of inter-utricular space that is available for segment calcification. Also note the species-specific thickness of the peripheral primary inter-utricular space that resembles the micro-anhedral carbonate rim of the segment. *U* utricle (*p* primary, *s* secondary, *t* tertiary, *m* medullary); *IUS* inter-utricular space (*p* primary, *s* secondary)

(e.g., remnants of primary needles) on the utricle wall. Both processes lead to the formation of MAC.

The role of calcification in *H. opuntia*

Calcification has a range of functions for marine organisms (Kleypas et al. 2006). Nevertheless, at first glance it is not obvious why a marine macro-alga invests energy into the formation of a rigid calcium carbonate skeletal structure, when other marine algae and plants do not. Hence, it is important to consider the species-specific habitat of *H. opuntia* and its environmental conditions to provide answers to this enigma.

H. opuntia calcifies not solely to gain CO_2 or protons for photosynthesis or nutrient uptake. The skeleton also plays a major structural role in the alga's ecology making it less susceptible to breakage in high-energy regimes (DeWreede 2006; Ries 2009). Additionally, a calcareous skeleton is an efficient method of protection from grazing. Heavily calcified *Halimeda* species are grazed to a lesser extent than less calcified ones (Littler 1976; Paul and Hay 1986; Schupp and Paul 1994). *H. opuntia* is primarily located in the high-energy regimes of the reef crest, fore reef, and deep reef of tropical coral reefs (Johns and Moore 1988). *Halimeda* species that grow in these habitats possess smaller, but much heavier calcified segments, which presumably is an adaption to environmental conditions (Multer 1988; Kooistra and Verbruggen 2005). The enhanced stage of the segment's primary cementation (MAC formation) might derive from their smaller but higher number of utricles and accordingly smaller but higher total volume of IUS (Fig. 6; Macintyre and Reid 1995; Verbruggen and Kooistra 2004), the given seawater parameters (e.g., light conditions, pCO_2) of the environment in which these species grow and also species-specific metabolism, i.e., respiratory activity. Strong primarily cemented segments are less susceptible to breakage or disintegration, especially when shed into the sediment. Together these characteristics may explain why *H. opuntia* is one of the main macro carbonate sediment producers (>2 mm) in the tropics. In fact, it is these small and heavily cemented segments by *Halimeda* species of the lineages of Opuntia and Micronesicae (Drew and Abel 1988; Freile et al. 1995; Hillis 2001; Verbruggen et al. 2005, 2007) that are responsible for the build-up of carbonate platforms characterized by *Halimeda* sediments and thus might contribute crucially to island formation as they get transported over long distances, from their origin on the fore reef and reef crest, down the slope, onto the reef flat and up to the beach or into the lagoon (Jindrich 1969; Moore et al. 1976; Drew and Abel 1988; Hine et al. 1988; Johns and Moore 1988; Freile et al. 1995; Wienberg et al. 2010).

Based on the observation of *H. opuntia*'s specific microstructural features, the calcification in *Halimeda* spp. obviously cannot be considered as simple abiotic $CaCO_3$ precipitation. The features that are present, namely acidic polysaccharides on the utricle walls, external carbonic anhydrase activity within the inter-utricular space, and an organic matrix in which the early primary needles are embedded, strongly suggest active calcification or at least the active initiation of crystal growth as in many other marine calcifying organisms. However, biologically induced calcification (i.e., secondary calcification) is present but restricted to parts of the inter-utricular space that are not in direct contact with the cell wall. Thus, formation of the distinct skeletal microstructure seen in *H. opuntia* is more complex than previously thought. Here, we propose that it is the interplay of biological processes with biochemical parameters of the seawater, which act in parallel to form this distinct $CaCO_3$ skeletal microstructure. Our model for calcification in *Halimeda* spp. considers both the biotically driven calcification and the abiotically

driven precipitation of $CaCO_3$ depending on seawater carbonate chemistry influenced by the physiology of the alga. The model explains the formation of skeletal features in the living alga, as well as the first sedimentary processes already starting during the segments lifetime. Our investigations show that it is necessary to combine insights from fields of biology and physiology with biogeochemistry and sedimentology to gain a better understanding of processes influencing each other in a biological system.

Further investigations are needed to test the postulated model and the explanations given for the development of the skeletal morphological features seen in the skeletal microstructure of *H. opuntia*. Beyond the detection of an organic matrix, some deeper insights may come from microsensor studies dealing with diurnal changes of the seawater parameters within the IUS including a high-resolution mineralogical analysis of the different skeletal features, as well as the role of external carbonic anhydrase activity in calcification, its molecular characterization and whether or not other extracellular matrix proteins are present and involved in the process of calcification. However, the development of the most prominent microstructural feature in the skeleton of *H. opuntia*, the micro-anhedral carbonate, is not biologically controlled and may depend directly on seawater carbon chemistry. The process of micro-anhedral carbonate formation that causes cementation of the segment during its lifetime has implications for the alga and for its environment. Reduced segment cementation may result directly in a loss of segments in the sediment with an impact on ecosystem functioning and shoreline and island stability.

Acknowledgments Sebastian Flotow (ZMT-Bremen) is thanked for preparing thin-sections and help with the SEM. Achim Meyer (ZMT-Bremen) provided help in conducting experiments and maintaining the aquaria. Claire Reymond and Julien Michel (ZMT-Bremen) thoughtfully reviewed the manuscript. We are grateful for the funding of this study by the ZMT-Bremen. We sincerely thank the associate editor and two reviewers for the helpful comments that greatly improved the manuscript.

References

Addadi L, Raz S, Weiner S (2003) Taking advantage of disorder: amorphous calcium carbonate and its roles in biomineralization. Adv Mater 15:959–970

Addadi L, Joester D, Nudelman F, Weiner S (2006) Mollusk shell formation: a source of new concepts for understanding biomineralization processes. Chemistry 12:980–987

Alexandersson ET (1972) Intragranular growth of marine aragonite and Mg-calcite; evidence of precipitation from supersaturated seawater. J Sediment Res 42:441–460

Alexandersson ET (1974) Carbonate cementation in coralline algal nodules in the Skagerrak, North Sea; biochemical precipitation in undersaturated waters. J Sediment Res 1:7–26

Alexandersson ET, Milliman JD (1981) Intragranular Mg-calcite cement in *Halimeda* plates from the Brazilian continental shelf. J Sediment Res 51:1309–1314

Arias JL, Fernández MS (2008) Polysaccharides and proteoglycans in calcium carbonate-based biomineralization. Chem Rev 108:4475–4482

Arnott HJ (1982) Three systems of biomineralization in plants with comments on the associated organic matrix. In: Nancollas GH (ed) Biological mineralization and demineralization., Springer, Berlin Heidelberg, pp 199–218

Bertucci A, Moya A, Tambutté S, Allemand D, Supuran CT, Zoccola D (2013) Carbonic anhydrases in anthozoan corals–a review. Bioorg Med Chem 21:1437–1450

Böhm EL (1973) Composition and calcium binding properties of the water soluble polysaccharides in the calcareous alga *Halimeda opuntia* (L.) (Chlorophyta, Udoteaceae). Internationale Revue der gesamten Hydrobiologie und Hydrogeographie 58:117–126

Böhm EL, Goreau T (1973) Rates of turnover and net accretion of calcium and the role of calcium binding polysaccharides during calcification in the calcareous alga *Halimeda opuntia* (L.). Internationale Revue der gesamten Hydrobiologie und Hydrogeographie 58:723–740

Bonucci E (2007) Main suggested calcification mechanisms: extracellular matrix. In: Schreck S (ed) Biological calcification: normal and pathological processes in the early stages. Springer, Heidelberg, pp 507–558

Borowitzka MA (1982a) Morphological and cytological aspects of algal calcification. Int Rev Cytol 74:127–162

Borowitzka MA (1982b) Mechanism in algal calcification. Progress in Phycological Research 1:137–177

Borowitzka MA, Larkum AWD (1976a) Calcification in the green alga *Halimeda*. III. The sources of inorganic carbon for photosynthesis and calcification and a model of the mechanism of calcification. J Exp Bot 27:879–893

Borowitzka MA, Larkum AWD (1976b) Calcification in the green alga *Halimeda* IV. The action of metabolic inhibitors on photosynthesis and calcification. J Exp Bot 27:894–907

Comeau S, Carpenter R, Edmunds PJ (2012) Coral reef calcifiers buffer their response to ocean acidification using both bicarbonate and carbonate. Proc R Soc B Biol Sci 280:1753

Cuif JP, Dauphin Y, Nehrke G, Nouet J, Perez-Huerta A (2012) Layered growth and crystallization in calcareous biominerals: impact of structural and chemical evidence on two major concepts in invertebrate biomineralization studies. Minerals 2:11–39

De Beer D, Larkum AWD (2001) Photosynthesis and calcification in the calcifying algae *Halimeda discoidea* studied with microsensors. Plant Cell Environ 24:1209–1217

DeWreede R (2006) Biomechanical properties of coenocytic algae (Chlorophyta, Caulerpales). Sci Asia Suppl 1:57–62

Dickson AG, Millero FJ (1987) A comparison of the equilibrium constants for the dissociation of carbonic acid in seawater media. Deep Sea Res A 34:1733–1743

Dickson AG, Afghan JD, Anderson GC (2003) Reference materials for oceanic CO_2 analysis: a method for the certification of total alkalinity. Mar Chem 80(2):185–197

Dickson AG, Sabine CL, Christopher JR (2007) Guide to best practices for ocean CO_2 measurements. North Pacific Marine Science Organization Special Publication 3, Sidney, British Columbia pp 176

Doney SC, Balch WM, Fabry VJ, Feely RA (2009) Ocean acidification: a critical emerging problem for the ocean sciences. North 22:16–25

Drew EEA (1983) *Halimeda* biomass, growth rates and sediment generation on reefs in the central Great Barrier Reef province. Coral Reefs 2:101–110

Drew E, Abel K (1988) Studies on *Halimeda* I. The distribution and species composition of *Halimeda* meadows throughout the Great Barrier Reef Province. Coral Reefs 6:195–205

Faatz M, Gröhn F, Wegner G (2004) Amorphous calcium carbonate: synthesis and potential intermediate in biomineralization. Adv Mater 16:996–1000

Falini G, Reggi M, Fermani S, Sparla F, Goffredo S, Dubinsky Z, Levi O, Dauphin Y, Cuif JP (2013) Control of aragonite deposition in colonial corals by intra-skeletal macromolecules. J Struct Biol 183:226–238

Folk RL (1959) Practical petrographic classification of limestones. Am Assoc Pet Geol Bull 43(1):1–38

Folk R, Robles R (1964) Carbonate sands of isla perez, alacran reef complex, Yucatan. J Geol 75:412–437

Freile D, Milliman J, Hillis L (1995) Leeward bank margin *Halimeda* meadows and draperies and their sedimentary importance on the western Great Bahama Bank slope. Coral Reefs 14:27–33

Hillis, L (1997) Coralgal reefs from a calcareous green alga perspective and a first carbonate budget. Proc 8th Int Coral Reef Symp 1:761–766

Hillis L (2001) The calcareous reef alga *Halimeda* (Chlorophyta, Byropsidales): a cretaceous genus that diversified in the Cenozoic. Palaeogeogr Palaeoclimatol Palaeoecol 166:89–100

Hillis-Colinvaux L (1980) Ecology and taxonomy of *Halimeda*: primary producer of coral reefs. Adv Mar Biol 17:1–327

Hine AC, Hallock P, Harris MW, Mullins HT, Belknap DF, Jaap WC (1988) *Halimeda* bioherms along an open seaway: Miskito Channel, Nicaraguan Rise, SW Caribbean Sea. Coral Reefs 6:173–178

Hoegh-Guldberg O, Mumby PJ, Hooten AJ, Steneck RS, Greenfield P, Gomez E, Harvell CD, Sale PF, Edwards AJ, Caldeira K, Knowlton N, Eakin CM, Iglesias-Prieto R, Muthiga N, Bradbury RH, Dubi A, Hatziolos ME (2007) Coral reefs under rapid climate change and ocean acidification. Science 318:1737–1742

Hofmann LC, Straub S, Bischof K (2013) Elevated CO_2 levels affect the activity of nitrate reductase and carbonic anhydrase in the calcifying rhodophyte *Corallina officinalis*. J Exp Bot 64(4):899–908

Hofmann LC, Heiden J, Bischof K, Teichberg M (2014) Nutrient availability affects the response of the calcifying chlorophyte *Halimeda opuntia* (L.) J.V. Lamouroux to low pH. Planta 239:231–242

Holcomb M, Cohen AL, Gabitov RI, Hutter JL (2009) Compositional and morphological features of aragonite precipitated experimentally from seawater and biogenically by corals. Geochim Cosmochim Acta 73:4166–4179

Isenberg H, Douglas S, Lavine L, Spicer S, Weissfeller H (1966) A protozoan model of hard tissue formation. Ann NY Acad Sci 136:157–188

Jindrich V (1969) Recent carbonate sedimentation by tidal channels in the Lower Florida Keys. J Sediment Res 39:531–553

Jinendradasa S, Ekaratne S (2002) Composition and monthly variation of fauna inhabiting reef-associated *Halimeda*. Proc 9th Int Coral Reef Symp 2:1059–1063

Johns H, Moore C (1988) Reef to basin sediment transport using *Halimeda* as a sediment tracer, Grand Cayman Island, West Indies. Coral Reefs 6:187–193

Kinsey D, Hopley D (1991) The significance of coral reefs as global carbon sinks–response to greenhouse. Palaeogeogr Palaeoclimatol Palaeoecol 89:363–377

Kleypas JA, Feely RA, Fabry VJ, Langdon C, Sabine CL, Robbins LL (2006) Impacts of ocean acidification on coral reefs and other marine calcifiers. A guide for future research. Report of a workshop sponsored by NSF, NOAA and USGS

Kooistra WHCF, Verbruggen H (2005) Genetic patterns in the calcified tropical seaweeds *Halimeda opuntia, H. distorta, H. hederacea*, and *H. minima* (Bryopsidales, Chlorophyta) provide insights in species boundaries and interoceanic dispersal. J Phycol 41:177–187

Larkum AWD, Salih A, Kühl M (2011) Rapid mass movement of chloroplasts during segment formation of the calcifying siphonalean green alga *Halimeda macroloba*. Plos One 6:e20841

Liebezeit G, Dawson R (1981) Changes in the polysaccharide matrix of calcareous green algae during growth. Indices biochemiques et milieux marins. Journées du GABIM 14:147–154

Littler M (1976) Calcification and its role among the macroalgae. Micronesica 12:27–41

Macintyre I, Reid RP (1995) Crystal alteration in a living calcareous alga (*Halimeda*): implications for studies in skeletal diagenesis. J Sediment Res A Sediment Petrol Process 65:143–153

Mann S (2001) Biomineralization: principles and concepts in bioinorganic materials chemistry, vol 5. Oxford University Press, New York

Marin F, Luquet G (2004) Molluscan shell proteins. C R Palevol 3:469–492

Marshall JF, Davies PJ (1988) *Halimeda* bioherms of the northern Great Barrier Reef. Coral Reefs 6:139–148

Merbach C, Culberson CH, Hawley JE, Pytkowicz RM (1973) Measurements of the apparent dissociation constants of carbonic acid in seawater at atmospheric pressure. Limnol Oceanogr 18:897–907

Milliman JD (1974) Recent sedimentary carbonates, part 1. Marine carbonates. Springer, Heidelberg

Milliman JD, Droxler AW (1996) Neritic and pelagic carbonate sedimentation in the marine environment: ignorance is not bliss. Geol Rundsch 85:496–504

Mitsunaga K, Akasaka K, Shimada H, Fujino Y, Yasumasu I, Numanoi H (1986) Carbonic anhydrase activity in developing sea urchin embryos with special reference to calcification of spicules. Cell Differ 18:257–262

Miyamoto H, Miyoshi F, Kohno J (2005) The carbonic anhydrase domain protein nacrein is expressed in the epithelial cells of the mantle and acts as a negative regulator in calcification in the mollusc *Pinctada fucata*. Zool Sci 22:311–315

Miyamoto H, Miyashita T, Okushima M, Nakano S, Morita T, Matsushiro A (1996) A carbonic anhydrase from the nacreous layer in oyster pearls. Proc Natl Acad Sci USA 93:9657–9660

Moore CH, Graham EA, Land LS (1976) Sediment transport and dispersal across the deep fore-reef and island slope (-55 m to -305 m), Discovery Bay, Jamaica. J Sediment Petrol 46:174–187

Moya A, Tambutté S, Bertucci A, Tambutté E, Lotto S, Vullo D, Supuran C, Allemand D, Zoccola D (2008) Carbonic anhydrase in the scleractinian coral *Stylophora pistillata*: characterization, localization, and role in biomineralization. J Biol Chem 283: 25475–25484

Multer HG (1988) Growth rate, ultrastructure and sediment contribution of *Halimeda incrassata* and *Halimeda monile*, Nonsuch and Falmouth Bays, Antigua, W.I. Coral Reefs 6:179–186

Multer HG, Clavijo I (2004) *Halimeda* investigations: progress and problems. NOAA/RSMAS

Nakahara H, Bevelander G (1978) The formation of calcium carbonate crystals in *Halimeda incrassata* with special reference to the role of the organic matrix. Jap J Phycol 26:9–12

Neumann AC, Land LS (1975) Lime mud deposition and calcareous algae in the Bight of Abaco, Bahamas; a budget. J Sediment Res 45:763–786

Orme GR, Salama MS (1988) Form and seismic stratigraphy of *Halimeda* banks in part of the northern Great Barrier Reef Province. Coral Reefs 6:131–137

Paul V, Hay M (1986) Seaweed susceptibility to herbivory: chemical and morphological correlates. Mar Ecol Prog Ser 33:255–264

Payri CE (1988) Halimeda contribution to organic and inorganic production in a Tahitian reef system. Coral Reefs 6:251–262

Phipps C, Roberts HH (1988) Seismic characteristics and accretion history of *Halimeda* bioherms on Kalukalukuang Bank, eastern Java Sea (Indonesia). Coral Reefs 6:149–159

Pierrot D, Lewis E, Wallace DWR (2006) CO_2SYS DOS Program developed for CO_2 system calculations. ORNL/CDIAC-105. Carbon Dioxide Information Analysis Center, Oak Ridge National Laboratory, US Department of Energy, Oak Ridge, TN

Pomar L, Kendall CGSC (2007) Architecture of carbonate platforms: a response to hydrodynamics and evolving ecology. In: Lukasik J, Simo JA (eds) Controls on carbonate platform and reef development. SEPM 89:187–216

Rahman MA, Oomori T, Uehara T (2008) Carbonic anhydrase in calcified endoskeleton: novel activity in biocalcification in alcyonarian. Mar Biotechnol 10:31–38

Rao VP, Veerayya M, Nair RR, Dupeuble PA, Lamboy M (1994) Late Quaternary *Halimeda* bioherms and aragonitic faecal pellet-dominated sediments on the carbonate platform of the western continental shelf of India. Mar Geol 121:293–315

Rees SA, Opdyke BN, Wilson PA, Henstock TJ (2007) Significance of *Halimeda* bioherms to the global carbonate budget based on a geological sediment budget for the Northern Great Barrier Reef, Australia. Coral Reefs 26:177–188

Reid RP, Macintyre GI (1998) Carbonate recrystallization in shallow marine environments: a widespread diagenetic process forming micritized grains. J Sediment Res 68:928–946

Ries JB (2009) Effects of secular variation in seawater Mg/Ca ratio (calcite-aragonite seas) on $CaCO_3$ sediment production by the calcareous algae *Halimeda*, *Penicillus* and *Udotea* - evidence from recent experiments and the geological record. Terra Nova 21:323–339

Ries JB, Cohen AL, McCorkle DC (2009) Marine calcifiers exhibit mixed responses to CO_2-induced ocean acidification. Geology 37:1131–1134

Roberts H, Phipps C, Effendi L (1987) *Halimeda* bioherms of the eastern Java Sea, Indonesia. Geology 15:371–374

Robinson C, Brooks SJ, Shore RC, Kirkham J (1998) The developing enamel matrix: nature and function. Eur J Oral Sci 106:282–291

Salgado LT, Amado Filho GM, Fernandez MS, Arias JL, Farina M (2011) The effect of alginates, fucans and phenolic substances from the brown seaweed *Padina gymnospora* in calcium carbonate mineralization in vitro. J Cryst Growth 321:65–71

Schupp PJ, Paul VJ (1994) Calcium carbonate and secondary metabolites in tropical seaweeds: variable effects on herbivorous fishes. Ecology 75:1172–1185

Sikes CS (1978) Calcification and cation sorption of *Cladophoha glomerata* (chlorophyta) 1, 2. J Phycol 14(3):325–329

Simkiss K (1965) The organic matrix of the oyster shell. Comp Biochem Phys 16:427–435

Simkiss K, Wilbur KM (1989) Biomineralization. Academic Press, San Diego, CA, USA

Stanley SM, Ries JB, Hardie LA (2010) Increased production of calcite and slower growth for the major sediment-producing alga *Halimeda* as the Mg/Ca ratio of seawater is lowered to a "Calcite Sea" level. J Sediment Res 80:6–16

Tambutté S, Tambutté E, Zoccola D, Caminiti N, Lotto S, Moya A, Allemand D, Adkins J (2007) Characterization and role of carbonic anhydrase in the calcification process of the azooxanthellate coral *Tubastrea aurea*. Mar Biol 151:71–83

Tussenbroek BI, van Dijk JK (2007) Spatial and temporal variability in biomass and production of psammophytic *Halimeda incrassata* (Bryopsidales, Chlorophyta) in a Caribbean reef lagoon. J Phycol 43:69–77

Tsuzuki M, Miyachi S (1989) The function of carbonic anhydrase in aquatic photosynthesis. Aquat Bot 34:85–104

Verbruggen H, Kooistra W (2004) Morphological characterization of lineages within the calcified tropical seaweed genus *Halimeda* (Bryopsidales, Chlorophyta). Eur J Phycol 39:213–228

Verbruggen H, Littler DS, Littler MM (2007) *Halimeda pygmaea* and *Halimeda pumila* (Bryopsidales, Chlorophyta): two new dwarf species from fore reef slopes in Fiji and the Bahamas. Phycologia 46:513–520

Verbruggen H, De Clerck O, Cocquyt E, Kooistra WHCF, Coppejans E (2005) Morphometric taxonomy of siphonous green algae: a methodological study within the genus *Halimeda* (Bryopsidales). J Phycol 41:126–139

Vroom PS, Smith CM, Coyer JA, Walters LJ, Hunter CL, Beach KS, Smith JE (2003) Field biology of *Halimeda tuna* (Bryopsidales, Chlorophyta) across a depth gradient: comparative growth, survivorship, recruitment, and reproduction. Hydrobiologia 501:149–166

Watanabe T, Fukuda I, China K, Isa Y (2003) Molecular analyses of protein components of the organic matrix in the exoskeleton of two scleractinian coral species. Comp Biochem Physiol B Biochem Mol Biol 136:767–774

Wefer G (1980) Carbonate production by algae *Halimeda, Penicillus* and *Padina*. Nature 285:323–324

Weiner S, Lowenstam H (1986) Organization of extracellularly mineralized tissues: a comparative study of biological crystal growth. Crit Rev Biochem Mol Biol 20:365–408

Weiss IM, Marin F (2008) The role of enzymes in biomineralization processes. In: Sigel A, Sigel H, Sigel RKO (eds) Biomineralization: from nature to application. Wiley, West Sussex, pp 71–126

Wheeler AP, Sikes CS (1984) Regulation of carbonate calcification by organic matrix. Integr Comp Biol 24:933–944

Wienberg C, Westphal H, Kwoll E, Hebbeln D (2010) An isolated carbonate knoll in the Timor Sea (Sahul Shelf, NW Australia): facies zonation and sediment composition. Facies 56:179–193

Wilbur KM, Hillis-Colinvaux L, Watabe N (1969) Electron microscope study of calcification in the alga *Halimeda* (order Siphonales) 1. Phycologia 8:27–35

Wiman SK, McKendree WG (1975) Distribution of *Halimeda* plants and sediments on and around a patch reef near Old Rhodes Key, Florida. J Sediment Res 45:415–421

Zhong C, Chu CC (2010) On the origin of amorphous cores in biomimetic $CaCO_3$ spherulites: new insights into spherulitic crystallization. Cryst Growth Des 10:5043–5049

3.1 Extended discussion on the calcification of the green macro-alga genus *Halimeda*

3.1.1 Primary calcification

In segments of the first day, precipitation of $CaCO_3$ onsets directly on the external utricle wall with crystals shaped as aragonite needles (< 1 µm). Henceforth these small needles are termed "primary needles" and their process of formation "primary calcification". These early precipitated needles are observed embedded in an organic matrix. However, the matrix that may play a role in the initiation of primary needle formation is identified in segments of all maturation stages. To allow primary needle crystallization the organic matrix and with it its cell wall components are proposed to disintegrate (Liebezeit and Dawson 1981; Borowitzka 1982a), similar as observed in studies on enamel (dentinogenesis) or hydroxyapatite (bone) biomineralization (Bonucci 2007; Holcomb et al. 2009), and which is typical for biomineralization of hard tissues in general. The distinct shape primary needles show is peculiar, as they do not resemble the morphology of abiotically precipitated aragonite needle-shaped crystals (Macintyre and Reid 1995). Primary needles have a roundish crystal shape often with soft edges and posses a distinct tip. This distinct acuminated tip, observed in SEM images, is likely the actual $CaCO_3$ growth layer of the single (mono-)crystal and suggests that active $CaCO_3$ biomineralization, biotically-initiated and -controlled crystal nucleation and crystallization is present in *Halimeda* (e.g., Mann 2001; Bonucci 2007). Primary needles are likely formed during daytime photosynthesis in the algal segment, as they are the only $CaCO_3$ present in young apical segments of one day of age (green color; sampled after 12 h of daylight at dusk, before "lights off"). The maximum length of primary needles in segments of all maturation stages does not exceed ~5 µm. They are supposed to become rapidly recrystallized in the formation process of micro-anhedral carbonate (MAC), induced by cell metabolism (release of respiratory CO_2) at nighttime (Macintyre and Reid 1995). Subsequently, new primary needles form daily during photosynthesis at the external utricle wall.

$CaCO_3$ nucleation as the onset of primary needle formation likely takes place at the acidic, sulfated polysaccharides on the utricle wall, which were identified by Wilbur et al. (1969) and Böhm (1973). Acidic polysaccharides are known to act as cation attractors and are present in most calcifying organisms (e.g., Mann 2001; Bonucci 2007; Weiss and Marin 2008). According to the "theory of Ionotropy" (Mann 2001), Ca^{2+} ions are adsorbed and accumulated at acidic (i.e., negatively charged) end-groups of molecules, such as sulfated-bonds of polysaccharides present at the cell wall. Böhm (1973) showed that in particular the sulfated polysaccharides (i.e. likely pectins) at the utricle cell wall of *Halimeda* have a high cation affinity but low cation binding strength, excluding them to be directly responsible or a

template for subsequent needle crystallization. He concluded that they might rather act as an ion pool to provide Ca^{2+} ions for crystallization by elevating Ca^{2+} saturation at the utricle wall. Should primary calcification proceed within an organic matrix as suggested, it is likely that other yet unidentified calcifying proteins use this Ca^{2+} ion pool for $CaCO_3$ formation. Noteworthy, calcification induced by proteins would imply that HCO_3^- is used for $CaCO_3$ crystallization, independently from CO_3^{2-} ion availability. Moreover, this would be in agreement to the presence of external carbonic anhydrase activity, as organic molecules, such as proteins (including enzymes), involved in $CaCO_3$ biomineralization of other organisms, are known to posses "carbonic-anhydrase-like" catalytic domains in their tertiary or quarterly structure (e.g., Marin and Luquet 2004; Bonucci 2007; Weiss and Marin 2008).

3.1.1.1 The role of external carbonic anhydrase activity (eCA) in the calcification of macro-algae genus *Halimeda*

Within the IUS of *Halimeda* external carbonic anhydrase activity (eCA) was detected (Borowitzka and Larkum 1976b). External CA catalyzes the (reversible) reaction $CO_2 + H_2O \leftrightarrow HCO_3^- + H^+$. The calcification in *Halimeda* was shown to be suppressed to the "dark calcification rate", when eCA is inhibited via sodium acetazolamide (0.25 mM) (Borowitzka and Larkum 1976b). Thus, here I propose that eCA may have a direct function in the process of calcification in *Halimeda.* Previous studies on the calcification mechanism of marine algae and plants argue that the product of eCA is CO_2 for photosynthesis by the use of HCO_3^- as a substrate (e.g., Simkiss 1965; Borowitzka and Larkum 1976b). Although that most likely seems to be the case for many aquatic plants and algae (reviewed by Tsuzuki and Miyachi 1989) for calcifying algae such as *Halimeda* it is not conclusively explainable. In the experiment by Borowitzka and Larkum (1976b), calcification of *Halimeda* is suppressed when eCA is inhibited. However, in parallel photosynthesis only is lowered to some extent (~25 % of initial control rate at 0.25 mM sodium acetazolamide (inhibitor); Borowitzka and Larkum 1976b). For further explanation why also photosynthesis is subsequently lowered by sodium acetazolamide see e.g. Moroney et al. (2001). Even with photosynthesis of the alga lowered to ~25 % of the initial control rate, $CaCO_3$ saturation state within the IUS is expected to become sufficiently elevated for (abiotic) $CaCO_3$ crystallization to proceed (i.e., secondary needle growth), which indeed is indicated by a rise in circumfluent seawater pH under light from ~8.3 to ~8.5 (in Borowitzka and Larkum 1976b; seawater pH in the IUS presumably higher). However, seawater with a pH > 8.5 likely sustains calcification according to hypotheses for abiotic (i.e., biologically-mediated) crystal growth in *Halimeda* (Borowitzka and Larkum 1976b; Borowitzka 1984; De Beer and Larkum 2001). Thus the reduced

calcification observed in *Halimeda* is not explainable by the decrease of the photosynthesis rate alone (cf., Vogel et al. 2015b). Additionally, it has to be recalled that *Halimeda* (of the same species) that grew in low light regimes (i.e., low photosynthesis rate) were observed to be much heavier calcified (Goreau 1963; Goreau and Goreau 1973; Jensen et al. 1985; Macintyre and Reid 1995; pers. obs.), strongly arguing against simple abiotic (biologically-mediated) primary calcification induced by photo-physiology.

External CA is one of the essential enzymatic activities present within the organic matrix of most marine calcifying organisms, such as bacteria, mollusks, echinoderms and, corals (e.g., Mitsunaga et al. 1986; Marin and Luquet 2004; Miyamoto et al. 2005; Tambutté et al. 2007; Moya et al. 2008; Li et al. 2011; Bertucci et al. 2013). In these organisms the enzyme catalyzes the hydration of CO_2 to HCO_3^- when involved in the process of $CaCO_3$ biomineralization. Calcifying proteins or enzymes inducing and controlling $CaCO_3$ biomineralization may then use HCO_3^- from eCA (e.g., Bonucci 2007; Weiss and Marin 2008; Jury et al. 2010; Findlay et al. 2011; Bertucci et al. 2013). Thereby, eCA may be a functional domain in the tertiary or quaternary structures of (calcifying and other) proteins (reviewed by Liljas and Laurberg 2000; Marin and Luquet 2004; Bertucci et al. 2013). Although, it is known that eCA (i.e., the enzyme) can be part of so-called "transport-metabolon(s)" associated with membrane-bound HCO_3^- transporters (e.g., Hassan et al. 2013), *Halimeda* may not rely on eCA involvement in inorganic carbon cell-uptake for photosynthesis (Hofmann et al. 2015, unpublished data). That further questions the role, eCA is supposed to have for photo-physiology of the alga. Now when eCA is considered, e.g. as a functional domain of matrix proteins, responsible for the formation of HCO_3^- in primary calcification, it is conclusive why calcification is suppressed when eCA is inhibited. I conclude that even when at first glance primary needle precipitation seems to be linked to photosynthesis, as these needles are initially observed on the first day after light exposure, the link of photosynthesis to calcification is limited to the uptake of CO_2 from the IUS to "aid" in sustainment of the seawater $CaCO_3$ saturation for the ease of crystallization (cf. discussion of the calcification model, paragraph 4.2.4). However, main CO_2 uptake for photosynthesis may rather proceed at the peripheral cell layer of the utricles (i.e., segment surface) where also chloroplasts are primarily located during daytime (Larkum et al. 2011) and thus CO_2 may not be taken up in major quantities over cell walls in the IUS. Intriguingly, the segment surface of *Halimeda* is not calcified, even so uptake of CO_2 and O_2 / OH^- evolution likely raise seawater pH and $CaCO_3$ saturation of the diffusive boundary layer (DBL) at the segment surface sufficiently for abiotic precipitation. However, seawater $CaCO_3$ saturation is the main driver for secondary calcification in IUS and thus without photosynthesis (i.e., O_2 evolution into IUS) this process likely is affected. Presumably, exactly this was observed in the experiment conducted by Borowitzka and Larkum (1976b), when in the end after eCA also

photosynthesis was completely inhibited (at sodium acetazolamide concentrations > 1 mM; cf., Moroney et al. 2001). Subsequently, the low calcification rate that is still observed at a concentration of 0.25 mM sodium acetazolamide (i.e., "dark calcification rate" mentioned by Borowitzka and Larkum 1967b) finally vanishes due to complete inhibition of photosynthesis. Thus, the low calcification rate observed at 0.25 mM acetazolamide likely represents abiotic (biologically-mediated) secondary calcification, which was sustained by the still significant photosynthesis rate (~25 % of control rate), and the consequently elevated seawater pH (> 8.5) and $CaCO_3$ saturation in the IUS and of the DBL, as in contrast eCA-driven primary calcification was inhibited.

3.1.1.2 Crystal growth initiation at acidic macro-molecules on the cell wall

Acidic polysaccharides and proteins that exhibit high cation affinity are present at the cell wall of coenocytic algae (Böhm 1973; Domozych et al. 2012). Evolutionary, acidic macro-molecules at the cell wall may have developed as a protection from salt and thus are, in the context of evolution, likely an adaption to the marine environment (e.g., Aquino et al. 2011). These specific cell wall molecules are found in a multitude of different marine (calcifying) genera, such as in bacteria, protozoans, invertebrates, but also seaweeds and seagrass. In many of these organisms acidic cell wall polysaccharides evolved further forming a variety of specific structural conformations that now serve distinct purposes (e.g., Dumitriu 2012). Interestingly, even if evolutionary most of these organisms are not closely related, many of them form $CaCO_3$ hard tissues (i.e., calcify). Thereby, exactly these specific cell wall components (acidic polysaccharides, acidic proteins and carbonic anhydrases) are involved in formation of the $CaCO_3$ crystals in all of these organisms, e.g. determine the $CaCO_3$ polymorph that is precipitated (Bonucci 2007; Arias and Fernández 2008; Weiss and Marin 2008). Moreover, all kind of species that form hard tissues today, such as formation of bone minerals (hydroxyapatite) in vertebrates, chitin in invertebrates, dentinogenesis (enamel) in both invertebrates and vertebrates, and silification in protozoan, also use such specific features in hard tissue formation (e.g., Kobayashi 1971; Bonucci 2007, 2009, Bonucci and Gomez 2012). As this alone may hint to an evolutionary active initiation of hard tissue formation such as calcification in marine organisms, moreover the mechanisms underlying the calcification process, e.g. like the acquisition and accumulation of cations at acidic polysaccharides are also so similar, it seems likely that they originate from one early bacterial or protozoan ancestor shortly after the adaption from a "soda sea" to a "sodium chloride" ocean. However, as recent calcifying organisms exhibit acidic cell wall macro-molecules of huge structural and even taxon-specific diversity, such as e.g. in marine green algae (e.g., Estevez et al. 2009; Domozych et al. 2012), convergent evolution might be equibrobable.

One specific group of acidic polysaccharides present at the external cell wall of green algae and known to have strong cation affinity are pectins (Böhm 1973; Sikes 1978; Pickard 2013). These molecules reversibly bind cations such as Ca^{2+} ions with their anionic end groups (e.g. sulfates; Arias and Fernández 2008; Fernández-Díaz et al. 2010). By their specific conformation, they may form a complex termed pectin-Ca^{2+}. Pectin-Ca^{2+} complexes allow cell wall proteins to anchor themselves in the extracellular matrix. For example, extracellular enzymes with specific Ca^{2+} binding domains are able to attach to these pectin-Ca^{2+} complexes and still maintain their enzymatic activity (Carpin et al. 2001). Most enzymes and some carbonic anhydrases in the extracellular matrix, not only of marine calcifying organism, are also known to exhibit Ca^{2+} binding domains (Maurer and Hohenester 1997; Marin and Luquet 2004; Bonucci 2007; Weiss and Marin 2008). Presumably calcifying proteins / enzymes are able to use Ca^{2+} ions adsorbed by polysaccharides (e.g., pectins) to calcify in active catalysis. However, in order to make Ca^{2+} ions available, their release from complexes has to be triggered through a decrease of the micro-environmental pH (Pickard 2013) with following degradation (or conformation change) of the polysaccharides. This process may be initiated and controlled by the discharge of protons into the IUS through H^+-ATPase (proton pump) activity (Weiss and Pick 1996), by extracellular alkaline phosphatase (AP) or triggered by protonation of the circumjacent microenvironment through CO_2 hydration in the catalysis of carbonic anhydrase-like domains of Ca^{2+}-affine proteins.

3.1.2 Micro-anhedral carbonate (MAC) formation

Small micron-sized $CaCO_3$ crystals of anhedral shape accumulate on the external utricle walls that face into the IUS. Henceforth, these crystals are termed “micro-anhedral carbonate (MAC)”. Macintyre and Reid (1995) use the term “mini-micrite” to describe this type of crystals. However, the general term “micrite” (Folk 1959) for crystals < 4 µm in size does not allow specification of crystals of different genesis and shape and thus also includes primary needles, whose genesis is different (e.g., Milliman 1974). The new term “micro-anhedral carbonate” allows differentiation between needle-like crystals and crystals of anhedral shape within the same size range (< 1 µm). It also considers crystal genesis and formation process, in order to discriminate between MAC crystals and micrite precipitated in the sedimentary process of secondary “intra-granular” cementation (Milliman 1974; Reid and Macintyre 1998).

Newly formed MAC shows remnants of primary needles embedded, which suggests that MAC forms out of the primary needle crystals. Furthermore, this indicates that the formation of MAC involves the physiology of the alga. During nighttime the evolution of respiratory CO_2 into the IUS leads to a decrease in seawater pH and $CaCO_3$ saturation. Subsequently,

primary needles break down to smaller crystals (i.e. recrystallization; Macintyre and Reid 1995). Additionally, dissolved $CaCO_3$ from etched primary needles may instantly re-precipitate along external utricle walls. The process alternates with the perpetual formation of new primary needles at daytime and leads to a dense MAC structure within the IUS during the segments lifetime. Subsequently, the small primary IUS become completely filled with MAC and form a stabilizing outer rim that surrounds the segment. Noteworthy, macro-algae of the genus *Halimeda*, e.g. of the species *H. opuntia*, are heavier calcified (i.e., high MAC content and density, sIUS entirely calcified) when growing in deep-water or shaded habitats (i.e., low light regimes; shade-leaf segment morphotype) and some *Halimeda* species are known from waterdepths of more than 100 m b.s.l. (e.g., Goreau and Goreau 1973; Macintyre and Reid 1995; Granier 2012; pers. obs.). In fact, this suggests that $CaCO_3$ biomineralization in *Halimeda* likely is independent from gross photosynthesis and additionally underlines the important role of respiratory CO_2 in MAC formation.

In my view, the process of MAC formation has to be regarded as an abiotic process that is not controlled by the alga. Thus the formation of MAC within the IUS, as well as its crystal mineralogy relies on the seawater carbon chemistry, which is unintentionally altered by the alga´s metabolism during the day - night cycle and the ionic composition of the seawater, such as the *m* Mg / Ca ion ratio. Evidence for the plausibility of this statement may be the seawater metal ion ratio modification experiments from Stanley et al. (2010) and Blättler et al. (2014). I propose that the extensive formation of the $CaCO_3$ polymorph calcite observed within the IUS at a *m* Mg / Ca ratio of 1.5 in the species of *Halimeda incrassata* (Stanley et al. 2010) and *Halimeda discoidea* (Blättler et al. 2014) likely was precipitated in the process of MAC formation and thus MAC that originates from primary needles, which became recrystallized to and re-precipitated as Mg-calcite due to the experimental seawater parameters. Moreover, Stanley et al. (2010) note that the X-ray diffraction pattern of the incorporated Mg^{2+} "resembles that of non-skeletal calcite" and Blättler et al. (2014) shows Ca^{2+} stable isotope fractionation that indicate a first-order control on the $CaCO_3$ polymorph precipitated (i.e., on primary needle formation).

However, calcitic cements may also occasionally form under "unmodified" natural seawater *m* Mg / Ca ion ratio (~5.2) within IUS of living segments. Contrary to the formation of typical aragonite MAC in the living segment the precipitation of calcite rather has to be referred to as early secondary "intra-granular" cementation (Milliman 1974). That might account for values reported of up to 8 % Mg-calcite in the skeleton of living *Halimeda* sampled in the field, even so the age of the analyzed segments is unknown (e.g., Stanley et al. 2010; Sinutok PhD-Thesis 2013; Blättler et al. 2014). In *Halimeda* segments obtained from the sediment, intra-granular infillings of Mg-calcite are quite common (Alexandersson and Milliman 1981; Roberts et al. 1988; Reid and Macintyre 1998). In particular, the innermost parts of the sIUS

that remained open during the lifetime of the segment and the utricles (i.e., former location of the algal cells) may become filled with calcite cements and make it even more obvious that calcite found in the IUS of *Halimeda*, whether in segments from the living alga or from the sediment, is not intentionally and actively formed by the alga in a biological sense as it is never found directly associated with external utricle walls where active calcification takes place. However, endolithic microbes and micro-bioeroders are known to produce calcitic and even dolomitic deposits (e.g., Nothdurft et al. 2007; Diaz-Pulido et al. 2014; Reyes-Nivia et al. 2014). Most likely, these microorganisms also are present and abundant within the IUS of living *Halimeda* segments (Macintyre and Reid 1995) and may also (partly) play a role in MAC formation by the release of CO_2 due to their metabolism and by erosive activity, both causing $CaCO_3$ recrystallization.

MAC formation in the living segment is already of importance for the sediment record of *Halimeda* as its extent subsequently decides over the fate of the segments in the sediment. Thus it is opportune to name this process consistently the "primary cementation", as marine or intra-granular cementation (henceforth termed "secondary cementation") within *Halimeda* segments that infills the inner sIUS as well as the utricles, has to be separated (Milliman 1974, Alexandersson and Milliman 1981; Reid and Macintyre 1998; Perry 2000). Secondary cementation mainly takes place in a deposited plate without the involvement of physiological processes of the alga (Reid and Macintyre 1998). However, a sharp temporal boundary between the processes of primary and secondary cementation cannot be drawn as e.g., Milliman (1974) observed the onset of secondary cementation within utricles of a (presumably) dead segment that was still attached to the living alga.

3.1.2.1 Segments of different *Halimeda* species and their density in MAC

The grade of MAC extent and density largely differs between *Halimeda* species. This is due to the species-specific total volume of IUS that is available for calcification, which is caused by the dimensions of utricles of the different species. Additionally, these internal morphological features of the microstructure seem to be linked to the segment size of different species. Thus the species-specific segment size may be used as an indicator for the overall density of the segments calcification. Species with small segments (~1 cm) exhibit a morphological high pIUS to sIUS size ratio that derives from the species-specific dimensions and arrangement of utricles. Especially secondary, tertiary or medullary (= central) utricles are relatively small. Thus the total volume of IUS in these segments is large and leads to a considerable internal segment calcification and a high $CaCO_3$ to organic content (utricle) ratio. In comparison species with larger segments (> ~2 cm) have a rather low pIUS to sIUS size ratio and often exhibit large central utricles. The larger central utricles reduce the total

volume of IUS that leads to a weak segment calcification even if the IUS is completely filled with MAC. The $CaCO_3$ to organics (utricle) ratio within these segments is low. Thus, in *Halimeda* species with larger segments (> ~2 cm) the MAC segment rim between primary (peripheral) utricles is, compared to their dimension in width, merely a thin band, whereas in *Halimeda* species with small segments the rim of MAC often resembles more than ¼ of the dimensions of the segment´s width and thus forms a thick stabilizing rim, a peripheral skeleton of $CaCO_3$. This species-specific internal morphology and the extent of MAC is the main feature from which it is possible to predict if a segment persists unbroken, as a whole, in the sediment after shed from the alga. Large segments (> 2 cm) with comparably to their size and due to their internal morphology, thin rims of MAC and also with weak internal MAC density (i.e., primary cementation) are much more prone to disintegrate rapidly under physical forces of sediment transport and erosion.

Even so *Halimeda* species of the lineage Opuntia exhibit some of the heaviest calcified (i.e., primary cemented) segments alterations in individual specimen exist, as MAC formation depends on the photosynthesis / respiration ratio of the algal segment and thus on the environment in which the alga grows. For example, at least two segment morphotypes are present in the species of *H. opuntia*. The more common wide "butterfly- or fan-like" segment shape (cf., reniform) that is the sun-leaf morphotype of *H. opuntia* and a more "trident-like" segment shape (cf., tripartite), which resembles the shade-leaf morphotype of *H. opuntia* when growing in deep-water (> 20 m) or in habitats with low light availability (< 100 µmol photons m^{-2} s^{-1}). Shade-leaf segments generally are more calcified (i.e., primary cemented, especially the sIUS) than sun-leaf segments, as the higher respiratory activity of the alga in these habitats likely induces the formation of abundant MAC from active biomineralization of primary needles (see primary calcification) and thus may facilitate complete primary cementation of segments (Goreau 1963; Goreau and Goreau 1973; Macintyre and Reid 1995; pers. obs.). A good example to underline this statement are segments from *Halimeda* species of the lineage Opuntia that originate from water depths well below 20 m sampled at a carbonate knoll ("Pee Shoal"; sea mount) in Timor Sea (South-East Indian Ocean) approx. three months after a tropical storm passed the area (Wienberg et al. 2010). These segments are exceptionally heavily primarily cemented, but show a pristine peripheral and internal microstructure that suggests recent deposition during the storm event (Appendix X.II, Fig. A5). Thus they may support statements from e.g., Goreau (1963), Goreau and Goreau (1973) and my assumption that processes of (primary) calcification and photosynthesis are most likely decoupled to a certain extent and thus plea for active calcification in the genus *Halimeda*.

However after segments are shed from the alga secondary cementation is the only $CaCO_3$ precipitation taking place. Subsequently, for following sedimentary processes the dimensions

of the IUS and those of the central utricles matter, as segments from *Halimeda* species that posses smaller segments (< ~2 cm) and exhibit a strong stabilizing skeleton become rapidly secondarily cemented, thus may gain high intra-granular density. In contrast, most larger (> ~2 cm) and less primarily cemented segments do not even start to cement secondarily and disintegrate forming carbonate (needle) mud (Neumann and Land 1975; Macintyre and Reid 1992).

3.1.3 Secondary calcification

Euhedral aragonite needles that may grow to a lenght of more than 20 µm are found in the innermost parts of secondary inter-utricular spaces (sIUS). Their crystal shape is prismatic, elongated in the c-axes with a blunt end that is typical for abiotically precipitated aragonite (Weiner and Lowenstam 1986; Holcomb et al. 2009). As their specific location on top of MAC or primary needles suggests a subsequent formation after development of these features, here they are forthwith called "secondary needles" and their process of formation "secondary calcification". Photosynthesis (i.e., O_2 evolution) elevates the seawater pH and $CaCO_3$ saturation within the IUS (Borowitzka 1984; De Beer and Larkum 2001). Seawater $CaCO_3$ oversaturation thus may explain the formation of secondary needles (cf., infillings of conceptacles in red algae, Alexandersson 1974; Basso 2012). To form, these needles may rely on a nucleus of $CaCO_3$, as they are not found in close vicinity to the utricle wall and are not found in the IUS of early segments (day < 1). Additionally, they radiate in typical bundles of several needles from specific points of origin, such as a dense local accumulation of MAC or remnants of primary needles (e.g., Weiner and Lowenstam 1986).

Interestingly, secondary needles never show any accumulation of MAC and never are observed within the MAC (Macinytre and Reid 1995). Thus, it seems likely that the daily formation of new MAC, through recrystallization of primary needles at the cell wall of utricles, moves the MAC "front" from the utricle wall further into the open IUS thereby subsequently closing open IUS (Macintyre and Reid 1995). Thus, the MAC in the living algal segment might not represent a strong solid or rigid structure, but rather is porous and permeable, like a loosely attached fine-granular phase of micron-sized $CaCO_3$ crystals. Presumably, in addition to seawater filled micropores within the MAC, this characteristic also may be caused by soluble organic molecules (e.g., polysaccharides, matrix components) in-between the MAC crystals that keep those in a hydrous semifluid-like (amorphous?) phase. These MAC crystals then represent nucleation points for secondary needles. This is further supported by analyses via inductively coupled plasma optical emission spectrometry (ICP-OES) on the elemental composition of the purified $CaCO_3$ skeleton. Within the $CaCO_3$ skeletal structure of *Halimeda* sulfur was found incorporated that likely derives from sulfated

polysaccharides or glycoproteins from the organic matrix (preliminary work, data not shown; cf., Jacob et al. 2008). Only this consistence of the MAC may explain the observed progression pattern of MAC formation in agreement with the specific location of and observations on the occurrence of secondary needles in the IUS (i.e., always nucleating on top of MAC, never within MAC, no accumulation of MAC among secondary needles).

3.1.4 Ca^{2+} ion fluxes in the *Halimeda* skeleton

More evidence for the previously proposed explanations of the observed pattern of calcification may come from the study of Böhm and Goreau (1973) where radioactive labeled calcium ion (^{45}Ca) fluxes in different parts of the *Halimeda* skeleton were measured. Experiments conducted reveal that different parts of the skeleton exchange calcium ions at different rates with the seawater in the IUS. Thus the skeleton is divided into an "exchangeable phase" and a "phase of lesser exchangeability" with respect to calcium ions. In fact, these two phases may refer to two different skeletal features and their respective calcification processes as discussed before. The "exchangeable phase" may be regarded as the process of primary calcification with Ca^{2+} adsorbtion by acidic polysaccharides at the cell wall. The "lesser exchangeable phase" may be regarded as the micro-anhedral carbonate (MAC) formation from primary needles. The concentration of returned calcium ions from the "exchangeable" skeleton phase that subsequently become incorporated into the skeleton´s "lesser exchangeable phase", is higher when compared to dead algae (i.e., abiotic $CaCO_3$ precipitation) suggesting a metabolic-induced calcification process (i.e., MAC formation). Additionally, Böhm and Goreau (1973) proposed that crystallization may rather proceed in a mucilage or organic matrix and not along polysaccharide fibers, as was suggested by Wilbur et al. (1969). Observed random orientation of primary needles may argue against $CaCO_3$ crystallization along polysaccharides. However, occasionally also ordered crystal orientation was observed thus the exact mechanism of crystallization is still to debate.

3.1.5 Seawater metal ion ratio alteration (*m* Mg / Ca ratio); Further evidence for biotic calcification in macro-algae genus *Halimeda*

A fair example of the steering functions the organic matrix components of *Halimeda* may hold is the seawater metal ion ratio modification experiment by Stanley et al. (2010). The seawater magnesium / calcium (*m* Mg / Ca) ion ratio was reduced, thus subsequently abiotic $CaCO_3$ precipitation of the polymorph calcite was favored over the polymorph aragonite. A closer look at the SEM images on the crystal morphology and mineralogy of *Halimeda*

incrassata provided in Stanley et al. (2010), allow identification of aragonite needles even under seawater conditions that were called "calcite seas". Seawater *m* Mg / Ca ratio was reduced to 1.5 (from todays ratio of 5.2), however 54 % of the algal skeleton remained aragonite. To place these findings into context one should be aware, that biological calcification is in general tightly regulated by organic molecules, which control the initiation as well as $CaCO_3$ crystallization, including crystal morphology and mineralogy (e.g., Levi et al. 1988; Feng et al. 2000; Bonucci 2007; Arias and Fernández 2008; Weiss and Marin 2008; Salgado et al. 2011). For example, in a comparable experimental approach (although in vitro) with the calcifying acidic protein "Aspein" that is involved in the formation of calcite crystals in the prismatic shell layer of bivalves, Takeuchi et al. (2008) showed that in its presence calcite is precipitated even under a *m* Mg / Ca ion ratio that favors the abiotic precipitation of aragonite. Thus, I argue that the precipitation of calcite seen in the experiment of Stanley et al. (2010) is mostly abiotically (re-)precipitated micro-anhedral carbonate (MAC) that is formed in another process (cf. discussion on recrystallization and MAC formation, paragraph 3.1.2). Moreover, secondary calcification (i.e., formation of secondary aragonite needles under "ambient" Mg / Ca ratio) during daytime also may become altered into abiotic precipitation of the calcite $CaCO_3$ polymorph. These findings strongly indicate that the formation of primary needles in *Halimeda* and their $CaCO_3$ mineralogy is controlled by the alga and is not altered by the *m* Mg / Ca ion ratio of the seawater. Notably, Blättler et al. (2014), in conducting a similar experiment to Stanley et al. (2010), also proposed the existence of a first-order control on $CaCO_3$ precipitation and mineralogy in *Halimeda discoidea* that was inferred from Ca^{2+} isotope ratio measurements of the skeleton. These experiments revealed that the *Halimeda* skeleton exhibits a shift in the Ca^{2+} isotope ratio other than expected from Ca^{2+} incorporation of abiotic $CaCO_3$ precipitation. Thus, results of previous studies taken together strongly indicate a biotically-initiated and mineralogically-controlled primary calcification by polysaccharides and presumably proteins / enzymes at the cell wall and within the organic matrix present.

4. Manuscript II :

Ocean acidification alters the calcareous microstructure of the green macro-alga *Halimeda opuntia*

(2015) Wizemann A, Meyer FW, Hofmann LC, Wild C, Westphal H

Coral Reefs 34:941-954

DOI: 10.1007/s00338-015-1288-9

Statement of personal contribution

Manuscript writing:

I wrote the initial manuscript.

(Total contribution: 70%)

Laboratory work:

I helped in maintaining the auqaria and in designing the experimental setup.

I occasionally conducted water parameter measurements (pH, salinity, temperature).

(Total contribution: 30%)

Analyses:

I collected and prepared the samples and conducted scanning electron microscopy.

(Total contribution: 100%)

Idea:

I contributed to the initial idea of the experiment.

I developed the initial idea of the analyses and of the manuscript.

(Total contribution: 50%)

Coral Reefs (2015) 34:941–954
DOI 10.1007/s00338-015-1288-9

REPORT

Ocean acidification alters the calcareous microstructure of the green macro-alga *Halimeda opuntia*

André Wizemann[1] · Friedrich W. Meyer[1] · Laurie C. Hofmann[2] · Christian Wild[1,2] · Hildegard Westphal[1,3]

Received: 5 June 2014 / Accepted: 12 March 2015 / Published online: 20 March 2015

Abstract Decreases in seawater pH and carbonate saturation state (Ω) following the continuous increase in atmospheric CO_2 represent a process termed ocean acidification, which is predicted to become a main threat to marine calcifiers in the near future. Segmented, tropical, marine green macro-algae of the genus *Halimeda* form a calcareous skeleton that involves biotically initiated and induced calcification processes influenced by cell physiology. As *Halimeda* is an important habitat provider and major carbonate sediment producer in tropical shallow areas, alterations of these processes due to ocean acidification may cause changes in the skeletal microstructure that have major consequences for the alga and its environment, but related knowledge is scarce. This study used scanning electron microscopy to examine changes of the $CaCO_3$ segment microstructure of *Halimeda opuntia* specimens that had been exposed to artificially elevated seawater pCO_2 of ~650 µatm for 45 d. In spite of elevated seawater pCO_2, the calcification of needles, located at the former utricle walls, was not reduced as frequent initiation of new needle-shaped crystals was observed. Abundance of the needles was ~22 % μm^{-2} higher and needle crystal dimensions ~14 % longer. However, those needles were ~42 % thinner compared with the control treatment. Moreover, lifetime cementation of the segments decreased under elevated seawater pCO_2 due to a loss in micro-anhedral carbonate as indicated by significantly thinner calcified rims of central utricles (35–173 % compared with the control treatment). Decreased micro-anhedral carbonate suggests that seawater within the inter-utricular space becomes $CaCO_3$ undersaturated ($\Omega < 1$) during nighttime under conditions of elevated seawater pCO_2, thereby favoring $CaCO_3$ dissolution over micro-anhedral carbonate accretion. Less-cemented segments of *H. opuntia* may impair the environmental success of the alga, its carbonate sediment contribution, and the temporal storage of atmospheric CO_2 within *Halimeda*-derived sediments.

Keywords Ocean acidification · Biomineralization · Marine cementation · Carbonate sediments · SEM

Communicated by Biology Editor Dr. Anastazia Banaszak

Electronic supplementary material The online version of this article (doi:10.1007/s00338-015-1288-9) contains supplementary material, which is available to authorized users.

✉ André Wizemann
andre.wizemann@zmt-bremen.de

[1] Leibniz Center for Tropical Marine Ecology (ZMT), Fahrenheitstraße 6, 28359 Bremen, Germany

[2] Faculty of Biology and Chemistry, University of Bremen, Leobener Straße NW2, 28359 Bremen, Germany

[3] Faculty of Geosciences, University of Bremen, Klagenfurter Straße 2, 28359 Bremen, Germany

Introduction

Atmospheric greenhouse gases, such as CO_2, rapidly equilibrate in the ocean. An increase in the atmospheric CO_2 concentration thus leads to an increase in the CO_2 concentration of seawater, causing a process known as ocean acidification (Caldeira and Wickett 2003). Progressive ocean acidification reduces seawater pH and shifts seawater carbon chemistry, thereby decreasing seawater carbonate ion (CO_3^{2-}) saturation (Feely et al. 2004; Orr et al. 2005). The seawater carbonate saturation state (Ω) is an important parameter for the formation of calcium carbonate structures, as it determines whether calcium

carbonate ($CaCO_3$) precipitation or dissolution is favored (Kleypas et al. 1999). Calcifying organisms in the ocean thus may face severe consequences when the carbonate saturation state is lowered (Doney et al. 2009). However, calcification processes of most marine organisms are not well understood. For example, elevated seawater pCO_2 experiments on the calcification of marine micro-algae such as coccolithophores revealed species-specific responses of $CaCO_3$ structure formation (Riebesell 2004; Langer et al. 2006). Generally, $CaCO_3$ biomineralization in most, if not all, marine organisms is an enzyme-driven process, whereby the use of bicarbonate (HCO_3^-) is predominant (Bonucci 2007; Weiss and Marin 2008; Jury et al. 2010). As an increase in seawater pCO_2 shifts the equilibrium toward a higher availability of HCO_3^-, $CaCO_3$ biomineralization may be enhanced by moderate ocean acidification in organisms where the ionic composition of the extracellular calcifying matrix or fluid is influenced by seawater. In contrast, abiotic $CaCO_3$ precipitation is negatively affected by elevation of seawater pCO_2 as seawater $CaCO_3$ saturation is consequently reduced (e.g., Morse et al. 2007; Stanley 2008).

Tropical marine calcifying green macro-algae of the genus *Halimeda* likely exhibit biotic induction of calcification, as external carbonic anhydrase activity is present (Borowitzka and Larkum 1976; Hofmann et al. 2014). Nevertheless, the formation of the algal calcareous skeleton of the $CaCO_3$ polymorph aragonite is also influenced by its physiology, which causes diurnal shifts in the seawater carbon chemistry in the inter-utricular space (Macintyre and Reid 1995; De Beer and Larkum 2001). Thereby, the extracellular calcareous microstructure is formed in semi-enclosed open spaces between the algal cells, i.e., tube-like filaments called utricles. The open space between these utricles is thus referred to as inter-utricular space. The formation of the $CaCO_3$ segment microstructure involves several time-dependent steps described by Macintyre and Reid (1995) and refined by Wizemann et al. (2014). The occurrence of different skeletal features (i.e., primary needles, micro-anhedral carbonate, secondary needles) is the result of complex interactions between physiological processes (i.e., photosynthesis and metabolism) and environmental parameters (e.g., seawater carbon chemistry, light availability, temperature).

With the formation of the extracellular calcareous skeleton likely driven by a combination of biotic and abiotic calcification processes, influenced by both cell physiology and seawater parameters, *Halimeda* is a model organism for studying the effects of ocean acidification on calcification in its entirety. Thus, the distinct formation of the calcareous skeletal microstructure and the importance of the genus *Halimeda* as a major carbonate sediment producer and bioherm builder have lead to several studies that assessed effects of ocean acidification on its calcification (Robbins et al. 2009; Ries et al. 2009, Ries 2011; Sinutok et al. 2011, 2012; Price et al. 2011; Hofmann et al. 2014). Whereas most studies have focused on the physiological response and the subsequent change of total calcification (total algal $CaCO_3$ content), little is known regarding alterations of the skeletal microstructure of *Halimeda* due to shifts in seawater carbon chemistry. The focus of this study is to identify alterations of the internal skeletal $CaCO_3$ microstructure of the species *Halimeda opuntia* that result from an elevation of seawater pCO_2.

Study organism

Halimeda opuntia (Lamouroux 1816) is a cosmopolitan marine macro-alga of tropical shallow seas. Macro-algae of the genus *Halimeda* exhibit a segmented, branched growth habit whereby the algae form calcareous segments of the $CaCO_3$ polymorph aragonite (Hillis-Colinvaux 1980; Macintyre and Reid 1995; Stanley et al. 2010; Fig. 1a). Because of a rapid growth rate of up to one segment per day on each branch, the genus *Halimeda* is one important $CaCO_3$ sediment producer in tropical coral reef environments (Wefer 1980; Drew 1983; Hine et al. 1988; Multer 1988; Freile et al. 1995; Rees et al. 2007; Wienberg et al. 2010). Within the genus of *Halimeda*, the species *H. opuntia* morphologically defines the lineage Opuntia (Hillis 2001; Verbruggen and Kooistra 2004). Generally, taxa of this lineage are characterized by the absence of a bulbous holdfast, but possess thin root-like filaments with which they are able to attach primarily to hard substrates. Thus, *Halimeda* species of the lineage Opuntia are often found in coral reef environments (Hillis-Colinvaux 1980; Johns and Moore 1988).

Materials and methods

Experimental setup

Macro-algae of the species *H. opuntia* from reefs of Cebu (Philippines, purchased from Marina Fauna Inc.®) were brought to the marine experimental facility of the Leibniz Center for Tropical Marine Ecology (ZMT) in Bremen (Germany). The algae were acclimatized for 1 month to laboratory seawater conditions (approx. temperature 27 °C, salinity 35 PSU, light regime 150 µmol photons m^{-2} s^{-1}). After acclimatization, the algae were placed into mesocosms (265-l) with carbonate live sand (Ocean Direct®) as substrate. A total of five algae were placed in each of six mesocosms. The mesocosms were fully closed (however, with an open water-filtering system) and equipped with an electronically controlled gas-mixing system (HTK®

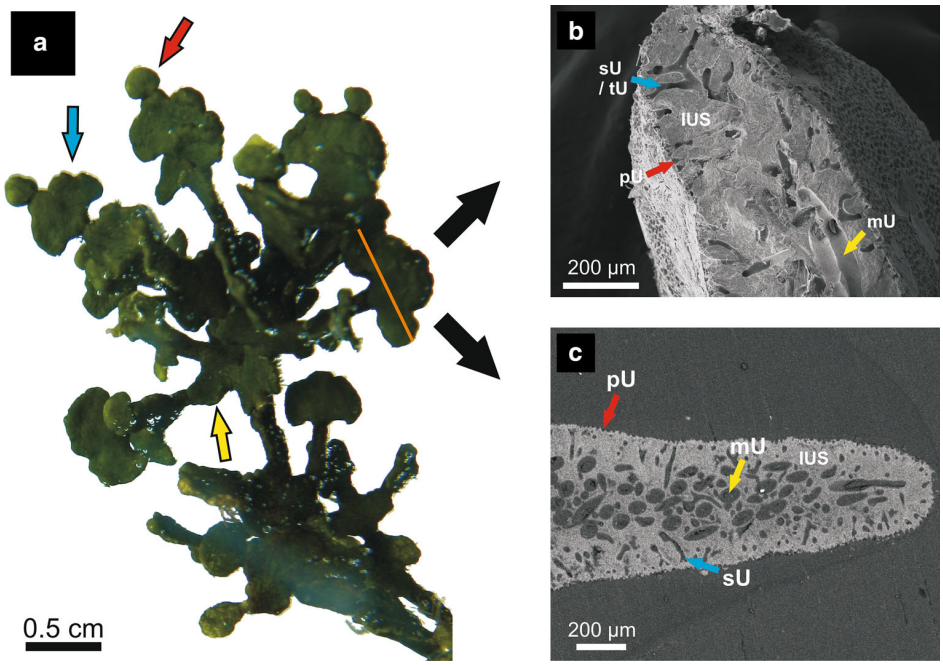

Fig. 1 Segmented *green* macro-alga *Halimeda opuntia*. **a** Growing alga with young segments (<2 d; *red arrow*), mature apical segments (2–7 d; *blue arrow*), and mature mid-growth segments (>7 d; *yellow arrow*). The *orange line* indicates the cutting plane of a segment when prepared for scanning electron microscope (SEM) analyses. **b** SEM image (via SE) of a stub sample from a segment cut in the middle plain. **c** SEM image (via BSE) of a thin section from a segment cut in the middle plane. U = utricle (p = primary, s = secondary, t = tertiary, m = medullary); IUS = inter-utricular space

Hamburg; pure CO_2 provided by Linde® Gas) that premixes air with pure CO_2 to adjust the pCO_2 concentration of the outflow air. On the gas-mix system, the pCO_2 level of the outflow air was set to 400 ppm (ambient air pCO_2) for three mesocosms of the control treatment and to max output provided by the system of >1500 ppm (elevated air pCO_2) for the three mesocosms of the high-pCO_2 treatment. The premixed air was directly bubbled into the mesocosms; no negative feedback mechanism regarding the actual equilibrated seawater pCO_2 was implemented (i.e., no stat system was used). T5 light bulbs switched in a 12/12 h d/night cycle provided a moderate light regime of 150 µmol photons m^{-2} s^{-1}. Artificial seawater (SW) was used both for acclimatization and the experiment in the mesocosms.

Artificial seawater preparation

The artificial SW was prepared in a 35,000-l tank with tap water prefiltered and UV sterilized using reverse-osmosis purification technique prior to filling the mesocosms. The salinity of the water in the tank was then adjusted to 35 (PSU). As the sea salt (custom made; Electronic Supplementary Materials, ESM, Table S1) that was used for artificial seawater preparation exhibited an unnatural high total alkalinity (A_T) of >3000 µmol kg^{-1} SW, the A_T of the artificial seawater in the tank was initially reduced to 2200 ± 100 µmol kg^{-1} SW with HCl (1 N), i.e., to an A_T range typical for tropical surface ocean waters in the Pacific region (e.g., Takahashi et al. 1981). The water was given adequate residual time of more than 2 weeks in the 35,000-l tank for proton/pH equilibration through outgassing of CO_2 prior to the start of the experiment (Riebesell et al. 2010).

Measurements of chemical and physical seawater parameters

During the experiment, seawater A_T of the mesocosms was measured twice per week with an automated titrator (SI Analytics®, TitroLine Alpha Plus) with an A_T standard provided by A.G. Dickson (batch 111) as certified reference material (Dickson et al. 2003, 2007). Seawater A_T in the mesocosms was re-adjusted to 2200 ± 100 µmol kg^{-1} SW by the addition of $NaHCO_3$ solution with a peristaltic pump during the experiment, when required. Temperature (T), salinity (S), and pH (NBS scale) were monitored multiple times a day, during daylight, with a multi-probe (WTW® Multi 3410, SenTix® ORP 900 pH probe, TetraCon® 925 conductivity probe). The pH probe was calibrated using two-point calibration with standard NBS buffer solutions (WTW®) for pH 4.01 and 7.

Seawater carbon chemistry

Measured seawater parameters (T, S, A_T, and pH_{NBS}) were used to calculate carbon chemistry and the respective $CaCO_3$ saturation state (Ω) of the seawater in the mesocosms with the program CO_2SYS (Pierrot et al. 2006; Table 1). Based on calculations, seawater in the three

Table 1 Measured seawater (SW) parameters (mean ± SD) and calculated SW carbon chemistry (via CO_2SYS; Pierrot et al. 2006) of control treatment (ambient pCO_2) and high-pCO_2 treatment (elevated pCO_2) mesocosms ($n = 3$)

Mesocosm	T (°C)	S (PSU)	pH_{NBS}	A_T	pCO_2	CO_2	HCO_3^-	CO_3^{2-}	Ω_{arag}	Ω_{cal}
1 (ambient)	25.9 ± 0.4	35.6 ± 0.2	8.15 ± 0.04	2053 ± 125	385 ± 28	11 ± 0.5	1587 ± 65	185 ± 35	2.9 ± 0.4	4.4 ± 0.6
2 (ambient)	26.4 ± 0.4	35.3 ± 0.1	8.15 ± 0.04	2287 ± 160	434 ± 15	12 ± 0.6	1775 ± 92	208 ± 31	3.3 ± 0.5	5.0 ± 0.7
3 (ambient)	26.3 ± 0.4	35.1 ± 0.5	8.15 ± 0.02	2208 ± 54	418 ± 15	12 ± 0.3	1714 ± 19	199 ± 15	3.2 ± 0.2	4.8 ± 0.3
1 (elevated)	26.3 ± 0.3	35.4 ± 0.3	8.01 ± 0.04	2159 ± 121	600 ± 31	16 ± 0.5	1782 ± 73	152 ± 22	2.4 ± 0.3	3.6 ± 0.5
2 (elevated)	26.2 ± 0.2	35.3 ± 0.2	7.98 ± 0.01	2119 ± 143	638 ± 18	17 ± 0.5	1770 ± 114	140 ± 14	2.2 ± 0.2	3.4 ± 0.4
3 (elevated)	26.2 ± 0.1	35.6 ± 0.3	7.97 ± 0.03	2280 ± 79	705 ± 34	20 ± 0.3	1914 ± 44	149 ± 15	2.4 ± 0.3	3.6 ± 0.4

Temperature (T), salinity (S), pH_{NBS}, and total alkalinity (A_T) were measured (at daytime). Carbon chemistry was calculated using $K1$, $K2$ constants from Merbach et al. (1973) refit by Dickson and Millero (1987). A_T and carbon species are given in μmol kg^{-1} SW, seawater pCO_2 in μatm. Ω = calculated $CaCO_3$ saturation state (arag = aragonite; cal = calcite)

mesocosms of the control treatment and the three mesocosms of the high-pCO_2 treatment reached a mean equilibrated pCO_2 in the range of 400 ± 50 μatm (ambient pCO_2; daylight) and 650 ± 50 μatm (elevated pCO_2; daylight), respectively. Natural fluctuations of the equilibrated seawater pCO_2 and seawater carbon chemistry are likely due to outgassing of CO_2 (10 % water exchange per week and open water-filtering system), photosynthesis (daytime)/respiration (nighttime) cycle of the mesocosm community (sediment, algae, epibionts), and the absence of a negative feedback mechanism to the gas-mix system. Calculated seawater pCO_2 and carbon species concentrations for the seawater in the mesocosms may be slightly off, as pH_{NBS} measurements used for calculations of seawater carbon chemistry are especially subject to drift (e.g., Riebesell et al. 2010). Direct measurements of the equilibrated seawater pCO_2 were not conducted.

Sampling

The algae were collected from the mesocosms after 45 d of growth, briefly rinsed with distilled water, and oven-dried at 35 °C for 48 h. Afterward, young segments (<2 d; $n = 9$), well-developed apical segments (2–7 d; $n = 9$), and mature mid-growth segments (>7 d; $n = 9$) were collected randomly from algae in each mesocosm for further analyses (Fig. 1a; ESM Table S2). The approximate segment age was visually determined from growing "branches" of the algae as illustrated in Fig. 1a. Due to the experimental duration (45 d) and the visually observed segment growth rate of the algae (2–3 segments per week on each branch), sampling of older, pre-existing segments was excluded. Algae were not stained as staining may disturb the mesocosm microbial sediment and epibiont communities, which would hamper the mesocosm approach (i.e., natural shifts in seawater carbon chemistry due to community respiration and photosynthesis; cf. alizarin and corals, Dodge et al. 1984). Additionally, all mature segments sampled (2–7 d and >7 d) showed the sun-leaf segment morphotype of *H. opuntia* (i.e., "butterfly-like" or "fan-like" segment shape; cf. Fig. 1a), as light intensity (i.e., photosynthesis vs. respiration rate) influences the segments grade in $CaCO_3$ density (i.e., micro-anhedral carbonate content; Macintyre and Reid 1995; pers. obs.).

Sample preparation for SEM analyses

Stub samples

Segments were cut in the middle plane with a razor blade and mounted on a stub with conductive glue, fractured surface facing upwards (Fig. 1a). They were gold sputtered and analyzed with a scanning electron microscope (TESCAN® VEGA3 XMU) with the secondary electron (SE) detector at 2.5, 6, and 10 keV (Fig. 1b).

Thin sections

Segments were embedded in epoxy and cut in the middle plane. Afterward, they were polished to ~35 μm, gold sputtered, and analyzed with an SEM with the detector for back-scattered electrons (BSE) at 10 keV (Fig. 1c).

Organics were not removed in order to allow identification of internal microstructural features. Organics were lost in some cases due to the preparation technique.

Microstructural analyses

Primary needle abundance and dimensions

Primary needle abundance and dimensions within central medullary utricles were obtained from SEM images with ImageJ. To measure needle abundance, a 100-μm^2 area was defined randomly and further subdivided into 16 squares of 6.25 μm^2 each. All needles within the squares were point-

counted, and the mean crystal density per μm^2 was calculated. This was carried out for three independent segments of each mesocosm from the control treatment and the high-pCO_2 treatment. Several medullary utricles (>5) within each segment were screened to ensure that areas counted showed needle densities representative of the whole segment.

To obtain needle dimension, the length and width were measured for 20 randomly and independently selected primary needles of central medullary utricles within a randomly selected area of 200 μm^2 of four independent apical segments (from different alga and/or mesocosm) from the control treatment and the high-pCO_2 treatment. Mean values and standard deviations were calculated. Only needles were measured whose extents and especially termini (for width determination) were mostly visible in the SEM images. In case crystals exhibited a polygonal shape, the longer axis of the crystal blunt end (terminus) was measured to determine needle width. However, the line of view to determine crystal extents on the SEM images often was not parallel due to individual needle growth direction; thus, measurements of crystal dimension are biased to some degree. To make sure that other medullary utricles showed a similar crystal habit, numerous areas of each segment were screened (>5).

Thickness of micro-anhedral carbonate utricle rims

The thickness of micro-anhedral carbonate rims around central medullary utricles from three segments at three consecutive maturation stages (<2, 2–7, >7 d; Fig. 1a; ESM Table S1) from both treatments was measured from SEM images of thin sections using ImageJ. Therefore, ten measurements distributed randomly but radially around each utricle were obtained. Visual screening of numerous utricles (>5) of each segment ensured that representative areas were chosen.

Statistical analyses

All statistical calculations were carried out with the program Sigma Plot® from raw measurement data. Between-group differences in primary needle abundance per μm^2 between control treatment and high-pCO_2 treatment algae were tested using a one-way ANOVA. Additionally, a pairwise multi-comparison analysis (Holm–Sidak method) was run to analyze significant in-group differences between the control treatment and the high-pCO_2 treatment groups. To check for significant differences in primary needle width and length and to compare the thickness of MAC utricle rims of all stages of segment maturation (<2, 2–7, >7 d; Fig. 1a) between the control treatment and the high-pCO_2 treatment, a paired *t* test was done. As the normality test failed with the data obtained from the early segment stages (<2 d) a Wilcoxon signed-rank test was performed for this group instead.

Results

The terms used for the description of the $CaCO_3$ segment microstructure follow Macintyre and Reid (1995) as refined by Wizemann et al. (2014).

Primary needles

Primary needles form directly at the external cell walls of utricles facing into the inter-utricular space and are the first $CaCO_3$ precipitated by the alga. They are up to 5 µm in length, often exhibit smooth edges with a roundish tip when newly formed, and may completely fill up the primary inter-utricular space of younger segments.

In apical segments grown under ambient seawater pCO_2, the inter-utricular space was densely filled with $CaCO_3$ (Fig. 2a); especially, within the primary inter-utricular space, but also to some extent within the secondary inter-utricular space, primary needles were abundant and the dominant needle type (Fig. 2b, c, d). In apical segments from algae of the high-pCO_2 treatment, the observation of primary needles was limited to an appearance on the utricle walls and partially to the primary inter-utricular space (Fig. 3b, c). In these segments, the $CaCO_3$ density of the inter-utricular space was not as pronounced as in segments of the control treatment (cf. Fig. 2a and 3a). Under elevated seawater pCO_2, apical segments are characterized by open inter-utricular space (Fig. 3b, d). On primary utricle walls of young segments (<2 d) grown under elevated pCO_2, a high abundance and density of $CaCO_3$ nuclei was observed (ESM Fig. S2a).

Primary needle abundance and dimensions

Apical segments of the control treatment and the high-pCO_2 treatment showed differences in primary needle abundance and dimensions (width and length; Fig. 4a, b and ESM Fig. S1a, b). In segments from the high-pCO_2 treatment, primary needle abundance measured per μm^2 was significantly higher (22 ± 7 %; $p < 0.001$; ESM Table S3). In segments of the high-pCO_2 treatment, primary needles investigated were 42 % (±21 %) thinner and 14 % (±6 %) longer (paired *t* test, $p < 0.001$ and $p < 0.05$, respectively; Fig. 4a, b; ESM Table S3). There was no significant in-group difference of needle abundance (pairwise multiple comparison test, $p > 0.05$) within the control treatment or the high-pCO_2 treatment group.

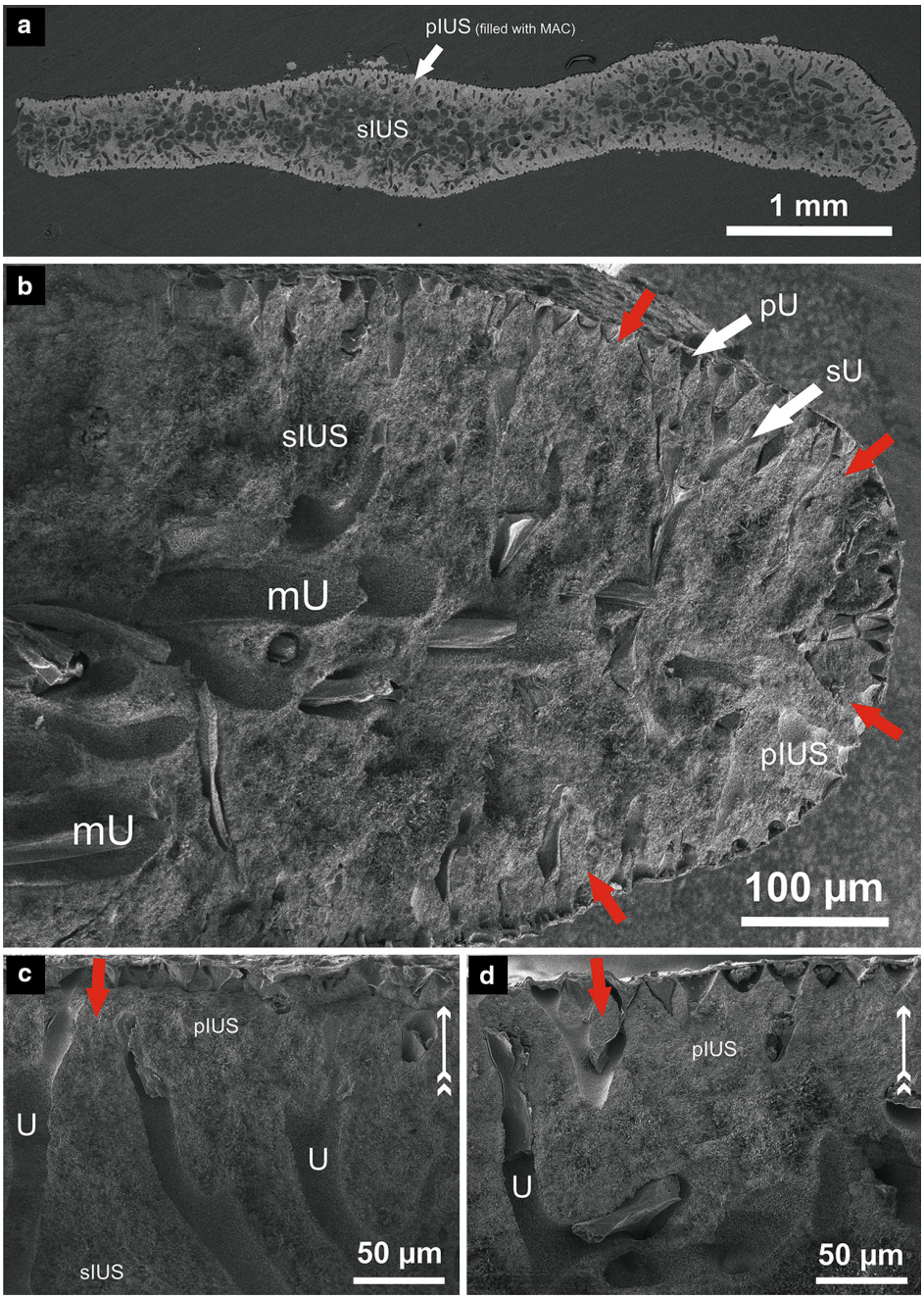

Fig. 2 SEM analyses of the $CaCO_3$ microstructure of an apical segment at ambient seawater pCO_2 (control treatment). **a** Cross-sectional overview of the microstructure of a complete segment (thin section via BSE). **b** Magnification from the tip of a segment showing the location of inter-utricular space (IUS) and utricles (*U*). Note the early stage of micro-anhedral carbonate formation (e.g., *red arrows*). **c**, **d** Detailed analyses of the primary inter-utricular space (pIUS) to illustrate stage of micro-anhedral carbonate density (=primary cementation; e.g., *red arrows*). *White arrows* indicate direction to segment surface. U = utricle (*p* = primary, *s* = secondary, *m* = medullary); IUS = inter-utricular space (*p* = primary, *s* = secondary)

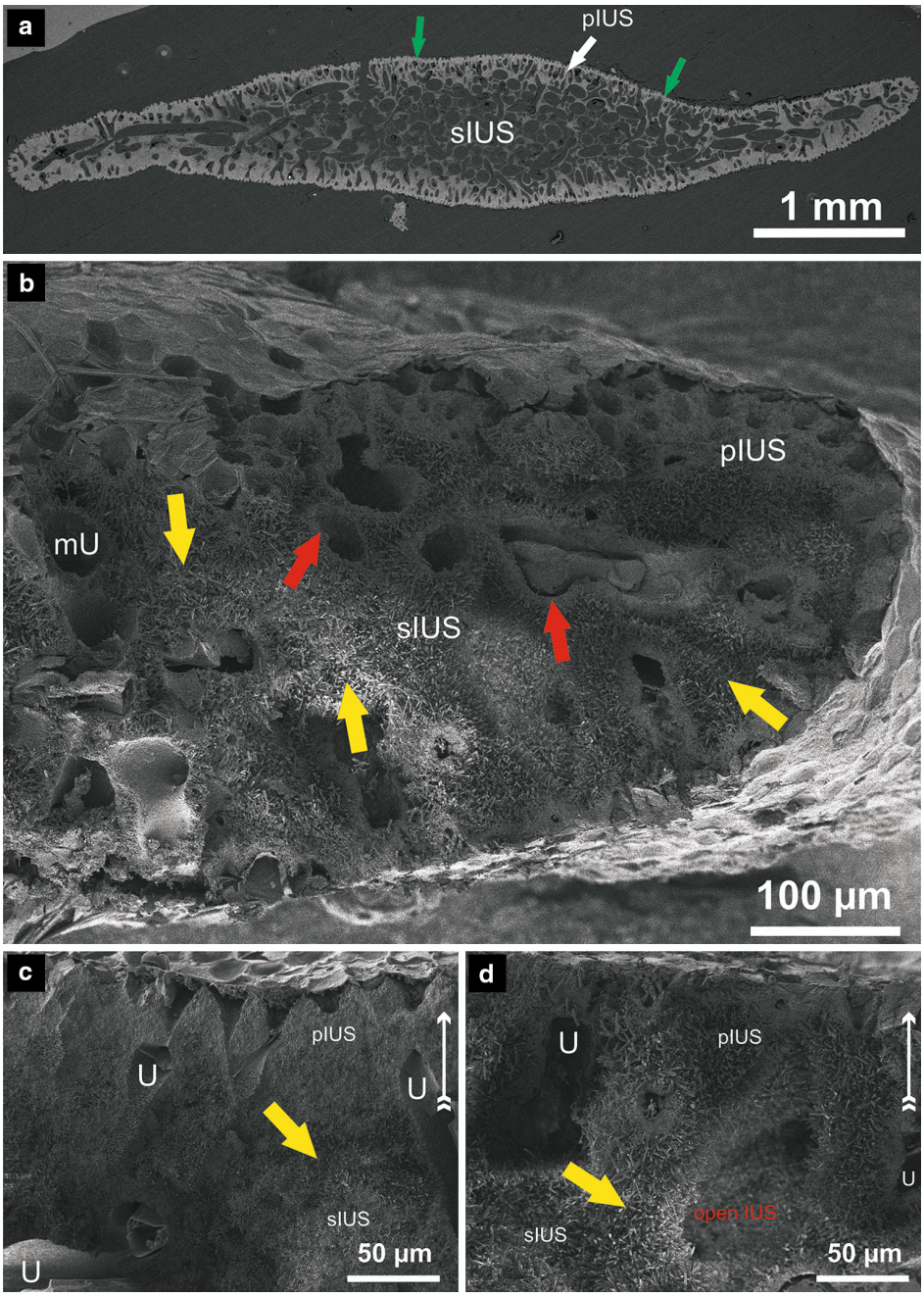

Fig. 3 SEM analyses of the $CaCO_3$ microstructure of an apical segment under elevated seawater pCO_2 (high-pCO_2 treatment). **a** Cross-sectional overview of the microstructure of a complete segment (thin section via BSE). Note the thin calcified segment rim (*green arrows*; cf. Fig. 2a). **b** Magnification from the tip of a segment showing the location of utricles (*U*) and inter-utricular space (IUS). Note that micro-anhedral carbonate (MAC) is mostly limited to utricle rims (e.g., *red arrows*) and the high abundance of secondary needles (e.g., *yellow arrows*; cf. Fig. 2b) in the inter-utricular space. **c**, **d** Detailed analyses of the primary inter-utricular space (pIUS) illustrate a lack of micro-anhedral carbonate density (=primary cementation; cf., Fig. 2c, d). Note the high abundance of secondary needles within the primary inter-utricular space (pIUS) and the open space within the secondary inter-utricular space (sIUS) observed in (**d**) (e.g., *yellow arrows*). *White arrows* indicate direction to segment surface. *U* = utricle (*m* = medullary); IUS = inter-utricular space (*p* = primary, *s* = secondary)

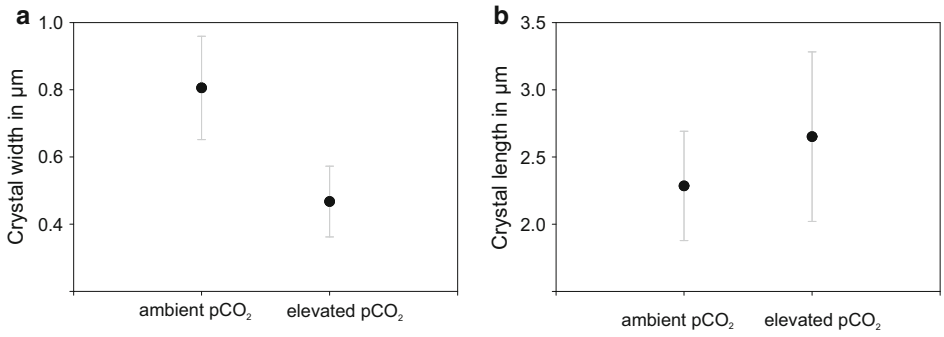

Fig. 4 Dimensions of primary needle single crystals that formed on the external cell wall of medullary utricles of segments from the control treatment (ambient pCO_2) and the high-pCO_2 treatment (elevated pCO_2). Shown in **a** is the mean (±SD) crystal width and in **b** the mean (±SD) crystal length

Primary cementation (micro-anhedral carbonate formation)

The grade of segment lifetime cementation (i.e., primary cementation) that is caused by the formation of micro-anhedral carbonate is an indicator for the overall calcification of the alga (Wizemann et al. 2014). Thus, the more micro-anhedral carbonate that is formed, the more heavily calcified is the carbonate skeleton of the algal segment. Generally, micro-anhedral carbonate is most pronounced in the primary inter-utricular space and at the central utricle rims. As the name indicates, micro-anhedral $CaCO_3$ crystals are micron-sized and of anhedral shape.

The primary inter-utricular space of apical segments from the control treatment was completely filled with micro-anhedral carbonate (Fig. 2a, b). The secondary inter-utricular space of these segments was partly filled with micro-anhedral carbonate (Fig. 2b, c, d). Micro-anhedral carbonate within the inter-utricular space of apical segments grown under elevated seawater pCO_2 was less developed than that in apical segments from the control (Fig. 3a, b). The secondary inter-utricular space was not densely filled with $CaCO_3$ in segments of algae grown under elevated seawater pCO_2 (Fig. 3c, d).

Growth-time series

In a growth-time series, segments sampled in consecutive order from a "branch" in the control treatment seemed to gain overall density in $CaCO_3$ with increasing segment age (Fig. 5a–f). In segments from the high-pCO_2 treatment, the secondary inter-utricular space was gradually less filled with micro-anhedral carbonate equivalent to an increase in segment size and thus increase in segment age (Fig. 5g–l).

Cementation of central utricle rims Central medullary utricles (mU) within the secondary inter-utricular space of segments from the control treatment showed thick $CaCO_3$ rims of micro-anhedral carbonate. The rim of micro-anhedral carbonate gains thickness with segment age, as seen in SEM images of the growth-time series (Fig. 5a, c, e). The micro-anhedral carbonate rims of central medullary utricles within the secondary inter-utricular space in segments of the high-pCO_2 treatment were thinner when segments of similar age were compared (Fig. 5). In young segments (<2 d), micro-anhedral carbonate thickness of utricle rims from segments in the control treatment was 35 ± 6 % higher than in segments from the high-pCO_2 treatment (Wilcoxon signed-rank test, $p < 0.05$). In older, mature segments (2–7, >7 d), the difference in micro-anhedral carbonate thickness was significant (paired t test, $p < 0.001$). The micro-anhedral carbonate utricle rim was 152 ± 12 % (2–7 d) to 173 ± 27 % (>7 d) thicker in mature segments from the control treatment than from the high-pCO_2 treatment. Medullary utricle rims of mature segments from the high-pCO_2 treatment did not show thicker layers of micro-anhedral carbonate than that of young apical segments (Fig. 5g, i, k).

Cementation of segment rims In segments from the control treatment, segment rims of micro-anhedral carbonate seemed to extend in dimension with proceeding segment maturation (Fig. 5b, d, f). Additionally, an extensive area of the secondary inter-utricular space was filled with micro-anhedral carbonate in mature mid-growth segments (Fig. 5f). In segments of the treatment, the micro-anhedral carbonate rim was well developed in young segments (<2 d; Fig. 5h), but did not seem to increase in its extent when compared with apical (2–7 d) and mature mid-growth segments (>7 d; Fig. 5j, l).

Secondary needles

Secondary needles are long euhedral orthorhombic $CaCO_3$ crystals (typically of more than 20 µm length) that face and grow into the inner inter-utricular space.

Within the inter-utricular space of segments from the control treatment, secondary needles were less abundant, shorter, and only observed within the secondary inter-

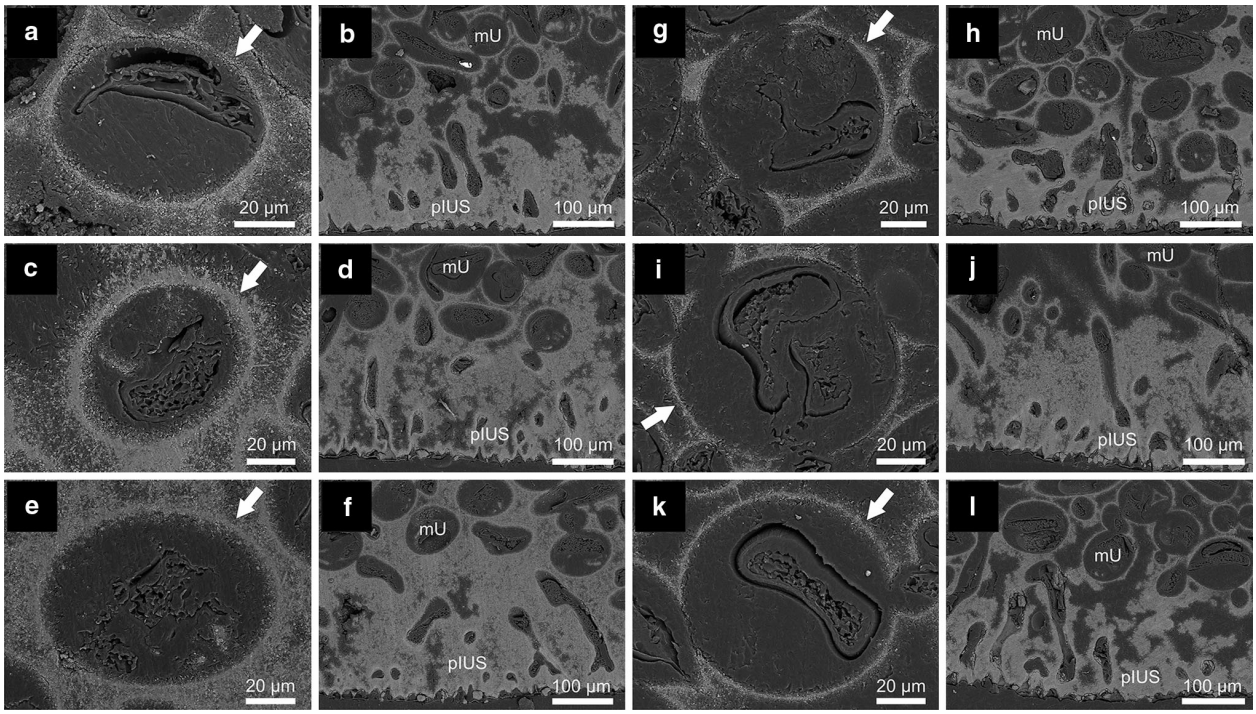

Fig. 5 SEM thin-section analyses (via BSE) of segments sampled in consecutive order from a "branch" grown under **a–f** ambient seawater pCO_2 and **g–l** elevated seawater pCO_2. Segment age for (**a** and **b**, **g** and **h**) <2 d, (**c** and **d**, **i** and **j**) 2–7 d, (**e** and **f**, **k** and **l**) >7 d (cf., ESM Table S2). **a**, **c**, **e** Micro-anhedral carbonate rims of central medullary utricles (mU) from segments of increasing maturation and **b**, **d**, **f** corresponding primary inter-utricular space (pIUS). Same order for **g**, **i**, **k** and **h**, **j**, **l** for the elevated seawater pCO_2, respectively. *White arrows* in **a**, **c**, **e**, **g**, **i**, **k** indicate micro-anhedral carbonate rims of medullary utricles. Note the decreasing $CaCO_3$ density of the inter-utricular space and the low accumulation of micro-anhedral carbonate at the rims of utricles with increasing segment maturation as shown in segments grown under elevated seawater pCO_2 **g–l**. mU = medullary utricle; pIUS = primary inter-utricular space

utricular space (Fig. 2b, c, d). In apical segments from the high-pCO_2 treatment, a high abundance of long secondary needles was observed within the secondary inter-utricular space (Fig. 3b). Moreover, secondary needles were also observed within parts of the primary inter-utricular space (Fig. 3d). In some cases, secondary needles were found directly on top of primary needles; no layer of micro-anhedral carbonate was visible (ESM Fig. S3a). Additionally, thin sections showed that secondary needles form a major part of the calcified skeleton of segments from the high-pCO_2 treatment (ESM Fig. S3b).

Discussion

Strong shifts in seawater pH and $CaCO_3$ saturation (Ω) naturally occur within the inter-utricular space as a result of physiological day and night cycles of the algal cell metabolism and influence the formation of the segment $CaCO_3$ microstructure (Macintyre and Reid 1995; De Beer and Larkum 2001). In the following paragraphs, the additional effect of elevated seawater pCO_2 on the development of each microstructural feature in the segment is discussed separately.

Primary calcification under elevated seawater pCO_2

Our observations of a high abundance of small, thin primary needles and numerous nuclei within the organic matrix of a primary utricle are consistent with previously reported effects of elevated seawater pCO_2 on *Halimeda* (Robbins et al. 2009; Sinutok et al. 2011). Primary calcification may be driven by organic matrix components and involve external carbonic anhydrase activity (Wizemann et al. 2014). Hofmann et al. (2014) showed that an increase in seawater pCO_2 leads to an elevation of external carbonic anhydrase activity in *H. opuntia*. If the product of external carbonic anhydrase is HCO_3^- that is used by calcifying proteins in $CaCO_3$ biomineralization (Bonucci 2007; Weiss and Marin 2008; Bertucci et al. 2013), it is likely that primary needle formation is actively enhanced. Additionally, the fast removal of CO_2 from the inter-utricular space through external carbonic anhydrase activity elevates the seawater $CaCO_3$ saturation (Ω) and the pH sufficiently to

sustain daytime calcification under moderately elevated seawater pCO_2.

Primary cementation (micro-anhedral carbonate formation) under elevated seawater pCO_2

Less micro-anhedral carbonate was observed within the inter-utricular space of apical and mature segments, as well as along utricle walls of segments grown under elevated seawater pCO_2 when compared to segments from the control treatment. Primary needle recrystallization and $CaCO_3$ re-precipitation that both cause micro-anhedral carbonate formation are most likely initiated and driven by exhaled respiratory CO_2 (Macintyre and Reid 1995; Wizemann et al. 2014). Micro-anhedral carbonate formation may strongly depend on the carbonate saturation state (Ω) of the seawater that enters the inter-utricular space. Presented results suggest that $CaCO_3$ oversaturation ($\Omega_{arag} > 1$) necessary for significant nighttime micro-anhedral carbonate accretion is no longer reached when seawater pCO_2 is elevated >650 µatm (cf., Vogel et al. 2015a, b). Thereby, the onset of $CaCO_3$ dissolution likely is caused by seawater $CaCO_3$ undersaturation ($\Omega_{arag} < 1$) inside the inter-utricular space, due to the fact that the combination of seawater pCO_2 and CO_2 from metabolism determines the $CaCO_3$ saturation state within the inter-utricular space. Additionally, species-specific respiratory activity of *H. opuntia* is significantly higher than that of other *Halimeda* species (ESM Table S4). That may cause onset of $CaCO_3$ dissolution and negative effects on micro-anhedral carbonate formation in *H. opuntia* even at moderately elevated seawater pCO_2. However, the extent to which seawater pCO_2 affects micro-anhedral carbonate formation depends on the respiratory activity of each individual alga and naturally differs under varying environmental conditions (e.g., water depth/light regime) and with other environmental stressors (e.g., seawater temperature). Furthermore, endolithic microbes are likely present within the inter-utricular space and the $CaCO_3$ skeletal structure (Macintyre and Reid 1995; Reyes-Nivia et al. 2014). These most certainly play an additional role in the add-up of metabolic-derived CO_2 and thus are an important steering factor for micro-anhedral carbonate formation to consider. Thus, a very complex multifactorial system influences the seawater $CaCO_3$ saturation (Ω) within the inter-utricular space that determines whether micro-anhedral carbonate accretion or $CaCO_3$ dissolution occurs.

Secondary calcification under elevated seawater pCO_2

High abundance of euhedral secondary needles was observed within the inter-utricular space in apical segments grown under elevated seawater pCO_2. Comparison between secondary needle dimensions in apical segments from both treatments indicates that under elevated seawater pCO_2 secondary needles are larger in size. Even so, this is likely caused by higher availability of open space within the inter-utricular space under elevated seawater pCO_2; it also emphasizes that despite elevated seawater pCO_2 the $CaCO_3$ saturation of the seawater in the inter-utricular space is sufficient for crystallization during photosynthesis. In some cases, secondary needles were observed initiating on top of primary needles without a micro-anhedral carbonate layer present, which deviates from identified calcification patterns of different *Halimeda* species that grew in unmodified seawater carbon chemistry (e.g., Weiner and Lowenstam 1986; Multer 1988; Macintyre and Reid 1995; Wizemann et al. 2014). However, discussed impacts of elevated seawater pCO_2 on micro-anhedral carbonate formation may explain this observation.

Alteration of the *Halimeda* segment $CaCO_3$ microstructure under ocean acidification

Wizemann et al. (2014) shows a schematic drawing of the development of the calcareous microstructure in the *Halimeda* segment that is based on Macintyre and Reid (1995). Here, it is modified to illustrate and compare the formation of the $CaCO_3$ segment microstructure with alterations observed under elevated seawater pCO_2 and lowered $CaCO_3$ saturation (Fig. 6).

Microstructural daytime processes in the segment under elevated pCO_2

During daytime, the formation of primary needles in an organic matrix at the external utricle wall represents the onset of segment calcification (Fig. 6 Ia, Ib). Under elevated pCO_2, a higher density of needles and longer needles are observed (Fig. 6 Ib; cf., ESM Figs. S1, S2a). Thus, the process of their formation might be stimulated by the shift in seawater carbon chemistry that enhances active primary calcification. CO_2 is a substrate for external carbonic anhydrase (eCA). It has been shown that external carbonic anhydrase activity in several calcifying macroalgae, including *H. opuntia*, increases under elevated seawater pCO_2 (Hofmann et al. 2013, 2014). The use of CO_2 via external carbonic anhydrase activity and CO_2 cell uptake allow the $CaCO_3$ saturation state in the inter-utricular space to reach a similar level as under ambient seawater pCO_2. Consequently, abundant growth of secondary needles is observed in segments grown under elevated pCO_2 (Fig. 6 IIIb, cf. Fig. 3).

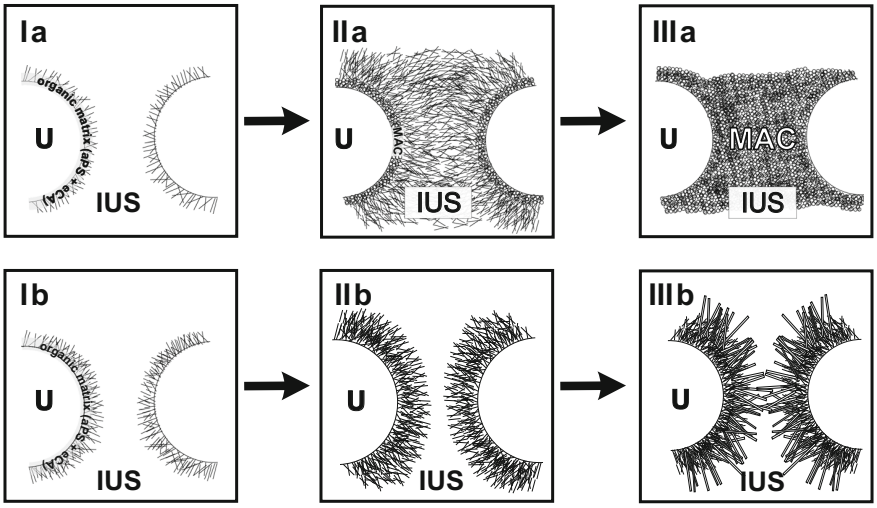

Fig. 6 Schematic drawing of the $CaCO_3$ microstructural segment development in the genus *Halimeda* lineage Opuntia; **Ia–IIIa** under ambient conditions and **Ib–IIIb** when altered under elevated seawater pCO_2 (modified from Wizemann et al. 2014 and references therein). **Ia** Primary needles form actively in an organic matrix at the external utricle wall. **IIa** Primary needles may completely fill in open inter-utricular space. Micro-anhedral carbonate (MAC) forms in vicinity of utricle walls out of recrystallized primary needles. **IIIa** Inter-utricular space (IUS) may become completely filled up with micro-anhedral carbonate (MAC), leading to a primary cementation of the segment. Potential formation of secondary needles in innermost secondary inter-utricular space (sIUS), which is in strong dependency to the availability of open space, is not shown in this illustration (cf., Wizemann et al. 2014). **Ib** Abundant and longer primary needles form actively in an organic matrix at the external utricle wall. **IIb** Proceeding active calcification fills inter-utricular space (IUS) with primary needles. Note that naturally extensive formation of micro-anhedral carbonate at external utricle walls is hampered by elevated seawater pCO_2 as it causes $CaCO_3$ undersaturation ($\Omega < 1$). **IIIb** Abundant and large secondary needles, which may nucleate directly on top of primary needles, form during daytime in inner inter-utricular space (IUS); no layer of micro-anhedral carbonate is present. Due to the availability of open space, inter-utricular space (IUS) is largely dominated by secondary needle growth, as extensive primary cementation does not occur (cf., Wizemann et al. 2014). Also see text for further explanation. U = utricle; IUS = inter-utricular space; aPS = acidic polysaccharides; eCA = external carbonic anhydrase; MAC = micro-anhedral carbonate

Microstructural nighttime processes in the segment under elevated pCO_2

At nighttime, respiratory CO_2 and presumably CO_2 as a product of cell-internal carbonic anhydrase activity are exhaled into the inter-utricular space. Under ambient seawater pCO_2 (<400 µatm), this leads to the formation of micro-anhedral carbonate and thus to an advancing cementation of the segment (Fig. 6 IIa, IIIa). However, if CO_2 from cell-metabolism equilibrates in seawater that is already enriched in CO_2, this results in a lower seawater pH in the inter-utricular space. The shift in seawater carbon chemistry may drive the seawater in the inter-utricular space to a state of $CaCO_3$ undersaturation ($\Omega_{arag} < 1$). Subsequently, $CaCO_3$ that is precipitated during daytime starts to dissolve and does not become recrystallized to and/or re-precipitated as micro-anhedral carbonate (Fig. 6 IIb). Micro-anhedral carbonate formation during nighttime is affected, which ultimately results in a less-cemented inter-utricular space. This is observed in segments grown under elevated seawater pCO_2 when secondary needles are partially initiating directly on top of primary needles without a layer of micro-anhedral carbonate present (Fig. 6 IIIb; cf. ESM Fig. S3a). Large secondary needles fan out into the available inter-utricular space where, in contrast, under ambient conditions, micro-anhedral carbonate may fill out most of that open space (cf. Fig. 6 IIIa).

Consequences of the impact of elevated seawater pCO_2 on micro-anhedral carbonate formation

The strong species-specific micro-anhedral carbonate density of the segments protects *H. opuntia* from grazing and from physical stress in high-energy regimes (Paul and Hay 1986; Johns and Moore 1988). Any impact on the segmental skeleton density may cause it to be accessible to a wider range of grazing organisms that normally avoid the segments because of their high $CaCO_3$ content. With a less-calcified internal microstructure, the environmental niche of *H. opuntia* may shift to lower energetic regimes whereby breakage of "branches" and an effect on upright growth is less likely. However, species competition is at its highest in habitats that exhibit high biodiversity, such as tropical coral reefs; thus, rapid niche turnover may not be an option (Verbruggen et al. 2009; Hoegh-Guldberg and Bruno 2010). Albeit moderately elevated seawater pCO_2 is

supposed to have a positive effect on algal growth rate (total biomass) as it is supposed to enhance photosynthesis (e.g., Cornwall et al. 2012), non-calcifying species (i.e., fleshy algae) exhibit a faster response to higher availability of CO_2 and may easily be able to outcompete calcifying species such as *H. opuntia* (Sinutok et al. 2011; Hofmann et al. 2012; Koch et al. 2013; Johnson et al. 2014).

Segments with high micro-anhedral carbonate content also are relevant for the sediment budget in reef ecosystems. The process of micro-anhedral carbonate formation leads to a lifetime cementation of the segment (i.e., primary cementation; Wizemann et al. 2014). Primary cementation is a precondition for subsequent intra-granular secondary cementation of the segment that takes place in the sediment after the organics have disintegrated (Milliman 1974; Reid and Macintyre 1998). Specifically, primary cementation of segments enables certain lithophytic *Halimeda* species (mainly of the lineages Opuntia and Micronesicae; Hillis 2001; Verbruggen and Kooistra 2004) to contribute significant amounts of macroscopic *Halimeda* segments to tropical shallow settings (Drew 1983; Drew and Abel 1988; Milliman 1993; Rees et al. 2007). Segments of *H. opuntia* with a low grade of primary cementation may share the fate of segments from other, lesser-calcified *Halimeda* species that are prone to disintegrate rapidly and particularly contribute to the formation of carbonate (needle) mud (<63 μm; Neumann and Land 1975; Macintyre and Reid 1992). Thus, impacts on the process of micro-anhedral carbonate formation may have major consequences for the carbonate sediment budget and grain-size structure of tropical shallow-water environments and sedimentary settings. Negative effects of ocean acidification observed on the primary cementation of *Halimeda* segments will lead to a fining of shallow-water sediments over the long term, when structures become less dense (cemented) and more susceptible to fragmentation (Guinotte and Fabry 2008; Manzello et al. 2008). Subsequently, segment contribution of heavily calcified *Halimeda* species to tropical carbonate sediments, to the buildup of tropical islands and carbonate platforms, may significantly decrease in the future.

Acknowledgments Sebastian Flotow (ZMT—Bremen) is acknowledged for the preparation of thin sections and support with the SEM analyses. Nils Rädecker and Florian Roth (ZMT—Bremen, University of Bremen) provided help in the setup of mesocosms, sample collection and water parameter measurements. Achim Meyer (ZMT—Bremen) helped to maintain the mesocosms and the gas-mixing system during the experiment. This research was funded by the Leibniz Center for Tropical Marine Ecology. Contribution of L.C. Hofmann was funded by the German Federal Ministry of Education and Research (BMBF) project Biological Impacts of Ocean Acidification (BIOACID). Helpful comments and suggestions from reviewers and the associate editor highly improved the manuscript.

Conflict of interest The authors declare no conflict of interest.

References

Bertucci A, Moya A, Tambutté S, Allemand D, Supuran CT, Zoccola D (2013) Carbonic anhydrases in anthozoan corals—a review. Bioorg Med Chem 21:1437–1450

Bonucci E (2007) Main suggested calcification mechanisms: extracellular matrix. In: Schreck S (ed) Biological calcification: normal and pathological processes in the early stages. Springer, Heidelberg, pp 507–558

Borowitzka MA, Larkum AWD (1976) Calcification in the green alga *Halimeda* IV. The action of metabolic inhibitors on photosynthesis and calcification. J Exp Bot 27:894–907

Caldeira K, Wickett ME (2003) Oceanography: anthropogenic carbon and ocean pH. Nature 425:365

Cornwall CE, Hepburn CD, Pritchard D, Currie KI, McGraw CM, Hunter KA, Hurd CL (2012) Carbon-use strategies in macroalgae: differential responses to lowered pH and implications for ocean acidification. J Phycol 48:137–144

De Beer D, Larkum AWD (2001) Photosynthesis and calcification in the calcifying algae *Halimeda discoidea* studied with microsensors. Plant Cell Environ 24:1209–1217

Dickson AG, Millero FJ (1987) A comparison of the equilibrium constants for the dissociation of carbonic acid in seawater media. Deep Sea Res 34:1733–1743

Dickson AG, Afghan JD, Anderson GC (2003) Reference materials for oceanic CO_2 analysis: a method for the certification of total alkalinity. Mar Chem 80.2:185–197

Dickson AG, Sabine CL, Christopher JR (2007) Guide to best practices for ocean CO_2 measurements. North Pacific Marine Science Organization Special Publication 3, Sidney, British Columbia, pp 176

Dodge RE, Wyers SC, Frith HR, Knap AH, Smith SR, Cook CB, Sleeter TD (1984) Coral calcification rates by the buoyant weight technique: effects of alizarin staining. J Exp Mar Biol Ecol 75:217–232

Doney SC, Balch WM, Fabry VJ, Feely RA (2009) Ocean acidification: a critical emerging problem for the ocean sciences. Oceanography 22:16–25

Drew EEA (1983) *Halimeda* biomass, growth rates and sediment generation on reefs in the central Great Barrier Reef province. Coral Reefs 2:101–110

Drew EEA, Abel KM (1988) Studies on Halimeda I. The distribution and species composition of *Halimeda* meadows throughout the Great Barrier Reef Province. Coral Reefs 6:195–205

Feely RA, Sabine CL, Lee K, Berelson W, Kleypas J, Fabry VJ, Millero FJ (2004) Impact of anthropogenic CO_2 on the $CaCO_3$ system in the oceans. Science 305:362–366

Freile D, Milliman J, Hillis L (1995) Leeward bank margin *Halimeda* meadows and draperies and their sedimentary importance on the western Great Bahama Bank slope. Coral Reefs 14:27–33

Guinotte JM, Fabry VJ (2008) Ocean acidification and its potential effects on marine ecosystems. Ann NY Acad Sci 1134:320–342

Hillis L (2001) The calcareous reef alga *Halimeda* (Chlorophyta, Byropsidales): a cretaceous genus that diversified in the Cenozoic. Palaeogeogr Palaeocl 166:89–100

Hillis-Colinvaux L (1980) Ecology and taxonomy of *Halimeda*: primary producer of coral reefs. Adv Mar Biol 17:1–327

Hine AC, Hallock P, Harris MW, Mullins HT, Belknap DF, Jaap WC (1988) *Halimeda* bioherms along an open seaway: Miskito Channel, Nicaraguan Rise, SW Caribbean Sea. Coral Reefs 6:173–178

Hoegh-Guldberg O, Bruno JF (2010) The impact of climate change on the world's marine ecosystems. Science 328:1523–1528

Hofmann LC, Straub S, Bischof K (2012) Competition between calcifying and noncalcifying temperate marine macroalgae under elevated CO_2 levels. Mar Ecol Prog Ser 464:89–105

Hofmann LC, Straub S, Bischof K (2013) Elevated CO_2 levels affect the activity of nitrate reductase and carbonic anhydrase in the calcifying rhodophyte *Corallina officials*. J Exp Bot 64:899–908

Hofmann LC, Heiden J, Bischof K, Teichberg M (2014) Nutrient availability affects the response of the calcifying chlorophyte *Halimeda opuntia* (L.) J.V. Lamouroux to low pH. Planta 239:231–242

Johns H, Moore C (1988) Reef to basin sediment transport using *Halimeda* as a sediment tracer, Grand Cayman Island, West Indies. Coral Reefs 6:187–193

Johnson MD, Price NN, Smith JE (2014) Contrasting effects of ocean acidification on tropical fleshy and calcareous algae. PeerJ 2:e411

Jury CP, Whitehead RF, Szmant AM (2010) Effects of variations in carbonate chemistry on the calcification rates of *Madracis auretenra* (=*Madracis mirabilis* sensu Wells, 1973): bicarbonate concentrations best predict calcification rates. Glob Change Biol 16:1632–1644

Kleypas JA, Buddemeier RW, Archer D, Gattuso JP, Langdon C, Opdyke BN (1999) Geochemical consequences of increased atmospheric carbon dioxide on coral reefs. Science 284:118–120

Koch M, Bowes G, Ross C, Zhang XH (2013) Climate change and ocean acidification effects on seagrasses and marine macroalgae. Glob Change Biol 19:103–132

Langer G, Geisen M, Baumann KH, Kläs J, Riebesell U, Thoms S, Young JR (2006) Species-specific responses of calcifying algae to changing seawater carbonate chemistry. Geochem Geophy Geosy 7:1–12

Macintyre IG, Reid RP (1992) Comment on the origin of aragonite needle mud: a picture is worth a thousand words. J Sediment Res 62:1095–1097

Macintyre IG, Reid RP (1995) Crystal alteration in a living calcareous alga (*Halimeda*): implications for studies in skeletal diagenesis. J Sediment Res A65:143–153

Manzello DP, Kleypas JA, Budd DA, Eakin CM, Glynn PW, Langdon C (2008) Poorly cemented coral reefs of the eastern tropical Pacific: possible insights into reef development in a high-CO_2 world. P Natl A Sci 105:10450–10455

Merbach C, Culberson CH, Hawley JE, Pytkowicz RM (1973) Measurements of the apparent dissociation constants of carbonic acid in seawater at atmospheric pressure. Limnol Oceanogr 18:897–907

Milliman JD (1993) Production and accumulation of calcium carbonate in the ocean: budget of a nonsteady state. Global Biogeochem Cy 7:927–957

Milliman JD (1974) Recent sedimentary carbonates, part 1. Marine carbonates. Springer, Heidelberg

Morse JW, Arvidson RS, Lüttge A (2007) Calcium carbonate formation and dissolution. Chem Rev 107:342–381

Multer HG (1988) Growth rate, ultrastructure and sediment contribution of *Halimeda incrassata* and *Halimeda monile*, Nonsuch and Falmouth Bays, Antigua, W.I. Coral Reefs 6:179–186

Neumann AC, Land LS (1975) Lime mud deposition and calcareous algae in the Bight of Abaco, Bahamas; a budget. J Sediment Res 45:763–786

Orr JC, Fabry VJ, Aumont O, Bopp L, Doney SC, Feely RA, Gnanadesikan A, Gruber N, Ishida A, Joos F, Key RM, Lindsay K, Maier-Reimer E, Matear R, Monfray P, Mouchet A, Najjar RG, Platter GK, Rodgers KB, Sabine CL, Sarmiento JL, Schlitzer R, Slater RD, Totterdell IJ, Weirig MF, Yamanaka Y, Yool A (2005) Anthropogenic ocean acidification over the twenty-first century and its impact on calcifying organisms. Nature 437:681–686

Paul V, Hay M (1986) Seaweed susceptibility to herbivory: chemical and morphological correlates. Mar Ecol-Prog Ser 33:255–264

Pierrot D, Lewis E, Wallace DWR (2006) CO_2SYS DOS Program developed for CO_2 system calculations. ORNL/CDIAC-105. Carbon Dioxide Information Analysis Center, Oak Ridge National Laboratory, US Department of Energy, Oak Ridge, TN

Price NN, Hamilton SL, Tootell JS, Smith JE (2011) Species-specific consequences of ocean acidification for the calcareous tropical green algae *Halimeda*. Mar Ecol-Prog Ser 440:67–78

Rees SA, Opdyke BN, Wilson PA, Henstock TJ (2007) Significance of *Halimeda* bioherms to the global carbonate budget based on a geological sediment budget for the Northern Great Barrier Reef, Australia. Coral Reefs 26:177–188

Reid RP, Macintyre IG (1998) Carbonate recrystallization in shallow marine environments: a widespread diagenetic process forming micritized grains. J Sediment Res 68:928–946

Reyes-Nivia C, Diaz-Pulido G, Dove S (2014) Relative roles of endolithic algae and carbonate chemistry variability in the skeletal dissolution of crustose coralline algae. Biogeosciences Discuss 11:2993–3021

Riebesell U (2004) Effects of CO_2 enrichment on marine phytoplankton. J Oceanogr 60:719–729

Riebesell U, Fabry VJ, Hansson L, Gattuso JP (2010) Guide to best practices for ocean acidification research and data reporting. Luxembourg: Publications Office of the European Union, p 260

Ries JB, Cohen AL, McCorkle DC (2009) Marine calcifiers exhibit mixed responses to CO_2-induced ocean acidification. Geology 37:1131–1134

Ries JB (2011) Skeletal mineralogy in a high-CO_2 world. J Exp Mar Biol Ecol 403:54–64

Robbins LL, Knorr PO, Hallock P (2009) Response of *Halimeda* to ocean acidification: field and laboratory evidence. Biogeosci Discuss 6:4895

Stanley SM (2008) Effects of global seawater chemistry on biomineralization: past, present, and future. Chem Rev 108:4483–4498

Stanley SM, Ries JB, Hardie LA (2010) Increased production of calcite and slower growth for the major sediment-producing alga *Halimeda* as the Mg/Ca ratio of seawater is lowered to a "Calcite Sea" level. J Sediment Res 80:6–16

Sinutok S, Hill R, Doblin MA, Wuhrer R, Ralph PJ (2011) Warmer more acidic conditions cause decreased productivity and calcification in subtropical coral reef sediment-dwelling calcifiers. Limnol Oceanogr 56:1200–1212

Sinutok S, Hill R, Doblin MA, Kühl M, Ralph PJ (2012) Microenvironmental changes support evidence of photosynthesis and calcification inhibition in Halimeda under ocean acidification and warming. Coral Reefs 31:1201–1213

Takahashi T, Broecker WS, Bainbridge AE (1981) The alkalinity and total carbon dioxide concentration in the world oceans. Carbon Cycle Modelling, SCOPE 16:271–286

Verbruggen H, Kooistra W (2004) Morphological characterization of lineages within the calcified tropical seaweed genus *Halimeda* (Bryopsidales, Chlorophyta). Eur J Phycol 39:213–228

Verbruggen H, Tyberghein L, Pauly K, Vlaeminck C, Nieuwenhuyze KV, Kooistra WH, Leliaert F, Clerck OD (2009) Macroecology meets macroevolution: evolutionary niche dynamics in the seaweed *Halimeda*. Global Ecol Biogeogr 18:393–405

Vogel N, Fabricius KE, Strahl J, Noonan SHC, Wild C, Uthicke S (2015a) Calcareous green alga *Halimeda* tolerates ocean acidification conditions at tropical carbon dioxide seeps. Limnol Oceanogr 60:263–275

Vogel N, Meyer F, Wild C, Uthicke S (2015b) Decreased light availability can amplify negative impacts of ocean acidification on calcifying coral reef organisms. Mar Ecol Prog Ser 521:49–61

Wefer G (1980) Carbonate production by algae *Halimeda, Penicillus* and *Padina*. Nature 285:323–324

Weiner S, Lowenstam H (1986) Organization of extracellularly mineralized tissues: a comparative study of biological crystal growth. Crit Rev Biochem Mol 20:365–408

Weiss IM, Marin F (2008) The role of enzymes in biomineralization processes. In: Sigel A, Sigel H, Sigel RKO (eds) Biomineralization: From nature to application. Wiley, West Sussex, pp 71–126

Wienberg C, Westphal H, Kwoll E, Hebbeln D (2010) An isolated carbonate knoll in the Timor Sea (Sahul Shelf, NW Australia): facies zonation and sediment composition. Facies 56:179–193

Wizemann A, Meyer FW, Westphal H (2014) A new model for the calcification of the green macro-alga *Halimeda opuntia* (Lamouroux). Coral Reefs 33:951–964

Electronic Supplementary Material (ESM)

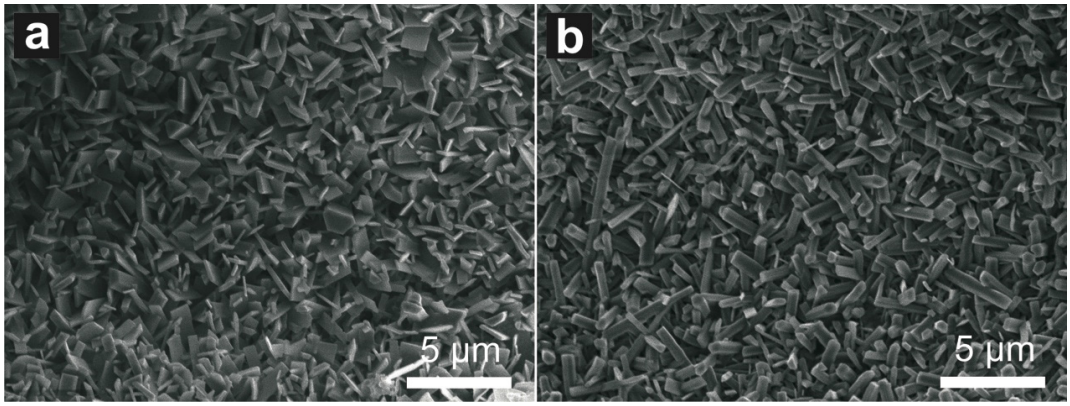

Figure S1 SEM images (via SE) of primary needles from the former external cell wall (organics lost) of a central (medullary) utricle in an apical segment grown under **(a)** ambient seawater pCO_2 and **(b)** elevated seawater pCO_2. Note the higher abundance and the thinner, but longer habit of these needles in **(b)** (images to scale; cf. Fig. 4).

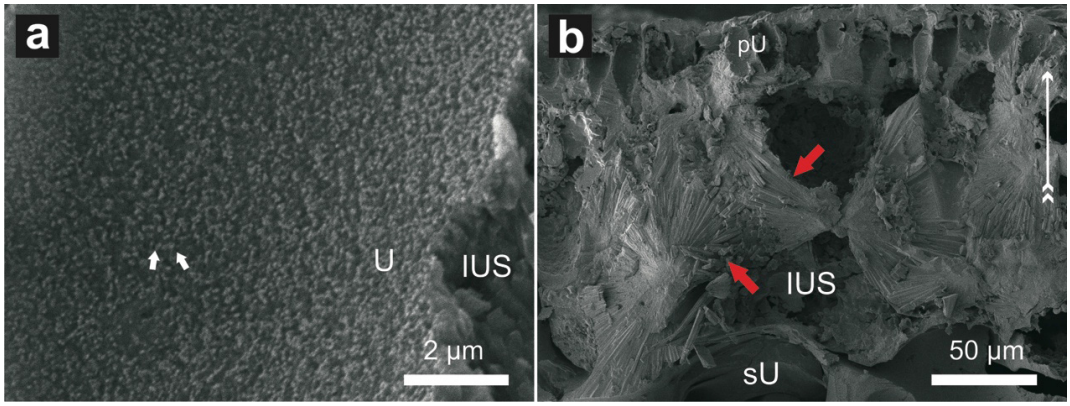

Figure S2 SEM images (via SE) of young segments (day < 2) grown under elevated seawater pCO_2. **(a)** High magnification of a primary utricle (pU) showing nuclei of primary needles within the organic matrix (e.g., white arrows; cell wall removed). Note the high abundance of nuclei per μm^2. **(b)** Large secondary needles (e.g., red arrows) within the inter-utricular space (IUS). Note the open areas within the IUS. White arrow indicates direction to segment surface.

U = utricle (p = primary; s = secondary); IUS = inter-utricular space.

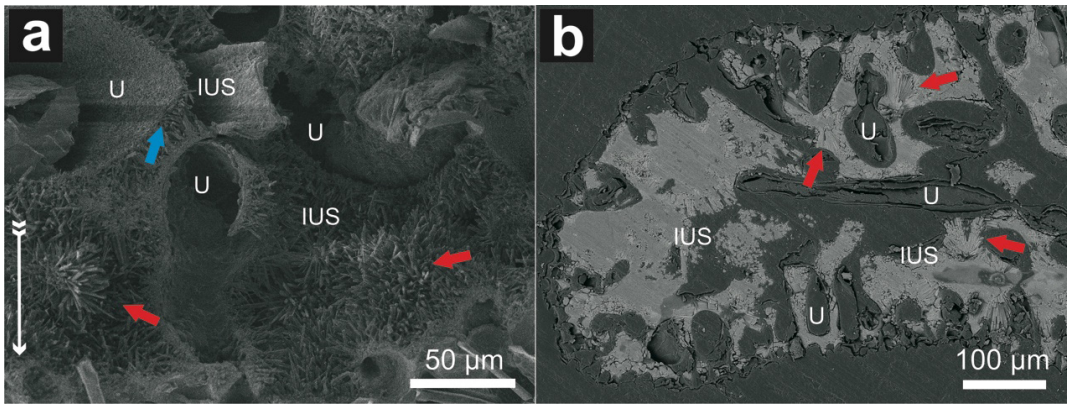

Figure S3 SEM images of secondary needles as observed in **(a)** stub-samples (via SE) and **(b)** thin-sections (via BSE) of apical segments grown under elevated seawater pCO_2. **(a)** Secondary needles fan-out in typical aragonite fiber-bundles (e.g., red arrows). Note that in some cases nucleation points of secondary needles are directly on top of primary needles, no micro-anhedral carbonate layer is observed (blue arrow). White arrow indicates direction to segment surface. **(b)** SEM image (via BSE) of a thin-section shows large bundles of secondary needles (e.g., red arrows) within the inter-utricular space (IUS). Note that the $CaCO_3$ skeleton of the segment consists almost entirely of secondary needles, polished in the process of thin-section preparation.
U = utricle; IUS = inter-utricular space.

Table S1 Physical and chemical water parameters and, concentrations of selected elements (measured via ICP-OES from freshly prepared seawater) of the artificial seawater (SW) that was used in the experiment compared to those of natural North Sea SW. Note the unnatural high initial total alkalinity (A_T) before adjustment with HCl (after Riebesell et al. 2010) and the high amount of silicate of the artificial SW that was prepared from tap water by reverse osmosis and custom made sea salt.
T = temperature; S = salinity; A_T = total alkalinity (in µmol kg^{-1}SW); Mn = Manganese; Zn = Zink; Si = Silicate; LOD = limit of detection.

SW	T (C°)	S (PSU)	pH_{NBS}	initial A_T	Mn (µg/L)	Zn (µg/L)	Si (µg/L)
Artificial	~27	~35	~8.1	3400 ± 50	240 ± 10	200 ± 5	1325 ± 25
North Sea	~27	~32	~8.1	2300 ± 50	< LOD	< LOD	80 ± 5

Table S2 Overview of analyzed segments of *H. opuntia* (cf. Fig. 1). Shown are the mesocosm number with respective pCO_2 treatment (ambient or elevated) from which the segments originate (cf. Table 1), the estimated segment age, and the method of analysis via SEM. When thin-sections and stub-samples from segments of the same age and grown within the same mesocosm were analyzed, segments were chosen randomly from different alga.

SE = secondary electrons; BSE = back-scattered electrons.

Figure	mesocosm (n = 3)	segment age in days	SEM analysis method
2a	2 / ambient pCO_2	2 to 7	thin-section / BSE
2b	2 / ambient pCO_2	2 to 7	stub / SE
2c	2 / ambient pCO_2	2 to 7	stub / SE
2d	2 / ambient pCO_2	2 to 7	stub /SE
3a	2 / elevated pCO_2	2 to 7	thin-section / BSE
3b	2 / elevated pCO_2	2 to 7	stub /SE
3c	2 / elevated pCO_2	2 to 7	stub /SE
3d	2 / elevated pCO_2	2 to 7	stub /SE
S2a	3 / elevated pCO_2	< 2	stub /SE
S2b	3 / elevated pCO_2	< 2	stub /SE
S1a	3 / ambient pCO_2	2 to 7	stub / SE
S1b	1 / elevated pCO_2	2 to 7	stub /SE
5a	1 / ambient pCO_2	< 2	thin-section / BSE
5b	1 / ambient pCO_2	< 2	thin-section / BSE
5c	1 / ambient pCO_2	2 to 7	thin-section / BSE
5d	1 / ambient pCO_2	2 to 7	thin-section / BSE
5e	1 / ambient pCO_2	> 7	thin-section / BSE
5f	1 / ambient pCO_2	> 7	thin-section / BSE
5g	1 / elevated pCO_2	< 2	thin-section / BSE
5h	1 / elevated pCO_2	< 2	thin-section / BSE
5i	1 / elevated pCO_2	2 to 7	thin-section / BSE
5j	1 / elevated pCO_2	2 to 7	thin-section / BSE
5k	1 / elevated pCO_2	> 7	thin-section / BSE
5l	1 / elevated pCO_2	> 7	thin-section / BSE
S3a	2 / elevated pCO_2	2 to 7	stub / SE
S3b	2 / elevated pCO_2	2 to 7	thin-section / BSE

Table S3 One-way ANOVA of mean primary needle abundance per μm^2 within a medullary utricle of n = 3 segments from each mesocosm of the control treatment and the high pCO_2 treatment.

Source of Variation	DF	SS	MS	F	P
Between subjects	15	1.406	0.0937		
Between treatments	5	3.275	0.655	14.548	< 0.001
Residual	75	3.377	0.0450		
Total	95	8.057			

Table S4 Overview of the respiratory activity of the *Halimeda* species *H. opuntia*, *H. incrassata* and *H. macroloba*. Shown is the respiration rate (mean ± SD) as oxygen (O_2) change measured in µmol O_2 cm^{-2} h^{-1}. Negative values indicate an uptake of oxygen. Respiration rate was measured over one hour under full darkness and standardized to surface area (per cm^2) identified from digital pictures via 2D planar projection. Note the distinctively higher mean respiration rate of *H. opuntia* compared to the sand-dwelling species *H. incrassata* and *H. macroloba*.

H. opuntia	*H. incrassata*	*H. macroloba*
-0.60 ± 0.15	-0.38 ± 0.16	-0.27 ± 0.05

4.1 Extended discussion on the effect of elevated seawater pCO_2 on the skeletal features of the green macro-alga genus *Halimeda*

The distinct microstructural features observed in the *Halimeda* skeleton are formed in relationship to different physiological processes of the alga. Thus they respond differently to changes in seawater carbon chemistry. Thereby, skeletal features that are either formed in active calcification (i.e., primary needles) or driven by the photo-physiology (i.e., secondary needles) of the alga likely show little to no change to moderate elevation of seawater pCO_2 (< 1000 µatm), as the influence of photo-physiology on the seawater carbon chemistry in the IUS is supposed to be strong. Contrariwise, skeletal features that are influenced by cell metabolism (i.e., respiratory CO_2, MAC formation) are affected. As the extent of the different features is not similarly pronounced between *Halimeda* species and their physiological responses to shifts in seawater carbon chemistry may also differ, the impact of elevated seawater pCO_2 and subsequent change in carbon chemistry on the segment microstructure is considered largely species-specific.

4.1.1 Primary calcification and elevated seawater pCO_2

At the utricle wall of early apical segments (< 2 days) from *H. opuntia* grown under elevated seawater pCO_2 (> 650 µatm) dense $CaCO_3$ nuclei formation was observed. Subsequently, in mature segments increased numbers of primary needles and of nucleating crystals were measured (per μm^2) when compared to control segments. Primary needles additionally were observed to be longer when compared to needles from segments grown at ambient seawater pCO_2 (~400 µatm). First of all, CO_2 is a substrate for photosynthesis thus elevated seawater pCO_2 is supposed to enhance the physiological performance (i.e. photosynthesis and growth rate) of any plant or alga (e.g., Cornwall et al. 2012; Koch et al. 2013). Generally, it is understood that the processes of calcification and photosynthesis in marine calcifying algae are closely linked. Thereby, the assumption is that photosynthesis elevates the carbonate saturation state within the IUS of *Halimeda*, which leads to the abiotic precipitation of $CaCO_3$. However, typical features involved in active $CaCO_3$ biomineralization of marine calcifying organisms are present at the external utricule cell walls of *Halimeda*, such as acidic polysaccharides and external carbonic anhydrase activity (Kobayashi 1971; Böhm 1973; Böhm and Goreau 1973; Borowitzka and Larkum 1976b; Bonucci 2007; Weiss and Marin 2008; Domozych et al. 2012). Studies have shown that eCA in various calcifying macro-algae, including the genus *Halimeda*, increased when seawater pCO_2 is elevated (Hofmann et al. 2013, 2014). In models of plant physiology, eCA is considered to increase the CO_2

concentration outside the cell to allow enhanced CO_2 uptake via diffusion (CO_2 concentration gradient) over the cell wall (Borowitzka and Larkum 1976b; Sültemeyer 1998). However, when seawater pCO_2 (and DIC) is already elevated there is little need for increased eCA. Thus, another more plausible explanation for this response is that the product of eCA is HCO_3^-, catalyzed from CO_2 as a substrate. This may further imply that eCA in *Halimeda* takes part in the calcification process in a similar way as in many other calcifying organisms (Borowitzka and Larkum 1976b; Bonucci 2007; Weiss and Marin 2008; Bertucci et al. 2013). If eCA plays a substantial role in the biotic calcification of *Halimeda* the consequence likely might be enhanced primary needle formation (primary calcification) under elevated seawater pCO_2. The observed formation of abundant $CaCO_3$ nuclei at the cell wall of utricles in early apical segments (< 2 days) and the higher density and overall longer growth dimensions of primary needles in mature segments under elevated seawater pCO_2 (> 650 µatm) may support this conclusion. As this also means that the uptake of CO_2 for photosynthesis is not the main driver for primary calcification in *Halimeda*, as additionally it might mainly take place at the segment surface and not within the IUS, photosynthesis eventually has to be considered a process that merely supports calcification by elevation of the $CaCO_3$ saturation in the IUS (i.e., through O_2 / OH^- efflux).

4.1.2 Primary cementation and elevated seawater pCO_2

Micro-anhedral carbonate (MAC) formation involves the metabolism of the alga. The micron-sized anhedral crystals thereby likely originate from break down and recrystallization of primary needles (Macintyre and Reid 1995). Nighttime CO_2 evolution into the IUS here is considered to be the main driving force as it leads to a decline in both seawater pH and carbonate ion saturation. Under normal seawater conditions (e.g., regular pH of ~8.1, A_T of ~2300 µmol kg^{-1}SW and, pCO_2 of ~400 µatm), $CaCO_3$ over-saturation ($\Omega_{arag} > 1$) allows (re-)precipitation of $CaCO_3$ as CO_2 evolution of the alga during nighttime is most likely buffered. The process is responsible for a cementation of the segment during its lifetime and here is termed “primary cementation”. Significant elevation of seawater pCO_2 diminishes this buffer effect. Dissolution of $CaCO_3$ then may exceed re-precipitation during nighttime, as the seawater $CaCO_3$ saturation state potentially drops $\Omega_{arag} < 1$. Depending on both, the elevation of seawater pCO_2 and metabolic activity (photosynthesis / respiration ratio) of the alga, the process of MAC formation in the segment is affected.

In summary, the negative effect of elevated seawater pCO_2 on the process of MAC formation depends on the combination of the respiratory activity, the rate seawater pCO_2 is elevated and the physiological response (e.g., eCA, photosynthesis), but also on the corresponding shifts in seawater carbon chemistry and the A_T of the seawater that moreover is coupled to the water-

flow regime around the alga, the thickness and chemical and nutritional composition (e.g., phosphate level) of the diffusive boundary layer (DBL) (Cornwall et al. 2014). The metabolic respiration of the alga is controlled by the light-regime (photosynthesis / respiration ratio), other environmental stressors, which drive its metabolism, such as elevated seawater temperature, respiring epibionts, bioeroders and endolithic microbes and finally the general health state of the alga. It is a very complex multifactor system that influences the $CaCO_3$ saturation within the IUS, which is responsible whether MAC formation or dissolution of $CaCO_3$ occurs. Ries et al. (2009) presented a parabolic response curve for total calcification (i.e., $CaCO_3$ content measured by organic combustion) of *Halimeda incrassata* under continuous elevation of seawater pCO_2. Total calcification of the alga was enhanced up to a seawater pCO_2 of ~600 µatm (A_T ~2000 µmol $kg^{-1}SW$; Ω_{arag} ~2.4). In contrast, with the increase in pCO_2 above 600 µatm total $CaCO_3$ content decreased, which likely was caused by the onset of dissolution. These findings perfectly illustrate the proposed enhancement and the observed impact on MAC formation as depending on the combination of respiratory CO_2 and seawater pCO_2, the seawater in the IUS becomes $CaCO_3$ undersaturated at a certain pCO_2 threshold, then favoring dissolution over (re-)precipitation. However, compared to *H. opuntia, H. incrassata* exhibits not as heavily, densely calcified segments under ambient seawater pCO_2 and natural environmental conditions. That may derive, besides its environmental niche preference, from its lower dark respiration rate and internal segment morphology (Jensen et al. 1985; Multer 1988; Macintyre and Reid 1995; Vogel et al. 2015a, b). In *H. opuntia*, whose segments are more prone to become completely filled with MAC under ambient seawater pCO_2 (~400 µatm) due to its comparably high dark respiration, an impact (= $CaCO_3$ accretion / dissolution turning point) is likely observed at slightly lower seawater pCO_2 (< ~600 µatm) than found by Ries et al. (2009) for *H. incrassata*. Also to keep in mind is that a laboratory experiment may not accurately simulate the daily shifts in seawater pH, DBL linked carbon chemistry and $CaCO_3$ saturation, as they may occur in the natural environment. For example, large-scale shifts in nighttime ecosystem respiration, especially in environments with weak current regime i.e. lagoon, back-reef environment, have been shown to be another, even stronger influencing factor that is moreover strongly up-scaling with seawater temperature (i.e., causing elevated metabolic rates), especially when mean seawater pCO_2 is already elevated due to anthropogenic ocean acidification (Shaw et al. 2013; Mongin and Baird 2014).

4.1.3 Secondary calcification and elevated seawater pCO_2

The euhedral prismatic shaped secondary needles in the inner IUS likely are abiotically precipitated. Their formation depends on the seawater $CaCO_3$ saturation during daytime

photosynthesis. Processes such as the uptake of CO_2 for photosynthesis and H^+ in proton-driven cell-uptake (nutrients / HCO_3^- symporters), as well as external carbonic anhydrase activity (eCA) elevate the CO_3^{2-} ion saturation within the IUS. These physiological daytime processes are not impacted by elevated pCO_2. In contrast the catalysis of additional CO_2 by eCA likely is fast and may sustain $CaCO_3$ saturation within the IUS. The appearance and growth of secondary needles thus is not altered. As MAC formation is reduced by elevated seawater pCO_2, the higher availability of open space within the IUS may then even allow extensive growth of secondary needles, as was observed in the mesocosm study.

4.2 A theoretical model for the process of calcification in macro-algae of the genus *Halimeda* and the effects of ocean acidification

Based on investigations on the segments microstructure and on known physiological processes, the different steps and processes taking place in the calcification of *Halimeda* are integrated in a simple theoretical model that may explain their formation depending on seawater carbon chemistry and cell physiology of the alga (Fig. 5a). Thus by taking into account known processes relevant for calcification, the model also aims to estimate alterations of the segment´s internal microstructure due to elevated seawater pCO_2 (Fig. 5b).

4.2.1 Daytime processes under ambient seawater carbon chemistry

Seawater enters the IUS and provides ions necessary for calcification processes (Fig. 5a, d(daytime)1). Acidic sulfated polysaccharides (and presumably other glycoproteins) located on the utricle wall attract cations, such as Ca^{2+} (Wilbur et al. 1969; Böhm 1973; Böhm and Goreau 1973; Domozych et al. 2012). Within the organic matrix, external carbonic anhydrase activity (eCA) catalyzes the (reversible) reaction of $H_2O + CO_2 \leftrightarrow HCO_3^- + H^+$ (Fig. 5a, d2). Here eCA is proposed to produce HCO_3^- that may be used in the formation of primary needles and cell-imported for photosynthesis. Presumably other yet unknown matrix proteins are present, which use Ca^{2+} ions reversibly adsorbed by the polysaccharides and HCO_3^- obtained from eCA-like domains for calcification. Membrane-bound channel proteins that function as ion symporters co-transport nutrients or HCO_3^- together with protons (H^+) into the cell. The removal of protons from the IUS and the removal of CO_2 both for photosynthesis (Fig. 5a, d3) and by eCA elevate the seawater $CaCO_3$ saturation (Ω) within the IUS. Subsequently secondary needles are able to crystallize abiotically on top of possible nucleation sites (remnants of primary needles and MAC) in the inner IUS (Fig. 5a, d4). Additionally, active primary calcification and abiotic precipitation of $CaCO_3$ (i.e., secondary calcification) in the

alga during daytime also may have the purpose to enrich the seawater within the IUS in CO_2, for the use in photosynthesis, for eCA to gain HCO_3^- for primary calcification and, in protons (H^+) for several H^+-driven trans-membrane symporters. That includes nutrient / H^+ symporters that are relevant for cell metabolism and photosynthesis (Borowitzka and Larkum 1976a; Price et al. 1985; McConnaughey and Whelan 1997). A light-physiology induced proton pump (H^+-ATPase) also elevates proton concentration in the IUS during daytime. Generally the proton discharge via H^+-ATPase might function as a pH balancing system to avoid acidification of the cell protoplasm. However, the possibility exists that the proton pump also may actively control the pH of the organic matrix for the process of primary calcification (e.g., for crystal nucleation and Ca^{2+} cycling at polysaccharides).

4.2.2 Nighttime processes under ambient seawater carbon chemistry

During nighttime processes related to photosynthesis cease. As cell metabolism continues, respiratory CO_2 builds up within the cell. Excessive respiratory CO_2 is exhaled into the IUS (Fig. 5a, n(nighttime)1). External CA in the IUS may produce additional CO_2. Primary needles precipitated on the utricle wall during daytime react with exhaled respiratory CO_2, become recrystallized and break down to smaller anhedral shaped crystals (Fig. 5a, n2). This process represents the formation of MAC that is driven by the local decrease in $CaCO_3$ saturation (Ω) in vicinity to the external cell wall. However, $CaCO_3$ under-saturation ($\Omega < 1$) in the IUS likely is not persistent, thus local re-precipitation may also occur (Fig. 5a, n3 and n4). The alternating diurnal processes of daytime primary calcification and nighttime formation of MAC build up the densely cemented internal skeleton of the *Halimeda* segment.

4.2.3 Daytime processes under elevated seawater pCO_2

Carbon species and Ca^{2+} ions enter the IUS with seawater that is elevated in pCO_2 (> 400 µatm) and lowered in pH (< 8) (Fig. 5b, d1). CO_2 is proposed to be the substrate of external carbonic anhydrase (i.e. the enzyme), thus a higher availability of CO_2 leads to higher enzymatic activity. As eCA is supposed to be involved in the primary calcification this process is likely enhanced (Fig. 5b, d2). The use-up of CO_2 via eCA and in photosynthesis (Fig. 5b, d3) may elevate the $CaCO_3$ saturation (Ω) likewise as under ambient seawater pCO_2 (< 400 µatm) thus abiotic secondary calcification is not negatively affected (Fig. 5b, d4). As protons (H^+) are used in nutrient / HCO_3^- symport, they may become a limiting factor in seawater with high $CaCO_3$ oversaturation ($\Omega > 4$). Seawater enriched in protons (i.e., high

pCO_2, low pH) may provide additional protons for enhanced nutrient uptake (via H^+ symporters) and thus may increase algal growth performance.

4.2.4 Nighttime processes under elevated seawater pCO_2

Within the IUS, respiratory CO_2 from the alga equilibrates in seawater elevated in pCO_2 (Fig. 5b, n1). Depending on seawater pCO_2 concentration and the respiratory activity of the alga, the resulting seawater pCO_2 might lead to persistent $CaCO_3$ under-saturation ($\Omega < 1$) of the seawater in the IUS during nighttime. Such conditions now may favor $CaCO_3$ dissolution over (re)precipitation (Fig. 5b, n2 and n3). As a consequence recrystallization of primary needles, i.e. MAC formation, is impacted (Fig. 5b, n4). Persistent $CaCO_3$ under-saturation ($\Omega < 1$) during nighttime thus may lead to an overall weaker calcified (i.e. primary cemented), needle dominated skeletal segment microstructure as was observed in segments grown under elevated seawater pCO_2.

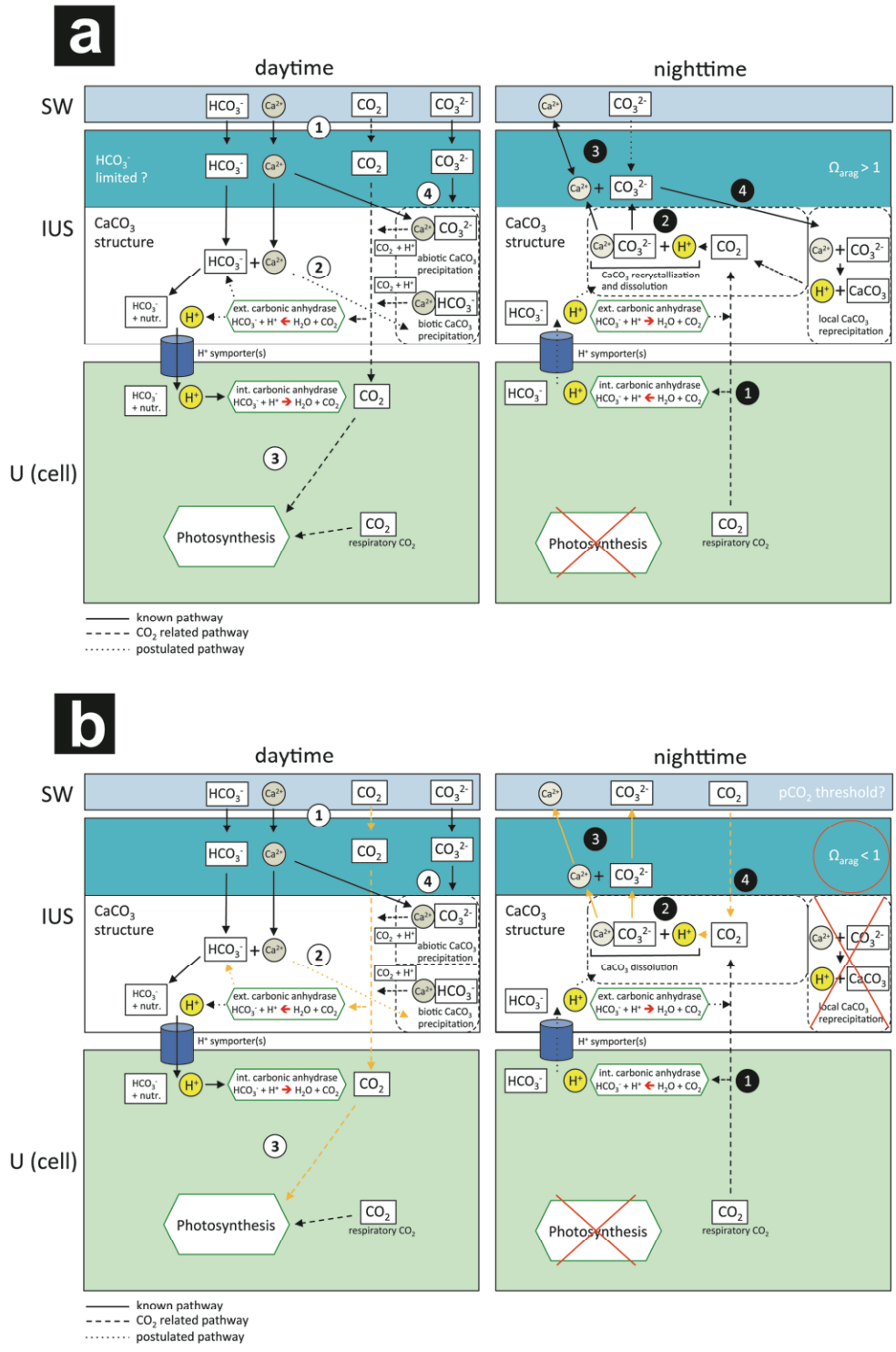

Fig. 5 Theoretical model for the calcification of *Halimeda*. (a) Day- and nighttime processes of calcification under ambient seawater pCO_2. (b) Day- and nighttime processes of calcification under elevated seawater pCO_2. Altered processes due to elevated seawater pCO_2 in (b) are highlighted in yellow. Red arrows within boxes of internal and external CA indicate preferred equilibrium reaction of enzyme activity depending on substrate availability.

Fig. 5 (continued)

Daytime processes: (1a, b) Seawater elevated in dissolved inorganic carbon (DIC) enters the IUS. (2a) CO_2 is used in photosynthesis and by external carbonic anhydrase. Primary needles are actively formed out of HCO_3^- and Ca^{2+} ions that are adsorbed by acidic polysaccharides. (2b) Under elevated seawater pCO_2, the shift in seawater carbon chemistry leads to a higher availability of CO_2 and HCO_3^-. External carbonic anhydrase activity is enhanced due to elevated seawater pCO_2 (cf., Hofmann et al. 2014) thus primary calcification is enhanced. Additionally, higher availability of HCO_3^- and protons (H^+) may no longer limit algal growth performance. (3a, b) Uptake of H^+, HCO_3^- and CO_2 elevate $CaCO_3$ saturation (Ω) within the IUS that leads to (4a, b) secondary needle precipitation.

Nighttime processes: (1a) Respiratory CO_2 enters the IUS and leads to (2a) recrystallization of primary needles and MAC formation. (1b) Respiratory CO_2 enters the IUS and equilibrates in seawater elevated in pCO_2 and (2b) as a consequence dissolution of primary needles is favored over recrystallization. (3a) Incoming seawater is well buffered, i.e. $CaCO_3$ saturated. (3b) Incoming seawater with high pCO_2 has no buffer effect, thus does not allow (4a, b) local re-precipitation of $CaCO_3$. (4b) Subsequently, formation of micro-anhedral carbonate (i.e., primary cementation) ceases due to $CaCO_3$ under-saturation ($\Omega < 1$) within the IUS (red circle).

Note (in b, nighttime) that due to the combination of respiratory activity (from metabolism) and the elevation of seawater pCO_2 a threshold may exist over which micro-anhedral carbonate formation starts to be affected.

U = utricle; IUS = inter-utricular space; SW = seawater.

5. Manuscript III :

Microstructural analyses of sedimentary *Halimeda* segments from the Spermonde Archipelago (SW Sulawesi, Indonesia): a new indicator for sediment transport in tropical reef islands?

(2015) Wizemann A, Mann T, Klicpera A, Westphal H

Facies 61:4

DOI: 10.1007/s10347-015-0429-5

Statement of personal contribution

Manuscript writing:

I wrote the initial manuscript.

(Total contribution: 70%)

Field and laboratory work:

I performed sediment sample screening and sediment picking.

(Total contribution: 10%)

Analyses:

I prepared the samples and conducted scanning electron microscopy.

(Total contribution: 100%)

Idea:

I developed the initial idea of the analyses and of the manuscript.

(Total contribution: 80%)

Facies (2015) 61:4
DOI 10.1007/s10347-015-0429-5

ORIGINAL ARTICLE

Microstructural analyses of sedimentary *Halimeda* segments from the Spermonde Archipelago (SW Sulawesi, Indonesia): a new indicator for sediment transport in tropical reef islands?

André Wizemann · Thomas Mann · André Klicpera · Hildegard Westphal

Received: 26 September 2014 / Accepted: 13 February 2015

Abstract Understanding the origin of sediments and the direction of sediment transport is a prerequisite for accurate reconstruction of reef island evolution. In tropical settings, island development depends on the accumulation of sediments on the reef flat, which are produced by calcifying organisms such as corals, foraminifera, and green macro-algae of the genus *Halimeda*. In certain areas of tropical regions, calcareous segments from these algae might account for more than 50 wt% of the coarser sediment fraction. *Halimeda*-rich sediments typically contain complete segments that become widely distributed to a range of sedimentary settings. However, the exact sedimentary pathway is either mostly unknown or was neglected. Here we show that the alteration of *Halimeda* segments from the Spermonde Archipelago (SW Sulawesi, Indonesia) is related to processes during transport and deposition. Using field observations and scanning electron microscopy we observed that *Halimeda* segments, sampled from the reef flat to the shore on four uninhabited islands, without exception belong to the grain-size class of pebble gravel (1.6 > 0.4 cm; medium-to-fine pebbles) and reveal characteristic patterns of external and internal microstructural alteration with respect to sampling area. Furthermore, *Halimeda* species, from which most of these segments originate, preferably inhabit hard substrates in the reef, on the reef crest, and the outer reef flat. Thus, the observed distinct microstructural alteration of the segments allows drawing conclusions on sediment transport and deposition. Particularly, rapid secondary cementation may preserve the segments as a sedimentary component for the development and maintenance of reef islands and coastlines in tropical shallow seas.

Keywords Carbonate sediments · *Halimeda* microstructure · Sediment alteration · Physical abrasion · Secondary cementation · SEM

A. Wizemann (✉) · T. Mann · A. Klicpera · H. Westphal
Leibniz Center for Tropical Marine Ecology (ZMT),
Fahrenheitstraße 6, 28359 Bremen, Germany
e-mail: andre.wizemann@zmt-bremen.de

H. Westphal
Department of Geosciences, University of Bremen,
Klagenfurterstraße 2, 28359 Bremen, Germany

Introduction

Reef islands in the tropics are often densely populated environments of high socio-economic and ecologic relevance (e.g., Moberg and Folke 1999; Hoffmann 2002; Ghina 2003). Thus, their maintenance and future development is important but threatened today by anthropogenic influence, processes of climate change, sea-level rise, and coastal erosion (e.g., McClanahan et al. 2002; Hughes et al. 2003; Woodroffe 2008). As tropical atoll and reef islands are formed by the accumulation of sediments, knowing sediment origin is necessary in order to be able to predict future effects of these processes. Thus, to identify proxies that may help to reconstruct past sedimentological and climatological events, an understanding of the long-term behavior of these highly dynamic systems is desirable. Thereby, tropical reef island formation relies on transport of sediments from areas of production to sites of deposition (e.g., Woodroffe et al. 1999; Kench et al. 2012). In tropical island settings, the predominant sources of sediments are the fringing coral reefs that border the reef flat (e.g., Renema 2002; Kench et al. 2005; Harris et al. 2014). As a consequence, most of the reef-derived sediments are of biogenic origin and the amount of calcium carbonate produced

in coral reef environments is essential for reef island formation and maintenance (Perry et al. 2011).

Next to corals and foraminifera, one of the prominent carbonate sediment-producing organisms in tropical coral reef environments are calcifying green macro-algae of the genus *Halimeda* (Milliman 1974; Hillis-Colinvaux 1980; Rees et al. 2007). Their aragonitic segments (also termed plates or flakes in sedimentary studies) are found in most tropical reef settings ranging from the shore over the reef flat and shallow-water inward reefs to the high-energetic reef crest, the fore reef, and reef slope (e.g., Jindrich 1969; Goreau and Goreau 1973; Wiman and McKendree 1975; Orme et al. 1978; Drew 1983; Scoffin and Tudhope 1985; Drew and Abel 1988; Johns and Moore 1988; Freile et al. 1995; Wienberg et al. 2010). Species of this macro-alga are characterized by a rapid segmental growth with rates of up to one segment per branch and day (Wefer 1980; Drew 1983). Thus, the genus of *Halimeda* represents, in terms of reproduction, a major carbonate sediment factory in tropical regions (Milliman 1974, 1993). Given the rapid growth and the wide distribution of the algae, segments found in the sediment might represent a valuable environmental archive. With additional knowledge on its segmental calcification, subsequent investigation of external and internal microstructural features of the segments may thus allow the reconstruction of distinct local sedimentation and transportation patterns.

The calcification of *Halimeda* segments follows a distinct pattern (Macintyre and Reid 1995; Wizemann et al. 2014). Short aragonite needles become recrystallized to smaller anhedral crystals (<1 μm) and form dense micro-anhedral carbonate (MAC), which leads to primary cementation of the segments already during lifetime. With increasing segment age, this process continues as the so-called interutricular spaces (IUS) between utricles become densely filled with MAC. Macro-algae of the genus *Halimeda* almost continuously shed their calcareous segments to the sediment (Wefer 1980; Multer 1988; Multer and Clavijo 2004). Typical coarse *Halimeda* sediments, which may accumulate to extensive sedimentary bodies, are mostly composed of single segments (e.g., Drew 1983; Hine et al. 1988; Mankiewicz 1988; Roberts et al. 1988; Freile et al. 1995; Martin et al. 1997; Granier 2012). Thereby the segment's external and internal microstructure is altered within the sediment due to physical and geochemical processes (e.g., Milliman 1974; Alexandersson and Milliman 1981; Reid and Macintyre 1998; Perry 1998, 2000; Perry and Taylor 2006). However, until now, species-specific types of *Halimeda* segments and their posthumous microstructural alteration have received little or no attention when sedimentary transport mechanisms on the reef flat have been reconstructed.

Here we analyze physical and biogeochemical alterations of the calcium carbonate ($CaCO_3$) microstructure of *Halimeda* segments that were sampled from surface sediments of reef islands in the Spermonde Archipelago, SW Sulawesi, Indonesia. Our intention is to relate changes in the skeletal microstructure of the segments to processes that act during sediment transport and deposition. Therefore, we investigated surface characteristics and morphology of single *Halimeda* segments for species identification by in situ photography and conducted internal microstructural analyses via scanning electron microscopy. We aim to provide a better understanding of the primary origin of *Halimeda* segments and to get a better insight into *Halimeda*-specific sedimentation processes that are part of the local carbonate factory. Furthermore, this study may help in estimating to what extent segments of calcareous macro-algae of the genus *Halimeda* contribute to the development and stabilization of coastlines, atolls, and reef islands in the tropics.

Study sites

The Spermonde Archipelago is situated in the Strait of Makassar west of South Sulawesi, Indonesia (Fig. 1). The Archipelago consists of a multitude of small and partly reef-fringed islands to the west-northwest of the city of Makassar (Fig. 1b). The outermost islands are located on a discontinuous barrier reef, with the water depth increasing rapidly from about 60 m to over 200 m, and lie approximately 60 km from the mainland (Renema and Troelstra 2001). Most of the islands are inhabited and paved by houses and huts of fishermen often covering the entire island. They provide excellent conditions to study sea-level change and island formation (Renema and Troelstra 2001; Renema et al. 2001; Imran et al. 2013), coral reef diversity and health (Edinger et al. 1998, 2000; Knittweis et al. 2009; Sawall et al. 2011), related socio-economic topics (Glaeser and Glaser 2010; Glaser et al. 2010; Ferse et al. 2014) and sedimentology of carbonate sediments (Renema 2002, 2006; Wilson and Vecsei 2005; this study). Here, four uninhabited islands (Fig. 1c–f) were investigated with three of them [Pulau Pamangangang (PP), Pulau Suranti (PS), Pulau Tambakulu (PT)] located in vicinity of the shelf edge and one islands situated closer to the mainland [Pulau Panambungan (PPB)].

Materials and methods

Sediment sampling

Surface sediment samples ($n = 71$; bulk ~200 g each) were carefully taken from the top ~5 cm of the substrate with a hand-shovel while snorkeling in October–November 2012 and 2013. Samples were taken along transects down to a

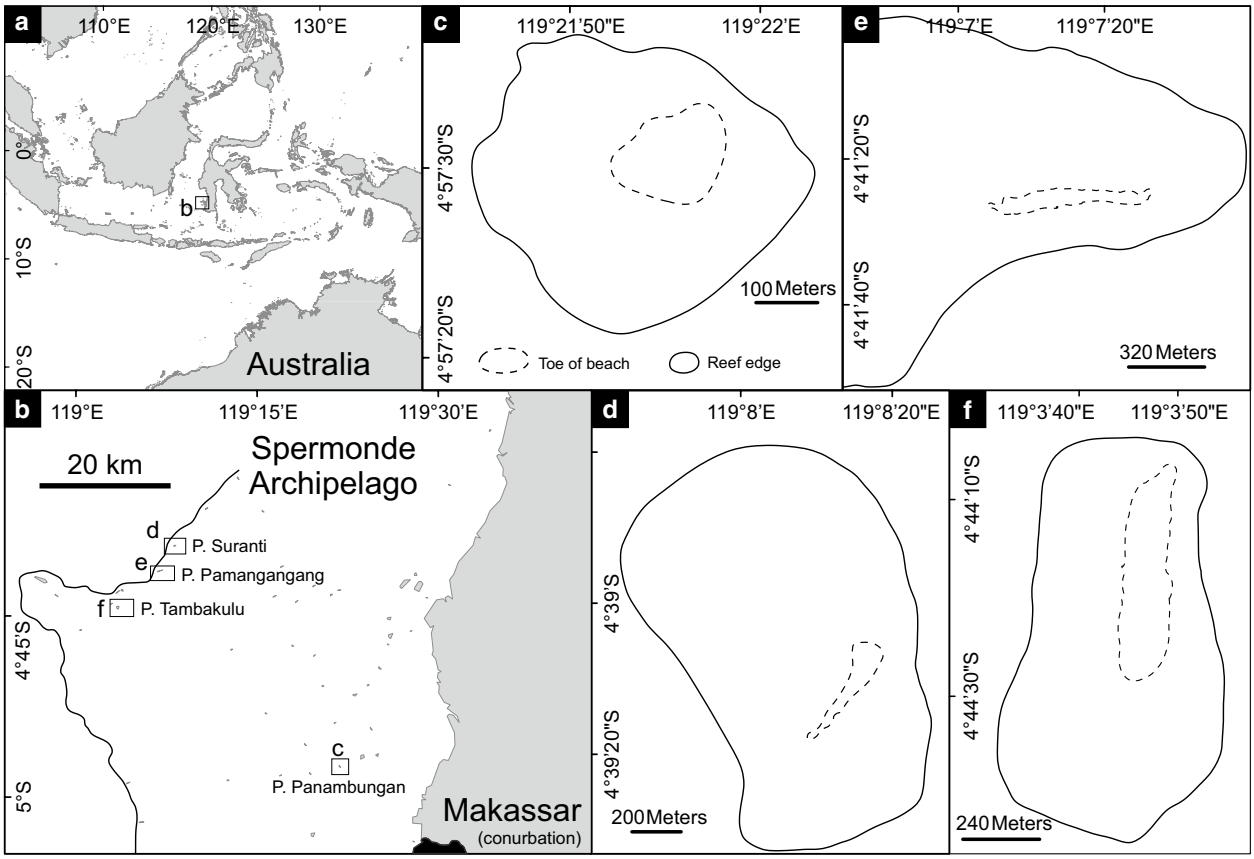

Fig. 1 Location of the Spermonde Archipelago (SW Sulawesi, Indonesia). **a** Overview map of the Indo-Pacific region. *Small quadrate* indicates the sampling area. **b** Close-up of the Spermonde region showing the location of the four uninhabited islands (**c**–**f**) from where surface sediment was sampled. **c** Island of Pulau Panambungan (PPB) on the inner shelf. **d** Island of Pulau Suranti (PS), **e** island of Pulau Pamangangang (PP) and, **f** island of Pulau Tambakulu (PT) located at the outer shelf. Reef edge in **c**–**d** indicates the location of increasing reef slope inclination

water depth of 1–2 m below sea level (m b.s.l.). Sampling followed the drift pathways in consecutive order from the reef flat in direction to the shore and drift line (Table 1; Fig. 2). Sediment samples were dried where possible, and directly brought to the Leibniz-Center for Tropical Marine Ecology (ZMT) in Bremen, Germany, to avoid biogenic alteration of fresh carbonate materials. In the laboratory, sediment samples were rinsed under fresh water in order to remove soluble components and afterwards oven-dried at 40 °C for 48 h. All further investigations (incl. thin-section preparation and SEM analyses) took place in the Geoecology and Carbonate Sedimentology group at ZMT.

Sediment screening and segment picking

Bulk sediment samples ($n = 71$) were screened for *Halimeda* segments and complete segmental plates of *Halimeda* were picked using a binocular microscope (Leica S6E) and a picking tray (Figs. 2, 3). Always the most pristine (based on shape and external microstructure) and unbroken segment was picked out of each sediment sample. This was done in order to ensure maximal preservation for internal microstructure analysis via scanning electron microscopy (SEM) and to be able to infer the exact preservation stage of segments within the sample with respect to sediment sampling location. From sediment samples where *Halimeda* segments were obtained, 14 specimens (i.e., single segments, each out of a single bulk sediment sample) are exemplarily and representatively shown in this study, and these are summarized in Table 1. The respective sample ID of analyzed segments in Table 1 directly refers to the depicted segments in Figs. 7, 8, and, 9 as well as to the sampling location of sediments in maps in Fig. 2. The sample ID also indicates out of which sediment sample from which island (PT, PS, PP, or PPB) the segment was picked. Please note that when the sample ID according to Table 1 is used in the text, the single segment is addressed.

Table 1 Overview of picked *Halimeda* segments that are exemplarily shown in this study, with sample ID, coordinates and environmental sampling location at the islands of Pulau Suranti (PS), Pulau Tambakulu (PT), Pulau Pamangangang (PP), and Pulau Panambungan (PPB) (cf. Figs 1, 2)

Analysis methods used involve back-scattered electron microscopy (BSE–SEM), energy-dispersive X-ray (EDX–SEM) both from thin-sections, and digital photography for determination of external morphological alteration (i.e., segment shape) of *Halimeda* segments sampled

Drift line = onshore, shoreline = in water; X = method used, – = not investigated

[a] Use of method based on BSE–SEM imaging information

Sample ID	Coordinates	Env. location	BSE–SEM	EDX–SEM[a]	Digital photography
PS2	S4°39.229′ E119°08.195′	Drift line	X	–	X
PS3	S4°39.226′ E119°08.193′	Shoreline	X	–	X
PS4	S4°39.222′ E119°08.187′	Reef flat	X	–	X
PS6	S4°39.238′ E119°08.219′	Drift line	X	–	X
PS7	S4°39.238′ E119°08.221′	Shoreline	X	–	X
PS8	S4°39.240′ E119°08.222′	Shoreline	X	–	X
PT8	S4°44.283′ E119°03.809′	Drift line	X	–	X
PT9	S4°44.281′ E119°03.816′	Shoreline	X	–	X
PT10	S4°44.275′ E119°03.852′	Reef flat	X	–	X
PP5	S4°41.434′ E119°07.296′	Reef flat	X	–	X
PP6	S4°41.403′ E119°07.292′	Drift line	X	–	X
PP7	S4°41.402′ E119°07.293′	Shoreline	X	–	X
PPB8	S4°57.360′ E119°21.914′	Drift line	X	X[a]	X
PPB10	S4°57.370′ E119°21.910′	Reef flat	X	–	X

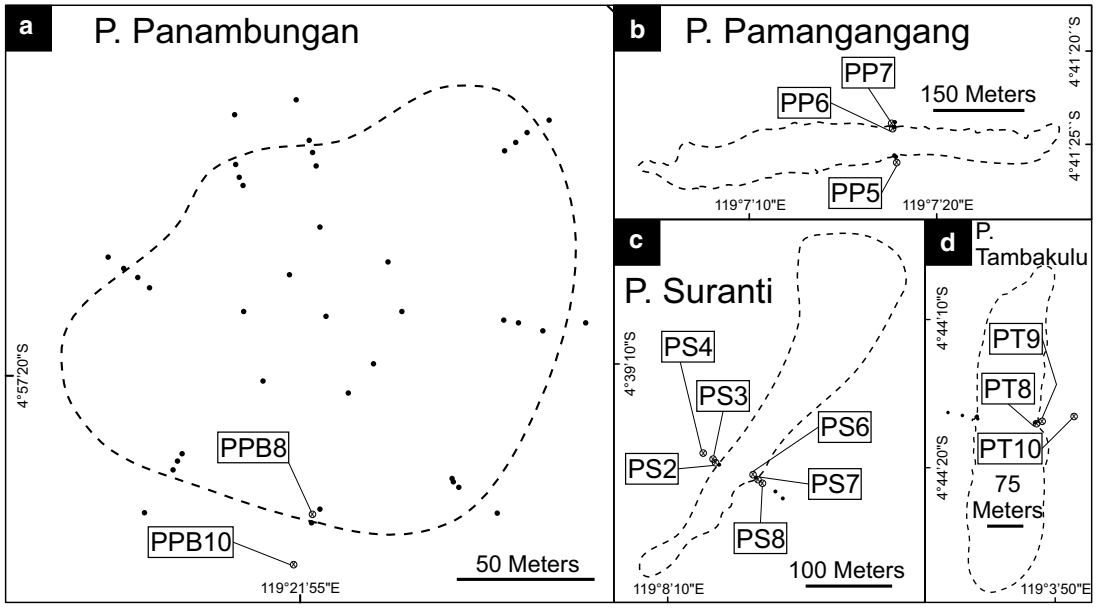

Fig. 2 Detailed maps of islands showing transects sampled. **a** Location of sediment samples taken from Pulau Panambungan (PPB), **b** from Pulau Pamangangang (PP), **c** from Pulau Suranti (PS), and **d** from Pulau Tambakulu (PT). *Crossed circles* with labels refer to the respective samples analyzed (Table 1). *Black dots* indicate sampling points (total $n = 71$)

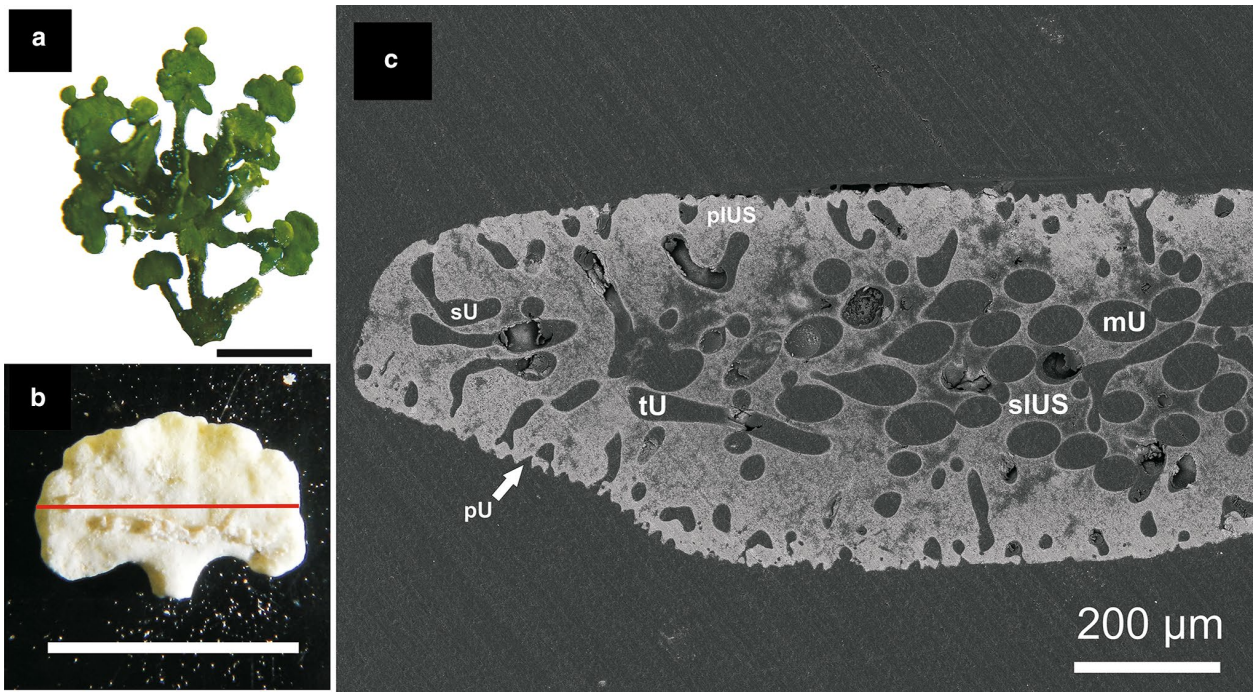

Fig. 3 The tropical green macro-alga genus *Halimeda* and its calcareous segments. **a** Segmented habit of the common Indo-Pacific calcareous macro-alga species *Halimeda opuntia*. *Scale bar* 1 cm. **b** Digital photograph of a typical segment from a *Halimeda* of the *H. opuntia* lineage obtained from surface sediment. The *red line* indicates the polished plain for thin-section analysis. *Scale bar* 0.5 cm **c** SEM image (via BSE) of a thin-section showing the internal skeletal microstructure of an almost pristine *Halimeda* segment from the sediment. *U* utricle (*p* primary, *s* secondary, *t* tertiary, *m* medullary); *IUS* interutricular space (*p* primary, *s* secondary)

Sample preparation and analyses

Collected *Halimeda* segments were photographed in the picking tray with a digital camera (Nikon AW100 using macro-focus) for species identification, size determination, and comparison of the alteration stage, as depicted in Fig. 3b. Afterwards, petrographic thin-sections were prepared for the analysis of the internal segment microstructure. Therefore, the sampled segments were embedded in epoxy resin, cut along the middle plane, and polished to thin-sections of 35-µm thickness. In the last preparation step, the thin-sections were gold sputtered and analyzed with a scanning electron microscope (SEM; TESCAN VEGA3 XMU) at 10 keV in back-scattered electron mode (BSE–SEM; Fig. 3c).

Energy-dispersive X-ray (SEM–EDX) element detection was used to identify $CaCO_3$ polymorphs through the presence or absence of Mg^{2+} if BSE–SEM imaging indicated mineralogical alteration of intra-granular cements. Point-measurements were conducted using the Oxford X-Max2 element detector (50 mm^2) of the SEM at 5 keV. Working distance between sample and Wehnelt cylinder was set to ~15.5 mm. Point-measuring live time was adjusted to 120 s (approx. >300 k total counts).

Results

Complete, unbroken *Halimeda* segments were present in 45 out of 71 sediment samples (*n* segments present in samples from PPB = 19, PP = 9, PS = 9, PT = 8). Fourteen single segments picked from the respective sediment samples according to Table 1 are representatively shown in this study (depicted in corresponding Figs. 7, 8, 9). Fragmented segments were scarcely observed in the 71 bulk sediment samples investigated, and not used for analyses. As a result of a heavily altered peripheral segment microstructure, the determination of the *Halimeda* species based on the segment's shape and surface characteristics was in some cases not possible by means of light microscopy and digital photographs. Further identification of the *Halimeda* species or at least *Halimeda* lineage of specimens (after Hillis 2001; Verbruggen and Kooistra 2004) was achieved by investigating the internal morphological microstructure from thin-sections under the SEM (cf., Figs. 3c, 4). Most *Halimeda* segments have a mean grain-size diameter of ~0.5 cm in the size class of pebble gravel (after Wentworth 1922; digital photographs in Figs. 3b, 7, 8, 9). In short on-site surveys in different reef zones, e.g., on the reef crest, outer and inner reef flat around the islands (an illustration of the

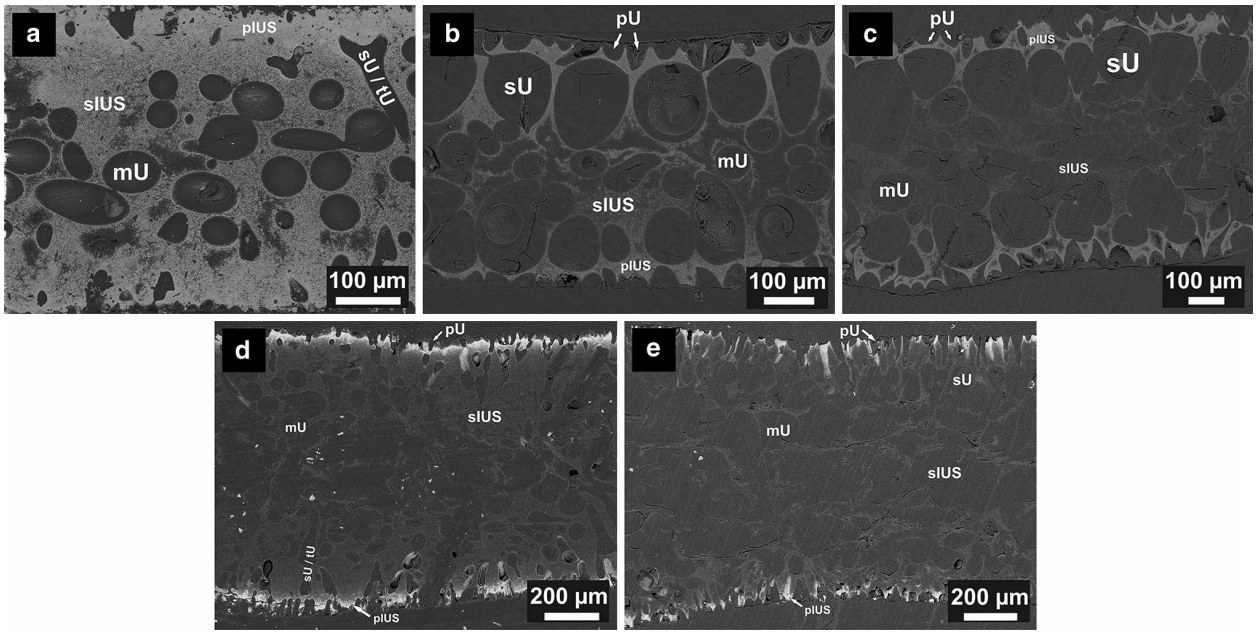

Fig. 4 Comparison of various common *Halimeda* species and their internal segment microstructure as observed in SEM images (via BSE–SEM) of thin-sections from mature segments that were obtained from living algae. Modified from Wizemann et al. (2014). Shown are the species **a** *Halimeda opuntia*, **b** *Halimeda copiosa*, **c** *Halimeda cuneata*, **d** *Halimeda incrassata*, and **e** *Halimeda macroloba*. Note the similarity of the internal morphology of sedimentary *Halimeda* segments (Figs. 3c, 7, 8, 9) with segments obtained from living *Halimeda opuntia*., *U* utricle (*p* primary, *s* secondary, *t* tertiary, *m* medullary); *IUS* interutricular space (*p* primary, *s* secondary)

local situation is given in Fig. 5), various species of *Halimeda* macro-algae were observed, some of which with significantly larger segments (>2 cm in diameter). These species (*Halimeda* cf. *cuneata* and *gigas*) were predominantly found in situ in sandy substrate on the inner reef flat in water depths <1–2 m b.s.l. (Figs. 5, 6). Sediment composition in the vicinity of these algae consisted mainly of fine-grained carbonate sand and mud (size fractions <2 mm). In sediment samples where complete and externally pristine-shaped *Halimeda* segments were present, none of these segments was larger in diameter than the grain size of medium pebbles (<1.6 cm, after Wentworth 1922; i.e., strong species-specificity of *Halimeda* segments in the sediment). Overall, it has to be noted that *Halimeda* segments were not a major component in carbonate sediments of these islands (<5 %), as also the occurrence of the living alga as sea-floor cover was not frequent. Nevertheless, by using the most conservative method, picking the "most pristine" segment per sample, the presented investigations and interpretations are applicable even with low abundances of *Halimeda* growth.

Alteration of the internal skeletal microstructure

For the description of the internal skeletal microstructure of *Halimeda* segments, it is important to separate between: (1) primary $CaCO_3$ infillings of MAC within the IUS during lifetime of the segment (i.e., primary cementation) and (2) secondary precipitated $CaCO_3$ from marine cementation (i.e., intra-granular or secondary cementation; Milliman 1974; Reid and Macintyre 1998; Wizemann et al. 2014). Particularly, primary cementation is induced by the alga's metabolism that causes recrystallization of skeletal $CaCO_3$ and only takes place in living segments (Macintyre and Reid 1995; Wizemann et al. 2014). In contrast, secondary cementation is the successive step of internal segment cementation that takes place in a dead segment after the organics have disintegrated. Additionally, secondary cementation may include precipitation of other $CaCO_3$ polymorphs, such as Mg-calcite (Alexandersson and Milliman 1981; Reid and Macintyre 1998).

Halimeda segments from the island Pulau Suranti (PS)

Halimeda segments were sampled at PS along two transects. Investigations of the internal $CaCO_3$ microstructure (evaluated by thin-sections and SEM) and the external grain shape (determined by digital photographs) indicate consecutive stages of microstructural alteration with respect to sampling location (Table 1; Figs. 2c, 7). In segments that were sampled close to and on the shore, the outward elongated edges that are typical for pristine (i.e., "butterfly"

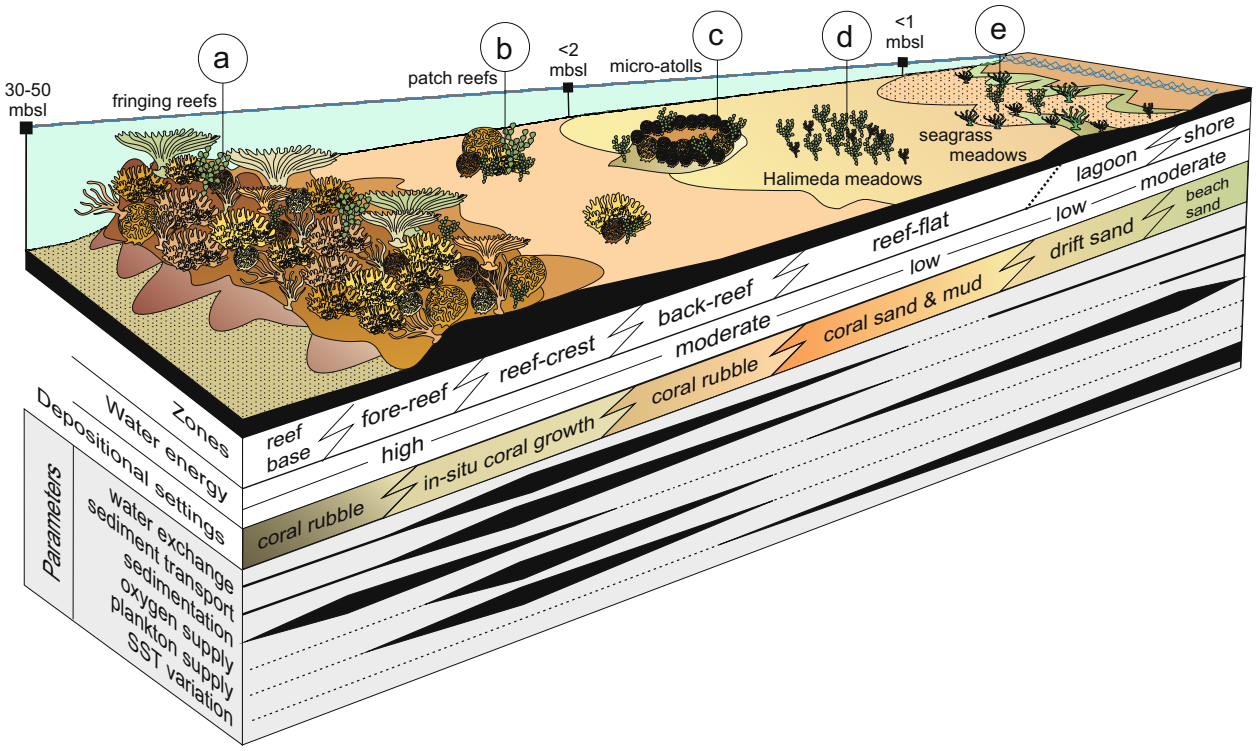

Fig. 5 Reef zones, sedimentology, and changes of physical and chemical parameters across a typical fringing reef of islands in the Spermonde Archipelago. Modified from Whitten et al. (2002) and references therein. *Letters* indicate sites of *Halimeda* growth: **a** lithophytic *Halimeda* species (e.g., *H. opuntia*) attached to coral rock within the coral reef and on the reef crest, **b** attached to coral rock (2–3 m b.s.l.) forming isolated reef patches in the back reef area and, **c** attached to micro-atolls (<1–2 m b.s.l.) on the reef flat. **d** Psammophytic *Halimeda* species (e.g., *H. gigas*, *H. cuneata*; Fig. 6) forming meter-sized meadows (<1–2 m b.s.l.) covering the inner reef flat. **e** Isolated psammophytic *Halimeda* within seagrass meadows (<1 m b.s.l.) on the innermost reef flat or lagoon. Note that seafloor sediment samples were taken from areas (**d**) and (**e**) close to the beach (inner and innermost reef flat; Fig. 2; Table 1)

or "fan"-shaped) segments (Fig. 3b) are lost (Table 1; Fig. 7b–f and corresponding digital photographs). Only the central parts of segments are preserved. Likewise, with respect to sampling location the stage of intra-granular, secondary cementation is observed to increase in segments towards the shore (Fig. 7a–c). Segments PS6, PS7, and PS8 were sampled close to each other and show advanced stages of secondary cementation (Table 1; Fig. 7d, e) with specimen PS8 completely cemented (Fig. 7f).

Halimeda segments from the islands Pulau Tambakulu (PT) and Pulau Pamangangang (PP)

Halimeda segments sampled at PT (Figs. 2d, 8a–c) and PP (Figs. 2b, 8d–f) show consecutive microstructural alteration in direction towards the shore (Table 1). Analyses of the internal $CaCO_3$ microstructure (thin-sections) and external grain shape (digital photographs) reveal similarities to observed alteration patterns of segments sampled at PS. Specimens PT10 and PP5 (Fig. 8a, d, respectively) that show pristine external morphology and internal microstructure, were sampled on the reef flat (Fig. 2b, d). Abraded segments and in an advanced stage of cementation were sampled at the shoreline and onshore in the drift line (Table 1; Fig. 8b, c, e, f).

Halimeda segments from the island Pulau Panambungan (PPB)

Two analyzed segments from PPB (Fig. 2a) show similar microstructural alteration stages with respect to sampling location as segments from PS, PT, and PP (Table 1). Specimen PPB10 (i.e., exemplarily for 19 analyzed segments at PPB) sampled on the reef flat shows microstructural features typical for a pristine segment, i.e., primary utricles and primary IUS, and no secondary cementation (Fig. 9a). Specimen PPB8 sampled within the drift line (Fig. 9b) is almost completely secondarily cemented. Secondary cements within larger central utricles and within secondary IUS may consist of the $CaCO_3$ polymorph Mg-calcite, which is inferred from energy-dispersive X-ray (SEM–EDX) measurements (Fig. 10) and which also is indicated

Fig. 6 Digital photograph of psammophytic macro-algae of the genus *Halimeda* (presumably specimen of *Halimeda* cf. *cuneata* or *H. gigas*) with segments >2 cm growing on sandy substrate in the inner reef flat area at PPB (Figs. 2a, 5). Note the fine-grained carbonate sediment in which these *Halimeda* grow and that they likely produce. No segments of these particular *Halimeda* species are observed in the nearby surface sediment depicted and within sediment samples taken

by a change in color (gray) in the back-scattered electron image (BSE–SEM). Seven more cemented *Halimeda* segments obtained from PPB showed Mg-calcite infillings of utricles.

Consecutive stages of segment alteration

Thin-section and morphological analyses (via SEM and digital photography) of the $CaCO_3$ microstructure of *Halimeda* segments from surface sediments allow the identification of consecutive stages of segment alteration. Two sedimentary processes (1) physical surface abrasion and (2) secondary cementation were identified to be primarily responsible for the alteration of the external and the internal $CaCO_3$ microstructure of the segments (Milliman 1974; Alexandersson and Milliman 1981; Perry 2000). Besides these two major processes, micro-bioerosion and surface dissolution (i.e., chemical abrasion; Perry and Taylor 2006) also were observed in some of the segments analyzed. A qualitative estimation of the alteration stages observed in segments presented in this study is given in Table 2.

Physical surface abrasion.–Segments that were sampled on the reef flat show porous surface structures of peripheral primary utricles and primary IUS typical for freshly dropped, pristine *Halimeda* segments (Figs. 7a, 8a, d, 9a; Table 1). Thus the external morphological segment shape is very similar to that of living segments (Fig. 3a). In contrast, most segments that originate from sediment samples which were taken close to and within the drift line of islands, exhibit a heavily abraded, smooth surface and lack typical peripheral porous structures from primary utricles (Figs. 7b, c, e, f, 8c, e, f, 9b; Table 1). Additionally, their typical grain shape is largely altered from a characteristic pristine "butterfly" or "fan-like" segment shape to a more roundish pebble-shaped grain (digital photographs in Figs. 7b–f, 8c).

Secondary cementation.–Segments sampled directly on the reef flat rarely show indications of secondary cementation and exhibit a typical *Halimeda*-like grain shape, pristine surface characteristics and an unaltered internal skeletal microstructure that hardly differs from mature living segments (Figs. 7a, 8a, d, 9a and corresponding digital photographs; Table 1; cf. Fig. 4a).

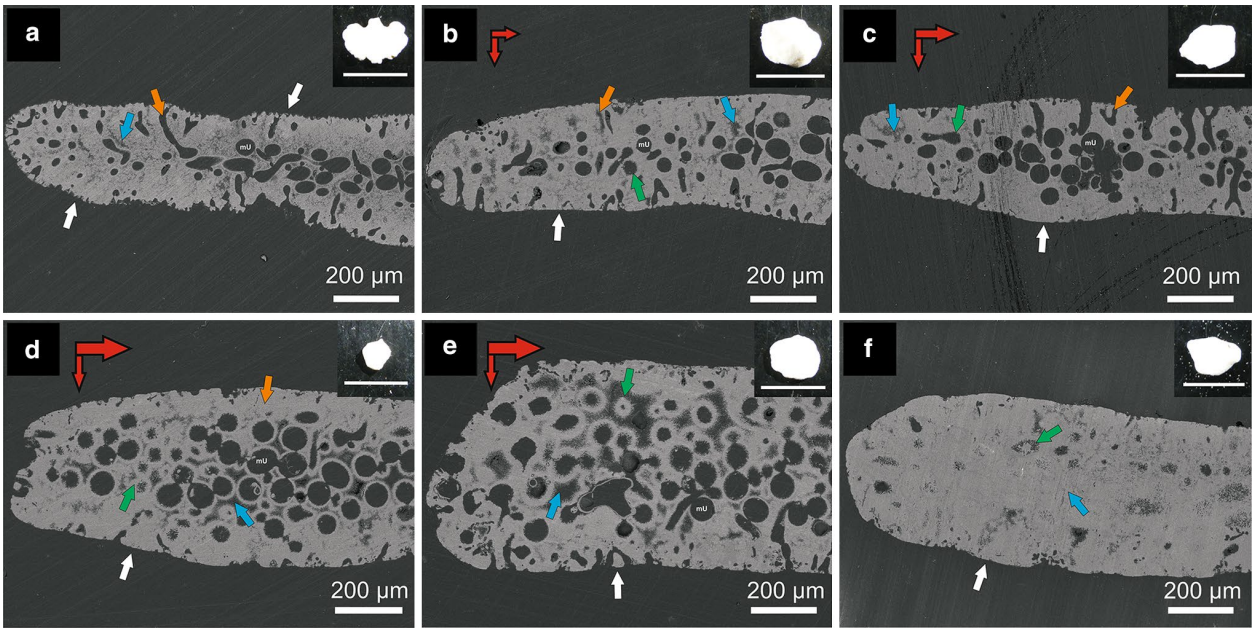

Fig. 7 SEM images (via BSE–SEM) of thin-sections and corresponding digital photographs (*small upper right box*) of selected *Halimeda* segments from transects at PS (6 of 9). **a** Nearly pristine segment shows primary utricle surface structure (*white arrow*), secondary utricles (*orange arrow*) and open interutricular space (*blue arrow*). **b** Abraded segment showing no primary utricles (*white arrow*), closing secondary (*orange arrow*), and medullary (*green arrow*) utricles, and left open interutricular space (*blue arrow*). **c** Abraded segment lacking primary utricles (*white arrow*) with partly secondary (*orange arrow*) and closing medullary (*green arrow*) utricles, and left open interutricular space (*blue arrow*). **d** Heavily abraded segment with no primary utricles present (*white arrow*), secondary utricles mainly closed (*orange arrow*), and partly left open interutricular space (*blue arrow*), medullary utricles in closing stage (*green arrow*). **e** Heavily abraded segment showing no primary utricles (*white arrow*), left open interutricular space (*blue arrow*) and closing medullary utricles (*green arrow*). **f** Heavily abraded and fully cemented segment with no primary utricle structure present (*white arrow*). Interutricular space and medullary utricles nearly closed (*blue* and *green arrow*, respectively). Thickness of *red arrows* in (b–e) qualitatively indicates the strength of the "physical erosional force" that shaped the external morphology of the segments. *mU* medullary utricle; *scale bar* in digital photographs 0.5 cm

In segments that were sampled close to the shore, secondary cementation is observed within the peripheral IUS (Table 1; Figs. 7b, e, 8b). In segments sampled in the drift line of islands, $CaCO_3$ infillings of the secondary IUS and secondary and tertiary utricles are present (Table 1; Figs. 7c, d, 8c, and, 9b). Additionally, in these segments, the entire IUS is (almost) completely cemented. Central medullary utricles are found cemented in segments sampled close to the shore (Figs. 7f and, 9b). However, in some specimens, medullary utricles are observed in an advanced stage of cementation when open space within the secondary IUS is still present (e.g., Fig. 7e). The analyzed secondary cements generally consist of the $CaCO_3$ polymorph aragonite (e.g., $CaCO_3$ needle infillings of utricles), but in some cases are likely formed by the $CaCO_3$ polymorph Mg-calcite (Figs. 9b and, 10).

Micro-bioerosion.–In *Halimeda* segments that show nearly pristine surface structures (i.e., primary utricles still present and not cemented) and grain shape (i.e., "butterfly" or "fan-like" segment shape, Fig. 3) the observation of micro-bioerosion (e.g., caused by fungi, micro-algae, and bacteria) is limited to the cemented primary IUS (Fig. 7a; Table 2). In partially cemented and completely cemented segments, micro-bioerosion occasionally also is observed in the inner secondary IUS and in cemented utricles (Figs. 7e, f, 8e).

Discussion

Assessing the grade of segment alteration

Primarily, two sedimentary processes, physical abrasion, and secondary cementation are responsible for the alteration of the external and internal $CaCO_3$ microstructure of the segments (Milliman 1974; Perry 2000). These processes act in parallel and as a result, segments show a variety of different morphological stages. Determining the progression of each stage to infer time periods of transport and deposition and thus the relative segment age without dating them is not trivial as both processes are non-uniform

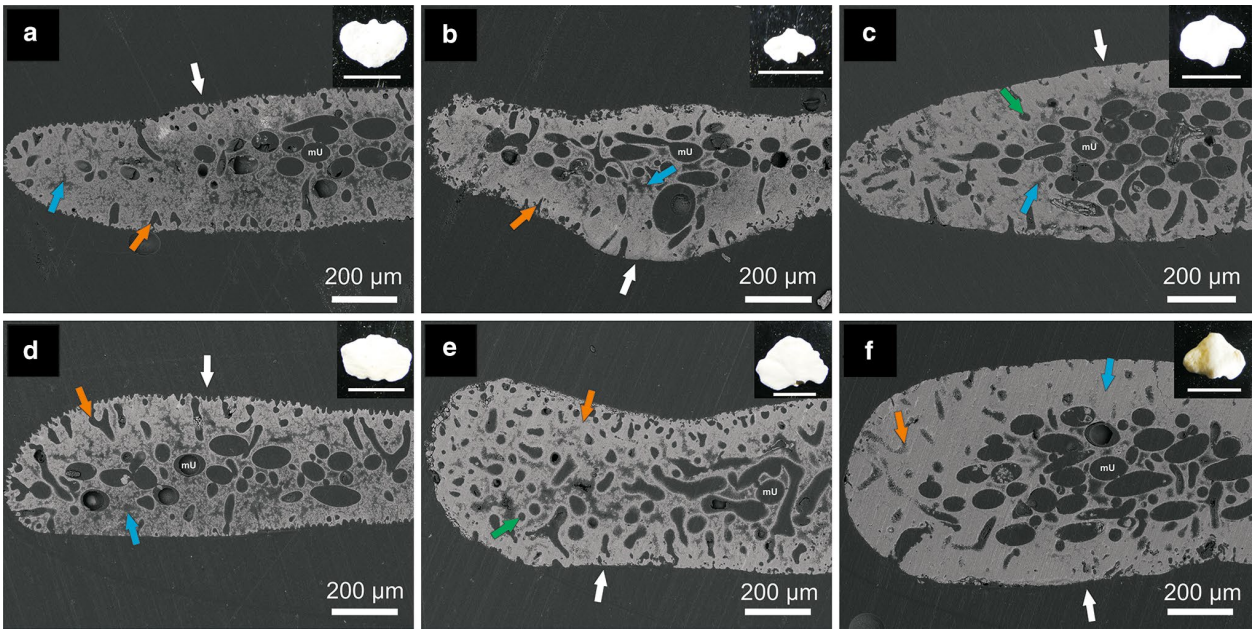

Fig. 8 SEM images (via BSE–SEM) of thin-sections and corresponding digital photographs (*small upper right box*) of selected *Halimeda* segments from transects PT (3 of 8) (a–c) and PP (3 of 9) (d–f). **a** Fairly pristine segment showing primary utricle structure (*white arrow*), secondary utricles (*orange arrow*), and left open interutricular space (*blue arrow*). **b** Abraded segment with no primary utricles present (*white arrow*), closing secondary utricles (*orange arrow*), and left open interutricular space (*blue arrow*). **c** Abraded segment showing no primary utricles (*white arrow*), closing medullary utricles (*green arrow*), and left open interutricular space (*blue arrow*). **d** Nearly pristine segment showing primary utricles (*white arrow*), secondary utricles (*orange arrow*), and left open interutricular space (*blue arrow*). **e** Abraded segment with no primary utricles (*white arrow*), partly closed secondary utricles (*orange arrow*), and closing medullary utricles (*green arrow*). **f** Abraded and cemented segment showing no primary utricles (*white arrow*) and closing secondary utricles (*orange arrow*). Interutricular space is almost completely closed (*blue arrow*). *mU* medullary utricle; *scale bar* in digital photographs 0.5 cm

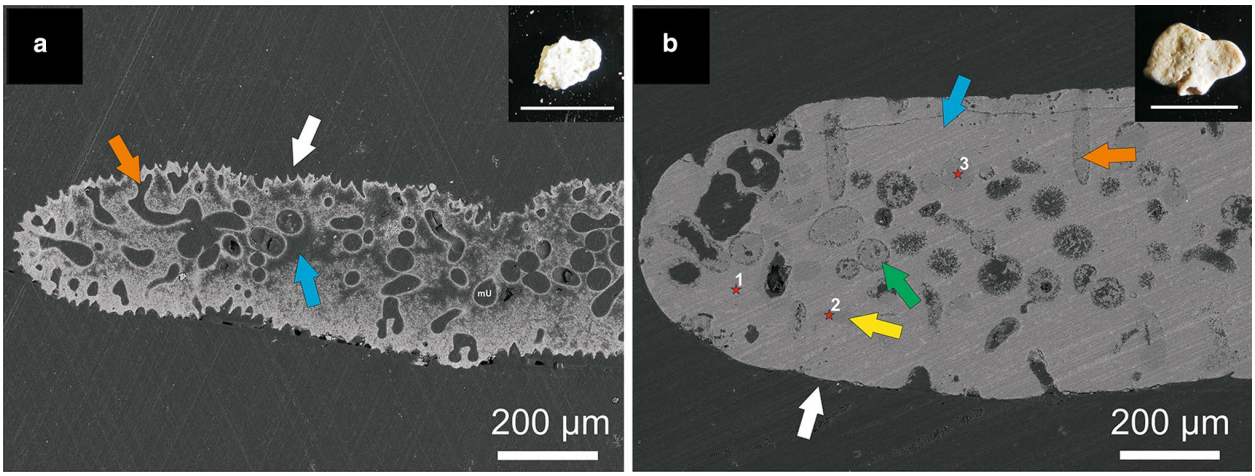

Fig. 9 SEM images (via BSE–SEM) of thin-sections and corresponding digital photographs (*small upper right box*) of selected *Halimeda* segments from transect PPB (2 of 19). **a** Pristine segment shows primary utricle surface structure (*white arrow*), secondary and tertiary utricles (*orange arrow*) and left open interutricular space (*blue arrow*). **b** Abraded and heavily cemented segment with no primary utricles (*white arrow*), secondary and medullary utricles closed (*orange* and *green arrow*, respectively), and interutricular space completely closed (*blue arrow*). Note the different $CaCO_3$ mineralogy of infillings of utricles (*orange* and *green arrow*) and within the innermost interutricular space (*blue* and *yellow arrows*) as indicated by energy-dispersive X-ray (EDX) measurements (Fig. 10). Secondary cements of seven more segments obtained from PPB consisted of the $CaCO_3$ polymorph calcite. *mU* medullary utricle; *scale bar* in digital photographs 0.5 cm

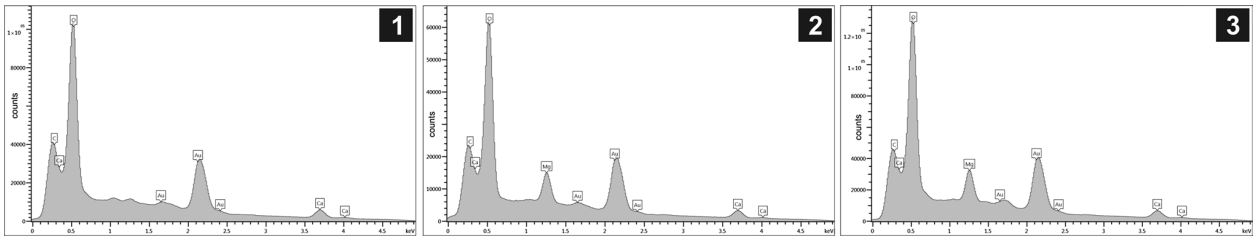

Fig. 10 Energy-dispersive X-ray (EDX–SEM) measurements of thin-section depicted in Fig. 9b. Element profiles 1–3 correspond to the marked spots (*red stars*) in Fig. 9b. (1) Original skeletal microstructure (2) cemented interutricular space, and (3) cemented medullary utricle. Note the absence and presence of Mg^{2+} in (1), (2), and (3), respectively. Thin-section was gold sputtered (Au)

Table 2 Details on analyzed *Halimeda* segments from surface sediment samples of transects from islands Pulau Suranti (PS), Pulau Tambakulu (PT), Pulau Pamangangan (PP), and Pulau Panambungan (PPB) in the Spermonde Archipelago (SW Sulawesi, Indonesia; Fig. 2)

Figure	Sample ID	Species or lineage	Surface abrasion	Secondary cementation	Surface dissolution	Micro-bioerosion	Preservation
7a	PS4	*Halimeda opuntia*	–	–	–	+/pmB	Unbroken, pristine
7b	PS3	Opuntia	+	+	I	–	Unbroken, well-rounded
7c	PS2	Opuntia	+	+	I	+/dmB	Unbroken, rounded
7d	PS6	?	++	++	I	+/pmB	Unbroken, rounded
7e	PS7	Opuntia	+++	++	I	++/dmB	Unbroken, rounded
7f	PS8	Opuntia	++	+++	I	++/dmB	Unbroken, rounded
8a	PT10	*Halimeda opuntia*	–	–	–	–	Unbroken, pristine
8b	PT9	*Halimeda opuntia*	+	+	II	++/pmB	Unbroken, bioeroded
8c	PT8	*Halimeda opuntia*	++	+	I	+/pmB	Unbroken, rounded
8d	PP5	*Halimeda opuntia*	–	–	–	–	Unbroken, pristine
8e	PP6	Opuntia?	+	+	I	+/dmB	Unbroken, pristine
8f	PP7	Opuntia	++	++	I	+/pmB	Unbroken, rounded
9a	PPB10	*Halimeda opuntia*	–	–	–	–	Fragmented, pristine
9b	PPB8	Opuntia	+	+++[a]	III	+/pmB	Unbroken, etched

Shown is the identified *Halimeda* species of segments analyzed or, where species identification was ambiguous, of *Halimeda* lineage (after Hillis 2001; Verbruggen and Kooistra 2004). Also shown is the qualitative grade of segment alteration (physical surface abrasion and secondary cementation), the qualitative stage of surface dissolution (after Perry and Taylor 2006), the extent and depth of micro-bioerosion and, the qualitative preservation of the morphological segment shape and surface structure

– = feature is absent; + to +++ = estimated grade of feature present; I to III = stages of surface dissolution; pmB = peripheral micro-bioerosion in primary interutricular space (pIUS); dmB = deep micro-bioerosion in secondary interutricular space (sIUS)

[a] specimen shows secondary cementation of $CaCO_3$ polymorph Mg-calcite, cf. Fig. 10

in nature. *Halimeda* segments become physically abraded when transported, whereas secondary cementation is a continuous process that nevertheless may largely depend on seawater and pore-water $CaCO_3$ saturation state (Ω) (e.g., Alexandersson 1972; Alexandersson and Milliman 1981; Friedman 1998; Perry 2000). Processes such as micro-bioerosion and surface dissolution (i.e., chemical abrasion) that additionally affect the external and internal $CaCO_3$ segment microstructure were not observed to play major roles for the overall extensive alterations of *Halimeda* segments presented in this study (cf., Perry 2000; Perry and Taylor 2006). Due to the strong primary cementation (i.e., high MAC content; Wizemann et al. 2014) of the segments analyzed these are unlikely to disintegrate in the sediment, even if micro-bioerosion is present. Additionally, sea- and surface sediment pore-water $CaCO_3$ saturation at these tropical islands likely is comparatively high (i.e., $\Omega_{arag} > 3$; Hoegh-Guldberg et al. 2007) and leads to secondary cementation (frequently observed, Table 2).

Stages of physical surface abrasion

Physical abrasion of carbonate grains is generally considered as an indication for sediment transport

(Milliman 1974). Thus the particular stage of abrasion may be related to the time period and intensity of sediment transport (i.e., current regime in relation to seabed or substrate roughness). Physical surface abrasion first causes loss of the small peripheral primary utricles and the primary IUS that form the characteristic porous surface microstructure of *Halimeda* segments. The process of physical abrasion does not seem to act with equal force on the entire segment, as the thinner distal elongated parts were observed to be much heavier abraded than the thicker central parts. Likely, a gentle rolling movement across the seabed and the high energy of waves onto the shore are responsible for this distinct segment shape. Heavily abraded segments show no peripheral primary utricles and only consist of the former central part of pristine segments. We assume that segments that show heavily altered surface microstructures and grain shapes were transported over longer distances (> ~100 m) from their source of origin, as these were predominantly sampled on the shore within the drift line of islands. It also has to be mentioned that physical abrasion is more common than fragmentation of segments in the sediment samples investigated. This may lead to the following conclusion. Small and heavily calcified segments (i.e., <1 cm in diameter, high MAC content) such as from the lineages of *Halimeda opuntia* and *H. micronesicae* (Hillis 2001; Verbruggen and Kooistra 2004) predominantly become preserved as complete segments and in most cases do not undergo fragmentation to needle-sized grains. In contrast, larger segments of many other *Halimeda* species (i.e., >2 cm in diameter; needle-dominated, acicular internal microstructure with low MAC content, cf. Fig. 4) rapidly break apart and form needle mud that only is identifiable via scanning electron microscopy (Neumann and Land 1975; Macintyre and Reid 1992). However, detailed analyses of the mud fraction (<63 µm) were out of the scope of this study and due to high wave energy this fraction likely would be transported off the reef. Furthermore, as sampling was done in vicinity to and on the shore, wave energy may have already fragmented most segments from these *Halimeda* species down to needle mud.

Stages of secondary cementation

Secondary cementation starts on the peripheral structures of the segment, i.e., in the primary utricles and the left open peripheral IUS. Advanced cementation stages show the onset of $CaCO_3$ infilling of larger utricles and secondary IUS. Often, full cementation of the IUS is observed before complete cementation of the largest medullary utricles, which then ultimately results in a completely cemented segment. However, in some cases medullary utricles may become filled at the time of, or even before, the secondary IUS. This probably also depends on the extents of primary cementation of the formerly living segment and on the $CaCO_3$ polymorph precipitated during secondary cementation.

The occurrence of secondary cementation is an indication of the relative age of a segment rather than of sediment transport. Thus, in combination with physical surface abrasion, the stage of intra-granular cementation may allow further evaluation of the time period a segment was transported. As the left open space within a freshly dropped *Halimeda* segment (i.e., utricles and open areas of the IUS) is relatively small in volume (<1 cm^3), particularly in small and heavily calcified segments from *Halimeda* species of the *H. opuntia* and *H. micronesicea* lineages (Hillis 2001; Verbruggen and Kooistra 2004), secondary cementation may happen almost as fast as physical abrasion (when transported). In contrast to abrasion, secondary cementation may start right after death of the segment even when still attached to the living alga (Milliman 1974). Intriguingly, none of the segments analyzed shows merely secondary cementation (e.g., of utricles) without any signs of physical surface abrasion of peripheral primary utricles. This strongly argues against in situ deposition of segments in these island settings. However, the time-scale of secondary cementation is not known, largely under-studied and thus is still to debate. Friedman (1998) observed that $CaCO_3$ cementation is rapid (oolite formation in <1 year) in areas such as the Bahamas, where seawater is $CaCO_3$ supersaturated ($\Omega_{arag} > 4$). Given the small volume of open IUS and utricles of well-calcified segments, it seems plausible to have rapid secondary cementation occurring even in tropical regions with slightly lower seawater $CaCO_3$ saturation ($\Omega_{arag} \sim 3$), although this depends further on local micro-environmental conditions such as pore-water saturation with $CaCO_3$. Alexandersson and Milliman (1981) dated entirely cemented *Halimeda* segments with in-filled utricles from surface sediments of the Brazilian continental shelf and obtained ages over 10 k years BP, without considerable recrystallization of the original $CaCO_3$ segment microstructure. Thus, it may be exactly the rapid progress of secondary cementation that enables freshly dropped *Halimeda* segments to persist as complete plates in surface sediments for such long periods of time. Undoubtedly, this time gap is very large and temporal partial dissolution followed by frequent re-cementation cannot be excluded. Nevertheless, these findings underline the high preservation potential of well-cemented segments.

Secondary cements of the $CaCO_3$ polymorph Mg-calcite, indicated by the presence of Mg^{2+} in the element composition of cements (via SEM–EDX) and by gray value change in the BSE–SEM image (Reid and Macintyre 1998), were observed in some fairly cemented segments

from the island PPB (Figs. 2a, 9b; only one out of seven specimens is shown here). Especially the larger medullary utricles and the innermost sIUS are filled with Mg-calcite (compare Alexandersson and Milliman 1981; Roberts et al. 1988; Reid and Macintyre 1998), whereas more peripheral utricles and peripheral IUS are filled with secondary aragonite cements. Thus, spaces that show Mg-calcite cements likely became filled in the latest stage of the cementation process. Moreover, analyzed segments still exhibit external characteristics of a typical *Halimeda*-shaped grain. The observed loss of primary utricles thus may not be due to long-lasting transport causing abrasion as this would result in a well-rounded grain. More likely, this favors rapid deposition by an extreme sedimentation event. In these segments, surface dissolution (i.e., corrosion) might account for the altered surface morphology (Perry 2000). We observed Mg-calcite infillings exclusively in segments from sediments of the island of PPB. Clearly, there has to be a specific environmental reason why this is (only) observed there. Potentially, it is an indicator that the freshwater lens under the island discharges into the shoreline and inner reef flat but it may also be the result of enhanced precipitation of rainwater as particularly this island is located closer to the mainland Sulawesi. Freshwater, being rich in CO_2, naturally exhibits a lower carbonate saturation state (Ω) and a lower Mg–Ca ratio than seawater, thus low-Mg calcite may be favored over aragonite in abiotic $CaCO_3$ precipitation (Hanor 1978; Longman 1980; Stanley et al. 2010). This may also explain the observed surface dissolution of the aragonitic peripheral microstructure with loss of primary utricles. Another possibility might be differing chemical and nutrient composition of water masses on the inner shelf area close to the mainland as well as an enhanced sediment load compared to those at offshore reefs (e.g., at islands PT, PS, and PP on the shelf edge; Fig. 1b) that are more influenced by open ocean waters (e.g., Renema 2002; Cleary et al. 2005). Such conditions may cause $CaCO_3$ dissolution as they decrease the $CaCO_3$ saturation state of seawater (McLaughlin et al. 2003; Mutti and Hallock 2003). However, besides physico-chemical environmental factors biological causes are equally likely. For example, endolithic microbes or micro-bioeroders that inhabit crevices (i.e., utricles and open IUS) may be responsible for the precipitation of Mg-calcite (Nothdurft et al. 2007; Reyes-Nivia et al. 2014). Nevertheless, we found no evidence of extensive micro-bioerosion and boring organisms in the skeletal microstructure and within the cements. Moreover, segments show calcitic infillings of central utricles and secondary IUS that were sampled in opposing transects around and on the island (data not shown). This may exclude a specific local microbiological community to be the reason for the Mg-calcite cements within these segments. Infillings of Mg-calcite cements in *Halimeda* segments sampled from the sediment are quite common and may occur both as low and high Mg-calcite (Alexandersson and Milliman 1981; Roberts et al. 1988; Reid and Macintyre 1998). In fact, this suggests that precipitation of Mg-calcite within segments may have different (abiotic and biotic) origins.

Surface dissolution

Several *Halimeda* segments show early stages of surface dissolution (Table 2; after Perry and Taylor 2006). However, in most cases surface dissolution is not a major process. Frequently observed segment cementation indicates that the seawater and pore-water of these islands is sufficiently $CaCO_3$ oversaturated to prevent abiotic chemophysical dissolution. Furthermore, physical abrasion is identified to be by far more intense and effective in modifying the external surface structure and segment morphology, thus it is difficult to estimate the stage of surface dissolution when extensive physical abrasion is present. Morphological changes of the grain shape, e.g., rounding of grains and subsequent loss of primary utricles and primary IUS, here almost completely result from physical abrasion. In some cases, especially where extensive peripheral micro-bioerosion is visible, predominantly bio-eroding endoliths may have caused observed surface dissolution. Nevertheless, in the particular case of a segment from the island PPB that shows secondary cements of Mg-calcite, surface dissolution is in an advanced stage (cf. Perry and Taylor 2006). As discussed in the previous paragraph, the specific type of segment cementation and the occurrence of extensive surface dissolution at this site may both have a similar cause such as low $CaCO_3$ saturation of pore-water induced by freshwater influence (Milliman 1974; Hanor 1978).

Micro-bioerosion

Many *Halimeda* segments show signs of micro-bioerosion (Table 2; ten out of 14 segments in this study). Micro-borings are most abundant and widespread in heavily cemented *Halimeda* segments (Perry 1998; Fig. 7e, f). As these segments are strongly abraded, with polished surface lacking porous primary utricle structure and primary IUS, this likely resembles “in situ” bioerosion during long-term sediment deposition. Pristine segments show signs of “lifetime” bioerosion that in most cases is only observed within the primary IUS (Fig. 7a). Micro-bioerosion is common in living *Halimeda* segments (Macintyre and Reid 1995; Wizemann et al. 2014) where it is limited to the well-calcified primary IUS. However, as soon as a segment is dropped from the algae, traces of this peripheral “lifetime” bioerosion subsequently become physically eroded via transport-induced surface abrasion (Perry 2000). Thus, the observation and the

extent of structurally deep micro-bioerosion on a segment may also be an indication for the retention time and the relative age of the segment in the sediment as it is presumably more likely to have settling of micro-bioeroders during phases of temporary deposition than during frequent relocation (Perry 1998). However, heavily cemented segments may be very old as mentioned above (e.g., Alexandersson and Milliman 1981), which might, without knowledge on the segment age, contradict the use of bioerosion as an indicator to infer relative time of deposition.

The origin of *Halimeda* sediments at tropical reef-fringed islands

Segments sampled in transects from the reef flat towards the shore show a consecutive increase in surface abrasion and subsequently exhibit a rounded external morphology that indicates significant sediment transport. Thus, segments with merely primary IUS and peripheral primary utricles cemented were likely sampled closer to *Halimeda* communities on the outer reef flat (i.e., high-energy intra-reef area) or at the reef crest (Fig. 5). Segments heavily abraded and additionally with secondary IUS and larger central utricles cemented were sampled further away from their source of origin (i.e., here at the shoreline and onshore).

The internal morphological microstructure of the investigated segments is similar to *Halimeda* species from taxonomic lineages that exhibit rather small segments. Analyses suggest that the origin of these complete *Halimeda* segments are lithophytic, heavily calcified *Halimeda* species such as *H. opuntia*, which inhabit hard substrates on the reef crest and coral patches on the outer reef flat (inter-reef area; Fig. 5). Segments of psammophytic *Halimeda* species that grow on inner reef flats or within the lagoon were not observed in sediment samples (Table 2). The mere occurrence of *Halimeda* segments in bulk sediments and sediment cores, even when sampled in areas where macro-algae of the genus *Halimeda* are observed growing, should therefore not be rashly regarded as "in situ" sediment production and "in situ" deposition without identification of the *Halimeda* species or lineage and taking into account their specific habitat preference. Moreover, in order to be able to retrace the actual source it is necessary to assess stages of surface abrasion and (intra-granular) secondary cementation of the segments via thin-section (scanning electron) microscopy (Figs. 3, 4).

Halimeda-segment alterations in the sediment: a proxy for sediment transport?

The distinct consecutive stages of abrasion and secondary cementation patterns observed in the microstructure of *Halimeda* segments allow for speculation on the spatial and temporal extent of sediment transport. Even in the comparably few sediment samples (45 out of 71) analyzed, *Halimeda* segments show different alteration stages in relation to sampling location, from fairly pristine to heavily altered plates, illustrating the full range of alteration stages possible. Thus, it might be possible to reconstruct the local sediment transport in tropical reef islands with the help of *Halimeda* segments. Ford and Kench (2012) already have drawn this conclusion, based on segment durability. However, to be able to relate to what extent segments become transported, assessment of a multitude of additional environmental data is necessary. This may include data from seasonal current regimes, such as water flow direction and energy, and knowledge about extreme sedimentation events, such as major storms, tsunamis, or spring tides (e.g., Harris et al. 2014). Moreover, as segments investigated exhibit similar dimensions (~0.5 cm; i.e., typical segment size of *Halimeda* species of the lineage of *H. opuntia*) they represent only the grain-size classes of medium to fine pebbles. For that reason sediment transport in areas with weak current regime likely does not apply. Nevertheless, pristine and freshly settled *Halimeda* segments may be transported together with grains of smaller size (<0.4 cm), as their flattened external "butterfly" or "fan-like" morphology provides them with higher buoyancy than roundish grains within the same grain-size range (e.g., Jindrich 1969; Kench and McLean 1996). These hydrodynamic characteristics of freshly dropped, pristine segments may then vanish after some time due to progressive abrasion of the elongated outer parts during transport and the gain in intra-granular $CaCO_3$ density due to secondary cementation.

Tracing *Halimeda* segments from a specific source area to a site of deposition requires mapping of patch reefs and a survey of the complete population structure of *Halimeda* species present around the specific island investigated (e.g., Wiman and McKendree 1975; Johns and Moore 1988). Furthermore, it may be beneficial to stain local assemblages of *Halimeda* algae (e.g., with Alizarin Red S) to be able to visually track dropped segments over time within the sediment similar to techniques used in field studies that analyzed algae growth rates (e.g., Wefer 1980; Multer 1988; Multer and Clavijo 2004). However, it is difficult to track single segments within the sediment if not a large number of algae is repeatedly and consistently stained over a period of time (e.g., one month).

From the presented analyses, it might be possible to reconstruct the transport pattern of dropped segments and the period of time that elapsed between drop of segments from the alga and their final deposition, as segments become abraded when distributed (transported) and gradually more cemented (Friedman 1998, Perry 2000). Consequently, segments that do not show extensive cementation of utricles and remnants of IUS and additionally do not

show signs of abrasion or corrosion of the primary utricle structure may be considered recent (<1 year). Therefore the stage of cementation within segments in relation to the stage of abrasion may be used as an indicator to infer how long these resided close to its source (e.g., algal communities). Drawing this conclusion may be valid only for segments sampled from surface sediments, which have constantly remained submerged and not for segments that are found onshore or are obtained from sediment cores. Segments from onshore sediments that lack secondary cementation and exhibit an almost pristine external and internal $CaCO_3$ microstructure can be very old (i.e., hundreds to thousands of years) when rapidly deposited by extreme events (i.e., storms, tsunamis). Thus pristine segments found in sediments onshore may be used as proxies for environmental reconstructions (e.g., via stable isotope measurements). However, the exact age of most segments in more recent surface sediments cannot be determined sufficiently yet by modern dating techniques, such as AMS, δC^{14}, and Th-U series, as most segments in surface sediments on the reef flat are likely much younger in age (<10 years; e.g., Clark et al. 2014). Presumably, complete *Halimeda* segments from surface sediments thus are a relatively contemporary tracer for sediment transport (e.g., Ford and Kench 2012; Dawson and Smithers 2014), but erroneous estimations of their relative age and preservation potential are more likely, if the *Halimeda* lineage or species is not identified and internal microstructural features of the segments such as primary and secondary cementation are not investigated. Segments that become deposited finally e.g., onshore, down the reef slope, or buried in the sediment are undoubtedly much older and well within the range of standard δC^{14} dating (>400 years) (cf., Alexandersson and Milliman 1981; Roberts et al. 1988; Kench, pers. com.). These may provide insights into past environmental conditions and processes of early island formation. However, care must be taken when dealing with segments that old, as these exhibit a higher likelihood of skeletal

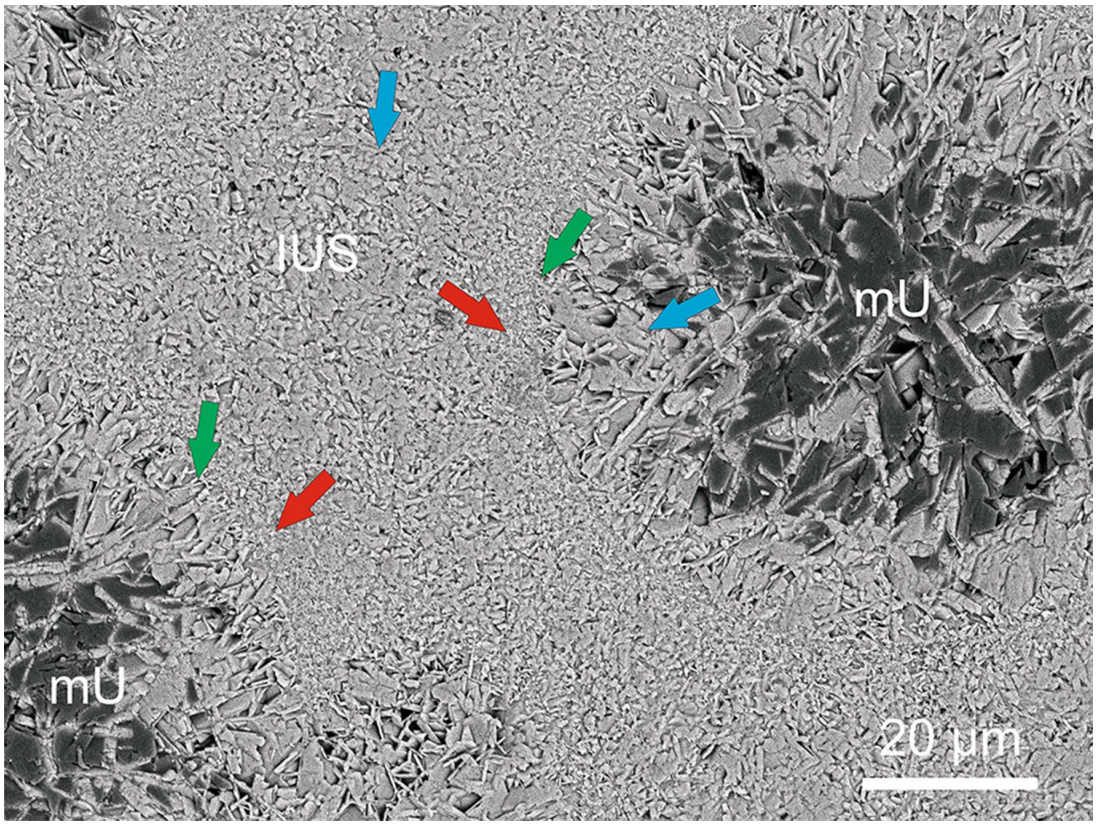

Fig. 11 SEM image (via BSE–SEM) of a thin-section from a heavily cemented *Halimeda* segment (*H. opuntia* lineage) obtained from surface sediments, illustrating unaltered original skeletal microstructure and secondary cementation within central parts. Shown are skeletal primary needles at the former location of utricle walls (e.g., *green arrows*) and micro-anhedral carbonate rims of medullary utricles (e.g., *red arrows*) (Wizemann et al. 2014). Secondary cements (e.g., *blue arrows*) fill-in medullary utricles in the form of long needle-like and granular, blocky $CaCO_3$ crystals (>1 µm). Granular $CaCO_3$ also infills voids between original secondary needles in the interutricular space. Note the remarkable difference in $CaCO_3$ crystal morphology of micro-anhedral carbonate when compared to secondary cements (Reid and Macintyre 1998). *IUS* interutricular space; *mU* medullary utricle

alterations (e.g., $CaCO_3$ recrystallization) caused by early diagenetic processes. Nevertheless, we investigated heavily cemented albeit undated segments from surface sediments that show an unaltered original microstructure with clearly distinguishable skeletal features and secondary cements (Fig. 11). Thus with both, knowledge of skeletal formation (i.e., calcification) and of secondary cementation, environmental reconstructions from segments may be indeed practicable, e.g. via high-resolution microanalyses such as Nano-SIMS (secondary-ion mass spectrometry).

Conclusions

Processes such as abrasion and secondary cementation, which alter biogenic carbonate grains and subsequently lead to their preservation in the sediment, are important for providing sediment supply of coral reef environments, for shoreline development and reef island formation. *Halimeda* species that contribute to the coarse carbonate grain-size fraction (>2 mm) of these settings are lithophytic species which typically inhabit hard substrates such as in the coral reef, on the reef crest and on reef patches of the outer reef flat of tropical reef-fringed islands (e.g., Johns and Moore 1988; Fig. 5). Thus, the main source of typical *Halimeda* sediments at tropical islands, e.g. in the Spermonde Archipelago, lies in close vicinity to, and also within, coral reefs fringing the islands. Most *Halimeda* species that grow on adjacent sandy substrates (e.g., on the inner reef flat; Figs. 5, 6) produce fine-grained carbonate sediments (<63 µm). Where typical coarse *Halimeda* sediments are present care should be taken with their interpretation, as that requires identification of the *Halimeda* species or lineage, knowledge on their environmental niche and detailed analyses of their external and internal skeletal microstructure. If these prerequisites are met, *Halimeda* segments will contribute substantially to the reconstruction of sediment transport and island evolution in the tropics.

Acknowledgments This study was funded by the Leibniz-Center for Tropical Marine Ecology (ZMT) in Bremen (Germany). Sebastian Flotow (ZMT-Bremen) is thanked for the preparation of thin-sections and support of SEM analyses. We sincerely thank the editor Franz Theodor Fürsich and reviewer Willem Renema for their effort, helpful comments, and suggestions that greatly improved the manuscript. Fieldwork for this study was conducted under Research Permit No. 399/SIP/FRP/SM/X/2012 and Working Permit No. 2C11JD5741-L of the Indonesian Ministry for Research and Technology (RISTEK).

References

Alexandersson ET (1972) Intragranular growth of marine aragonite and Mg-calcite; evidence of precipitation from supersaturated seawater. J Sediment Res 42:441–460

Alexandersson ET, Milliman JD (1981) Intragranular Mg-calcite cement in *Halimeda* plates from the Brazilian continental shelf. J Sediment Res 51:1309–1314

Clark TR, Roff G, Zhao JX, Feng YX, Done TJ, Pandolfi JM (2014) Testing the precision and accuracy of the U-Th chronometer for dating coral mortality events in the last 100 years. Quat Geochronol 23:35–45

Cleary DF, Becking LE, de Voogd NJ, Renema W, de Beer M, van Soest RW, Hoeksema BW (2005) Variation in the diversity and composition of benthic taxa as a function of distance offshore, depth and exposure in the Spermonde Archipelago, Indonesia. Estuar Coast Shelf Sci 65:557–570

Dawson JL, Smithers SG (2014) Carbonate sediment production, transport, and supply to a coral cay at Raine Reef, Northern Great Barrier Reef, Australia: a facies approach. J Sediment Res 84:1120–1138

Drew EEA (1983) *Halimeda* biomass, growth rates and sediment generation on reefs in the central Great Barrier Reef province. Coral Reefs 2:101–110

Drew EEA, Abel K (1988) Studies on *Halimeda* I. The distribution and species composition of *Halimeda* meadows throughout the Great Barrier Reef Province. Coral Reefs 6:195–205

Edinger EN, Jompa J, Limmon GV, Widjatmoko W, Risk MJ (1998) Reef degradation and coral biodiversity in Indonesia: effects of land-based pollution, destructive fishing practices and changes over time. Mar Pollut Bull 36:617–630

Edinger EN, Kolasa J, Risk MJ (2000) Biogeographic variation in coral species diversity on coral reefs in three regions of Indonesia. Divers Distrib 6:113–127

Ferse SC, Glaser M, Neil M, Mánez KS (2014) To cope or to sustain? Eroding long-term sustainability in an Indonesian coral reef fishery. Reg Environ Change 14:2053–2065

Ford MR, Kench PS (2012) The durability of bioclastic sediments and implications for coral reef deposit formation. Sedimentology 59:830–842

Freile D, Milliman JD, Hillis L (1995) Leeward bank margin *Halimeda* meadows and draperies and their sedimentary importance on the western Great Bahama Bank slope. Coral Reefs 14:27–33

Friedman GM (1998) Rapidity of marine carbonate cementation—implications for carbonate diagenesis and sequence stratigraphy: perspective. Sediment Geol 119:1–4

Ghina F (2003) Sustainable development in small island developing states. Environ Dev Sustain 5:139–165

Glaeser B, Glaser M (2010) Global change and coastal threats: the Indonesian case. An attempt in multi-level social-ecological research. Hum Ecol Rev 17:135–147

Glaser M, Baitoningsih W, Ferse SC, Neil M, Deswandi R (2010) Whose sustainability? Top–down participation and emergent rules in marine protected area management in Indonesia. Mar Policy 34:1215–1225

Goreau T, Goreau N (1973) The ecology of Jamaican coral reefs. II. Geomorphology, zonation, and sedimentary phases. Bull Mar Sci 23:399–464

Granier B (2012) The contribution of calcareous green algae to the production of limestones: a review. Geodiversitas 34:35–60

Hanor JS (1978) Precipitation of beachrock cements: mixing of marine and meteoric waters vs. CO_2-degassing. J Sediment Res 48:489–501

Harris DL, Vila-Concejo A, Webster JM (2014) Geomorphology and sediment transport on a submerged back-reef sand apron: one Tree Reef, Great Barrier Reef. Geomorphology 222:132–142

Hillis L (2001) The calcareous reef alga *Halimeda* (Chlorophyta, Byropsidales): a Cretaceous genus that diversified in the Cenozoic. Palaeogeogr Palaeoclimatol Palaeoecol 166:89–100

Hillis-Colinvaux L (1980) Ecology and taxonomy of *Halimeda*: primary producer of coral reefs. Adv Mar Biol 17:1–327

Hine AC, Hallock P, Harris MW, Mullins HT, Belknap DF, Jaap WC (1988) *Halimeda* bioherms along an open seaway: Miskito Channel, Nicaraguan Rise, SW Caribbean Sea. Coral Reefs 6:173–178

Hoegh-Guldberg O, Mumby PJ, Hooten AJ, Steneck RS, Greenfield P, Gomez E, Harvell CD, Sale PF, Edwards AJ, Caldeira K, Knowlton N, Eakin CM, Iglesias-Prieto R, Muthiga N, Bradbury RH, Dubi A, Hatziolos ME (2007) Coral reefs under rapid climate change and ocean acidification. Science 318:1737–1742

Hoffmann TC (2002) Coral reef health and effects of socio-economic factors in Fiji and Cook Islands. Mar Pollut Bull 44:1281–1293

Hughes T, Baird A, Bellwood D, Card M, Connolly S, Folke C, Grosberg R, Hoegh-Guldberg O, Jackson JBC, Kleypas J, Lough JM, Marshall P, Nyström M, Palumbi SR, Pandolfi JM, Rosen B, Roughgarden J (2003) Climate change, human impacts, and the resilience of coral reefs. Science 301:929–934

Imran AM, Suriamihardja DA, Sirajuddin H (2013) Geology of Spermonde platform. In: Proceedings of the 7th International Conference on Asian and Pacific Coasts, Hasanuddin University Press, Bali, pp 1062–1067

Jindrich V (1969) Recent carbonate sedimentation by tidal channels in the Lower Florida Keys. J Sediment Res 39:531–553

Johns H, Moore C (1988) Reef to basin sediment transport using *Halimeda* as a sediment tracer, Grand Cayman Island, West Indies. Coral Reefs 6:187–193

Kench PS, McLean RF (1996) Hydraulic characteristics of bioclastic deposits: new possibilities for environmental interpretation using settling velocity fractions. Sedimentology 43:561–570

Kench PS, McLean RF, Nichol SL (2005) New model of reef-island evolution: Maldives, Indian Ocean. Geology 33:145–148

Kench PS, Smithers SG, McLean RF (2012) Rapid reef island formation and stability over an emerging reef flat: Bewick Cay, northern Great Barrier Reef, Australia. Geology 40:347–350

Knittweis L, Jompa J, Richter C, Wolff M (2009) Population dynamics of the mushroom coral *Heliofungia actiniformis* in the Spermonde Archipelago, South Sulawesi, Indonesia. Coral Reefs 28:793–804

Longman MW (1980) Carbonate diagenetic textures from nearsurface diagenetic environments. AAPG Bullet 64:461–487

Macintyre IG, Reid RP (1992) Comment on the origin of aragonite needle mud: a picture is worth a thousand words. J Sediment Res 62:1095–1097

Macintyre IG, Reid RP (1995) Crystal alteration in a living calcareous alga (*Halimeda*): implications for studies in skeletal diagenesis. J Sediment Res A65:143–153

Mankiewicz C (1988) Occurrence and paleocologic significance of *Halimeda* in late Miocene reefs, southeastern Spain. Coral Reefs 6:271–279

Martin J, Braga J, Riding R (1997) Late Miocene *Halimeda* algamicrobial segment reefs in the marginal Mediterranean Sorbas Basin, Spain. Sedimentology 44:441–456

McClanahan T, Polunin N, Done T (2002) Ecological states and the resilience of coral reefs. Conserv Ecol 6:18

McLaughlin CJ, Smith CA, Buddemeier RW, Bartley JD, Maxwell BA (2003) Rivers, runoff, and reefs. Global Planet Change 39:191–199

Milliman JD (1974) Recent sedimentary carbonates, part 1. Marine carbonates. Springer, New York

Milliman JD (1993) Production and accumulation of calcium carbonate in the ocean: budget of a nonsteady state. Global Biogeochem Cycles 7:927–957

Moberg F, Folke C (1999) Ecological goods and services of coral reef ecosystems. Ecol Econ 29:215–233

Multer HG (1988) Growth rate, ultrastructure and sediment contribution of *Halimeda incrassata* and *Halimeda monile*, Nonsuch and Falmouth Bays, Antigua, W.I. Coral Reefs 6:179–186

Multer HG, Clavijo I (2004) *Halimeda* investigations: progress and problems. NOAA/RSMAS

Mutti M, Hallock P (2003) Carbonate systems along nutrient and temperature gradients: some sedimentological and geochemical constraints. Int J Earth Sci 92:465–475

Neumann AC, Land LS (1975) Lime mud deposition and calcareous algae in the Bight of Abaco, Bahamas; a budget. J Sediment Res 45:763–786

Nothdurft LD, Webb GE, Bostrom T, Rintoul L (2007) Calcite-filled borings in the most recently deposited skeleton in live-collected Porites (Scleractinia): implications for trace element archives. Geochim Cosmochim Act 71:5423–5438

Orme G, Flood P, Sargent G (1978) Sedimentation trends in the lee of outer (ribbon) reefs, northern region of the Great Barrier Reef province. Philos Trans R Soc A 291:85–99

Perry CT (1998) Grain susceptibility to the effects of microboring: implications for the preservation of skeletal carbonates. Sedimentology 45:39–51

Perry CT (2000) Factors controlling sediment preservation on a north Jamaican fringing reef: a process-based approach to microfacies analysis. J Sediment Res 70:633–648

Perry CT, Taylor KG (2006) Inhibition of dissolution within shallow water carbonate sediments: impacts of terrigenous sediment input on syn-depositional carbonate diagenesis. Sedimentology 53:495–513

Perry CT, Kench PS, Smithers SG, Riegl B, Yamano H, O'Leary MJ (2011) Implications of reef ecosystem change for the stability and maintenance of coral reef islands. Glob Change Biol 17:3679–3696

Rees SA, Opdyke BN, Wilson PA, Henstock TJ (2007) Significance of *Halimeda* bioherms to the global carbonate budget based on a geological sediment budget for the Northern Great Barrier Reef, Australia. Coral Reefs 26:177–188

Reid RP, Macintyre IG (1998) Carbonate recrystallization in shallow marine environments: a widespread diagenetic process forming micritized grains. J Sediment Res 68:928–946

Renema W (2002) Larger foraminifera as marine environmental indicators. Scripta Geol 124:1–263

Renema W (2006) Large benthic foraminifera from the deep photic zone of a mixed siliciclastic-carbonate shelf off East Kalimantan, Indonesia. Mar Micropaleontol 58:73–82

Renema W, Troelstra SR (2001) Larger foraminifera distribution on a mesotrophic carbonate shelf in SW Sulawesi (Indonesia). Palaeogeogr Palaeoclimatol Palaeoecol 175:125–146

Renema W, Hoeksema BW, Van Hinte JE (2001) Larger benthic foraminifera and their distribution patterns on the Spermonde shelf, South Sulawesi. Zool Verh Leiden 334:115–149

Reyes-Nivia C, Diaz-Pulido G, Dove S (2014) Relative roles of endolithic algae and carbonate chemistry variability in the skeletal dissolution of crustose coralline algae. Biogeosci Discuss 11:2993–3021

Roberts H, Aharon P, Phipps C (1988) Morphology and sedimentology of *Halimeda* bioherms from the eastern Java Sea (Indonesia). Coral Reefs 6:161–172

Sawall Y, Teichberg MC, Seemann J, Litaay M, Jompa J, Richter C (2011) Nutritional status and metabolism of the coral *Stylophora subseriata* along a eutrophication gradient in Spermonde Archipelago (Indonesia). Coral Reefs 30:841–853

Scoffin TP, Tudhope AW (1985) Sedimentary environments of the central region of the Great Barrier Reef of Australia. Coral Reefs 4:81–93

Stanley SM, Ries JB, Hardie LA (2010) Increased production of calcite and slower growth for the major sediment-producing alga *Halimeda* as the Mg/Ca ratio of seawater is lowered to a "Calcite Sea" level. J Sediment Res 80:6–16

Verbruggen H, Kooistra W (2004) Morphological characterization of lineages within the calcified tropical seaweed genus *Halimeda* (Bryopsidales, Chlorophyta). Europ J Phycol 39:213–228

Wefer G (1980) Carbonate production by algae *Halimeda, Penicillus* and *Padina*. Nature 285:323–324

Wentworth CK (1922) A scale of grade and class terms for clastic sediments. Geology 30:377–392

Whitten T, Mustafa M, Henderson GS (2002) The Ecology of Sulawesi. PT Java Books Indonesia, Jakarta 777 p

Wienberg C, Westphal H, Kwoll E, Hebbeln D (2010) An isolated carbonate knoll in the Timor Sea (Sahul Shelf, NW Australia): facies zonation and sediment composition. Facies 56:179–193

Wilson MEJ, Vecsei A (2005) The apparent paradox of abundant foramol facies in low latitudes: their environmental significance and effect on platform development. Earth Sci Rev 69:133–168

Wiman SK, McKendree WG (1975) Distribution of *Halimeda* plants and sediments on and around a patch reef near Old Rhodes Key, Florida. J Sediment Res 45:415–421

Wizemann A, Meyer FW, Westphal H (2014) A new model for the calcification of the green macro-alga *Halimeda opuntia* (Lamouroux). Coral Reefs 33:1–14

Woodroffe CD (2008) Reef-island topography and the vulnerability of atolls to sea-level rise. Global Planet Change 62:77–96

Woodroffe CD, McLean RF, Smithers SG, Lawson EM (1999) Atoll reef-island formation and response to sea-level change: West Island, Cocos (Keeling) Islands. Mar Geol 160:85–104

5.1 Extended discussion on the carbonate sediment formation of the green macro-alga genus *Halimeda*

Because of their rapid segmental growth and high abundance, algae of the genus *Halimeda* contribute significant quantities of carbonate sediment to tropical marine settings (e.g., Milliman 1974; Wefer 1980; Drew 1983; Drew and Abel 1988; Hine et al. 1988; Johns and Moore 1988; Milliman 1993; Freile et al. 1995; Rees et al. 2007). Segments from *Halimeda* meadows and bioherms, are known to take part in the formation of carbonate platforms, carbonate banks and ramps, atoll and reef islands, continental shelf rims and, carbonate knolls in the open ocean (Milliman 1974; Alexandersson and Milliman 1981; Roberts and Phipps 1987; Drew and Abel 1988; Hine et al. 1988; Orme and Salama 1988; Phipps and Roberts 1988; Roberts et al. 1988; Freile et al. 1995; Pomar and Kendall 2007; Rees et al. 2007; Wienberg et al. 2010). Sedimentary components of *Halimeda* that are present in sediments are either aragonite needle mud (< 63 µm; Neumann and Land 1975; Macintyre and Reid 1992) or complete to partly fragmented segments in the grain size class of pebble gravel (1.6 > 0.4 cm; Wentworth 1922; Jindrich 1969; Alexandersson and Milliman 1981; Hine et al. 1988; Roberts et al. 1988; Freile et al. 1995). Explanations for the observed sediment characteristics and sediment contribution of macro-algae from the genus *Halimeda* base on the common assumption that dropped *Halimeda* segments undergo rapid fragmentation and finally form carbonate mud (e.g., Milliman 1974; Perry et al. 2011). Even so *Halimeda* segments contribute to fine-grained needle mud, extents of segment calcification and segment size largely differ among *Halimeda* species (Hillis-Colinvaux 1980; Multer 1988; Verbruggen and Kooistra 2004). The existence of species-specific *Halimeda* sediments is often neglected and detailed species-specific analyses of *Halimeda* components are scarce. The general assumption of a consecutive breakdown (i.e., to needle-sized grains) of *Halimeda* segments, no matter what species, led to interpretations that most of the needle mud in tropical settings may derive from calcareous algae (Neumann and Land 1975). Albeit segments of some, if not most, *Halimeda* species rapidly become fragmented and form distinct needle mud, the larger quantity of carbonate muds nevertheless may be either precipitated abiotically or by other organisms (Macintyre and Reid 1992; Milliman et al. 1993; Gischler et al. 2013; Enrique and Schubert 2014). This contradicts the assumption that especially those segments of certain *Halimeda* species that are observed in tropical carbonate sediments worldwide (cf., Tab. 5.1.I, Figs. A1-A14) are a main source for such carbonate muds. In contrast, the species-specific *Halimeda* segments found within tropical marine sediments are an unique persistent component type in tropical carbonate sediments and may endure as complete grains even longer than 10k years in the surface sediments (Alexandersson and Milliman 1981). Besides

they are also frequently observed preserved in the paleo-record, e.g. accumulations in sediment cores and in lime stones (packstones, float- and rudstones) (Mankiewicz 1988; Roberts et al. 1988; Braga et al. 1996; Martin et al. 1997; Granier 2012). Nevertheless, these species-specific segments found in sediments undergo strong morphological alteration, however contrary to the general theory of rapid fragmentation to needle-sized grains (< 63 μm) as widely assumed hitherto.

5.1.1 *Halimeda* segments from sediments worldwide

Carbonate sediments sampled in shallow water environments of tropical shorelines and reef islands worldwide were screened for *Halimeda* segments (Table 5.1.I and Appendix X.II, corresponding Figs. A1 - A14). Thin-sections of sampled segments were used to analyze species and lineage, external morphology (e.g., shape and surface characteristics) and internal microstructure with the SEM. All analyzed segments are in the size range of 1.6 > 0.4 cm pebble gravel (medium to fine pebbles; Wentworth 1922) and if externally pristine, exhibit a characteristic "butterfly", "fan-like" or "trident-like" morphological shape (e.g., Jindrich 1969; Freile et al. 1995; Kooistra and Verbruggen 2005). The internal microstructure (e.g., utricle structure and IUS) of the segments is very similar, thus it is likely that they originate from closely related *Halimeda* species and lineages that inhabit similar habitats. The majority of observed *Halimeda* segments in these sediments are identified to originate from lithophytic species of the lineages Opuntia and Micronesicae (Hillis 2001; Verbruggen and Kooistra 2004). Species within these lineages have small segments (< 1 cm), are widely ramified with thin root-like filaments and are typically found on hard substrates (lithophytic) and within high-energy environments (e.g., fore reef, reef crest; patch reefs on the outer reef flat; Johns and Moore 1988). The close structural similarity of the analyzed segments suggests that only few species and their morphotypes, which especially grow within such habitats, form these typical *Halimeda*-rich (i.e., segment-rich) carbonate sediments that are observed in present tropical settings.

Tab. 5.1.I Origin and number of analyzed *Halimeda* segments (from thin-sections via SEM-BSE) obtained from tropical sediments worldwide (Appendix X.II, Figs. A1 - A14). For further information on sampling location see also figure captions.

Plate (Fig.-Nr.)	Sampling location	Number of segments depicted	by courtesy of
A1	Great Barrier Reef	6	J.D. Milliman
A2	Fiji	4	P. Meyer / H. Westphal
A3	Maldives	3	C. Betzler
A4	Maldives (historical)	2	Natural History Museum Berlin
A5	Timor Sea (Pee Shoal)	3	C. Wienberg / H. Westphal
A6	Brazil (Abrolhos)	3	M. Naumann
A7	Mexico (Yucatan)	16	F.W. Meyer
A8 - A11	Indonesia (Spermonde)	38	T. Mann / A. Klicpera / H. Westphal
A12	Bahamas / Florida / Belize	9	H. Westphal / P. Reid / D. McNeill
A13	Zanzibar	3	N. Hérran / H. Westphal
A14	Hawaii	2	T. Mann / H. Westpal

5.1.2 Origin and alteration of *Halimeda* segments in the sediment

Halimeda species of the lineages Opuntia and Micronesicae that exhibit small segments (< 1.6 cm; high pIUS / sIUS ratio; high $CaCO_3$ / organic ratio; comparably small central utricles) are the source of coarse *Halimeda* sediments (Hillis 2001; Verbruggen and Kooistra 2004). Larger segments (> ~2 cm) of weaker calcified species (e.g., from *Halimeda* lineages Halimeda and Rhipsalis) breack down to needle-sized grains and are a source of aragonite needle muds (Neumann and Land 1975; Drew 1983; Multer 1988; Macintyre and Reid 1992; Verbruggen and Kooistra 2004). Heavily fragmented segments and needles cannot be traced back precisely to communities of calcifying macro-algae. Their source of origin (e.g., algal bioherms or communities vs. abiotic precipitation) thus is difficult to determine (Macintyre and Reid 1992; Milliman et al. 1993). Furthermore, as detailed analyses of carbonate needle mud are rarely undertaken, the total carbonate sediment contribution of the genus *Halimeda* is largely unknown. Overall contribution to tropical carbonate sediments that originate from the genus *Halimeda* (i.e., needle mud and preserved segments combined) may be underestimated.

Complete and heavily calcified *Halimeda* segments that are found in reef sediments become altered in processes such as physical abrasion, micro-bioerosion, dissolution and secondary cementation (Perry 1998, 2000; Perry and Taylor 2006). Dissolution and cementation are predominantly controlled by the $CaCO_3$ saturation of the sea and pore-water of the vicinal microenvironment that is also influenced by bacterial and micro-algal overgrowth, whereas physical abrasion and endolithic micro-bioerosion are concurring processes depending whether the segment is transported or deposited.

5.1.2.1 Cementation and dissolution as in-situ processes

In $CaCO_3$ supersaturated seawater ($\Omega_{arag} > 4$) of tropical shallow seas the process of cementation is rapid (e.g., Friedman 1998; Grammer et al. 1999). Secondary cementation of open spaces in dropped *Halimeda* segments starts at the segment rim and subsequently proceeds to the inner core part. Firstly the peripheral primary utricles (pU) and secondary utricles (sU) as well as open areas in the pIUS in vicinity to the segment rim become filled with $CaCO_3$. Cementation advances to the central parts of the segment and, gradually in-fills tertiary utricles (tU), medullary utricles (mU) and the innermost sIUS. The "ideal" end-stage of the cementation process is an entirely cemented *Halimeda* segment whereby the IUS and utricles become completely filled (e.g., Appendix X.II Fig. A10g). Contrary to the $CaCO_3$ polymorph aragonite that characterizes the skeleton of a living segment, secondary cementation occasionally may consist of other $CaCO_3$ polymorphs such as (low and high) Mg-calcite (Alexandersson and Milliman 1981; Roberts et al. 1988; Reid and Macintyre 1998). However, depending on environmental parameters, such as the $CaCO_3$ saturation of the sea and pore-water, the rapidity and extent of secondary cementation is limited. Physical abrasion (i.e., transport-derived erosion) or micro-bioerosion and other biotically-induced processes, e.g. $CaCO_3$ dissolution and precipitation processes caused by epibionts and endoliths, act in parallel on the segment and may further alter its external habit and internal $CaCO_3$ microstructure (Roberts et al. 1988; Perry 1998; 2000; Nothdurft et al. 2007; Reyes-Nivia et al. 2014). However, surface dissolution and intra-granular cementation may not exclude each other as both were observed in some of the specimens analyzed (e.g., Appendix X.II Figs. A1-14). This is possible when these processes occur at different time scales and are caused by different (abiotic and biotic) processes. Dissolution mainly affects the peripheral porous primary utricle structure and the pIUS and is likely not persistent in $CaCO_3$ oversaturated tropical waters. Well-calcified, primary cemented segments may withstand temporary dissolution longer than lesser-calcified ones. Additionally, they may gain intra-granular density over time (Alexandersson and Milliman 1981; Perry and Taylor 2006).

5.1.2.2 Physical surface abrasion during sediment transport

Physical abrasion of the segment surface structure is a common process and may be interpreted as an indication for the transport of a segment (Perry 2000). Abrasion starts at peripheral parts of the segment with removal of the primary utricles and the pIUS. Heavily abraded segments are reduced to their central parts, i.e. central medullary utricles and sIUS, by loosing the typical "butterfly" or "fan-like" segment shape (i.e., common sun-leaf segment morphotype of *H. opuntia*), which is altered into a more roundish pebble-like grain shape. This also allows separation of the process from surface dissolution (i.e., chemical abrasion), which may not alter the grain shape of *Halimeda* segments in such a specific way (Perry 2000; Perry and Taylor 2006). During transport the physical abrasive force does not act with the same strength on the whole surface area of the segment. The outer elongated parts become abraded faster than the central parts. It is safe to assume, that this distinct abrasion pattern is induced by a rolling transport of the segment over the seafloor, presumably polished in-between other grains, which forms the observed roundish pebble-like grain shape of extensively altered segments. Finally the inner core part of a segment is preserved. This succession is in close dependency to the process of secondary cementation. Without cementation, most segments likely disintegrate before becoming a roundish grain. Particularly that may happen to transported segments of *Halimeda* species and segment morphotypes with wider central utricles (sU, tU and mU) and narrow IUS, lower $CaCO_3$ / organic ratio, and thus with a low grade of lifetime primary cementation (i.e., MAC content and density).

5.1.2.3 Micro-bioerosion

Although micro-bioerosion is frequently observed within living segments, its subsequent occurrence in a sedimentary segment may largely depend on whether it was transported or long-term deposited. Physical surface abrasion during transportation will remove signs of "lifetime" bioerosion, as it particularly affects the outer MAC rim (pIUS) where "lifetime" bioerosion primarily takes place (Perry 1998). During phases of transportation, it is safe to assume that segments rarely become bioeroded, as constant relocation may hardly allow settlement of micro-bioeroders. As some heavily cemented and thus presumably very old segments show considerable deep intra-granular micro-bioerosion, the observation of both may indicate long-term deposition. Thus together with the segments surface characteristics and its grade of secondary cementation, the occurrence of deep intra-granular micro-bioerosion may argue for an interpretation as final and long-term sediment deposition.

5.1.3 The potential of *Halimeda* segments as proxies for sediment transport

Processes that alter the microstructure of the segment in the sediment, such as intra-granular secondary cementation, physical surface abrasion and micro-bioerosion, might be used as indicators for sediment transport, deposition and estimations on the relative age of *Halimeda* segments, as the alteration of the segment follows a distinct pattern that correlates with transport and age. Furthermore, heavy calcified segments that are preserved in the sediments originate primarily from morphotypes of lithophytic *Halimeda* species, which are found in wave-exposed reef environments, e.g. in the fore reef and reef crest (Goreau and Goreau 1973; Hillis-Colinvaux 1980; Verbruggen et al. 2006). Similar observations of time- and sampling area-related microstructural alterations were made in analyses of sedimentary tests (shells) from tropical benthic foraminifera (Dawson and Smithers 2014). The use of species-specific *Halimeda* segments however has some benefits over other sedimentary components for the use as proxies for sediment transport. (1) The origin and source of sedimentary segments is more defined as the alga is benthic and immobile with strong habitat / substrate specificity. (2) Secondary (peripheral and deep intra-granular) microstructural alterations start only when, however as soon as, segments become part of the sediment. (3) Alteration stages are well defined and proceed in time dependent patterns. (4) In analyses of the segment $CaCO_3$ microstructure, lifetime calcification and subsequent sedimentary processes are visually distinguishable, if diagenesis is not present. (5) Algal segments turn over from the alga to the sediment in less than one month, thus segment contribution to sediments is steady, high and rapid. (6) Due to the fair preservation potential of segments in surface sediments, even low abundances of algae and segments are sufficient for analyses and interpretation. (7) Staining of local algal communities, i.e. the segments $CaCO_3$ skeleton, may be practicable and thus may allow visual tracing of sediment transport.

The alteration stage of complete *Halimeda* segments found onshore in island sediments may enable estimations on the rapidity of transport until final deposition when the source area is know. Thereby, analyses of intra-species calcification patterns undertaken in this study may allow determining the place of origin of most of these segments. Due to the dependence of MAC formation on the environmental-specific photosynthesis / respiration ratio, especially those segments may become transported to the island shore that originate from algal specimen growing in deeper and wave-exposed areas with lesser light availability (i.e., reef and reef crest) as that leads to a stronger segment primary cementation (i.e., MAC content), which renders them less prone to fragmentation. Thus segments from the same lithophytic species that grow on hard-substrates (i.e., small patch reefs, micro-atolls) in the back reef area are less calcified and presumably become not that often preserved as complete segments in sediments onshore. However, pristine segments that are present in surface sediments and sediment cores

taken onshore may function as valuable indicators of extreme sedimentation events and when dated allow to evaluate time periods of island development (Mann et al., in prep; data not shown).

6. Conclusions and scientific outlook

6.1 Insights into the process of calcification of macro-algae genus *Halimeda*

The process of skeletal formation of the *Halimeda* segment is complex and may not be considered as simple abiotic or physiological-induced precipitation of $CaCO_3$. Likely, *Halimeda* is able to initiate calcification actively (i.e., primary calcification) regardless of the seawater $CaCO_3$ saturation and is also able to control the $CaCO_3$ polymorph that forms directly at the utricle wall regardless of e.g. the *m* Mg / Ca ratio of the seawater. The identification of an organic matrix, in which nucleation and early crystallization of the primary needles takes place, the existence of acidic (sulfated) polysaccharides on the utricle wall and the presence of external carbonic anhydrase activity are strong indications for active calcification, similar as observed in other marine calcifying organisms. However, neither a molecular nor a functional characterization of the extracellular matrix components, the cell wall or external carbonic anhydrase (i.e., the enzyme or enzymatic domains of a protein) was conducted within the research for this dissertation. Clearly this needs investigation in future work by techniques such as "cell wall proteomics" (Jamet et al. 2008). As that allows identification and characterization of cell wall proteins present, it may also reveal their specific localization at the cell wall.

Knowledge on the abundance, distribution and location of e.g. membrane-bound HCO_3^- / H^+ symporters and H^+-ATPase (i.e. at segment surface or inter-utricular) may contribute to characterize their role in the physiology of the alga. Furthermore, the exact cation (i.e., Ca^{2+}) binding / cycling mechanisms at the cell wall have to be clarified (cf., stable isotope / trace element fractionation) as in recent work on green macro-algae a number of candidate macromolecules (so called Ca^{2+} capacitors) on the external cell wall were identified (Domozych et al. 2012). These include not only acidic polysaccharides like pectins, but also glycosylated proteins such as from the diverse class of arabino-galactan proteins (AGP). Especially AGP serve multiple regulatory functions at the cell wall, such as cell wall signalling, cell growth, sectretion of exudates, give structural integrity by cytoskeletal linkage (Estevez et al. 2009; Ellis et al. 2010; Lamport and Várnai 2013; Pickard 2013), and interestingly many exhibit intrinsically disordered secondary structures (cf., proteins in biomineralization; Wojtas et al. 2012). Thereby the cell wall composition and conformation of macro-molecules (e.g., of polysaccharides and glycoproteins, AGP) so far investigated from different groups of marine coenocytic algae seem to have developed very taxon-specifically and significantly differ to higher plants and freshwater algae (Estevez et al. 2009; Ciancia et al. 2012).

Besides, the existence of pectin-Ca^{2+} binding motifs identified in some extracellular enzymes may be another promising focus of future research on (algal) calcification, as many proteins in the calcifying matrix, including some with external carbonic anhydrase-like domains, exhibit high Ca^{2+} affinity (Carpin et al. 2001; Marin and Luquet 2004; Bonucci 2007).

6.1.1 The role of alkaline phosphatase in $CaCO_3$ biomineralization

Alkaline phosphatase (AP) is an enzyme located in the extracellular matrix of calcifying organisms, including green macro-algae (Bevelander and Benzer 1948; Simkiss 1964; Atkinson 1987; Delgado and Lapointe 1994). AP activity catalyzes pyrophosphate (PP_i), which in high concentrations permits $CaCO_3$ nucleation, into orthophosphate (P_i). AP also exhibits high Ca^{2+} affinity and is considered a key enzyme in the process of calcification. AP may also play a role in the initiation of organic matrix degradation and post-functional structural modification of matrix components (e.g., by de- and phosphorylation of matrix proteins) to allow $CaCO_3$ crystallization (Hernandez et al. 2002; Bonucci and Gomez 2012). For example, de-phosphorylation of intrinsically disordered proteins (IDP), which probably most calcifying proteins are (e.g., Weiss and Marin 2008; Wojtas et al. 2012), modifies their tertiary structure (i.e., by disorder-order transition, conformation change) and therewith protein functionality (Bah et al. 2015).

For optimal catalysis, AP generally requires the pH in the matrix to be alkaline (pH >8). Interestingly, AP activity and H^+ fluxes may hypothetically fit to measurements of pH and Ca^{2+} concentrations with a microsensor in the species of *Halimeda discoidea* by De Beer and Larkum (2001). Under light, firstly Ca^{2+} ions are adsorbed at matrix components (e.g., acidic polysaccharides) when pH is elevated due to onset of photosynthesis and eCA (Fig. 6). Elevation of extracellular pH may also trigger AP activity that catalyzes PP_i to inorganic phosphate (P_i), and which then is bioavailable for take-up by algal cells. Symport of P_i / H^+ (and of other nutrients) into the cell decreases the intracellular pH that subsequently triggers H^+-ATPase activity balancing cell internal pH. H^+ efflux decreases extracellular pH, diminishes AP activity and leads to the release of adsorbed Ca^{2+} ions from matrix components. Release of Ca^{2+} from matrix components now facilitates $CaCO_3$ crystallization (cf., gradual increase in Ca^{2+} concentration in the IUS; De Beer and Larkum 2001). Thus nutrient (here P_i) uptake and AP activity may precede primary calcification, as the enzyme catalyzes PP_i to P_i and directly or indirectly may initiate matrix degradation. Thereby the observed increase in Ca^{2+} concentration likely follows the change in seawater pH (i.e., lag phase of Ca^{2+} release), as onset of AP activity (PP_i and P_i removal by cell uptake) and subsequent polysaccharide degradation depend on seawater pH change. However this

reasoning is highly speculative, thus investigations on the potential role of AP in the (primary) calcification of *Halimeda* in future research may be beneficial.

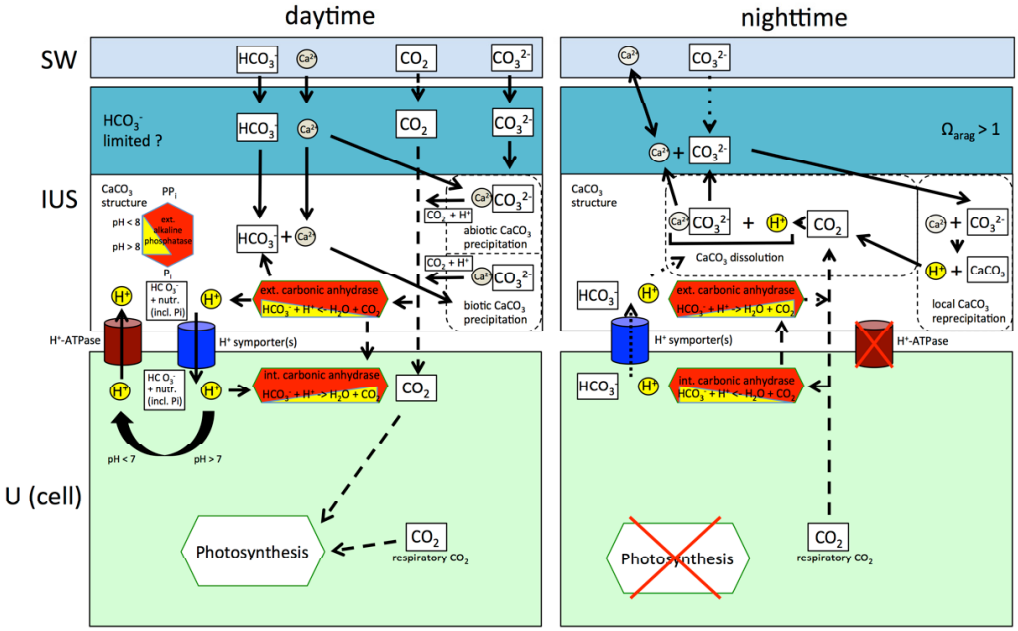

Fig. 6 Theoretical model for *Halimeda* calcification including the hypothetical process of alkaline phosphatase (AP) and light-physiology induced H^+-ATPase activity. Yellow triangles within red boxes indicate the preferred equilibrium reaction of enzyme activity (internal and external CA and external AP) depending on substrate availability and seawater pH. See paragraph 6.1.1 for further explanations.
SW = seawater; IUS = inter-utricular space; U = utricle; AP = alkaline phosphatase; CA = carbonic anhydrase.

6.1.2. High resolution structural analyses on the composition of the $CaCO_3$ skeleton

To reveal if organic molecules (e.g., glycoproteins, polysaccharides) are involved and act in the buildup of the calcium carbonate skeleton, high-resolution mineralogical, structural analyses (e.g., via synchrotron-SEM, cryo electron microscopy; transmission scanning electron microscopy, atomic-force microscopy or Raman-spectroscopy) of the different skeletal components may give further insights. These may include analyses of the $CaCO_3$ crystal angles and crystal lattices of the different skeletal features, as it is known that these may show alterations in biotically-formed calcified structures when compared to abiotically precipitated $CaCO_3$ (e.g., Berman et al. 1993). From observations of the buildup pattern of the microskeletal structure evidence is present that organic molecules are incorporated in the fine-

crystalline MAC as in preliminary analyses by ICP-OES sulfur was observed in purified skeletal $CaCO_3$. Such skeletal-associated organic molecules may keep the granular MAC in a hydrous gel-like (partly amorphous?) state (cf., bivalves; Jacob et al. 2008). Only that may explain the progression of MAC accumulation in the IUS during lifetime in accordance with secondary needle formation and their specific location.

6.2 The alteration of the internal microstructure and the process of calcification under elevated seawater pCO_2

Calcification in *Halimeda* likely involves biotically and abiotically derived skeletal features, thus the response of both to elevated seawater pCO_2 varies significantly. In biogenic calcification calcifying proteins, which possess enzyme-like activity, drive the formation of $CaCO_3$ structures within an extracellular organic matrix. Biogenic calcification may rely on HCO_3^-, including HCO_3^- from enzymatic CO_2 hydration (via eCA). Abiotic precipitation in contrast is dependent on the $CaCO_3$ saturation of the seawater within the IUS. Thus, the first process rather profits from a moderate elevation of seawater pCO_2 (< ~1000 µatm), contrariwise the latter is gradually impacted. Additionally, respiration of endolithic microbes or micro-bioeroders living in the calcareous structure likely also influences the carbonate saturation state within the IUS to the disadvantage of abiotic $CaCO_3$ formation especially under elevated seawater pCO_2.

6.2.1 Analyses to investigate microstructural alteration under elevated seawater pCO_2

To estimate the overall change in seawater carbonate saturation, direct measurements of seawater parameters in the DBL and within the IUS during specific daytimes are beneficial, similar as undertaken in a first experimental approach by De Beer and Larkum (2001). That may also include micro-probe analyses of the pH change directly on the external cell wall surface in the IUS to reveal cation (Ca^{2+}) binding and release mechanisms by cell wall and matrix components (i.e., Ca^{2+} capacitors like pectins and AGPs), as generally these processes are considered to be pH dependent. Cation release from cell-wall polysaccharides and protein complexes is typically triggered by a decrease in pH (e.g., to pH < 3 in land plants) of the extracellular matrix, whereas cation binding is induced by higher pH (e.g., cell wall pH > 5 in terrestrial plants; pH 6 - 7 in calcifying cyanobacteria; Dittrich and Sibler 2010; Pickard 2013). However calcification relies on the release of Ca^{2+} ions previously accumulated by cation capacitors (cf., Hunter 1987) thus a lowering of the pH on the cell wall may be necessary for crystallization to initiate and proceed. Moreover that may indicate high dynamic

of the cell wall pH and active regulation of the pH in the extracellular matrix, presumably over controlled proton efflux (to remind here is the proton efflux by H^+-ATPase activity on the cell wall of *Halimeda* in daylight; De Beer and Larkum 2001). If so, these complex dynamics also might be influenced by elevated seawater pCO_2 and thus seawater lower in pH.

6.2.2 Expression of extracellular and cell wall components under elevated pCO_2

Studies on marine organisms often reveal changes in activity and expression rates (i.e., abundance) of cell wall components such as H^+-ATPase, HCO_3^- / H^+ symporters and carbonic anhydrases under conditions of elevated seawater pCO_2 (e.g., Beniash et al. 2011; Hofmann et al. 2014; Hu et al. 2014). Several of these components are present at the cell wall or within the extracellular matrix of *Halimeda* (Borowitzka and Larkum 1976a, b, 1977; De Beer and Larkum 2001). Detailed responses of these components (i.e., protein expression and activity) may help to reveal physiological pathways and processes that are related to seawater carbon chemistry and calcification, e.g. of CO_2, HCO_3^-, CO_3^{2-} and proton (H^+) availability and usage, $CaCO_3$ saturation, and cation (e.g., Ca^{2+}) binding and cycling. Analyzes of the specific responses of multiple physiological components may also provide a better picture how these are linked with, and influence each other.

For example, in extremophile green micro-algae H^+-ATPase expression (i.e., of the proton pump protein complex) is induced over changes in pH of the external medium (Weiss and Pick 1996). Thus the potential observation of an increased expression of H^+-ATPase in *Halimeda* under elevated seawater pCO_2, as was observed for other marine organisms (e.g. Beniash et al. 2011; Hu et al. 2014), would indicate faster cell acidosis and presumably also an active control of *Halimeda* over the extracellular matrix pH.

6.2.3 Consequences of elevated seawater pCO_2 for the ecology of *Halimeda*

The physiology of the alga itself, the microbial (calcifying?) community living in and attached to the $CaCO_3$ structures clearly has to be a major field of research, not only in case of calcareous macro-algae of the genus *Halimeda.* It is important to understand how microbes modify the vicinal microenvironment (i.e., DBL) around and within extracellular calcareous structures, as evolutionary "higher organisms" (i.e., metazoans) certainly have to be considered as holobionts (i.e., the host and its microbiota). Furthermore, this may have numerous implications also for sedimentary processes such as for intra-granular secondary cementation (e.g., $CaCO_3$ polymorph; Nothdurft et al. 2007). The microstructural change under moderately elevated seawater pCO_2 may not have severe implications for the alga itself, as the physiological performance (i.e. photosynthesis and segmental growth) might be

even enhanced (e.g., Vogel et al. 2015a, b). However, it is the abiogenic process of MAC formation (i.e. primary cementation) that enables the algal segments to play important ecological roles, e.g. providing coarse substrate in tropical coral reef ecosystems. Thus presented investigations indicate an impact on carbonate sediment structure (i.e., cemented segments vs. needle mud) and $CaCO_3$ budget of tropical reef sediments. Presumably also many other $CaCO_3$ secreting organisms, not only of tropical coral reefs, may incorporate phases of abiogenic $CaCO_3$ into their skeleton (e.g., Alexandersson 1974; Braithwaite et al. 2000; Basso 2012). Further research thus should focus on the identification and understanding of such complex multi-structural and multi-genetic skeletal formations in order to be able to more precisely predict effects caused by environemntal changes on skeletal formation and on the budget of carbonate sediments produced by these organisms.

6.3 *Halimeda* segment alteration in sedimentary processes and their potential use as sediment tracers

Complete *Halimeda* segments that are found in sediments worldwide show a typical "butterfly", "fan-like" or "trident-like" shape depending on segment leaf morphotype or species morphotype and are within the grainsize class of pebble gravel (1.6 > 0.4 cm, medium to fine pebbles; Wentworth 1922; Milliman 1974). Thus it is obvious as only a specific type of segments is observed in tropical sediments that it is a limited number of species contributing to typical coarse *Halimeda*-rich sediments (i.e., consisting of partly fragmented and complete segments). This species-specific segment contribution to carbonate sediments is caused by a species-specific internal morphological segment microstructure and species-specific physiology (photosynthesis and respiration) that likely derives from niche adaption these *Halimeda* species developed (Hillis-Colinvaux 1980; Johns and Moore 1988; Granier 2012). Both, species-specific internal segment microstructure and physiology, lead to different extents of species- and environment-specific segment calcification, particularly of primary cementation (i.e. segment MAC content). This species-specificity has to be considered when *Halimeda* segments are used in interpretations of e.g., island formation. Interpretations based merely on the segments surface structure and grain shape are not sufficient to reconstruct the sediment transport or to identify the origin of these sediments and their discharge areas. Moreover, the occurrence of seemingly little superficially altered segments from the sediments (i.e., surface not significantly abraded) combined with the lack of species identification might both mislead to an interpretation as in-situ production and deposition, e.g. when these segments are present in lagoonary facies types, but may have become rapidly deposited, e.g. in extreme sedimentation events such as storms. Thus species

identification, knowledge on habitat preference of species, the investigation of the internal skeletal microstructure and its alteration due to sedimentary processes like secondary cementation, dissolution, micro-bioerosion and the progress patterns of physical abrasion might widen the interpretation range and help in accurate sedimentological reconstruction of sediment source and sink areas in tropical regions.

Furthermore, in most cases the original *Halimeda* skeleton is preserved in segments from surface sediments. Thus, it is possible to distinguish between sedimentary $CaCO_3$ precipitation and the original $CaCO_3$ skeletal structure, as e.g. primary and secondary cements differ in crystal morphology and occasionally also in mineralogy. Therefore it may be also practicable to measure specific stable isotopes ratios ($\delta^{13}C$, $\delta^{18}O$) and elements (e.g., Su, Mg, Sr, B) from regions of different $CaCO_3$ genesis and gain insight into environmental conditions from the segment´s lifetime period and from the time period the segment was deposited and / or became transported within the sediment (Wefer and Berger 1981; Macintyre and Reid 1998; Hover et al. 2001). However, it should be noted that due to the calcification pattern, isotope analyses of the segment skeleton as a whole are not recommended and will result in a mix up of $CaCO_3$ precipitated from different environmental and physiological sources and in time-dependent processes (Wefer and Berger 1981; Milliman et al. 1993; Delaney et al. 1996; Blättler et al. 2014).

6.3.1 Anthropogenic influences on carbonate sediment production of *Halimeda*

Any impact on the process of calcification and subsequent cementation of the *Halimeda* segment caused by anthropogenic processes such as ocean acidification may lead to a noticeable decrease of segments present in tropical sediments. In this work, I present evidence that the process of primary cementation in *H. opuntia* is affected by ocean acidification, leading to a more needle-dominated, acicular skeletal microstructure of the segment. Subsequent faster disintegration and fragmentation of segments in the water column may lead to a fining of sediment (i.e., grain size composition), particularly in areas where lithophytic *Halimeda* species are major sediment contributors of complete segments and represent a larger portion of coarse carbonate sediments (i.e., pebble gravel). An impact on community structures in the sink area is also expectable, as many organisms rely on well-aerated coarse macro sediments (e.g., species of seagrass, the interstitial fauna, and many other burrowing animals). In addition, as coarse and cemented sediments presumably take more time to dissolve, which is indicated by the age of cemented *Halimeda* segments from surface sediments that were dated to be over 6k years (Mann et al., in prep.) and 10k years (Alexandersson and Milliman 1981), the carbonate pool and long-term carbon storage of carbonate sediments may be affected as fine-grained and less cemented carbonate material

dissolves faster. Thus, over long-term (i.e., geological timescales), a diminished contribution of cemented grains that aditionally undergo rapid fragmentation, coupled with fast dissolution due to low(ered) seawater $CaCO_3$ saturation may have the potential to affect ocean´s carbonate buffer capacity and the buildup of carbonate platforms, atoll and reef islands in the tropics.

7. References

Addadi L, Raz S, Weiner S (2003) Taking advantage of disorder: amorphous calcium carbonate and its roles in biomineralization. Adv Mater 15:959–970

Addadi L, Joester D, Nudelman F, Weiner S (2006) Mollusk shell formation: a source of new concepts for understanding biomineralization processes. Chemistry 12:980–987

Alexandersson ET (1972) Intragranular growth of marine aragonite and Mg-calcite; evidence of precipitation from supersaturated seawater. J Sediment Res 42:441–460

Alexandersson ET (1974) Carbonate cementation in coralline algal nodules in the Skagerrak, North Sea; biochemical precipitation in undersaturated waters. J Sediment Res 1:7–26

Alexandersson ET, Milliman JD (1981) Intragranular Mg-calcite cement in *Halimeda* plates from the Brazilian continental shelf. J Sediment Res 51:1309–1314

Andersson AJ, Mackenzie FT, Lerman A (2005) Coastal ocean and carbonate systems in the high CO_2 world of the Anthropocene. Am J Sci 305:875–918

Arias JL, Fernández MS (2008) Polysaccharides and proteoglycans in calcium carbonate-based biomineralization. Chem Rev 108:4475–82

Arnott HJ (1982) Three systems of biomineralization in plants with comments on the associated organic matrix. In: Nancollas GH (ed) Biological mineralization and demineralization. Springer, Berlin Heidelberg, pp 199–218

Aquino RS, Grativol C, Mourão PAS (2011) Rising from the sea: correlations between sulfated polysaccharides and salinity in plants. PloS One 6:e18862

Atkinson MJ (1987) Alkaline phosphatase activity of coral reef benthos. Coral Reefs 6:59-62

Bach LT (2015) Reconsidering the role of carbonate ion concentration in calcification by marine organisms. Biogeosciences Discuss 12:6689–6722

Bah A, Vernon RM, Siddiqui Z, Krzeminski M, Muhandiram R, Zhao C, Sonenberg N, Kay LE, Forman-Kay JD (2014) Folding of an intrinsically disordered protein by phosphorylation as a regulatory switch. Nature 519:106–109

Basso D (2012) Carbonate production by calcareous red algae and global change. Geodiversitas 34:13–33

Beniash E, Ivanina A, Lieb N, Kurochkin I, Sokolova I (2010) Elevated level of carbon dioxide affects metabolism and shell formation in oysters *Crassostrea virginica* (Gmelin). Mar Ecol Prog Ser 419:95–108

Berman A, Hanson J, Leiserowitz L (1993) Biological control of crystal texture: a widespread strategy for adapting crystal properties to function. Science 259:776–779

Bernstein L, Bosch P, Canziani O, Chen Z, Christ R, Davidson O (2007) Climate change 2007: synthesis report. Summary for policymakers. In: Climate change 2007: synthesis report. Summary for policymakers. Intergovernmental Panel on Climate Change (IPCC)

Bertucci A, Moya A, Tambutté S, Allemand D, Supuran CT, Zoccola D (2013) Carbonic anhydrases in anthozoan corals–a review. Bioorg Med Chem 21:1437–1450

Bevelander G, Benzer P (1948) Calcification in marine molluscs. Biol Bull 94:176–183

Blättler CL, Stanley SM, Henderson GM, Jenkyns HC (2014) Identifying vital effects in *Halimeda* algae with Ca isotopes. Biogeosciences Discuss 11:3559–3580

Böhm EL (1973) Composition and calcium binding properties of the water soluble polysaccharides in the calcareous alga *Halimeda opuntia* (L.) (Chlorophyta, Udoteaceae). Internationale Revue der gesamten Hydrobiologie und Hydrogeographie 58:117–126

Böhm EL, Goreau T (1973) Rates of turnover and net accretion of calcium and the role of calcium binding polysaccharides during calcification in the calcareous alga *Halimeda opuntia* (L.). Internationale Revue der gesamten Hydrobiologie und Hydrogeographie 58:723–740

Bonucci E (2007) Main suggested calcification mechanisms: extracellular matrix. In: Schreck S (ed) Biological calcification: normal and pathological processes in the early stages. Springer, Heidelberg, pp 507–558

Bonucci E (2009) Calcification and silicification: a comparative survey of the early stages of biomineralization. J Bone Miner Metab 27:255–264

Bonucci E, Gomez S (2012) Cartilage Calcification. In: Seto J (ed) Advanced topics in biomineralization. InTech Europe, Croatia, pp 85–110

Borowitzka MA, Larkum AWD (1976a) Calcification in the green alga *Halimeda*. III. The sources of inorganic carbon for photosynthesis and calcification and a model of the mechanism of calcification. J Exp Bot 27:879–893

Borowitzka MA, Larkum AWD (1976b) Calcification in the green alga *Halimeda* IV. The action of metabolic inhibitors on photosynthesis and calcification. J Exp Bot 27:894–907

Borowitzka MA, Larkum AWD (1977) Calcification in the green alga *Halimeda* I. an ultrastructure study of thallus development. J Phycol 13:6–16

Borowitzka MA (1982a) Morphological and cytological aspects of algal calcification. Int Rev Cytol 74:127–162

Borowitzka MA (1982b) Mechanism in algal calcification. Progr Phycol Res 1:137–177

Borowitzka MA (1984) Calcification in aquatic plants. Plant Cell Environ 7:457–466

Brachert TC, Dullo WC (2000) Shallow burial diagenesis of skeletal carbonates: selective loss of aragonite shell material (Miocene to Recent, Queensland Plateau and Queensland Trough, NE Australia)—implications for shallow cool-water carbonates. Sediment Geol 136:169–187

Braga J, Martín J, Riding R (1996) Internal structure of segment reefs: *Halimeda* algal mounds in the Mediterranean Miocene. Geology 24:35–38

Braithwaite CJR, Taylor JD, Glover EA (2000) Marine carbonate cements, biofilms, biomineralization, and skeletogenesis: some bivalves do it all. J Sediment Res 70:1129–1138

Brennan ST, Lowenstein TK, Horita J (2004) Seawater chemistry and the advent of biocalcification. Geology 32:473–476

Broecker WS, Sanyal A (1998) Does atmospheric CO_2 police the rate of chemical weathering? Global Biogeochem Cy 12:403–408

Caldeira K, Wickett ME (2003) Oceanography: anthropogenic carbon and ocean pH. Nature 425:365–365

Carpin S, Crèvecoeur M, de Meyer M, Simon P, Greppin H, Penel C (2001) Identification of a Ca^{2+}-pectate binding site on an apoplastic peroxidase. The Plant Cell 13:511–520

Ciancia M, Alberghina J, Arata PX, Benavides H, Leliaert F, Verbruggen H, Estevez JM (2012) Characterization of cell wall polysaccharides of the coencocytic green seaweed *Bryopsis plumosa* (Bryopsidaceae, Chlorophyta) from the Argentine coast. J Phycol 48:326–335

Clark TR, Roff G, Zhao JX, Feng YX, Done TJ, Pandolfi JM (2014) Testing the precision and accuracy of the U-Th chronometer for dating coral mortality events in the last 100 years. Quat Geochronol 23:35–45

Clarkson MO, Kasemann SA, Wood RA, Lenton TM, Daines SJ, Richoz S, Ohnemueller F, Meixner A, Poulton SW, Tipper ET (2015) Ocean acidification and the Permo-Triassic mass extinction. Science 348:229–233

Cleary DF, Becking LE, de Voogd NJ, Renema W, de Beer M, van Soest RW, Hoeksema BW (2005) Variation in the diversity and composition of benthic taxa as a function of distance offshore, depth and exposure in the Spermonde Archipelago, Indonesia. Estuar Coast Shelf S 65:557–570

Comeau S, Carpenter R, Edmunds PJ (2012) Coral reef calcifiers buffer their response to ocean acidification using both bicarbonate and carbonate. Proc R Soc B Biol Sci 280:1753

Cornwall CE, Hepburn CD, Pritchard D, Currie KI, McGraw CM, Hunter KA, Hurd CL (2012) Carbon-use strategies in macroalgae: differential responses to lowered pH and implications for ocean acidification. J Phycol 48:137–144

Cornwall CE, Boyd PW, McGraw CM, Hepburn CD, Pilditch CA, Morris JN, Smith AM, Hurd CL (2014) Diffusion boundary layers ameliorate the negative effects of ocean acidification on the temperate coralline macroalga *Arthrocardia corymbosa*. PloS One 9:e97235

Cuif JP, Dauphin Y, Nehrke G, Nouet J, Perez-Huerta A (2012) Layered growth and crystallization in calcareous biominerals: impact of structural and chemical evidence on two major concepts in invertebrate biomineralization studies. Minerals 2:11–39

Dawson JL, Smithers SG (2014) Carbonate sediment production, transport, and supply to a coral cay at Raine Reef, Northern Great Barrier Reef, Australia: a facies approach. J Sediment Res 84:1120–1138

Dawson JL, Smithers SG, Hua Q (2014) The importance of large benthic foraminifera to reef island sediment budget and dynamics at Raine Island, northern Great Barrier Reef. Geomorphology 222:68–81

De Beer D, Larkum AWD (2001) Photosynthesis and calcification in the calcifying algae *Halimeda discoidea* studied with microsensors. Plant Cell Environ 24:1209–1217

Delaney ML, Linn LJ, Davies PJ (1996) Trace and minor element ratios in *Halimeda* aragonite from the Great Barrier Reef. Coral Reefs 15:181–189

Delgado O, Lapointe BE (1994) Nutrient-limited productivity of calcareous versus fleshy macroalgae in a eutrophic, carbonate-rich tropical marine environment. Coral Reefs 13:151–159

DeWreede R (2006) Biomechanical properties of coenocytic algae (Chlorophyta, Caulerpales). Sci Asia Suppl 1:57–62

Diaz-Pulido G, Nash MC, Anthony KRN, Bender D, Opdyke BN, Reyes-Nivia C, Troitzsch U (2014) Greenhouse conditions induce mineralogical changes and dolomite accumulation in coralline algae on tropical reefs. Nature Comm 5:3310

Dickson AG, Millero FJ (1987) A comparison of the equilibrium constants for the dissociation of carbonic acid in seawater media. Deep Sea Res 34:1733–1743

Dickson AG, Afghan JD, Anderson GC (2003) Reference materials for oceanic CO_2 analysis: a method for the certification of total alkalinity. Mar Chem 80.2:185–197

Dickson AG, Sabine CL, Christopher JR (2007) Guide to best practices for ocean CO_2 measurements. North Pacific Marine Science Organization Special Publication 3, Sidney, British Columbia, p 176

Dittrich M, Sibler S (2010) Calcium carbonate precipitation by cyanobacterial polysaccharides. Geol Soc, London, Special Publications 336:51–63

Dodge RE, Wyers SC, Frith HR, Knap AH, Smith SR, Cook CB, Sleeter TD (1984) Coral calcification rates by the buoyant weight technique: effects of alizarin staining. J Exp Mar Biol Ecol 75:217–232

Domozych DS, Ciancia M, Fangel JU, Mikkelsen MD, Ulvskov P, Willats WGT (2012) The cell walls of green algae: a journey through evolution and diversity. Front Plant Sci 3:1–7

Doney SC, Balch WM, Fabry VJ, Feely RA (2009) Ocean acidification: a critical emerging problem for the ocean sciences. North 22:16–25

Drew EEA (1983) *Halimeda* biomass, growth rates and sediment generation on reefs in the central Great Barrier Reef province. Coral Reefs 2:101–110

Drew EEA, Abel K (1988) Studies on *Halimeda* I. The distribution and species composition of *Halimeda* meadows throughout the Great Barrier Reef Province. Coral Reefs 6:195–205

Dumitriu S (ed) (2012) Polysaccharides: structural diversity and functional versatility. CRC Press, p 1224

Eberli GP, Swart PK, McNeill DF, Kenter JAM, Anselmetti FS, Melim LA, Ginsburg RN (1997) A synopsis of the Bahamas Drilling Project: results from two deep core borings drilled on the Great Bahama Bank. In: Proceedings of the ODP, initial reports, 166:23–41

Edinger EN, Jompa J, Limmon GV, Widjatmoko W, Risk MJ (1998) Reef degradation and coral biodiversity in Indonesia: effects of land-based pollution, destructive fishing practices and changes over time. Mar Pollut Bull 36:617–630

Edinger EN, Kolasa J, Risk MJ (2000) Biogeographic variation in coral species diversity on coral reefs in three regions of Indonesia. Divers Distrib 6:113–127

Edmond JM, Huh Y (1997) Chemical weathering yields from basement and orogenic terrains in hot and cold climates. In: Ruddiman WF (ed) Tectonic uplift and climate change Springer US, pp 329–351

Enríquez S, Schubert N (2014) Direct contribution of the seagrass *Thalassia testudinum* to lime mud production. Nature Comm 5:3835

Estevez JM, Fernández PV, Kasulin L, Dupree P, Ciancia M (2009) Chemical and in situ characterization of macromolecular components of the cell walls from the green seaweed *Codium fragile*. Glycobiology 19:212–228

Faatz M, Gröhn F, Wegner G (2004) Amorphous calcium carbonate: synthesis and potential intermediate in biomineralization. Adv Mater 16:996–1000

Falini G, Reggi M, Fermani S, Sparla F, Goffredo S, Dubinsky Z, Levi O, Dauphin Y, Cuif JP (2013) Control of aragonite deposition in colonial corals by intra-skeletal macromolecules. J Struct Biol 183: 226–238

Feely RA, Sabine CL, Lee K, Berelson W, Kleypas J, Fabry VJ, Millero FJ (2004) Impact of anthropogenic CO_2 on the $CaCO_3$ system in the oceans. Science 305:362–366

Feely RA, Doney SC, Cooley SR (2009) Ocean acidification: Present conditions and future changes in a high-CO_2 world. Oceanography 6:36–47

Feng Q, Pu G, Pei Y, Cui F, Li H, Kim T (2000) Polymorph and morphology of calcium carbonate crystals induced by proteins extracted from mollusk shell. J Cryst Growth 216:459–465

Fernández PV, Ciancia M, Miravalles AB, Estevez JM (2010) Cell-wall polymer mapping in the coenocytic macroalga *Codium vermilara* (Bryopsidales, Chlorophyta). J Phycol 46:456–465

Ferse SC, Glaser M, Neil M, Mánez KS (2012) To cope or to sustain? Eroding long-term sustainability in an Indonesian coral reef fishery. Reg Environ Change pp 1–13

Findlay HS, Wood HL, Kendall MA, Spicer JI, Twitchett RJ, Widdicombe S (2009) Calcification, a physiological process to be considered in the context of the whole organism. Biogeosciences Discuss 6:2267–2284

Findlay HS, Wood HL, Kendall MA, Spicer JI, Twitchett RJ, Widdicombe S (2011) Comparing the impact of high CO_2 on calcium carbonate structures in different marine organisms. Mar Biol Res 7:565–575

Folk RL (1959) Practical petrographic classification of limestones. Am Assoc Pet Geol Bull 43.1:1–38

Folk R, Robles R (1964) Carbonate sands of isla perez, alacran reef complex, Yucatan. J Geol 75:412–437

Ford MR, Kench PS (2012) The durability of bioclastic sediments and implications for coral reef deposit formation. Sedimentology 59:830–842

Freile D, Milliman J, Hillis L (1995) Leeward bank margin *Halimeda* meadows and draperies and their sedimentary importance on the western Great Bahama Bank slope. Coral Reefs 14:27–33

Friedlingstein P, Cox P, Betts R, Bopp L, von Bloh W, Brovkin V, and others (2006) Climate-carbon cycle feedback analysis: Results from the C4MIP model intercomparison. J Clim 19:3337–3353

Friedman GM (1998) Rapidity of marine carbonate cementation – implications for carbonate diagenesis and sequence stratigraphy: perspective. Sediment Geol 119:1–4

Ghina F (2003) Sustainable development in small island developing states. Environ Dev Sustain 5:139–165

Gischler E, Dietrich S, Harris D, Webster JM, Ginsburg RN (2013) A comparative study of modern carbonate mud in reefs and carbonate platforms: Mostly biogenic, some precipitated. Sediment Geol 292:36–55

Glaeser B, Glaser M (2010) Global change and coastal threats: The Indonesian case. An attempt in multi-level social-ecological research. Hum Ecol Rev 17:135–147

Glaser M, Baitoningsih W, Ferse SC, Neil M, Deswandi R (2010) Whose sustainability? Top–down participation and emergent rules in marine protected area management in Indonesia. Mar Policy 34:1215–1225

Goreau TF (1963) Calcium carbonate deposition by coralline algae and corals in relation to their roles as reef-builders. Ann NY Acad Sci 109:127–167

Goreau TF, Goreau N (1973) The ecology of Jamaican coral reefs. II. Geomorphology, zonation, and sedimentary phases. B Mar Sci 23:399–464

Granier B (2012) The contribution of calcareous green algae to the production of limestones: a review. Geodiversitas 34:35–60

Grammer GM, Crescini CM, McNeill DF, Taylor LH (1999) Quantifying rates of syndepositional marine cementation in deeper platform environments-new insight into a fundamental process. J Sediment Res 69:202–207

Guinotte JM, Fabry VJ (2008) Ocean acidification and its potential effects on marine ecosystems. Ann NY Acad Sci 1134:320–342

Hanor JS (1978) Precipitation of beachrock cements: mixing of marine and meteoric waters vs. CO_2-degassing. J Sediment Res 48:489–501

Harris DL, Vila-Concejo A, Webster JM (2014) Geomorphology and sediment transport on a submerged back-reef sand apron: One Tree Reef, Great Barrier Reef. Geomorphology 222:132–142

Hassan I, Shajee B, Waheed A, Ahmad F, Sly WS (2013) Structure, function and applications of carbonic anhydrase isozymes. Bioorgan Med Chem 21:1570–1582

Hernández I, Niell F, Whitton B (2002) Phosphatase activity of benthic marine algae. an overview. J Appl Phycol 3:475–487

Hillis, L (1997) Coralgal reefs from a calcareous green alga perspective and a first carbonate budget. Proc 8th Int Coral Reef Symp 1:761–766

Hillis L (2001) The calcareous reef alga *Halimeda* (Chlorophyta, Byropsidales): a cretaceous genus that diversified in the Cenozoic. Palaeogeogr Palaeocl 166:89–100

Hillis-Colinvaux L (1980) Ecology and taxonomy of *Halimeda*: primary producer of coral reefs. Adv Mar Biol 17:1–327

Hillis-Colinvaux L (1986) *Halimeda* growth and diversity on the deep fore-reef of Enewetak Atoll. Coral Reefs 5:19–21

Hine AC, Hallock P, Harris MW, Mullins HT, Belknap DF, Jaap WC (1988) *Halimeda* bioherms along an open seaway: Miskito Channel, Nicaraguan Rise, SW Caribbean Sea. Coral Reefs 6:173–178

Hoegh-Guldberg O, Mumby PJ, Hooten AJ, Steneck RS, Greenfield P, Gomez E, Harvell CD, Sale PF, Edwards AJ, Caldeira K, Knowlton N, Eakin CM, Iglesias-Prieto R, Muthiga N, Bradbury RH, Dubi A, Hatziolos ME (2007) Coral reefs under rapid climate change and ocean acidification. Science 318:1737–1742

Hoegh-Guldberg O, Bruno JF (2010) The impact of climate change on the world's marine ecosystems. Science 328:1523–1528

Hoffmann TC (2002) Coral reef health and effects of socio-economic factors in Fiji and Cook Islands. Mar Pollut Bull 44:1281–1293

Hofmann LC, Straub S, Bischof K (2012) Competition between calcifying and noncalcifying temperate marine macroalgae under elevated CO_2 levels. Mar Ecol Prog Ser 464:89–105

Hofmann LC, Straub S, Bischof K (2013) Elevated CO_2 levels affect the activity of nitrate reductase and carbonic anhydrase in the calcifying rhodophyte *Corallina officials*. J Exp Bot 64:899–908

Hofmann LC, Heiden J, Bischof K, Teichberg M (2014) Nutrient availability affects the response of the calcifying chlorophyte *Halimeda opuntia* (L.) J.V. Lamouroux to low pH. Planta 239:231–242

Hofmann LC, Bischof K, Baggini C, Johnson A, Koop-Jakobson K, Teichberg M (2015) CO_2 and inorganic nutrient enrichment affect the performance of a calcifying green alga and its noncalcifying epiphyte. Oecologica 1–13

Holcomb M, Cohen AL, Gabitov RI, Hutter JL (2009) Compositional and morphological features of aragonite precipitated experimentally from seawater and biogenically by corals. Geochim Cosmochim Acta 73:4166–4179

Hover VC, Walter LM, Peacor DR (2001) Early marine diagenesis of biogenic aragonite and Mg-calcite: new constraints from high-resolution STEM and AEM analyses of modern platform carbonates. Chem Geol 175:221–248

Hu MY, Guh YJ, Stumpp M, Lee JR, Chen RD, Sung PH, Chen YC, Hwang PP, Tseng YC (2014) Branchial NH^{4+}-dependent acid–base transport mechanisms and energy metabolism of squid (*Sepioteuthis lessoniana*) affected by seawater acidification. Front Zool 11:55

Hughes T, Baird A, Bellwood D, Card M, Connolly S, Folke C, Grosberg R, Hoegh-Guldberg O, Jackson JBC, Kleypas J, Lough JM, Marshall P, Nyström M, Palumbi SR, Pandolfi JM, Rosen B, Roughgarden J (2003) Climate change, human impacts, and the resilience of coral reefs. Science 301:929–934

Hunter G (1987) An ion-exchange mechanism of cartilage calcification. Connect Tissue Res 16:111–120

Imran AM, Suriamihardja DA, Sirajuddin H (2013) Geology of Spermonde platform. Proceedings of the 7th International Conference on Asian and Pacific Coasts pp 1062–1067

IPCC (2013) Climate Change 2013: The Physical Science Basis, The Fifth Assessment Report of the United Nations Intergovernmental Panel on Climate Change. Intergovernmental Panel on Climate Change (IPCC)

Isenberg H, Douglas S, Lavine L, Spicer S, Weissfeller H (1966) A protozoan model of hard tissue formation. Ann NY Acad Sci

Jakob U, Kriwacki R, Uversky VN (2014) Conditionally and transiently disordered proteins: awakening cryptic disorder to regulate protein function. Chem Rev 114:6779–6805

Jamet E, Albenne C, Boudart G, Irshad M, Canut H, Pont-Lezica R (2008) Recent advances in plant cell wall proteomics. Proteomics 8:893–908

Jensen PR, Gibson RA, Littler MM, Littler DS (1985) Photosynthesis and calcification in four deep-water *Halimeda* species (Chlorophyceae, Caulerpales). Deep-Sea Res Oceanogr A 32:451–464

Jindrich V (1969) Recent carbonate sedimentation by tidal channels in the Lower Florida Keys. J Sediment Res 39:531–553

Jinendradasa S, Ekaratne S (2002) Composition and monthly variation of fauna inhabiting reef-associated *Halimeda*. Proc 9th Int Coral Reef Symp 2:1059–1063

Johns H, Moore C (1988) Reef to basin sediment transport using *Halimeda* as a sediment tracer, Grand Cayman Island, West Indies. Coral Reefs 6:187–193

Johnson MD, Price NN, Smith JE (2014) Contrasting effects of ocean acidification on tropical fleshy and calcareous algae. PeerJ 2:e411

Jury CP, Whitehead RF, Szmant AM (2010) Effects of variations in carbonate chemistry on the calcification rates of *Madracis auretenra* (= *Madracis mirabilis* sensu Wells, 1973): bicarbonate concentrations best predict calcification rates. Glob Change Biol 16:1632–1644

Kench PS, McLean RF (1996) Hydraulic characteristics of bioclastic deposits: new possibilities for environmental interpretation using settling velocity fractions. Sedimentology 43:561–570

Kench PS, McLean RF, Nichol SL (2005) New model of reef-island evolution: Maldives, Indian Ocean. Geology 33:145–148

Kench PS, Smithers SG, McLean RF (2012) Rapid reef island formation and stability over an emerging reef flat: Bewick Cay, northern Great Barrier Reef, Australia. Geology 40:347–350

Kiessling W (2009) Geologic and biologic controls on the evolution of reefs. Ann Rev Ecol Sys 40:173–192

Kiessling W, Simpson C (2011) On the potential for ocean acidification to be a general cause of ancient reef crises. Glob Change Biol 17:56–67

Kinsey D, Hopley D (1991) The significance of coral reefs as global carbon sinks–response to greenhouse. Palaeogeogr Palaeoclimatol Palaeoecol 89:363–377

Kleypas JA, Buddemeier RW, Archer D, Gattuso JP, Langdon C, Opdyke BN (1999) Geochemical consequences of increased atmospheric carbon dioxide on coral reefs. Science 284:118–120

Kleypas JA, Feely RA, Fabry VJ, Langdon C, Sabine CL, Robbins LL (2006) Impacts of ocean acidification on coral reefs and other marine calcifiers. A guide for future research. Report of a workshop sponsored by NSF, NOAA and USGS

Knittweis L, Jompa J, Richter C, Wolff M (2009) Population dynamics of the mushroom coral *Heliofungia actiniformis* in the Spermonde Archipelago, South Sulawesi, Indonesia. Coral Reefs 28:793–804

Kobayashi S (1971) Acid mucopolysaccharides in calcified tissues. Int Rev Cytol 30:257–371

Koch M, Bowes G, Ross C, Zhang XH (2013) Climate change and ocean acidification effects on seagrasses and marine macroalgae. Glob Change Biol 19:103–132

Kooistra WHCF, Verbruggen H (2005) Genetic patterns in the calcified tropical seaweeds *Halimeda opuntia, H. distorta, H. hederacea*, and *H. minima* (Bryopsidales, Chlorophyta) provide insights in species boundaries and interoceanic dispersal. J Phycol 41:177–187

Kump LR, Brantley SL, Arthur MA (2000) Chemical weathering, atmospheric CO_2, and climate. Annu Rev Earth Planet Sci 28:611–667

Kump LR, Bralower TJ, Ridgwell A (2009) Ocean acidification in deep time. Oceanography 22:94–107

Lamport D, Várnai P (2013) Periplasmic arabinogalactan glycoproteins act as a calcium capacitor that regulates plant growth and development. New Phytologist 197:58–64

Langer G, Geisen M, Baumann KH, Kläs J, Riebesell U, Thoms S, Young JR (2006) Species-specific responses of calcifying algae to changing seawater carbonate chemistry. Geochem Geophy Geosy 7

Larkum AWD, Salih A, Kühl M (2011) Rapid mass movement of chloroplasts during segment formation of the calcifying siphonalean green alga *Halimeda macroloba*. Plos One 6:e20841

Levi Y, Albeck S, Brack A, Weiner S, Addadi L (1998) Control over aragonite crystal nucleation and growth: an in vitro study of biomineralization. Chem-Eur J 4:389–396

Li W, Liu L, Zhou P, Cao L, Jiang SY (2011) Calcite precipitation induced by bacteria and bacterially produced carbonic anhydrase. Curr Sci 100:502–508

Liebezeit G, Dawson R (1981) Changes in the polysaccharide matrix of calcareous green algae during growth. Indices biochemiques et milieux marins. Journées du GABIM 14:147–154

Liljas A, Laurberg M (2000) A wheel invented three times. The molecular structures of the three carbonic anhydrases. EMBO Reports 1:16–17

Littler M (1976) Calcification and its role among the macroalgae. Micronesica 12:27–41

Longman MW (1980) Carbonate diagenetic textures from nearsurface diagenetic environments. AAPG Bulletin 64:461-487

Macintyre IG, Reid RP (1992) Comment on the origin of aragonite needle mud: a picture is worth a thousand words. J Sediment Res 62

Macintyre IG, Reid RP (1995) Crystal alteration in a living calcareous alga (*Halimeda*): implications for studies in skeletal diagenesis. J Sediment Res A Sediment Petrol Process 65:143–153

Mankiewicz C (1988) Occurrence and paleocologic significance of *Halimeda* in late Miocene reefs, southeastern Spain. Coral Reefs 6:271–279

Mann S (2001) Biomineralization: principles and concepts in bioinorganic materials chemistry. Oxford University Press Vol. 5

Manzello DP, Kleypas JA, Budd DA, Eakin CM, Glynn PW, Langdon C (2008) Poorly cemented coral reefs of the eastern tropical Pacific: possible insights into reef development in a high-CO_2 world. P Natl A Sci 105:10450–10455

Marin F, Luquet G (2004) Molluscan shell proteins. Cr Acad Sci II A 3:469–492

Marshall JF, Davies PJ (1988) *Halimeda* bioherms of the northern Great Barrier Reef. Coral Reefs 6:139–148

Martin J, Braga J, Riding R (1997) Late Miocene *Halimeda* alga-microbial segment reefs in the marginal Mediterranean Sorbas Basin, Spain. Sedimentology 44:441–456

Maurer P, Hohenester E (1997) Structural and functional aspects of calcium binding in extracellular matrix proteins. Matrix Biology 15:569–580

McClanahan T, Polunin N, Done T (2002) Ecological states and the resilience of coral reefs. Conserv Ecol 6:18

McConnaughey TA, Whelan JF (1997) Calcification generates protons for nutrient and bicarbonate uptake. Earth-Sci Rev 42:95–117

McLaughlin CJ, Smith CA, Buddemeier RW, Bartley JD, Maxwell BA (2003) Rivers, runoff, and reefs. Global Planet Change 39:191–199

Melzner F, Stange P, Trübenbach K, Thomsen J, Casties I, Panknin U, Gorb SN, Gutowska MA (2011) Food supply and seawater pCO_2 impact calcification and internal shell dissolution in the blue mussel *Mytilus edulis*. PloS One 6:e24223

Merbach C, Culberson CH, Hawley JE, Pytkowicz RM (1973) Measurements of the apparent dissociation constants of carbonic acid in seawater at atmospheric pressure. Limnol Oceanogr 18:897–907

Milliman JD (1974) Recent sedimentary carbonates, part 1. Marine carbonates. Springer, Heidelberg

Milliman JD (1993) Production and accumulation of calcium carbonate in the ocean: Budget of a nonsteady state. Global Biogeochem Cy 7:927–957

Milliman JD, Droxler AW (1996) Neritic and pelagic carbonate sedimentation in the marine environment: ignorance is not bliss. Geol Rundsch 85:496–504

Mitsunaga K, Akasaka K, Shimada H, Fujino Y, Yasumasu I, Numanoi H (1986) Carbonic anhydrase activity in developing sea urchin embryos with special reference to calcification of spicules. Cell Differ 18:257–262

Miyamoto H, Miyashita T, Okushima M, Nakano S, Morita T, Matsushiro A (1996) A carbonic anhydrase from the nacreous layer in oyster pearls. Proc Natl Acad Sci USA 93:9657–9660

Miyamoto H, Miyoshi F, Kohno J (2005) The carbonic anhydrase domain protein nacrein is expressed in the epithelial cells of the mantle and acts as a negative regulator in calcification in the mollusc *Pinctada fucata*. Zool Sci 22:311–315

Moberg F, Folke C (1999) Ecological goods and services of coral reef ecosystems. Ecol Econ 29:215–233

Mongin M, Baird M (2014) The interacting effects of photosynthesis, calcification and water circulation on carbon chemistry variability on a coral reef flat: a modelling study. Ecol Model 284:19–34

Moore CH, Graham EA, Land LS (1976) Sediment transport and dispersal across the deep fore-reef and island slope (-55 m to -305 m), Discovery Bay, Jamaica. J Sediment Petrol 46:174–187

Moroney JV, Bartlett SG, Samuelsson G (2001) Carbonic anhydrases in plants and algae. Plant Cell Environ 24:141–153

Morse JW, Arvidson RS, Lüttge A (2007) Calcium carbonate formation and dissolution. Chem Rev 107:342–381

Moya A, Tambutté S, Bertucci A, Tambutté E, Lotto S, Vullo D, Supuran C, Allemand D, Zoccola D (2008) Carbonic anhydrase in the scleractinian coral *Stylophora pistillata*: characterization, localization, and role in biomineralization. J Biol Chem 283:25475–25484

Multer HG (1988) Growth rate, ultrastructure and sediment contribution of *Halimeda incrassata* and *Halimeda monile*, Nonsuch and Falmouth Bays, Antigua, W.I. Coral Reefs 6:179–186

Multer HG, Clavijo I (2004) *Halimeda* investigations: progress and problems. NOAA/RSMAS

Mutti M, Hallock P (2003) Carbonate systems along nutrient and temperature gradients: some sedimentological and geochemical constraints. Int J Earth Sci 92:465–475

Nakahara H, Bevelander G (1978) The formation of calcium carbonate crystals in *Halimeda incrassata* with special reference to the role of the organic matrix. Jap J Phycol 26:9–12

Nelson W (2009) Calcified macroalgae–critical to coastal ecosystems and vulnerable to change: a review. Mar Freshw Res 60:787–801

Neumann AC, Land LS (1975) Lime mud deposition and calcareous algae in the Bight of Abaco, Bahamas; a budget. J Sediment Res 45:763–786

Noé S, Titschack J, Freiwald A, Dullo WC (2006) From sediment to rock: diagenetic processes of hardground formation in deep-water carbonate mounds of the NE Atlantic. Facies 52:183–208

Nothdurft LD, Webb GE, Bostrom T, Rintoul L (2007) Calcite-filled borings in the most recently deposited skeleton in live-collected Porites (Scleractinia): implications for trace element archives. Geochim Cosmochim Ac 71:5423–5438

Orme G, Flood P, Sargent G (1978) Sedimentation trends in the lee of outer (ribbon) reefs, Northern Region of the Great Barrier Reef Province. Philos Trans R Soc A 291:85–99

Orme GR, Salama MS (1988) Form and seismic stratigraphy of *Halimeda* banks in part of the northern Great Barrier Reef Province. Coral Reefs 6:131–137

Orr JC Fabry VJ, Aumont O, Bopp L, Doney SC, Feely RA, Gnanadesikan A, Gruber N, Ishida A, Joos F, Key RM, Lindsay K, Maier-Reimer E, Matear R, Monfray P, Mouchet A, Najjar RG, Platter GK, Rodgers KB, Sabine CL, Sarmiento JL, Schlitzer R, Slater RD, Totterdell IJ, Weirig MF, Yamanaka Y, Yool A (2005) Anthropogenic ocean acidification over the twenty-first century and its impact on calcifying organisms. Nature 437:681–686

Paul V, Hay M (1986) Seaweed susceptibility to herbivory: chemical and morphological correlates. Mar Ecol Prog Ser 33:255–264

Payri CE (1988) *Halimeda* contribution to organic and inorganic production in a Tahitian reef system. Coral Reefs 6:251–262

Perry CT (1998) Grain susceptibility to the effects of microboring: implications for the preservation of skeletal carbonates. Sedimentology 45:39–51

Perry CT (2000) Factors controlling sediment preservation on a North Jamaican fringing reef: a process-based approach to microfacies analysis. J Sediment Res 70:633-648

Perry CT, Taylor KG (2006) Inhibition of dissolution within shallow water carbonate sediments: impacts of terrigenous sediment input on syn-depositional carbonate diagenesis. Sedimentology 53:495–513

Perry CT, Kench PS, Smithers SG, Riegl B, Yamano H, O'Leary MJ (2011) Implications of reef ecosystem change for the stability and maintenance of coral reef islands. Glob Change Biol 17:3679–3696

Phipps C, Roberts HH (1988) Seismic characteristics and accretion history of *Halimeda* bioherms on Kalukalukuang Bank, eastern Java Sea (Indonesia). Coral Reefs 6:149–159

Pickard B (2013) Arabinogalactan proteins – becoming less mysterious. New Phytologist 197:3–5

Pierrot D, Lewis E, Wallace DWR (2006) CO_2SYS DOS Program developed for CO_2 system calculations. ORNL/CDIAC-105. Carbon Dioxide Information Analysis Center, Oak Ridge National Laboratory, US Department of Energy, Oak Ridge, TN

Pomar L, Kendall CGSC (2007) Architecture of carbonate platforms: a response to hydrodynamics and evolving ecology. In: Lukasik J, Simo JA (eds) Controls on carbonate platform and reef development. SEPM 89:187–216

Pörtner H (2008) Ecosystem effects of ocean acidification in times of ocean warming: a physiologist's view. Mar Ecol Prog Ser 373:203–217

Price G, Badger M, Bassett M, Whitecross M (1985) Involvement of plasmalemmasomes and carbonic anhydrase in photosynthetic utilization of bicarbonate in *Chara corallina*. Funct Plant Biol 12:241–256

Price NN, Hamilton SL, Tootell JS, Smith JE (2011) Species-specific consequences of ocean acidification for the calcareous tropical green algae *Halimeda*. Mar Ecol Prog Ser 440:67–78

Rahman MA, Oomori T, Uehara T (2008) Carbonic anhydrase in calcified endoskeleton: novel activity in biocalcification in alcyonarian. Mar Biotechnol 10:31–38

Rao VP, Veerayya M, Nair RR, Dupeuble PA, Lamboy M (1994) Late Quaternary *Halimeda* bioherms and aragonitic faecal pellet-dominated sediments on the carbonate platform of the western continental shelf of India. Mar Geol 121:293–315

Raven J, Caldeira K, Elderfield H, Hoegh-Guldberg O, Liss P, Riebesell U, Shepherd J, Turley C, Watson A (2005) Ocean acidification due to increasing atmospheric carbon dioxide. R Soc June, pp 1–60

Raymo ME, Ruddiman WF (1992) Tectonic forcing of late Cenozoic climate. Nature 359:117–122

Rees SA, Opdyke BN, Wilson PA, Henstock TJ (2007) Significance of *Halimeda* bioherms to the global carbonate budget based on a geological sediment budget for the Northern Great Barrier Reef, Australia. Coral Reefs 26:177–188

Reid RP, Macintyre GI (1998) Carbonate recrystallization in shallow marine environments: a widespread diagenetic process forming micritized grains. J Sediment Res 68:928–946

Renema W, Hoeksema BW, Van Hinte JE (2001) Larger benthic foraminifera and their distribution patterns on the Spermonde shelf, South Sulawesi. Zool. Verh. Leiden 334:115–149

Renema W, Troelstra SR (2001) Larger foraminifera distribution on a mesotrophic carbonate shelf in SW Sulawesi (Indonesia). Palaeogeogra Palaeocl 175:125–146

Renema W (2002) Larger foraminifera as marine environmental indicators. Scripta Geologica 124, PhD thesis, Nationaal Natuurhistorisch Museum, p 263

Renema W (2006) Large benthic foraminifera from the deep photic zone of a mixed siliciclastic-carbonate shelf off East Kalimantan, Indonesia. Mar Micropaleontol 58:73–82

Reyes-Nivia C, Diaz-Pulido G, Dove S (2014) Relative roles of endolithic algae and carbonate chemistry variability in the skeletal dissolution of crustose coralline algae. Biogeosciences Discuss 11:2993–3021

Riebesell U (2004) Effects of CO_2 enrichment on marine phytoplankton. J Oceanogr 60:719–729

Riebesell U, Fabry VJ, Hansson L, Gattuso JP (2010) Guide to best practices for ocean acidification research and data reporting. Luxembourg: Publications Office of the European Union, p 260

Ries JB (2009) Effects of secular variation in seawater Mg/Ca ratio (calcite-aragonite seas) on $CaCO_3$ sediment production by the calcareous algae *Halimeda*, *Penicillus* and *Udotea* - evidence from recent experiments and the geological record. Terra Nova 21:323–339

Ries JB, Cohen AL, McCorkle DC (2009) Marine calcifiers exhibit mixed responses to CO_2-induced ocean acidification. Geology 37:1131–1134

Ries JB (2011) Skeletal mineralogy in a high-CO_2 world. J Exp Mar Biol Ecol 403:54–64

Robbins LL, Knorr PO, Hallock P (2009) Response of *Halimeda* to ocean acidification: field and laboratory evidence. Biogeosciences Discuss 6

Roberts H, Phipps C, Effendi L (1987) *Halimeda* bioherms of the eastern Java Sea, Indonesia. Geology 15:371–374

Roberts H, Aharon P, Phipps C (1988) Morphology and sedimentology of *Halimeda* bioherms from the eastern Java Sea (Indonesia). Coral Reefs 6:161–172

Robinson C, Brooks SJ, Shore RC, Kirkham J (1998) The developing enamel matrix: nature and function. Eur J Oral Sci 106:282–291

Salgado LT, Amado Filho GM, Fernandez MS, Arias JL, Farina M (2011) The effect of alginates, fucans and phenolic substances from the brown seaweed *Padina gymnospora* in calcium carbonate mineralization in vitro. J Cryst Growth 321:65–71

Sawall Y, Teichberg MC, Seemann J, Litaay M, Jompa J, Richter C (2011) Nutritional status and metabolism of the coral *Stylophora subseriata* along a eutrophication gradient in Spermonde Archipelago (Indonesia). Coral Reefs 30:841–853

Schupp PJ, Paul VJ (1994) Calcium carbonate and secondary metabolites in tropical seaweeds: variable effects on herbivorous fishes. Ecology 75:1172–1185

Scoffin TP, Tudhope AW (1985) Sedimentary environments of the central region of the Great Barrier Reef of Australia. Coral Reefs 4:81–93

Shaw EC, Mcneil BI, Tilbrook B, Matear R, Bates ML (2013) Anthropogenic changes to seawater buffer capacity combined with natural reef metabolism induce extreme future coral reef CO_2 conditions. Glob Change Biol 19:1632-1641

Sikes CS (1978) Calcification and cation sorption of *Cladophoha glomerata* (chlorophyta). J Phycol 14.3:325–329

Simkiss K (1964) Phosphates as crystal poisons of calcification. Biol Rev 39:487–504

Simkiss K (1965) The organic matrix of the oyster shell. Comp Biochem Phys 16:427–435

Simkiss K, Wilbur KM (1989) Biomineralization. Academic Press, San Diego, California 92101

Sinutok S, Hill R, Doblin MA, Wuhrer R, Ralph PJ (2011) Warmer more acidic conditions cause decreased productivity and calcification in subtropical coral reef sediment-dwelling calcifiers. Limnol Oceanogr 56:1200–1212

Sinutok S, Hill R, Doblin MA, Kühl M, Ralph PJ (2012) Microenvironmental changes support evidence of photosynthesis and calcification inhibition in *Halimeda* under ocean acidification and warming. Coral Reefs 31:1201–1213

Sinutok S (2013) Interactive effects of ocean acidification and warming on sediment-dwelling marine calcifiers. PhD-Thesis, University of Technology, Sydney, p 268

Stanley S, Hardie LA (1998) Secular oscillations in the carbonate mineralogy of reef-building and sediment-producing organisms driven by tectonically forced shifts in seawater chemistry. Palaeogeogr Palaeoclimatol Palaeoecol 144:3–19

Stanley SM (2008) Effects of global seawater chemistry on biomineralization: past, present, and future. Chem Rev 108:4483–4498

Stanley SM, Ries JB, Hardie LA (2010) Increased production of calcite and slower growth for the major sediment-producing alga *Halimeda* as the Mg/Ca ratio of seawater is lowered to a "Calcite Sea" level. J Sediment Res 80:6–16

Sültemeyer D (1998) Carbonic anhydrase in eukaryotic algae: characterization, regulation, and possible function during photosynthesis. Can J Bot 76:962–972

Takahashi T, Broecker WS, Bainbridge AE (1981) The alkalinity and total carbon dioxide concentration in the world oceans. Carbon Cycle Modelling, SCOPE, 16:271–286

Takeuchi T, Sarashina I, Iijima M, Endo K (2008) In vitro regulation of $CaCO_3$ crystal polymorphism by the highly acidic molluscan shell protein Aspein. FEBS Letters 582:591–596

Tambutté S, Tambutté E, Zoccola D, Caminiti N, Lotto S, Moya A, Allemand D, Adkins J (2007) Characterization and role of carbonic anhydrase in the calcification process of the azooxanthellate coral *Tubastrea aurea*. Mar Biol 151:71–83

Tsuzuki M, Miyachi S (1989) The function of carbonic anhydrase in aquatic photosynthesis. Aquat Bot 34:85–104

Tussenbroek BI, van Dijk JK (2007) Spatial and temporal variability in biomass and production of psammophytic *Halimeda incrassata* (Bryopsidales, Chlorophyta) in a Caribbean reef lagoon. J Phycol 43:69–77

Verbruggen H, Kooistra W (2004) Morphological characterization of lineages within the calcified tropical seaweed genus *Halimeda* (Bryopsidales, Chlorophyta). Eur J Phycol 39:213–228

Verbruggen H, De Clerck O, Cocquyt E, Kooistra WHCF, Coppejans E (2005) Morphometric taxonomy of siphonous green algae: a methodological study within the genus *Halimeda* (Bryopsidales). J Phycol 41:126–139

Verbruggen H, De Clerck O, N'yeurt ADR, Spalding H, Vroom PS (2006) Phylogeny and taxonomy of *Halimeda incrassata*, including descriptions of *H. kanaloana* and *H. heteromorpha* spp. nov. (Bryopsidales, Chlorophyta). Eur J Phycol 41:337–362

Verbruggen H, Littler DS, Littler MM (2007) *Halimeda pygmaea* and *Halimeda pumila* (Bryopsidales, Chlorophyta): two new dwarf species from fore reef slopes in Fiji and the Bahamas. Phycologia 46:513–520

Verbruggen H, Tyberghein L, Pauly K, Vlaeminck C, Nieuwenhuyze KV, Kooistra WH, Leliaert F, Clerck OD (2009) Macroecology meets macroevolution: evolutionary niche dynamics in the seaweed *Halimeda*. Global Ecol Biogeogr 18:393–405

Veron JEN (2008) Mass extinctions and ocean acidification: biological constraints on geological dilemmas. Coral Reefs 27:459–472

Vidal-Dupiol J, Zoccola D, Tambutté E, Grunau C, Cosseau C, Smith KM, Freitag M, Dheilly NM, Allemand D, Tambutté S (2013) Genes related to ion-transport and energy production are upregulated in response to CO_2-driven pH decrease in corals: new insights from transcriptome analysis. PloS One 8:e58652

Vogel N, Fabricius KE, Strahl J, Noonan SHC, Wild C, Uthicke S (2015a) Calcareous green alga *Halimeda* tolerates ocean acidification conditions at tropical carbon dioxide seeps. Limnol Oceanogr 60:263–275

Vogel N, Meyer F, Wild C, Uthicke S (2015b) Decreased light availability can amplify negative impacts of ocean acidification on calcifying coral reef organisms. Mar Ecol Prog Ser 521:49–61

Vroom PS, Smith CM, Coyer JA, Walters LJ, Hunter CL, Beach KS, Smith JE (2003) Field biology of *Halimeda tuna* (Bryopsidales, Chlorophyta) across a depth gradient: comparative growth, survivorship, recruitment, and reproduction. Hydrobiologia 501:149–166

Watanabe T, Fukuda I, China K, Isa Y (2003) Molecular analyses of protein components of the organic matrix in the exoskeleton of two scleractinian coral species. Comp Biochem Physiol B Biochem Mol Biol 136:767–774

Weber J, Woodhead P (1970) Carbon and oxygen isotope fractionation in the skeletal carbonate of reef-building corals. Chem Geol 6:93–117

Wefer G (1980) Carbonate production by algae *Halimeda, Penicillus* and *Padina*. Nature 285:323–324

Wefer G, Berger WH (1981) Stable isotope composition of benthic calcareous algae from Bermuda. J Sediment Res 51:2–8

Weiner S, Lowenstam H (1986) Organization of extracellularly mineralized tissues: a comparative study of biological crystal growth. Crit Rev Biochem Mol Biol 20:365–408

Weiss M, Pick U (1996) Primary structure and effect of pH on the expression of the plasma membrane H^+-ATPase from *Dunaliella acidophila* and *Dunaliella salina*. Plant Physiol 112:1693–1702

Weiss IM, Marin F (2008) The role of enzymes in biomineralization processes. In: Sigel A, Sigel H, Sigel RKO (eds) Biomineralization: from nature to application. Wiley, West Sussex, pp 71–126

Wentworth CK (1922) A scale of grade and class terms for clastic sediments. J Geol 30:377–392

Wheeler AP, Sikes CS (1984) Regulation of carbonate calcification by organic matrix. Integr Comp Biol 24:933–944

Wienberg C, Westphal H, Kwoll E, Hebbeln D (2010) An isolated carbonate knoll in the Timor Sea (Sahul Shelf, NW Australia): facies zonation and sediment composition. Facies 56:179–193

Wilbur KM, Hillis-Colinvaux L, Watabe N (1969) Electron microscope study of calcification in the alga *Halimeda* (order Siphonales). Phycologia 8:27–35

Wilson MEJ, Vecsei A (2005) The apparent paradox of abundant foramol facies in low latitudes: their environmental significance and effect on platform development. Earth Sci Rev 69:133–168

Wiman SK, McKendree WG (1975) Distribution of *Halimeda* plants and sediments on and around a patch reef near Old Rhodes Key, Florida. J Sediment Res 45:415–421

Wojtas M, Dobryszycki P, Andrzej O (2012) Intrinsically Disordered Proteins in Biomineralization. In: Seto J (ed) Advanced topics in biomineralization, InTech Europe, Croatia, p 174

Wood HL, Spicer JI, Widdicombe S (2008) Ocean acidification may increase calcification rates, but at a cost. Proc R Soc B 275:1767–1773

Wood HL, Spicer JI, Lowe DM, Widdicombe S (2010) Interaction of ocean acidification and temperature; the high cost of survival in the brittlestar *Ophiura ophiura*. Mar Biol 157:2001–2013

Woodroffe CD, McLean RF, Smithers SG, Lawson EM (1999) Atoll reef-island formation and response to sea-level change: West Island, Cocos (Keeling) Islands. Mar Geol 160:85–104

Woodroffe CD (2008) Reef-island topography and the vulnerability of atolls to sea-level rise. Global Planet Change 62:77–96

Zachos JC, Röhl U, Schellenberg SA, Sluijs A, Hodell DA, Kelly DC, Thomas E, Nicolo M, Raffi I, Lourens LJ, McCarren H, Kroon D (2005) Rapid acidification of the ocean during the Paleocene-Eocene thermal maximum. Science 308:1611–1615

Zeebe RE (2012) History of seawater carbonate chemistry, atmospheric CO_2, and ocean acidification. Annu Rev Earth Planet Sci 40:141–165

Zhong C, Chu CC (2010) On the origin of amorphous cores in biomimetic $CaCO_3$ spherulites: new insights into spherulitic crystallization. Cryst Growth Des 10:5043–5049

X. Appendix

X.I Abbreviations

AGP = arabino-galactan protein

AP = extracellular alkaline phosphatase

A_T = total alkalinity of the seawater

atm = atmospheres (here used in µatm)

ATPase = adenosine tri-phosphate(ase); enzyme, ionic pump

B = Borate

C^{14} AMS = isotope of carbon (radiocarbon dating via accelerator mass spectrometry)

Ca, Ca^{2+} = Calcium, ion

$CaCO_3$ = calcium carbonate

CO_2 = carbon dioxide; p = partial pressure (of)

CO_3^{2-} = carbonate

DBL = diffusive boundary layer

DIC = dissolved inorganic carbon

eCA = extracellular carbonic anhydrase activity

ekV = electron kilo Volt

H^+ = proton; hydrogen ion

HCO_3^- = bi-carbonate

H_2CO_3 = carbonic acid

H_2O = water

IDP = intrinsically disordered protein

IUS = inter-utricular space; p = primary, s = secondary

k = thousand (years)

Ma = million years

MAC = micro-anhedral carbonate

m b.s.l. = meters below sea level

Mg, Mg^{2+} = Magnesium, ion

m Mg /Ca = molar ratio, Magnesium / Calcium

Micrite = micro-crystalline calcite (Folk 1959)

OH^- = hydroxide anion

pH_{NBS} = pH, measured in NBS-scale

P_i = inorganic ortho-phosphate

PP_i = inorganic pyro-phosphate

ppm = parts per million

S = salinity

Su = Sulfur

SEM = scanning electron microscope

SEM-BSE = SEM - back-scattered electron, detector

SEM-EDX = SEM - energy dispersive X-ray, detector

Sr, Sr^{2+} = Strontium, ion

T = temperature (here of the seawater)

U = utricle; p, s, t, m = primary, secondary, tertiary, medullary

U / Th = uranium / thorium ratio (for dating)

$\delta^{13}C$ = stable isotope of carbon

$\delta^{18}O$ = stable isotope of oxygen

Ω = calcium carbonate saturation state of the seawater; arag = aragonite; cal = calcite

X.II Plates of thin-sections from *Halimeda* segments from surface sediment samples.

Scale bar in BSE-SEM images of thin-sections from *Halimeda* segments is 200 µm (Figs. A1 - A14). Rim of golden frame in upper right digital photographs of segments (in a picking tray) is 1 cm. Note the similarities of segments in grain size, internal morphological microstructure (cf., species-specificity, habitat-specificity) and stages of grain abrasion (i.e., roundness of the grain) in correspondence to stages of secondary cementation of segments that were sampled worldwide (from Atlantic, Indic, and Pacific locations; cf. Table 5.1.I). Also note that it is not possible to predict the stage of segment alteration only from external segment shape (cf. digital photographs), as a pristinely shaped segment may show abundant intra-granular secondary cementation and vice versa. Estimations on the age or transport of a segment merely from its surface structure and shape thus may lead to erroneous interpretations (e.g., in studies on island formation and sediment transport).

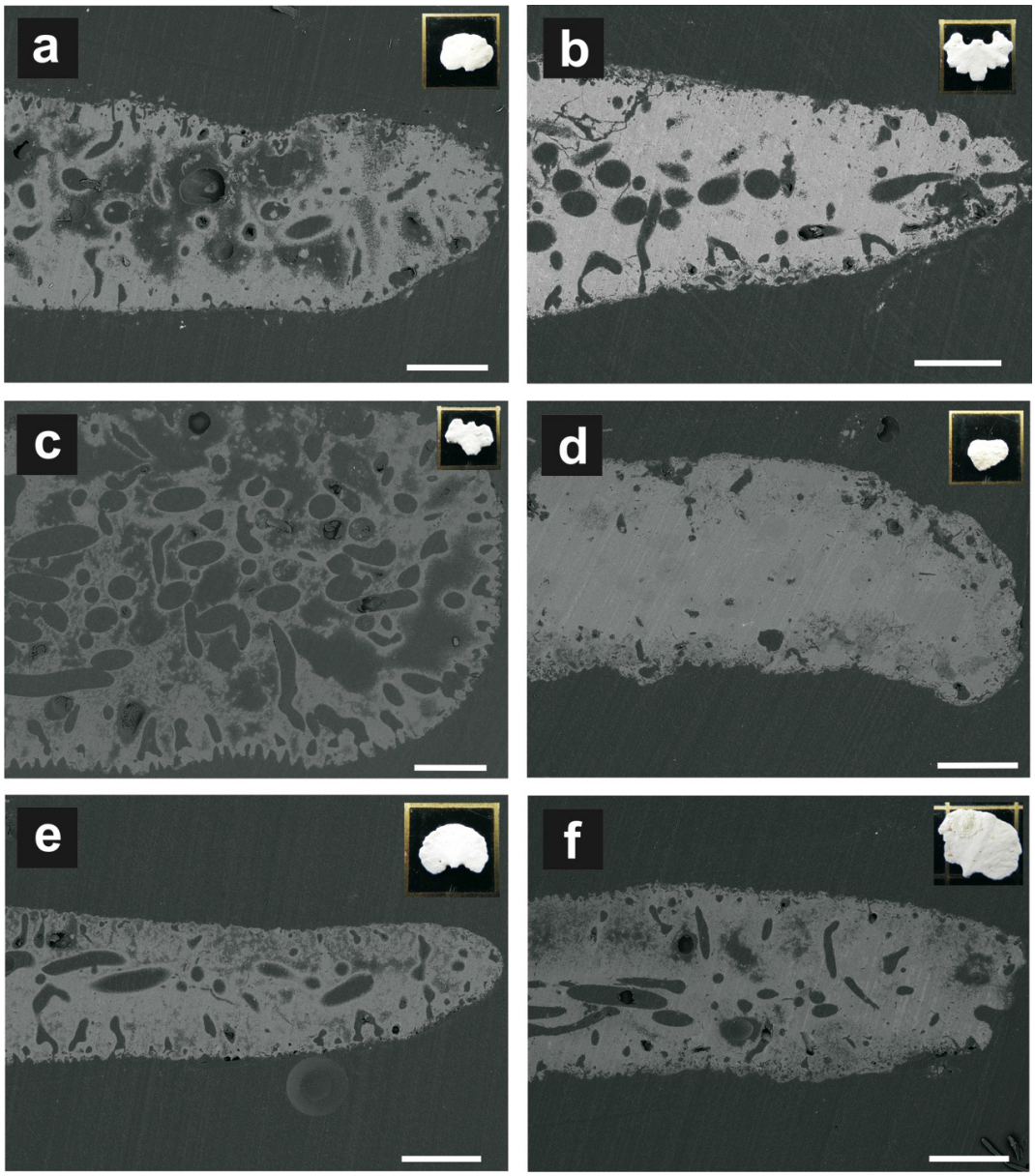

Fig. A1 BSE-SEM images of thin-sections from *Halimeda* segments and corresponding photographs that originate from surface sediments sampled in the Great Barrier Reef Province (Australia). Courtesy of J. D. Milliman (Virginia Institute of Marine Science). All specimens depicted are most likely of *Halimeda* lineage Opuntia. Sample ID: (a) 3533, (b) 3538, (c) 3540, (d) 3543, (e) 3549, (f) 3551. No data available on sampling water depth.

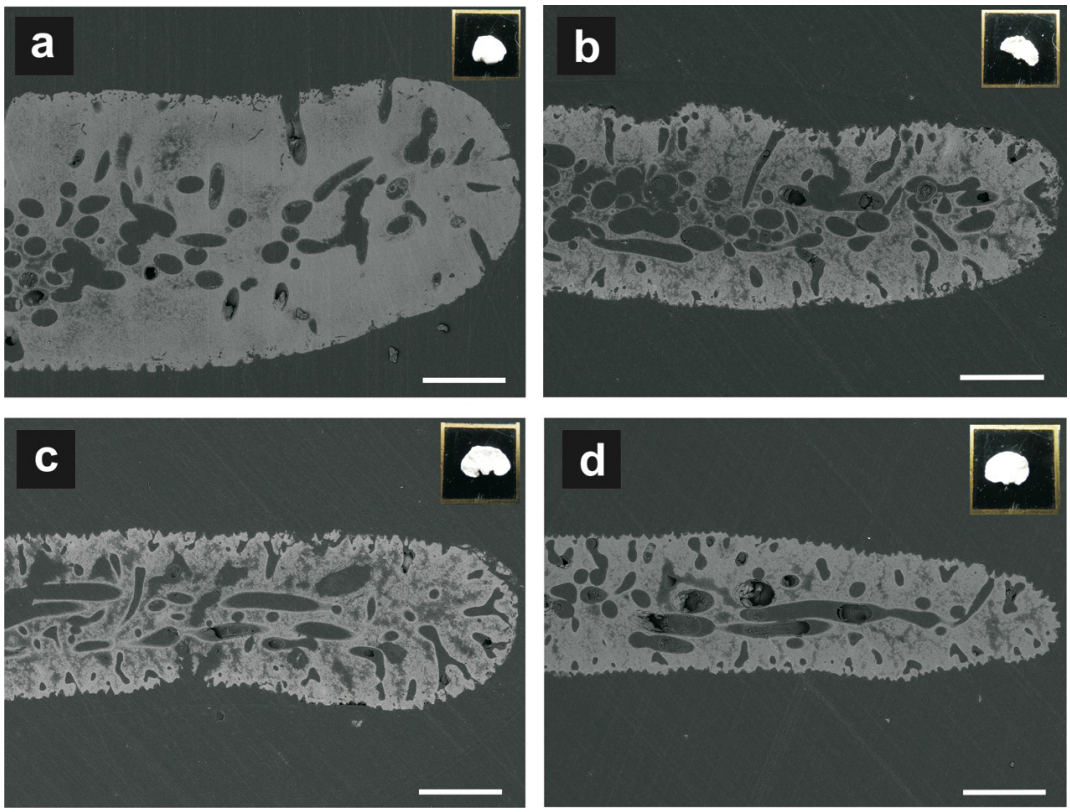

Fig. A2 BSE-SEM images of thin-sections from *Halimeda* segments and corresponding photographs that originate from surface sediments sampled at Fiji Atoll (Southern Pacific). Courtesy of P. Mayer and H. Westphal (University of Bremen and ZMT-Bremen). All specimens depicted are most likely of *Halimeda* lineage Opuntia. Sample ID: (a) 3-01_Nacumbuko, (b) 4-01_Nananu-i-ra, (c) 5-01_Nananu-i-ra, (d) 8-01_Nananu-i-ra. Samples taken from onshore (beach) and water depths < 1 m b.s.l.

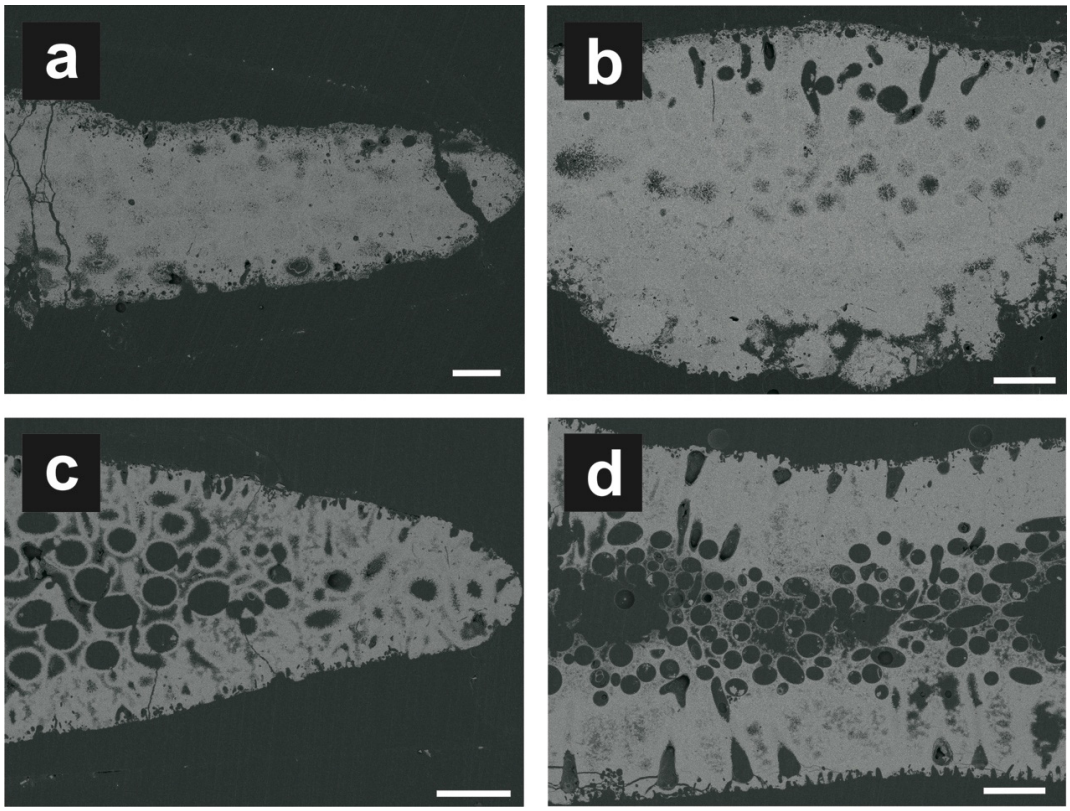

Fig. A3 BSE-SEM images of thin-sections from *Halimeda* segments that originate from surface sediments sampled in the Maldives (Kudahuvadhoo Atoll; Indian Ocean). Courtesy of C. Betzler (University of Hamburg). No photographs are available. (a) and (b) show heavily cemented segments where species identification is ambigous. (c) Specimen shows typical internal microstructure of *Halimeda* lineage Opuntia. (d) Specimen probably of *Halimda* lineage Opuntia or Micronesicae. Sample ID: (a) 08-SH-4P (b) 08-SH-4P_2, (c) 35-SH-B6, (d) 35-SH-B6_2. Samples taken from water depths < 2 m b.s.l.

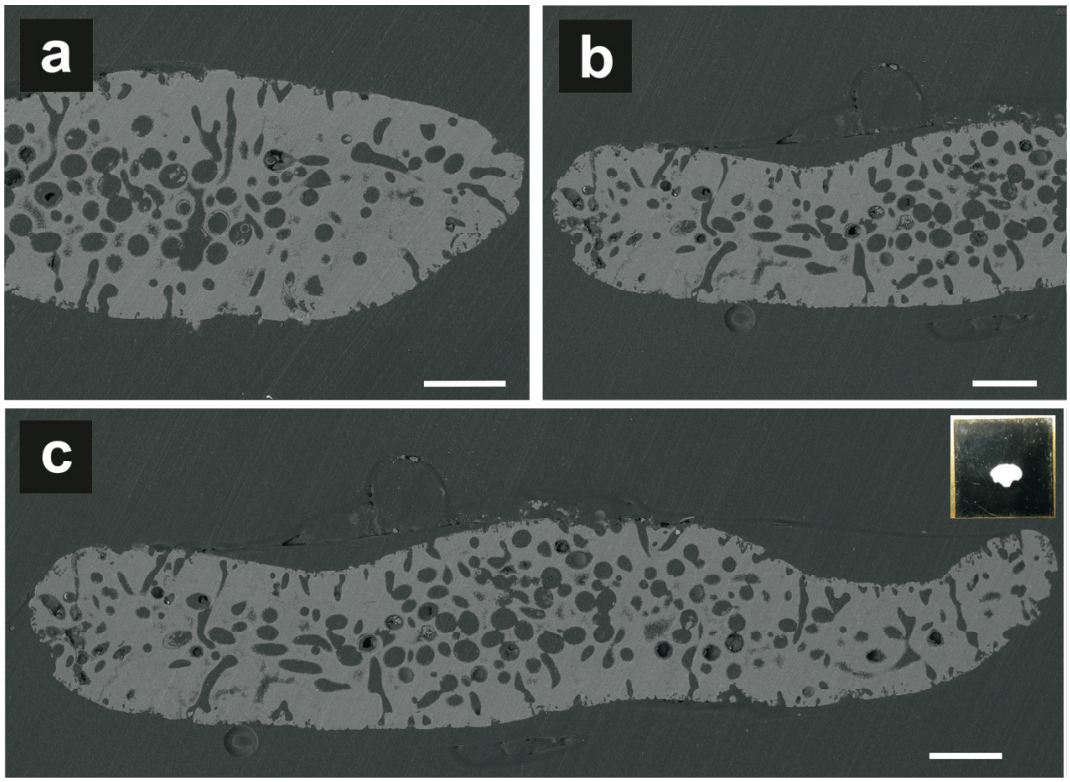

Fig. A4 BSE-SEM images of thin-sections from *Halimeda* segments and corresponding photograph that originate from historical surface sediment sampled in the Maldives during the German deep-sea expedition "Valdivia" 1898 - 1899 (Sample Nr. 219; Suvadiva, Huvadhu Atoll, "Kanduhulhudhoo Beach", Indian Ocean). Courtesy of the Natural History Museum Berlin. No photograph available for (a). (b) and (c) show same specimen. All specimens depicted most likely from *Halimeda* lineage Opuntia. Sample ID: (a) DTE1899_01, (b) and (c) DTE1899_02. Samples taken from onshore sediments (beach area).

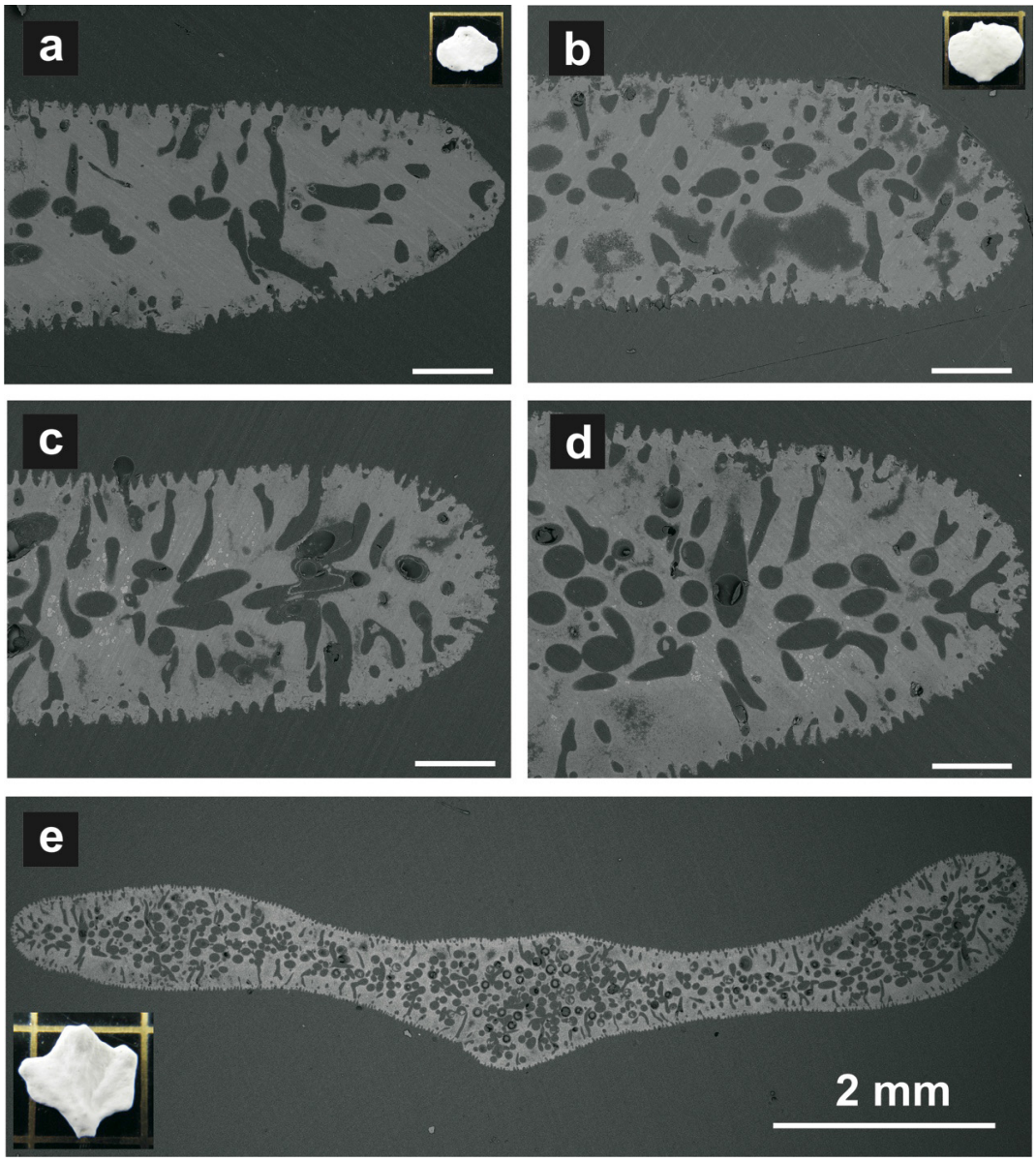

Fig. A5 BSE-SEM images of thin-sections from *Halimeda* segments and corresponding photographs that originate from surface sediments sampled at Pee Shoal (seamount; Timor Sea; South-Eastern Pacific Ocean; Wienberg et al. 2010; GeoB100_71). Courtesy of C. Wienberg and H. Westphal (MARUM Bremen and ZMT-Bremen). All specimens depicted most likely from *Halimed*a lineage Opuntia. No photograph available for (c). (d) and (e) show same specimen. (a) 71-3, (b) 71-4, (c) 71-5, (d) and (e) 71-5_2. Samples taken from water depths > 20 m b.s.l.

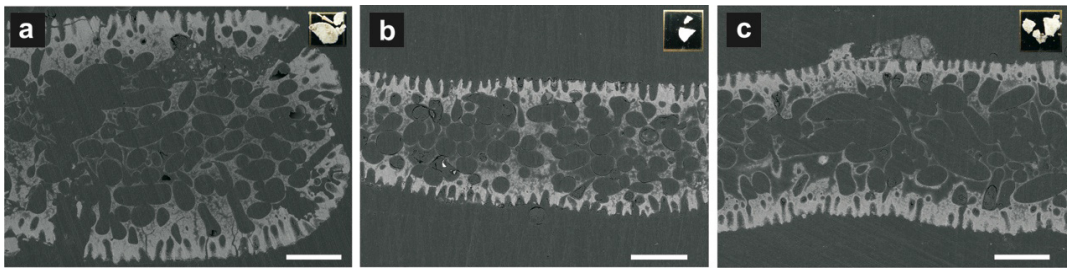

Fig. A6 BSE-SEM images of thin-sections from *Halimeda* segments and corresponding photographs that originate from surface sediments sampled in the Abrolhos Archipelago (coast off Brazil, Atlantic Ocean). Courtesy of M. Naumann (ZMT-Bremen). All specimens are from fragmented segments hampering species identification. (a) Specimen depicted presumably from *Halimeda* lineage Opuntia. Specimens depicted in (b) and (c) may originate from other *Halimeda* lineage. Sample ID: (a) Pedra_deLeste_10m, (b) Pedra_deLixia_3m, (c) Pedra_deLixia_9m. Sampling water depth indicated in sample ID.

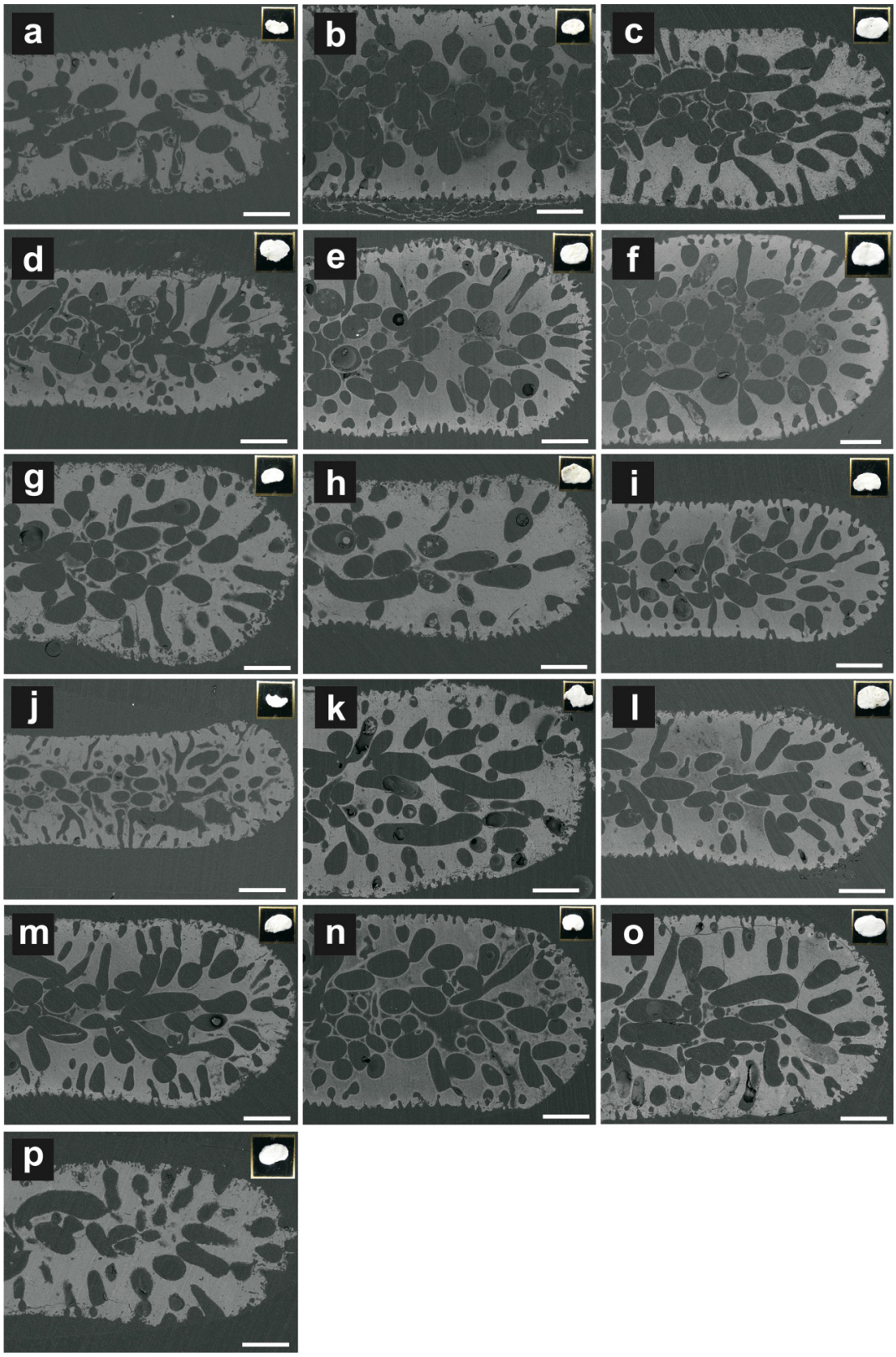

Fig. A7 (legend next page)

Fig. A7 (continued) BSE-SEM images of thin-sections from *Halimeda* segments and corresponding photographs that originate from surface sediments sampled at fringing reefs off Yucatan Peninsula (Puerto Morelos, Carribean Sea, Mexico). Courtesy of F. W. Meyer (ZMT-Bremen). All specimens depicted likely from *Halimeda* lineage Opuntia. Sample ID: (a) 01_5_5, (b) 01_5_50, (c) 01_5_R, (d) 02_5_5, (e) 02_5_50, (f) 02_5_R, (h) 03_5_5, (i) 03_5_II, (j) 03_5_R, (k) 72_R_I, (l) CO_1_R, (m) CO_1, (n) CO_2_5m, (o) CO_2_R, (p) OC_2. Samples taken from water depths < 5 m b.s.l.

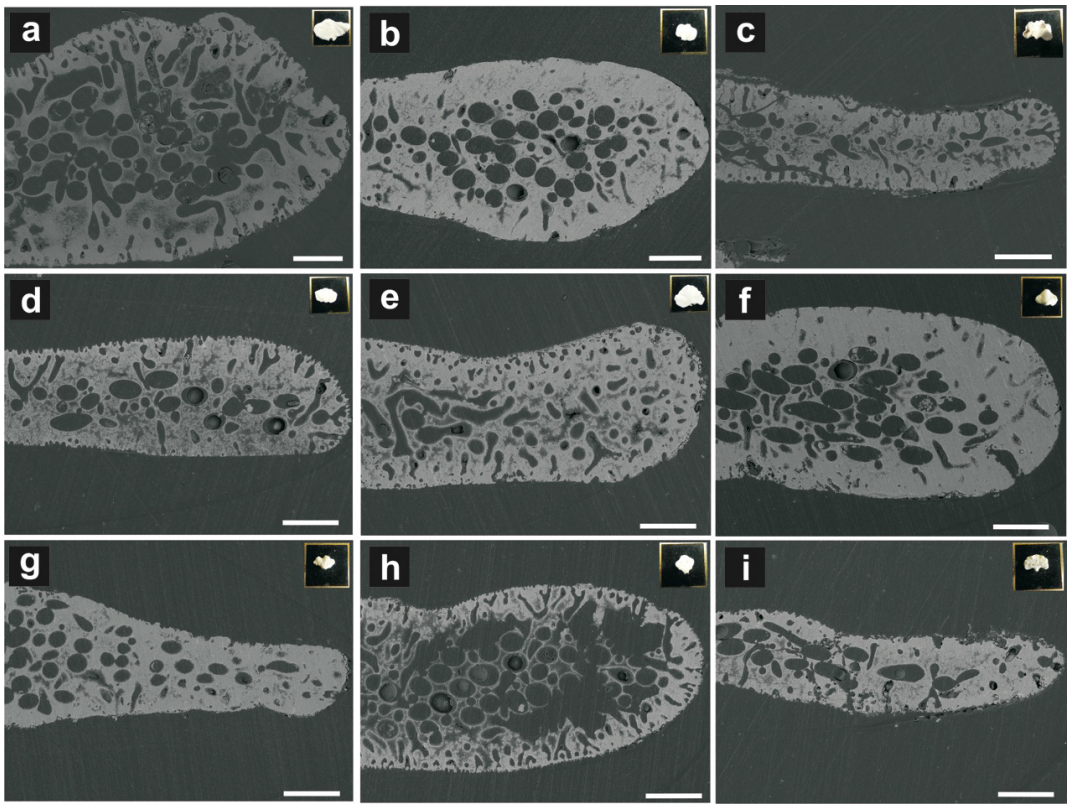

Fig. A8 BSE-SEM images of thin-sections from *Halimeda* segments and corresponding photographs that originate from surface sediments sampled at the island Pulau Pamangangan (PP) (Spermonde Archipelago, Sulawesi, Indonesia). Courtesy of T. Mann, A. Klicpera and H. Westphal (ZMT-Bremen). Most specimens depicted likely from *Halimeda* lineage Opuntia. Specimen in (e) probably of other *Halimeda* lineage. Sample ID: (a) PP1, (b) PP2, (c) PP4, (d) PP5, (e) PP6, (f) PP7, (g) PP8, (h) PP9, (i) PP10. Samples taken from onshore (beach area) and water depths < 2 m b.s.l.

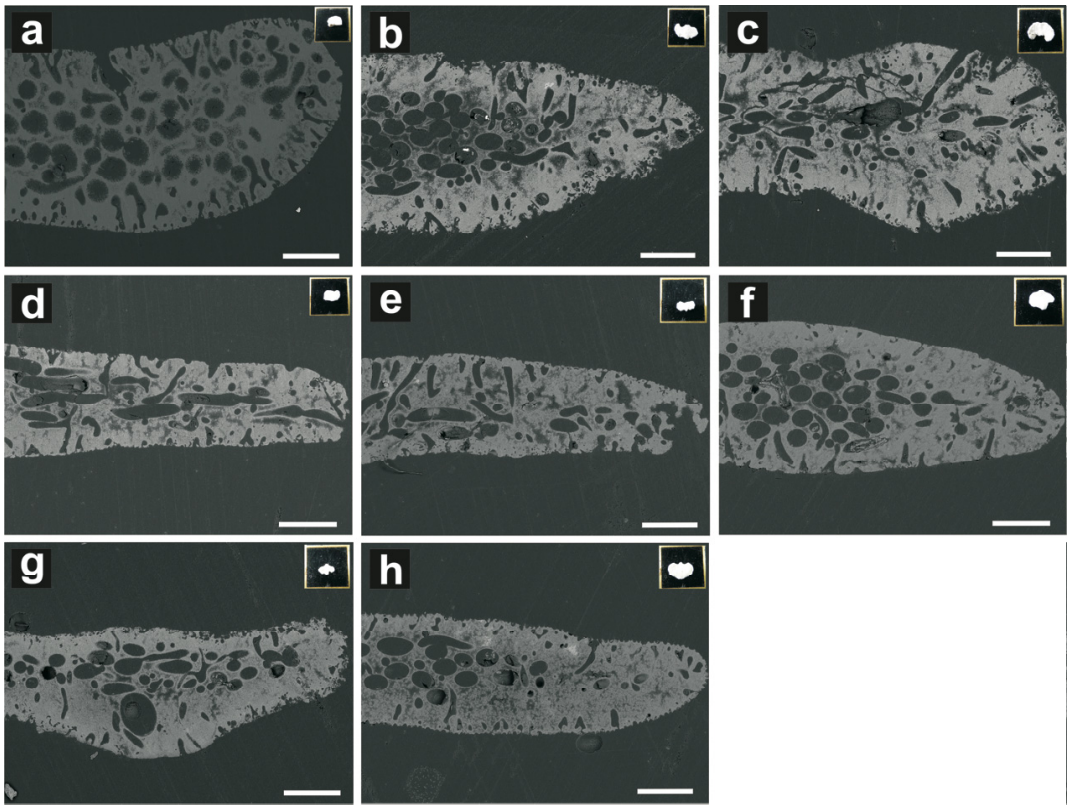

Fig. A9 BSE-SEM images of thin-sections from *Halimeda* segments and corresponding photographs that originate from surface sediments sampled at the island Pulau Tambakulu (PT) (Spermonde Archipelago, Sulawesi, Indonesia). Courtesy of T. Mann, A. Klicpera and H. Westphal (ZMT-Bremen). All specimens depicted likely from *Halimeda* lineage Opuntia. Sample ID: (a) PT1, (b) PT4, (c) PT5, (d) PT6, (e) PT7, (f) PT8, (g) PT9, (h) PT10. Samples taken from onshore (beach area) and water depths < 2 m b.s.l.

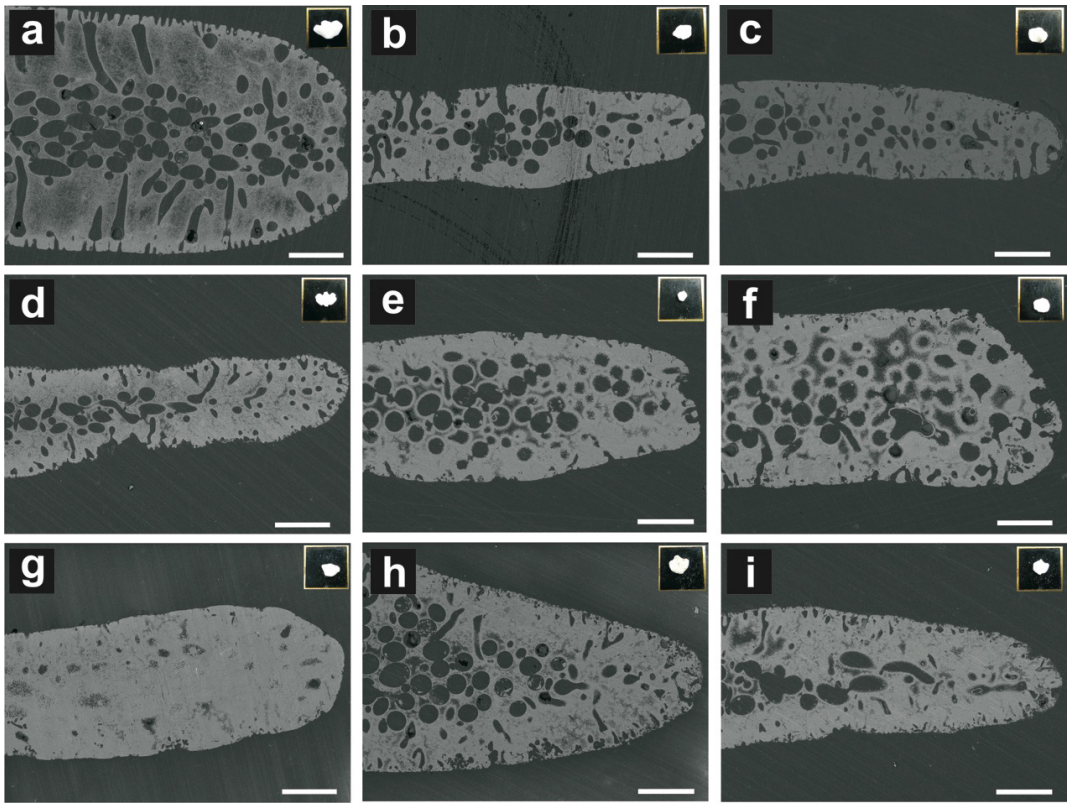

Fig. A10 BSE-SEM images of thin-sections from *Halimeda* segments and corresponding photographs that originate from surface sediments sampled at the island Pulau Suranti (PS) (Spermonde Archipelago, Sulawesi, Indonesia). Courtesy of T. Mann, A. Klicpera and H. Westphal (ZMT-Bremen). All specimens depicted likely from *Halimeda* lineage Opuntia. Sample ID: (a) PS1, (b) PS2, (c) PS3, (d) PS4, (e) PS6, (f) PS7, (g) PS8, (h) PS9, (i) PS10. Samples taken from onshore (beach area) and water depths < 2 m b.s.l.

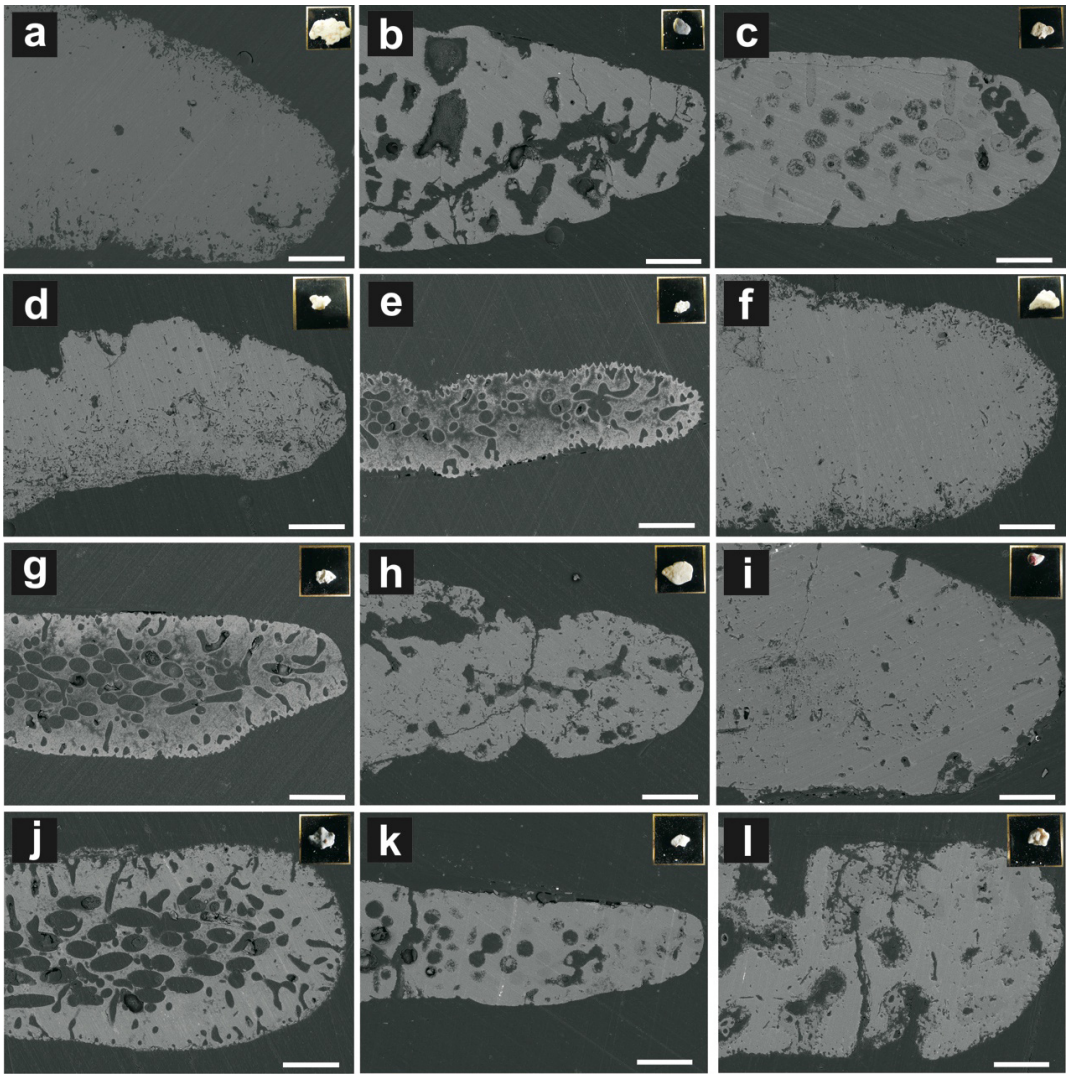

Fig. A11 BSE-SEM images of thin-sections from *Halimeda* segments and corresponding photographs that originate from surface sediments sampled at the island Pulau Pamanbungan (PPB) (Spermonde Archipelago, Sulawesi, Indonesia). Courtesy of T. Mann, A. Klicpera and H. Westphal (ZMT-Bremen). All specimens depicted likely from *Halimeda* lineages Opuntia or Micronesicae. Note that due to strong secondary cementation and abrasion of grains shown in (a), (b), (d), (f), (i) and (l), an identification as *Halimeda* segment may be questionable. Sample ID: (a) PPB1, (b) PPB2, (c) PPB8, (d) PPB9, (e) PPB10, (f) PPB11, (g) PPB12, (h) PPB13, (i) PPB14, (j) PPB21, (k) PPB22, (l) PPB23. Samples taken from onshore (beach area) and water depths < 2 m b.s.l.

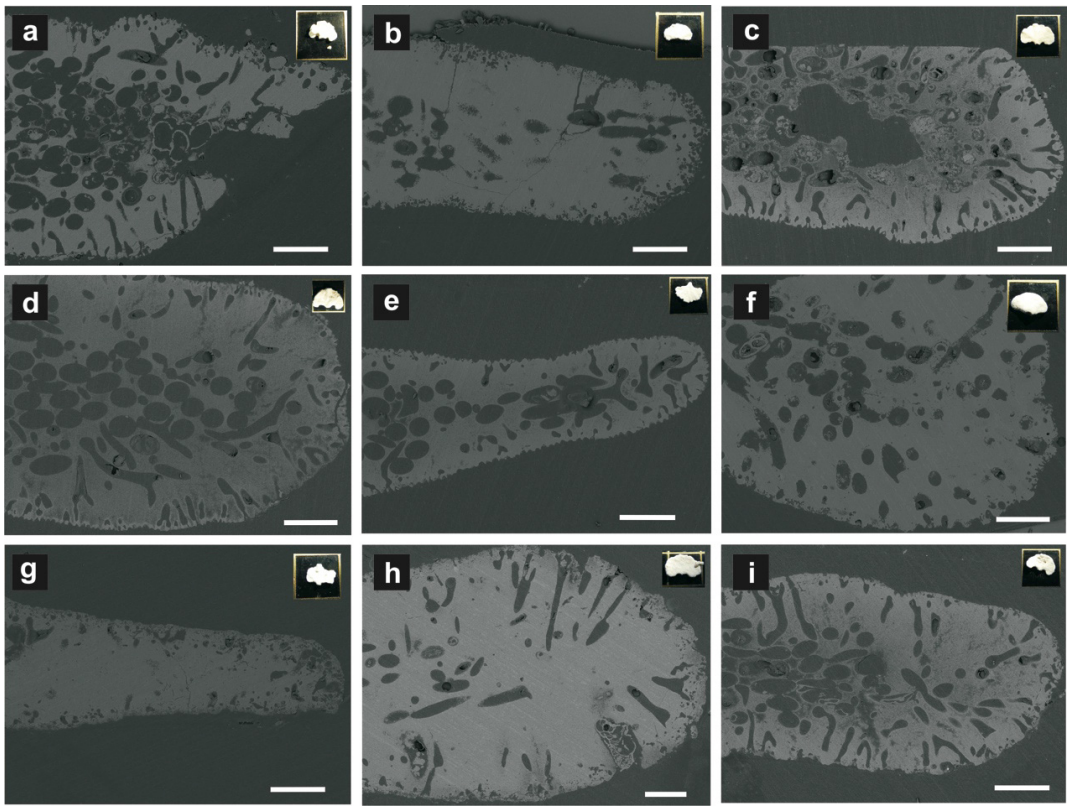

Fig. A12 BSE-SEM images of thin-sections from *Halimeda* segments and corresponding photographs that originate from surface sediments (van Veen Grab) sampled in the Bahamas, Florida shelf and in Belize (Caribbean Sea, Atlantic Ocean). Courtesy of H. Westphal, P. Reid and D. McNeill (ZMT-Bremen, Rosenstiel School of Marine and Atmospheric Science Miami and University of Miami). All specimens depicted likely from *Halimeda* lineage Opuntia. Sample ID: (a) Bah2_Belize (Tabacco_Cay, reef flat), (b) Bah3_Belize (SW_Cay), (c) Bah4_Belize (South_of_Placentia, Palmeto Cay), (d) Bah5_Florida_Keys (Marathon_Key), (e) Bah7_Florida_Keys (Biscayne), (f) Bah8_Bahamas (Lee_Stock_Island), (g) Bah9_Bahamas (Toto_Dive_1847, slope), (h) Bah10_Bahamas (Toto_Dive_1869, slope), (i) Bah11_Belize (Spruce_Key). Samples taken from various depths, < 2 m b.s.l. (reef flat) down to ~1900 m b.s.l. (slope) indicated by sample ID.

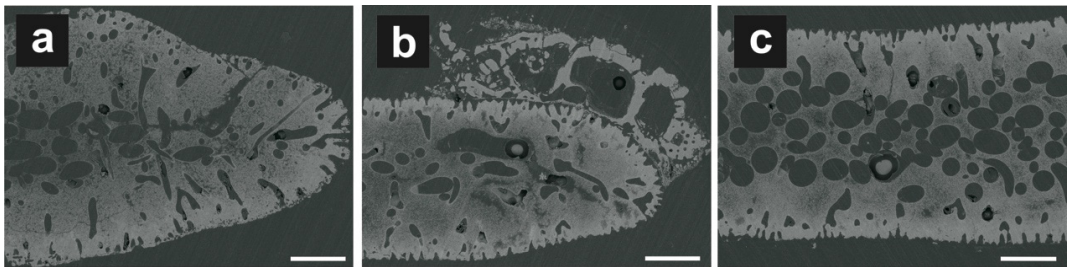

Fig. A13 BSE-SEM images of thin-sections from *Halimeda* segments that originate from surface sediments sampled in Zanzibar (Chwaka Bay, Tanzania, Africa, Indian Ocean). Courtesy of N. Hérran and H. Westphal (ZMT-Bremen). No photographs available. All specimens depicted likely from *Halimeda* lineage Opuntia. (b) With epiphyte, coralline red alga on the surface. Sample ID: (a) Sediment_Zanzibar, (b) Sediment_Zanzibar_2, (c) Sediment_Zanzibar_3. Samples taken from water depths < 2 m b.s.l.

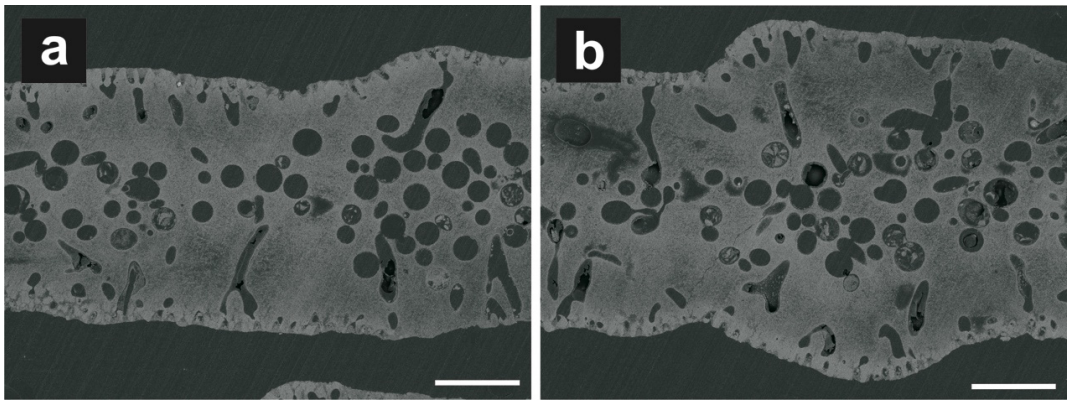

Fig. A14 BSE-SEM images of thin-sections from *Halimeda* segments that originate from surface sediments sampled in Hawaii (O´ahu Island, USA, Equatorial Pacific). Courtesy of T. Mann and H. Westphal (ZMT-Bremen). No photographs available. Specimens depicted likely from *Halimeda* lineages Opuntia or Micronesicae. Sample ID: (a) Sediment_Hawaii, (b) Sediment_Hawaii_2. Samples taken onshore (beach area).